

Final Report Compilation for Fault Detection and Diagnostics for Rooftop Air Conditioners



TECHNICAL REPORT

October 2003
P-500-03-096-A1



Gray Davis, *Governor*

CALIFORNIA ENERGY COMMISSION

Prepared By:
Architectural Energy Corporation
Vernon A. Smith
Boulder, CO

Purdue University
James Braun
West Lafayette, IN

CEC Contract No. 400-99-011

Prepared For:
Christopher Scruton
Contract Manager

Nancy Jenkins
PIER Buildings Program Manager

Terry Surles
PIER Program Director

Robert L. Therkelsen
Executive Director

DISCLAIMER

This report was prepared as the result of work sponsored by the California Energy Commission. It does not necessarily represent the views of the Energy Commission, its employees or the State of California. The Energy Commission, the State of California, its employees, contractors and subcontractors make no warrant, express or implied, and assume no legal liability for the information in this report; nor does any party represent that the uses of this information will not infringe upon privately owned rights. This report has not been approved or disapproved by the California Energy Commission nor has the California Energy Commission passed upon the accuracy or adequacy of the information in this report.

Acknowledgements

Jim Braun and Haorong Li with Purdue University conducted the research with support from Todd Rossi and Doug Dietrich with Field Diagnostic Services, Inc. David Jump with Nexant, Inc. and Lanny Ross with Newport Design Consultants provided field support.

Preface

The Public Interest Energy Research (PIER) Program supports public interest energy research and development that will help improve the quality of life in California by bringing environmentally safe, affordable, and reliable energy services and products to the marketplace.

The Program's final report and its attachments are intended to provide a complete record of the objectives, methods, findings and accomplishments of the Energy Efficient and Affordable Commercial and Residential Buildings Program. This attachment is a compilation of reports from Project 2.1, *Fault Detection and Diagnostics for Rooftop Air Conditioners*, providing supplemental information to the final report (Commission publication #P500-03-096). The reports, and particularly the attachments, are highly applicable to architects, designers, contractors, building owners and operators, manufacturers, researchers, and the energy efficiency community.

This document is one of 17 technical attachments to the final report, consolidating five research reports from Project 2.1:

- [*Description of Field Test Sites \(Feb 2003, rev.\)*](#)
- [*Description of FDD Modeling Approach For Normal Performance Expectation \(Dec 2001\)*](#)
- [*Description And Evaluation Of An Improved FDD Method For Rooftop Air Conditioners \(Aug 2002\)*](#)
- [*Decoupling-Based FDD Approach For Multiple Simultaneous Faults \(June 2003\)*](#)
- [*Automated Fault Detection and Diagnostics of Rooftop Air Conditioners For California, Final Report and Economic Assessment \(Aug 2003\)*](#)

The Buildings Program Area within the Public Interest Energy Research (PIER) Program produced this document as part of a multi-project programmatic contract (#400-99-011). The Buildings Program includes new and existing buildings in both the residential and the nonresidential sectors. The program seeks to decrease building energy use through research that will develop or improve energy-efficient technologies, strategies, tools, and building performance evaluation methods.

For the final report, other attachments or reports produced within this contract, or to obtain more information on the PIER Program, please visit www.energy.ca.gov/pier/buildings or contact the Commission's Publications Unit at 916-654-5200. The reports and attachments, as well as the individual research reports, are also available at www.archenergy.com.

Abstract

Project 2.1, *Fault Detection and Diagnostics for Rooftop Air Conditioners.*

Packaged air conditioners are the most poorly maintained type of HVAC system. In California, they use about 54% of the HVAC energy in the commercial sector. The Purdue research team developed thermo-fluids based fault detection methods that can pinpoint five common maintenance problems.

- This project was highly successful, resulting in a cost-effective method to detect simultaneous faults using only temperature sensors and models of normal operations.
- Controllers that embed these diagnostics methods will save energy and maintenance costs by providing alerts only when maintenance is needed and giving the mechanic better information.
- The historical data from the diagnostic system will also serve as a database for manufacturers to improve the reliability of components.

This document is a compilation of five technical reports from the research.

DESCRIPTION OF FIELD TEST SITES
Revision for Walgreens Field Sites

Deliverables 2.1.1a, 2.1.1b, and 3.1.1a

Progress report submitted to:
Architectural Energy Corporation

For the Building Energy Efficiency Program
Sponsored by:
California Energy Commission

Submitted By:
Purdue University

Principal Investigator: James Braun, Ph.D., P.E.
Research Assistants: Tom Lawrence, P.E.
Kevin Mercer
Haorong Li

April 2001
Revision February 2003

Mechanical Engineering
1077 Ray W. Herrick Laboratories
West Lafayette, IN 47907-1077
(765) 496-6008
(765) 494-0787 (fax)

RAY W. HERRICK
LABORATORIES
PURDUE ENGINEERING



TABLE OF CONTENTS

	<u>Page</u>
LIST OF TABLES	ii
LIST OF FIGURES	iii
1. INTRODUCTION	1
1.1 Purdue Research Projects under this Program	1
2.2 Related Reports	1
2. SELECTION OF FIELD TEST SITES	3
2.1 Criteria for selection of the building and climate types	3
2.2 California climate types	4
2.3 Method for selecting sites	4
3. DESCRIPTION OF FIELD TEST SITES	7
3.1 Modular School Rooms	9
3.2 Fast Food Restaurants	17
3.3 Retail Stores	36
4. TESTING PLAN	39

LIST OF TABLES

	<u>Page</u>
1 – Data List for Modular School Room Field Test Sites	12
2 - Data List for Inland Restaurant Field Test Sites (Watt Avenue and Castro Valley)	23
3 - Data List for Inland Restaurant Field Test Sites (Bradshaw Road and Milpitas)	26

LIST OF FIGURES

	<u>Page</u>
1 – Field Test Sites Data Collection and Communication Overview	8

1. INTRODUCTION

Purdue University is under contract to Architectural Energy Corporation on behalf of the California Energy Commission (CEC) to conduct several research projects. This work is being done under the Building Energy Efficiency Program as part of the CEC's Public Interest Energy Research (PIER) Program.

1.1 Purdue Research Projects under this Program

The work at Purdue is focused on four specific projects and is being coordinated under the direction of Dr. James Braun, P.E. Each project covers different technologies or concepts that have shown promise for improving energy efficiency in building heating, ventilation and air conditioning (HVAC) systems. Specifically, the four projects that Purdue is working on include evaluations and studies of the following. (1) fault detection and diagnostics (FDD) of rooftop air conditioning units (Project 2.1); (2) demand controlled ventilation (DCV) assessment (Project 3.1); (3) assessment and field testing of ventilation recovery heat pumps (Project 4.2); and (4) night ventilation with building thermal mass (Project 3.2).

The first three of these projects are currently active, with the Project 3.2 scheduled to start in September of 2001. All four of the projects involve both theoretical analysis and field demonstration and evaluation. This report describes the field test sites selected for use in projects 2.1 and 3.1. Monitoring equipment has been installed at modular school room and restaurant field sites in Northern California. We have an agreement with the Walgreens Company to allow use of retail store sites in the Los Angeles metropolitan area, and installation is expected to begin in August of 2001. An update to this report will be issued when the retail store installations are finalized.

1.2 Related Reports

This report describes the field test sites selected for use with the CEC PIER project. Other related reports submitted in parallel with this report are: (1) "Description of Laboratory Setup" and (2) "Modeling And Testing Strategies for Evaluating Ventilation Load Reduction Technologies."

The report “Description of Laboratory Setup” provides a description of the York rooftop unit and Honeywell Demand Controlled Ventilation system that are installed outside the Purdue Herrick Laboratory and the instrumentation used for monitoring the setup.. This setup follows closely the field site setups in California. The instrumentation includes measurement of system temperatures, pressures, relative humidities and carbon dioxide concentrations. The Laboratory Setup report covers in detail the setup and operation of the Virtual Mechanic hardware and ACRx ServiceTool Suite of monitoring software, both provided by Field Diagnostic Services. Finally, the report describes the general process for collecting and retrieving data downloaded from the field test sites.

The “Ventilation Strategy Analysis” report presents an overview of the modeling approach and input data to be used in evaluating the energy savings associated with several ventilation load reduction technologies. In addition, an overview of the preliminary test plan and field site monitoring setup for the heat pump heat recovery unit is given.

2. SELECTION OF FIELD TEST SITES

Projects 2.1 and 3.1 involve the use of 12 common field sites for evaluation of FDD and demand-controlled ventilation. In these two projects, field performance data will be obtained from heating/cooling units. Three different building types are being utilized in two different climate zones.

2.1 Criteria for selection of the building types

All of the Purdue projects are focused on small commercial buildings that utilize packaged air conditioning and heating equipment. The criteria used for selecting the types of buildings to include as field test sites focused on the typical building occupancy schedule, the building size and typical HVAC system installed, and the ability to identify multiple sites of similar design and construction within the same climate region. To reduce costs, the same test buildings are being used for the field studies in Projects 2.1 (fault detection and diagnostics) and 3.5 (demand-controlled ventilation). Earlier studies on demand-controlled ventilation indicated that the greatest benefits (in terms of energy savings) are possible with buildings that have variable occupancy schedules. Thus, the three building types selected for the field test sites are smaller retail stores, restaurants and schools. For each type of building, two nearly identical sites will be used in two different climates. This will allow comparative analysis of the energy savings associated with demand-controlled ventilation in terms of building type and climate. The fault detection and diagnostics project is focused strictly on small commercial packaged air conditioning units, so the field sites provide a range of equipment for demonstration and evaluation of this technology. A single site will be used to demonstrate a heat pump heat recovery unit. However, the data obtained from the demand-controlled ventilation sites can also be used to estimate savings for the heat pump heat recovery unit if it were installed in these additional sites.

A large number of modular schoolrooms are installed throughout the state of California. These rooms are all very similar in design and construction, and all typically use wall

mounted heat pumps for heating and cooling. One advantage of the modular schoolroom for this study is that essentially identical rooms can be monitored side-by-side.

For the restaurant building type, the systems used to condition the children's play areas that are common in many fast food chains will be monitored. These rooms typically are self-contained, or nearly so, and only require one or two rooftop units for cooling and heating. By monitoring only the play areas in these restaurants, the study can gather data on spaces that have the greatest variability in occupancy, and also will eliminate the effects of the kitchen area and its associated ventilation systems.

The third building type selected is a small retail store. Small retail stores can have an extremely wide variation in occupancy patterns. Chain stores were considered for the study since essentially identical buildings can be found.

2.2 California Climate Types

Although California has a wide range of climate types, much of the state can be characterized as a Mediterranean climate. This climate type experiences warm, dry summers and temperate moist winters. The state also includes desert regions in southern California (such as Palm Springs) and coastal regions. The specific climate type for a given locality may vary significantly within a small distance due to the influence of factors such as topology and the proximity to the ocean. Some of the best examples of these variations occur in the San Francisco Bay area where the distance of just a few miles can lead to significant variations in rainfall patterns and sky conditions

2.3 Method for selecting sites

It is not possible within the scope of this project to evaluate the new technologies for all possible climate regions in California using field data. However, it will be possible to perform more extensive evaluations through simulation. For the field studies, representative buildings were selected in two different macroclimate types (coastal and

inland). In addition, some of the selected sites are in northern California and some are in southern California, which gives as wide a range of location and climate type as practical within the context of these projects. The inland sites vary from the Mediterranean climate type of the Central Valley around Sacramento to the desert regions around Palm Springs. Although it was not possible to have field sites for all technologies in all climate regions, the areas selected for study represent those with the greatest concentration of population and commercial development.

Before the projects officially started, contacts were made with the owners of potential building sites within the school, restaurant and retail store categories. The identification of sites has been a time consuming process that has required the help of several of the participating organizations, including Honeywell, Schiller Associates, Carrier Corporation, Southern California Edison, and Architectural Energy Corporation.

The first buildings identified were schools. During the summer of 2000, contacts were made and meetings held with representatives of the Oakland Unified School District and the Woodland Joint Unified School District. Woodland is approximately 20 miles west of Sacramento and represents an inland climate type. The monitoring systems were installed at two rooms located side-by-side at each of the two school districts in December of 2000. More details on these sites are contained later in this report.

The restaurant building type is represented by two franchisee owned McDonald's stores in the Sacramento area and by two corporate owned stores on the southeastern San Francisco Bay area. These stores have PlayPlace areas with similar construction and HVAC system installations, although it was not possible to find stores with identical design and sun orientation. Sun orientation can be particularly important for the PlayPlace areas, since they typically include a large percentage of glass area. Monitoring equipment was installed in the Sacramento McDonalds during the middle of March, 2001. In the San Francisco Bay Area, a representative of McDonalds corporate office identified two stores for inclusion in our study that will be the best fit for our needs. Monitoring equipment were installed in May of 2001 at these two stores. More details on these sites are also given in the later sections of this report.

The retail stores are in Southern California. The Walgreens corporation has agreed to our using their stores as part of this program. Monitoring systems are installed at stores located in Rialto (near Riverside) and Anaheim. The Rialto store is located in a near desert climate, while Anaheim is a more coastal climate type.

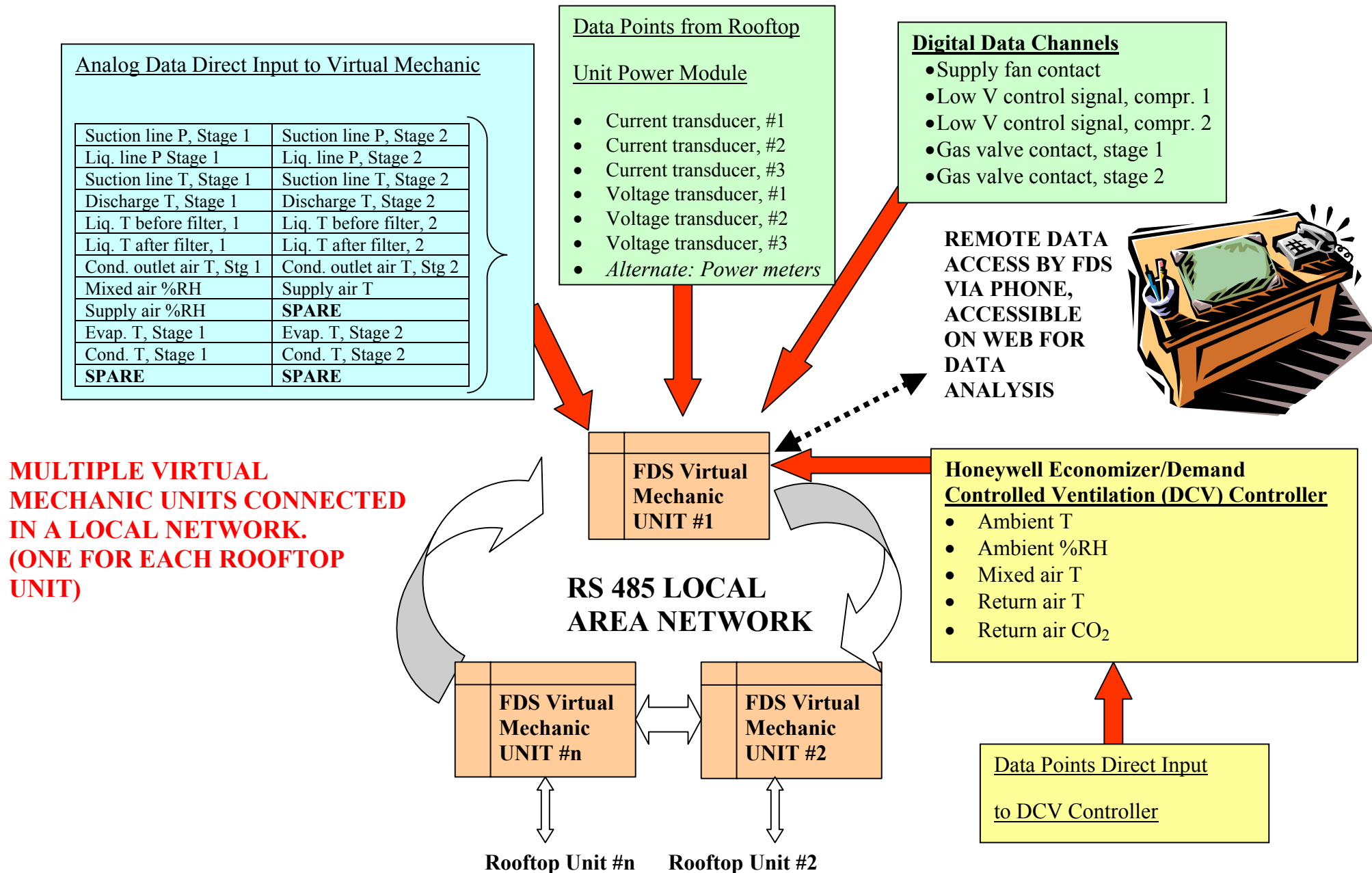
3. DESCRIPTION OF FIELD TEST SITES

Figure 1 presents a general overview of how data are monitored and collected from the field sites. Proprietary equipment from Honeywell controls ventilation dampers using economizer and demand-control ventilation algorithms. The Honeywell controller incorporates sensors to measure ambient temperature and humidity, return air temperature and carbon-dioxide concentration, and mixed air temperature. Additional sensors are installed to monitor other air state variables, refrigerant states, power consumption, and operational status. The primary data acquisition is accomplished using hardware from Field Diagnostics Services (FDS) called the Virtual Mechanic (VM). The VM communicates with the Honeywell controller across an RS485 network to obtain sensor information and to change control strategies. The additional sensors are wired directly to the VM. Data are sampled at approximately 5-minute intervals and are stored in the VM. For some field sites, multiple VMs are employed for multiple packaged air conditioners. Data are downloaded each day using cell phones connected to the master Virtual Mechanic at each test site.

A detailed description of the field test sites is provided in the following subsections. Some of the detailed technical information needed to simulate the performance of the different technologies for these buildings will be compiled later in the project. This section contains information on the following test sites:

- Modular School Rooms – Inland Climate Type
- Modular School Rooms – Coastal Climate Type
- Fast Food Restaurants – Inland Climate Type
- Fast Food Restaurants – Coastal Climate Type
- Retail Stores – Inland Climate
- Retail Stores – Coastal Climate

Figure 1 – Field Test Sites Data Collection and Communication Overview



BUILDING TYPE:**Modular School Rooms*****Inland Climate Locations*****ADDRESS:**

Gibson Elementary School
312 Gibson Road
Woodland, CA 95695
(530) 662-3944

EQUIPMENT INSTALLATION DATE: December 14-19, 2000**CELL PHONE NUMBER:**

(765) 427-0311

DETAILED BUILDING DESCRIPTION:

Floor Area	20 feet by 40 feet (800 sq. ft.)
Building Orientation	East – West
Wall Construction	Walls are 2x4 stud construction with R-11 insulation. Internal walls have $\frac{3}{4}$ " vinyl covered fiberboard over $\frac{5}{8}$ " gypsum wallboard.
Windows/ Shading	Wood panel exterior with no windows on south or north sides. East and west sides have one 4' x 8' window, with door on east side. Two-foot overhang on west wall and three-foot overhang on east wall entrance area. Windows are double-pane with $\frac{1}{4}$ " air gap.
Roof/Ceiling Construction	Flat roof with reflective paint coating. Roof has R-19 insulation. Interior drop ceiling is 8' above occupied space with t-bar 18" below the roof.
Floor	Crawl space below is ventilated with R-11 insulation below floor.
Lighting	10 sets of fluorescent lights, 120 W each with magnetic ballast.
Other Loads and Equipment	One desktop computer and one small refrigerator.
Occupancy Patterns	8:30 am to 3:00 pm weekdays. Usually one or two hours on Saturday mornings. The rooms are occupied by 15-20 small children per room, plus teacher. (These are kindergarten – first grade rooms.)

Gibson School (Cont'd)



**Woodland School Site –
Rear View Looking East**



**Woodland School Site –
Front View Looking West**

Each building (modular school room) has its own packaged air conditioner/heat pump. Two side-by-side units have been retrofit with the Honeywell economizer and demand control ventilation system and fully instrumented. Two VMs are networked together with one of units linked to a cell phone. The heat pump units were originally set up for fixed percentage of outdoor air, and did not have outdoor air flow control dampers. It was estimated that, based on the installation configuration, the airflow control was set up for approximately 15% outdoor air at these sites before the retrofit.

HEATING / AIR CONDITIONING EQUIPMENT:

Each building (room) has a sidewall-mounted heat pump as described in the table below.

Manufacturer	Bard Manufacturing
Model	WH 421-A
Nominal Cooling Capacity	3½ Tons
Number of Stages	1
SEER / HSPF	10.0 / 6.8
Supplemental Heating Capacity	10 kW nominal electric resistance heater.
Electrical	Single phase, 220 V
Supply Fan Rating	1400 cfm @ 0.3"

TEST INSTRUMENTATION:

Table 1 lists the input data channels used at the modular schoolrooms. The same data list is used at both the Woodland and Oakland school sites.

Table 1 – Data List for Modular School Room Field Test Sites

Channel # Data Point

Power Transducer Channels

1	Unit voltage
2	Compressor 1 voltage
3	Common
4	Unit total current
5	Compressor 1 current
6 - 8	Spare - Not Used

Other Analog Input Data

9	Suction line pressure, Stage 1
10	Liquid line pressure, Stage 1
11 - 14	Spare - Not Used
15	Mixed air temperature
16	Return air temperature
17	Supply air temperature, before heater
18	Supply air temperature, after heater
19	Condenser inlet air temperature
20	Condenser outlet air temperature
21	Suction line temperature, Stage 1
22	Discharge line temperature, Stage 1
23	SPARE - Used as additional ambient T
24	SPARE - Used as additional ambient T
25	Evaporation temperature, Stage 1
26	Condensation temperature, Stage 1
27- 32	Spare - Not Used

Calculated Data Channels

33-50	NOT USED
51	Honeywell DCV indoor (and outdoor) CO2 conc.
52	Honeywell DCV mixed air temperature
53	Honeywell DCV return air temperature
54	Honeywell DCV return / outdoor humidity
55	Honeywell DCV outdoor air temp & damper position
56	Honeywell DCV minimum damper position
57	superheat, stage 1
58	subcooling, stage 1
59	evaporating temperature, stage 1
60	condensing temperature, stage 1
61	condensing temperature over ambient (CT-AIC), stage 1
62	superheat, stage 2
63	subcooling, stage 2
64	evaporating temperature, stage 2
65	condensing temperature, stage 2
66	condensing temperature over ambient (CT-AIC), stage 2

Table 1 – Data List for Inland Modular School Room Field Test Site (Cont'd)

Channel	Data Point
67	evaporator temperature difference (RA-SA)
68	NOT USED
69	NOT USED
70	unit power (kW)
71	unit KWh
72	unit MWh
73	compressor 1 power (kW)
74	compressor 1 KWh
75	compressor 1 MWh
76	compressor 2 power (kW)
77	compressor 2 KWh
78	compressor 2 MWh
79	digital input 1, supply fan, run time (8 hours)
80	digital input 1, supply fan, run time (seconds)
81	digital input 2, cooling 1, run time (8 hours)
82	digital input 2, cooling 1, run time (seconds)
83	digital input 3, cooling 2, run time (8 hours)
84	digital input 3, cooling 2, run time (seconds)
85	digital input 4, heat 1, run time (8 hours)
86	digital input 4, heat 1, run time (seconds)
87	digital input 5, heat 2, run time (8 hours)
88	digital input 5, heat 2, run time (seconds)
89	digital input 6 run time (8 hours)
90	digital input 6 run time (seconds)
91	time since reset accumulators (8 hours)
92	time since reset accumulators (seconds)
93	up time (8 hours)
94	up time (seconds)
95	board temperature (F)
96	board battery voltage (V)
Digital Channels	
1	Supply fan contact (fan on / fan off)
2	Low voltage control signal for compressor contact
3	Spare
4	Heat on
5	Electric heat
6	

BUILDING TYPE:**Modular School Rooms***Coastal Climate Location***ADDRESS:**

Fremont High School
4610 Foothill Blvd.
Oakland, CA
(510) 879-3020

EQUIPMENT INSTALLATION DATE: December 19-21, 2000**CELL PHONE NUMBER:**

(765) 427-0325

DETAILED DESCRIPTION:

Floor Area	20 feet by 40 feet (800 sq. ft.)
Building Orientation	East – West
Wall Construction	Walls are 2x4 stud construction with R-11 insulation. Internal walls have $\frac{3}{4}$ " vinyl covered fiberboard over $\frac{5}{8}$ " gypsum wallboard.
Windows/ Shading	Wood panel exterior with no windows on south or north sides. East and west sides have one 4' x 8' window, with door on east side. Two-foot overhang on west wall and three-foot overhang on east wall entrance area. Windows are double-pane with $\frac{1}{4}$ " air gap.
Roof/Ceiling Construction	Flat roof with reflective paint coating. Roof has R-19 insulation. Interior drop ceiling is 8' above occupied space with t-bar 18" below the roof.
Floor	Crawl space below is ventilated with R-11 insulation below floor.
Lighting	Approximately 10 sets of fluorescent lights, 120 W each with magnetic ballast.
Other Loads and Equipment	One desktop computer. (To be verified)
Occupancy Patterns	8:30 am to 3:00 pm weekdays. The rooms are occupied by 15-20 high school students per classroom.

Fremont High School (Cont'd)



Oakland School Site (Fremont High School) - View Looking Along North Walls

Each building (modular school room) has its own packaged air conditioner/heat pump. Two side-by-side units have been retrofit with the Honeywell economizer and demand control ventilation system and fully instrumented. Two VMs are networked together with one of units linked to a cell phone. The heat pump units were originally set up for fixed percentage of outdoor air, and did not have outdoor air flow control dampers. It was estimated that, based on the installation configuration, the airflow control was set up for approximately 15% outdoor air at these sites before the retrofit.

HEATING / AIR CONDITIONING EQUIPMENT:

Each building (room) has a sidewall-mounted heat pump manufactured by Bard Industries, Model WH 421A. These are the same units as used at the Woodland school site. The units are contained within a fenced off area on the north end of the buildings.

Nominal Cooling Capacity	3½ Tons
SEER / HSPF	10.0 / 6.8
Heating Capacity	10 kW nominal electric resistance heater. Note: The electrical resistance heaters are not functioning for these rooms.
Electrical	Single phase, 220 V
Supply Fan Performance	1400 cfm @ 0.3"

TEST INSTRUMENTATION:

The Fremont school site uses the same data point list given in Table 1 for the Woodland schools.

BUILDING TYPE:**Fast Food Restaurants*****Inland Climate Locations*****ADDRESS:**

McDonalds Restaurant
2434 Watt Ave.
Sacramento, CA 95821
(916) 971-0244

3560 Bradshaw Road
Sacramento, CA 95827
(916) 361-8186

CONTACT:

Mike Godlove (Owner)
2508 Garfield Ave
Carmichael, CA 95608
(916) 483-6065

EQUIPMENT INSTALLATION DATE: March 12-14, 2001**CELL PHONE NUMBERS:** (765) 427-7714 and 427-7919**DETAILED DESCRIPTION:**

Equipment at two nearly identical McDonald's PlayPlaces in Sacramento have been retrofit with the Honeywell economizer and demand control ventilation system and fully instrumented. Each system has its own dedicated VM with a cell phone for data transmission. The Watt Avenue site has a slightly smaller floor area (approximately 20 square feet less take from two corners). The following subsections give some details on the building construction and operation. Additional details will be obtained later.

Sacramento Area McDonalds PlayPlace Construction (Watt Avenue and Bradshaw Road)

Floor Area	Approximately 20 feet by 30 feet (600 sq. ft.) that is for the most part isolated from the dining and cooking areas.
Building Orientation	Primary axis for this room is North - South. Major glass surfaces on the East and South walls. West face is interior wall shared with the dining area.
Wall Construction	“Stucco” exterior covering.
Windows/ Shading	Major glass surfaces on the East and South walls. West face is interior wall shared with the dining area. Some window area on North wall. No exterior shading. Windows are tinted with double pane, 1/4” air gap construction.
Roof/Ceiling Construction	Flat roof with light colored asphalt coating.
Floor	Tile on slab construction.
Lighting	Approximately six sets of fluorescent lights, with four bulbs each with magnetic ballast.
Other Loads and Equipment	Some air exchange with dining area and outdoor air via door in the common vestibule. Ceiling fans keep air in motion.
Occupancy Patterns	PlayPlace hours are: 9 am to 9:30 pm. Occupancy varies from 0 to a maximum of approximately 40.

Watt Avenue (Sacramento Area) McDonalds PlayPlace Pictures



Interior view of Watt Avenue McDonalds PlayPlace Area showing location of return air and supply air ducts.



Watt Avenue McDonalds – View Looking Southwest



Watt Avenue McDonalds – Rooftop Units Undergoing Equipment Installation

Bradshaw Road (Sacramento Area) McDonalds PlayPlace Pictures



Interior view of Bradshaw Road McDonalds PlayPlace Area



**Bradshaw Road McDonalds –
View Looking Northwest**



**Bradshaw Road McDonalds –
Rooftop Units Undergoing Equipment Installation**

HEATING / AIR CONDITIONING EQUIPMENT:

Each PlayPlace uses rooftop-mounted units for providing heating, cooling and ventilation air to the room. The two sites differ in the number of rooftop units used, with the Watt Avenue building using one two-stage unit and the Bradshaw Road building using two smaller single-stage units. According to York International's regional support representative, the units are custom designed for supply to McDonalds Corporation for the PlayPlace areas. The following tables describe the units used at each site. Since they

are custom designs, published performance ratings and other technical details were not readily available. This information will be obtained later.

Watt Avenue

Manufacturer	York International
Model	D3CG120N20025MKD
Nominal Cooling Capacity	10 Tons
Number of Stages	2
SEER / HSPF	TBD
Heating Capacity	200,000 Btu/hr nominal output
Electrical	Three phase, 220 V
Supply Fan Performance	4,000 cfm manufacture rated

Bradshaw Road

Manufacturer	York International
Model	D1CG072N07925ECC
Nominal Cooling Capacity	6 Tons
Number of Stages	1
SEER / HSPF	TBD
Heating Capacity	100,000 Btu/hr nominal output
Electrical	Three phase, 220 V
Supply Fan Performance	2,400 cfm manufacture rated (each)

TEST INSTRUMENTATION:

Tables 2 and 3 list the data channels used at the restaurants. A slightly different list is required for each site since the HVAC equipment setup is different. In particular, the Watt Avenue site has one larger (10 ton) unit with 2-stage cooling to condition the entire room. The Bradshaw Road site, on the other hand, has two smaller (6 ton) single-stage cooling units operating in parallel. Instrumentation for fault detection and diagnostics and monitoring was set-up for one rooftop unit per site, as originally planned in the project proposal stage. Therefore, one unit at the Bradshaw Road site was fully instrumented for both FDD and DCV purposes, while the second unit was instrumented only for the purposes of collecting data for the DCV project. The Watt Avenue site has only one rooftop unit and was fully instrumented according to the standard data list. All data will be collected using one Virtual Mechanic at each site.

Table 2 – Data List for Inland Restaurant Field Test Site (Watt Avenue)

Channel # Data Point

SENSOR CHANNELS

Power Transducer Channels

1	Unit voltage
2	Compressor 1 voltage
3	Compressor 2 voltage
4	Unit total current
5	Compressor 1 current
6	Compressor 2 current

Other Analog Input Data

7	SPARE - Not used
8	SPARE - Not used
9	Suction line pressure, Stage 1
10	Discharge pressure, Stage 1
11	Suction line pressure, Stage 2
12	Discharge pressure, Stage 2
13	SPARE - Not used
14	SPARE - Not used
15	Mixed air temperature
16	Return air temperature
17	Supply air temperature, before heater
18	Supply air temperature, after heater
19	Condenser inlet air temperature
20	Condenser outlet air temperature
21	Suction line temperature, Stage 1
22	Discharge line temperature, Stage 1
23	Liquid line temperature before filter/drier, Stage 1
24	Liquid line temperature after filter/drier, Stage 1
25	Evaporation temperature, Stage 1
26	Condensation temperature, Stage 1
27	Suction line temperature, Stage 2
28	Discharge line temperature, Stage 2
29	Liquid line temperature before filter/drier, Stage 2
30	Liquid line temperature after filter/drier, Stage 2
31	Evaporation temperature, Stage 2
32	Condensation temperature, Stage 2

Calculated Data Channels

33-50	NOT USED
51	Honeywell DCV indoor (and outdoor) CO2 conc.
52	Honeywell DCV mixed air temperature
53	Honeywell DCV return air temperature
54	Honeywell DCV return / outdoor humidity
55	Honeywell DCV outdoor air temp & damper position

Table 2 – Data List for Inland Restaurant Field Test Site (Watt Avenue) – Cont'd

Channel	Data Point
56	Honeywell DCV minimum damper position
57	superheat, stage 1
58	subcooling, stage 1
59	evaporating temperature, stage 1
60	condensing temperature, stage 1
61	condensing temperature over ambient (CT-AIC), stage 1
62	superheat, stage 2
63	subcooling, stage 2
64	evaporating temperature, stage 2
65	condensing temperature, stage 2
66	condensing temperature over ambient (CT-AIC), stage 2
67	evaporator temperature difference (RA-SA)
68	NOT USED
69	NOT USED
70	unit power (kW)
71	unit KWh
72	unit MWh
73	compressor 1 power (kW)
74	compressor 1 KWh
75	compressor 1 MWh
76	compressor 2 power (kW)
77	compressor 2 KWh
78	compressor 2 MWh
79	digital input 1, supply fan, run time (8 hours)
80	digital input 1, supply fan, run time (seconds)
81	digital input 2, cooling 1, run time (8 hours)
82	digital input 2, cooling 1, run time (seconds)
83	digital input 3, cooling 2, run time (8 hours)
84	digital input 3, cooling 2, run time (seconds)
85	digital input 4, heat 1, run time (8 hours)
86	digital input 4, heat 1, run time (seconds)
87	digital input 5, heat 2, run time (8 hours)
88	digital input 5, heat 2, run time (seconds)
89	digital input 6 run time (8 hours)
90	digital input 6 run time (seconds)
91	time since reset accumulators (8 hours)
92	time since reset accumulators (seconds)
93	up time (8 hours)
94	up time (seconds)
95	board temperature (F)
96	board battery voltage (V)

Table 2 – Data List for Inland Restaurant Field Test Site (Watt Avenue) – Cont’d

Digital Channels

1	Supply fan contact (fan on / fan off)
2	Low voltage control signal for compressor 1 contact
3	Low voltage control signal for compressor 2 contact
4	Heating 1
5	Heating 2
6	

Table 3 – Data List for Inland Restaurant Field Test Site (Bradshaw Road)

Channel # Data Point

SENSOR CHANNELS

Power Transducer Channels

1	Unit 1 input voltage
2	Compressor voltage, Unit 1
3	Unit 2 input voltage
4	Unit 1 total current
5	Compressor current, Unit 1
6	Unit 2 total current

Other Analog Input Data

7	SPARE - Not used
8	SPARE - Not used
9	Suction line pressure, Unit 1
10	Discharge pressure, Unit 1
11	SPARE - Not used
12	SPARE - Not used
13	SPARE - Not used
14	SPARE - Not used
15	Mixed air temperature - Unit 1
16	Return air temperature - Unit 1
17	Supply air temperature, before heater - Unit 1
18	Supply air temperature, after heater - Unit 1
19	Condenser inlet air temperature - Unit 1
20	Condenser outlet air temperature - Unit 1
21	Suction line temperature - Unit 1
22	Discharge line temperature - Unit 1
23	Liquid line temperature before filter/drier - Unit 1
24	Liquid line temperature after filter/drier - Unit 1
25	Evaporation temperature - Unit 1
26	Condensation temperature - Unit 1
27	SPARE - Not used
28	SPARE - Not used
29	Mixed air temperature - Unit 2
30	Mixed air humidity - Unit 2
31	Supply air temperature - Unit 2
32	Supply air humidity - Unit 2

CALCULATED DATA CHANNELS

33-50	NOT USED
51	Honeywell DCV indoor (and outdoor) CO2 conc.
52	Honeywell DCV mixed air temperature
53	Honeywell DCV return air temperature
54	Honeywell DCV return / outdoor humidity
55	Honeywell DCV outdoor air temp & damper position

Table 3 – Data List for Inland Restaurant Field Test Site (Bradshaw Road) – Cont’d

Channel	Data Point
56	Honeywell DCV minimum damper position
57	superheat, stage 1
58	subcooling, stage 1
59	evaporating temperature, stage 1
60	condensing temperature, stage 1
61	condensing temperature over ambient (CT-AIC), stage 1
62	NOT USED
63	NOT USED
64	NOT USED
65	NOT USED
66	NOT USED
67	NOT USED
68	NOT USED
69	NOT USED
70	unit power (kW)
71	unit KWh
72	unit MWh
73	compressor 1 power (kW)
74	compressor 1 KWh
75	compressor 1 MWh
76	compressor 2 power (kW)
77	compressor 2 KWh
78	compressor 2 MWh
79	digital input 1, supply fan, run time (8 hours)
80	digital input 1, supply fan, run time (seconds)
81	digital input 2, cooling 1, run time (8 hours)
82	digital input 2, cooling 1, run time (seconds)
83	digital input 3, cooling 2, run time (8 hours)
84	digital input 3, cooling 2, run time (seconds)
85	digital input 4, heat 1, run time (8 hours)
86	digital input 4, heat 1, run time (seconds)
87	digital input 5, heat 2, run time (8 hours)
88	digital input 5, heat 2, run time (seconds)
89	digital input 6 run time (8 hours)
90	digital input 6 run time (seconds)
91	time since reset accumulators (8 hours)
92	time since reset accumulators (seconds)
93	up time (8 hours)
94	up time (seconds)
95	board temperature (F)
96	board battery voltage (V)

Table 3 – Data List for Inland Restaurant Field Test Site (Bradshaw Road) – Cont’d

Digital Channels

1	Supply fan contact (fan on / fan off)
2	Low voltage control signal for compressor contact
3	Spare
4	Heating
5	Spare
6	

BUILDING TYPE:**Fast Food Restaurants*****Coastal Climate Locations*****ADDRESS:**99 N. Milpitas Blvd.
Milpitas, CA 95035
(408) 263-01811620 Storbridge Ave.
Castro Valley, CA 94546
(510) 537-9566**CONTACT:**Paul Martin
(408) 422-2339**EQUIPMENT INSTALLATION DATE:** May 2001**CELL PHONE NUMBERS:**(765) 427-2988
(765) 427-3052**DETAILED DESCRIPTION:**

The PlayPlace areas at these two sites are not as close in design and orientation as are the two Sacramento sites. This is a compromise in order to get two sites that are reasonably close together and in a similar coastal climate zone. Both restaurants are located south of Oakland on the east edge of the San Francisco Bay and have a floor space of around 1300 square feet, which is larger than the PlayPlace areas at the two Sacramento stores. The Castro Valley restaurant is oriented with its main glass area facing west. The Milpitas store, however, contains a larger glass area and is oriented facing north. The following subsections contain some descriptions of the room construction and heating/cooling equipment for these two coast climate restaurant sites. Additional details of the construction and building operation will be obtained later.

Castro Valley (San Francisco Bay Area) McDonalds PlayPlace Construction

Floor Area	Approximately 26 feet by 50 feet (1300 sq. ft.) that is isolated from the dining and cooking areas by an interior glass wall with two doors.
Building Orientation	Primary axis for this room is northwest - southeast. The long axis glass surface area faces southwest, with the smaller sides facing northwest and southeast. Northeast wall is interior wall shared with the dining area.
Wall Construction	“Stucco” exterior covering.
Windows/ Shading	Windows are tinted with double pane, 1/4” air gap construction. Overhang of 24” at top that provides minimal shading. Total glass area of about 490 sq. ft. on southwest wall and 195 sq. ft. each on the northwest and southeast walls.
Roof/Ceiling Construction	Flat roof with light colored asphalt coating.
Floor	Tile on slab construction.
Lighting	Total of 26 fixtures of 48” fluorescent lights, with four bulbs each with magnetic ballast. Several had missing bulbs, only approximately 80% of bulbs in place.
Other Loads and Equipment	One TV and four video games. Ceiling fans keep air in motion.
Occupancy Patterns	PlayPlace operating hours are 9am – 9pm. During visit on a Sunday afternoon, occupied by approximately 70 children and adults.

Milpitas (San Francisco Bay Area) McDonalds PlayPlace Construction

Floor Area	Approximately 24 feet by 50 feet with 6' by 6' corner that shares internal wall with kitchen storage. Total floor is approximately 1170 sq. ft. Zone is isolated from the dining and cooking areas by an interior glass wall with two doors.
Building Orientation	Primary axis for this room is east - west. The long axis glass surface area faces north, with the smaller sides facing west and east. South wall is interior wall shared with the dining area.
Wall Construction	"Stucco" exterior covering.
Windows/ Shading	Windows are tinted with double pane, 1/4" air gap construction. Overhang of 24" at top that provides minimal shading. Exterior walls are essentially floor to ceiling covered in glass. Total glass area of about 1000 sq. ft. on north wall, 480 sq. ft. on the east wall and 360 sq. ft. on the west wall.
Roof/Ceiling Construction	Flat roof with light colored asphalt coating.
Floor	Tile on slab construction.
Lighting	Total of 19 fixtures of 48" fluorescent lights, with four bulbs each with magnetic ballast.
Other Loads and Equipment	No TVs or video games. Ceiling fans keep air in motion.
Occupancy Patterns	PlayPlace operating hours are 8am – 9pm.

Castro Valley McDonalds PlayPlace Pictures



Interior view of Castro Valley McDonalds PlayPlace Area.



**Castro Valley McDonalds –
View Looking Southeast**



**Castro Valley McDonalds PlayPlace Area.
York Rooftop Unit**

Milpitas McDonalds PlayPlace Pictures



Interior view of Milpitas McDonalds PlayPlace Area (NW Corner)



Milpitas McDonalds – View Looking Southeast



Milpitas McDonalds PlayPlace Area. Two York Rooftop Units

HEATING / AIR CONDITIONING EQUIPMENT:

Each building (room) uses rooftop-mounted units for providing heating, cooling and ventilation air to the room. The two sites differ in the number of rooftop units used. Just like the two restaurants in Sacramento, one restaurant uses one two-stage York rooftop unit (Castro Valley) and the other (Milpitas) uses two smaller single-stage units. The units are of the same series that were designed and built specifically for the McDonalds PlayPlace areas. The following tables describe the units used at each site. Since they are

more or less custom design, published performance ratings and other technical details were not readily available.

Castro Valley

Manufacturer	York International
Model	D4CG150N16525MDB
Nominal Cooling Capacity	12 Tons
Number of Stages	2
SEER / HSPF	TBD
Heating Capacity	204,000 Btu/hr nominal output
Electrical	Three phase, 220 V
Supply Fan Performance	4,000 cfm manufacture rated

Milpitas

Manufacturer	York International
Model	D1CG072N09925C
Nominal Cooling Capacity	6 Tons
Number of Stages	1
SEER / HSPF	TBD
Heating Capacity	125,000 Btu/hr nominal output
Electrical	Three phase, 220 V
Supply Fan Performance	2,400 cfm manufacture rated (each)

TEST INSTRUMENTATION:

Similar test instrumentation will be used as for the Sacramento McDonalds. The system at the restaurant with only one rooftop unit (Castro Valley) will be fully instrumented for both FDD and DCV studies, like the Watt Avenue site in Sacramento. The data list is presented in Table 2. The Milpitas site is analogous to the Bradshaw Road store in Sacramento, whereby one unit will be fully instrumented for both FDD and DCV purposes, while the second unit will be instrumented only for the purposes of collecting data for the DCV project. Table 3 provides this data list. All data will be collected using one VM at each site.

BUILDING TYPE:**Retail Store****ADDRESS:*****Inland Climate Location***

Walgreens
550 S. Riverside
Rialto, CA
Contact: Gabriel Reyes (Store Manager)
(709) 874-6600

Coastal Climate Location

Walgreens
946 S. Brookhurst
Anaheim, CA
Contact: Lee Anderson (Store Manager)
(714) 520-5444

EQUIPMENT INSTALLATION DATES:

Rialto Store: VM Monitoring Equipment: August 1-5, 2001
Functioning Honeywell Controls: June, 2002

Anaheim Store: VM Monitoring Equipment: June, 2002
Functioning Honeywell Controls: Fall 2002

CELL PHONE NUMBERS: Dedicated land phone lines were installed in August 2002 to replace the cell phone arrangement.

DETAILED BUILDING DESCRIPTION: Rialto Store (Common Design)

Floor Area	100 feet by 90 feet (9,000 sq. ft.) in retail store space, 40 feet by 20 feet in the pharmacy. An additional 35 feet by 90 feet of backroom storage and 20 feet by 100 feet for office and equipment that is not part of the DCV study.
Building Orientation	Generally north - south, with front door on northeast corner.
Wall Construction	Brick and stucco exterior.
Windows/ Shading	<p>A total of 20 windows on the two exterior walls to the retail store area. Windows are 5 feet by 8 feet, tinted, double-pane with 1/4" air gap. Windows are on the east and north walls.</p> <p>A five-foot overhang covers the sidewalk and shades the exterior windows.</p>

Roof/Ceiling Construction	Flat roof with light store coating.
Floor	Floor tiles over concrete slab.
Lighting	Retail store has total of 170 fixtures with 2 bulbs, 8-foot long fluorescent lights. Pharmacy has 33 fixtures of 2 bulb, four-foot long fixtures.
Other Loads and Equipment	Refrigerated drink and food open to store, 25 feet linear feet. Freezer section with doors, 20 feet long. Photo processing machine plus two cash registers.
Occupancy Patterns	Store hours are 8 am to 10 pm, seven days a week.

HEATING / AIR CONDITIONING EQUIPMENT:

Four rooftop heat pumps condition the retail store space and one additional unit is dedicated to the pharmacy area. A separate unit is installed at the store to condition the storage room, but since this is an isolated area not normally occupied, it is not part of the DCV installation study. The rooftop units are manufactured by Trane.

Manufacturer	Trane
Model	WFD090C30BBC - Retail Store WFD075C30BBC - Pharmacy
Nominal Cooling Capacity	Retail store units - 7½ tons Retail store units - 6¼ tons
Number of Stages	1
SEER / HSPF	8.9 EER
Electrical	Three phase, 208 V
Supply Fan Performance	2,500 nominal supply airflow @ 0.5 in. w.c. - 6¼ tons 3,000 nominal supply airflow @ 0.5 in. w.c. - 7½ tons

TEST INSTRUMENTATION:

Similar test instrumentation is used as for the McDonalds sites. Individual VM monitoring systems are installed for each rooftop unit, and networked together to one master VM that communicates via the cell phone. These rooftop units are single stage compressor systems, and the same monitoring data as listed in Table 3 are used.



Trane rooftop heat pump installed on Walgreens Rialto store

4. TESTING PLAN

This test plan as outlined below was set up during the initial phases of the project. The test plan has changed as the result of equipment installation schedules and problems. The field sites were rotated more regularly between demand control ventilation ON and OFF remotely using procedures developed by Field Diagnostic Services.

Data is downloaded on a daily basis using cell phones connected to the master Virtual Mechanic at each test site. The data monitoring and collection process was outlined earlier in this report in Figure 1.

There are separate test plans for the two projects that share the 12 field test site buildings.

Project 2.1: Fault Detection and Diagnostics

A testing plan for this project is included in a separate report being submitted by Purdue for deliverable 2.1.1b. This report is titled, “Description of Laboratory Setup” and was described in Section 1.2 above.

Project 3.1: Demand Controlled Ventilation

The following is a general overview of the testing plan for Project 3.1. The separate report titled “*Modeling and Testing Strategies for Evaluating Ventilation Load Recovery Technologies*” being submitted by Purdue describes how the data being collected will be analyzed.

Key parameters to measure for this project are:

- Unit power consumption for the compressors and fans.
- Energy input during heating mode. This will be expressed either in terms of compressor and electrical resistance heater power for the sites with heat pump heating, or in terms of natural gas usage for rooftop units with heating.
- Total cycle time for compressor (and heater) operation.
- Levels of carbon dioxide in the occupied space.

- Temperature and humidity levels for the ambient air, mixed air, supply air and the conditioned space.

The following is a general outline of the data gathering and test plan.

SCHOOLS:

March – May 2001: Monitor building performance for each of the four schoolrooms. Use this data to build baseline data for each room.

May – June, 2001: For the remaining part of this school year, set up one building at each site to run in Demand Controlled Ventilation (DCV) mode and the other building with the standard economizer mode. During this time visit each room and characterize the nominal usage patterns, etc.

Summer, 2001 (June-August): If the rooms are not to be occupied regularly during the summer months when regular school is not in session (mid-June to early September), then set up each room to operate in one common mode. Since the units at both school sites were setup for fixed outdoor air ventilation rates originally, we will duplicate that situation with the same percentage of outdoor air for each room. This will allow for a full characterization of the building thermal performance and any baseline differences between rooms at each site.

Fall, 2001: Around the beginning of the new school year, the control strategy will be changed to include one building on DCV and the other on a fixed ventilation rate. The fixed ventilation rate will be for the maximum setting required for schoolroom occupancy as determined by ASHRAE Standard 62. The control strategies will be reversed from that during the initial cooling season monitoring time (May to June).

November 2001 – January 2002: Maintain the same control strategy for each building for the beginning of the heating season.

January 2002 – March 2002: Reverse ventilation control strategies between the buildings at each climate type. Do this during a site visit in late December 2001 or early January

2002, or remotely if possible. Change back to the same settings for each room as with the first cooling season phase of May-June, 2001.

RESTAURANTS:

March – May 2001: Monitor building performance for each of the restaurants using one common ventilation control strategy. This will likely be the use of the existing economizer control. Use this time to build baseline data for each building. During this time, visit each site (March and/or May) and characterize the nominal usage patterns, etc.

June-July, 2001: For each climate type, set up one building with DCV mode and the other with normal economizer mode. (Sacramento sites have Honeywell economizers currently installed.)

August-Fall, 2001: At each climate type, reverse the ventilation control strategies, with one building using DCV and the other set-up for fixed position dampers.

November 2001 – December/January 2002: Maintain the same control strategy for each building for the beginning of the heating season.

December 2001 – February 2002: Reverse ventilation control strategies between the buildings at each climate type. (Do this during a site visit in December 2001 or January 2002.) Change back to the same settings for each room as with the first cooling season phase of June-July, 2001.

RETAIL STORES

The detailed plan for monitoring the retail stores will be finalized after completion of the equipment installation. The plan will likely be as follows.

August-Fall, 2001: After the initial installation and checkout of the control equipment, begin to monitor the buildings at the inland and coastal climate sites with one building in DCV mode and the other using normal economizer control mode.

November 2001 – December/January 2002: Maintain the same control strategy for each building for the beginning of the heating season.

December 2001 – February 2002: Reverse ventilation control strategies between the buildings at each climate type. (Do this during a site visit in December 2001 or January 2002.)

Spring 2002: Reverse the ventilation control strategies from the cooling season data gathered during August and the fall of 2001.

DESCRIPTION OF FDD MODELING APPROACH FOR NORMAL PERFORMANCE EXPECTATION

Deliverable 2.1.2

Progress report submitted to:
Architectural Energy Corporation

For the Building Energy Efficiency Program
Sponsored by:
California Energy Commission

Submitted By:
Purdue University

Principal Investigator: James Braun, Ph.D., P.E.
Research Assistant: Haorong Li

December 2001

**Mechanical Engineering
1077 Ray W. Herrick Laboratories
West Lafayette, IN 47907-1077
(765) 496-6008
(765) 494-0787 (fax)**

**RAY W. HERRICK
LABORATORIES
PURDUE ENGINEERING**



Table of Contents

1. Introduction.....	4
2. Background work.....	7
2.1 Physical modeling and gray-box modeling.....	7
2.2 Black-box modeling.....	8
2.2.1 Polynomials.....	8
2.2.2 General Regression Neural Network.....	11
2.2.3 Back-propagation neural network	15
2.2.4 Radial basis function.....	16
3. Comparison of black-box modeling approaches using laboratory data	18
3.1 Laboratory experimental data	18
3.2 Comparisons.....	21
3.3 Polynomial plus GRNN model.....	27
4. Modeling field site data.....	31
4.1 Impact of unmeasured weather variables	31
4.1.1 Solar radiation impact on the system	31
4.1.2 Rainfall impact on the system	35
4.2 Data Processing.....	37
4.2.1 Driving condition problems.....	37
4.2.2 Steady-State Detector	40
4.2.3 Clustering of steady-state data.....	43
4.3 Purdue Field Site Results.....	44
4.4 California Rooftop unit model	52
5. Adaptive Polynomial plus GRNN	55
6. Conclusions and future work.....	58
7. Reference	59

NOMENCLATURE

A	Sensor surface area
ANN	Artificial neural network
BP	Back-propagation
ΔT_{ca}	Condenser air temperature difference
ΔT_{ea}	Evaporator air temperature difference
FDD	Fault detection and diagnosis
GRNN	General regression neural network
h_o	Heat transfer coefficient between sensor and ambient air
I_t	Irradiation on sensor exterior surface
ma	Mixed air
oa	Outdoor air
ra	Return air
RBF	Radial basis function
RMS	Root mean square
RTU	Rooftop unit
T_{amb}	Ambient temperature
t_a	Air temperature
T_{cond}	Condensing temperature
T_{dis}	Discharge line temperature
T_{evap}	Evaporating temperature
T_{ll}	Liquid line temperature
T_{ma}	Mixed air temperature
T_{oa}	Outdoor air temperature
T_{ra}	Return air temperature
t_s	Sensor surface temperature (sensor's reading)
T_{sc}	Subcooling
T_{sh}	Superheat
W_{ma}	Mixed air humidity ratio
W_{oa}	Outdoor air humidity ratio
W_{ra}	Return air humidity ratio
τ	Transmittance
ρ	Reflectance
α	Absorptance

1. Introduction

All the thermodynamic states of a rooftop air conditioning unit (RTU) are functions of external driving conditions and various faults, as is shown in figure 1.1. It is important for fault detection and diagnosis (FDD) not to misinterpret variations in thermodynamic states caused by changes in the driving conditions for faults. If measurements are classified directly, the classification rules have to be complicated to consider the effect of external driving conditions.

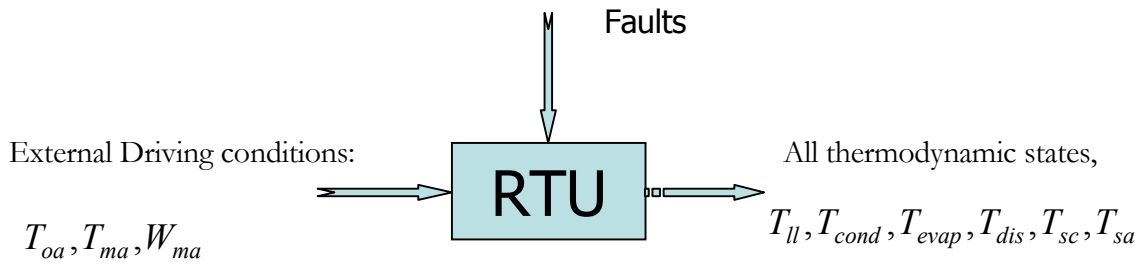


Figure 1.1 Rooftop system

In order to simplify classification and improve overall FDD performance, model-based FDD techniques usually use some type of model to predict expected values (normal behavior) of measured performance indices using measured external driving conditions for the equipment which is being monitored. Often, the difference between expected and actual measurement values (residuals) will always be zero mean when there are no faults. The probability distribution of residuals is a weak function of driving conditions and is strongly dependent on faults. So if residuals are used to detect and diagnose faults, the classifier may not need to consider driving conditions and is simplified considerably.

There are three general types of models: physical, black box and gray box. Physical models, whose parameters and structures have some physical significance, are derived from fundamental physical laws. An accurate physical model is capable of extrapolating performance expectations well in case of limited training data. However, it is difficult and expensive to develop an accurate physical model. Also, a complex physical model involves large collections of nonlinear equations which are difficult to solve. In addition, physical models are not accurate enough for a given system and require detailed data for training.

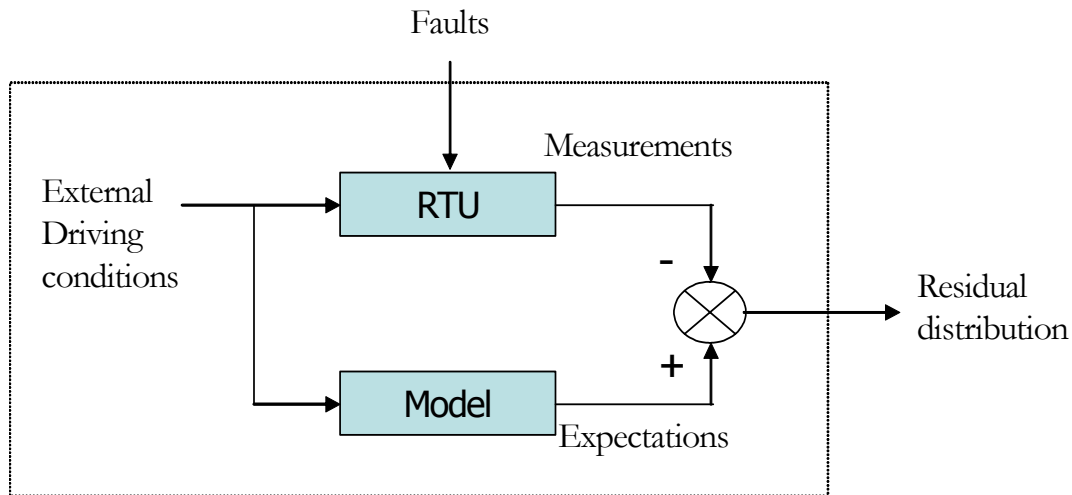


Figure 1.2 Rooftop system with a normal performance model

Gray-box modeling approaches use lumped system parameters and some semi-empirical expressions. Strictly speaking, there are no pure physical models in engineering; most of so-called physical models are gray-box models. Although easier to build and faster to solve than a physical model, a gray-box model may not be practical for commercial HVAC FDD.

Black-box models, which can overcome the shortcomings of physical models, use empirical input/output relationships that are fit to training data. There are many black-box modeling approaches. Different approaches have different characteristics and interpolating abilities. Generally speaking, in the mathematical point of view a black-box model can not be expected to have good extrapolating ability. However, in the physical point of view, most real systems normally would not change dramatically and have major linear components, so black-box models can have some extrapolating abilities near the training data range. What's more, different approaches have different extrapolating abilities and different parameters and structure of the same approach have different interpolating and extrapolating abilities. This report reviews some relevant literature, and then documents comparisons between several modeling approaches, and proposes an improved modeling approach.

Table 1.1 Comparisons of Three Modeling Approaches

	Characteristics	Advantages	Disadvantages
Physical models	Derived from fundamental physical laws; Large collections of nonlinear equations	Model parameters are meaningful; Extrapolates well in case of limited training data	Difficult to develop and solve the model; Need more detailed physical description and data
Black-box models	Input/output relationship to fit the train data by optimizing performance index	Easy to develop and realize; Accurate fits within the training data range; Computational simplicity	Poor extrapolation; Model parameters have no meaning
Gray-box models	Combination of physical and black box model; Use semi-empirical expressions	Easier to develop than physical model and has good interpolating and extrapolating performance	A little difficult and expensive to develop

2. Background work

There are a lot of literature on modeling of vapor compression systems. The following sections contain a review some models that were developed for FDD.

2.1 Physical modeling and gray-box modeling

Rossi and Braun (1995) developed a steady-state physical model, known as ACMODEL, which simulates the operation of vapor compression cycles. The model solves the mass, momentum, and energy balances for each component and performs a charge inventory for the entire system. This model was used to aid in the original development and evaluation of an FDD method. ACMODEL is a modular toolkit. Individual components are modeled as subroutines (e.g., compressor, condenser, evaporator, expansion device) with specified inputs and outputs. A robust numerical equation solver capable of converging to the operating state with a tight tolerance is included. A tuning program adjusts less well known model parameters based on simple measurements at an operating point to provide for more accurate performance predictions at different operating conditions.

The compressor of the ACMODEL is semi-empirical and uses empirical curve fits to manufacturer's performance data for compressor volumetric efficiency (to calculate mass flow rate) and power. The outlet enthalpy is calculated assuming a polytropic compression process with a constant polytropic efficiency.

The condenser and evaporator models use physically based tube-by-tube analyses where each tube is broken into small segments. Mass, momentum, and energy balance are applied to each tube segment, and the heat transfer, pressure drop, and refrigerant mass are calculated for the segment. However, there are some differences between the condenser and evaporator models. The condenser model considers only heat transfer whereas the evaporator model considers both heat transfer and mass transfer. The condenser and evaporator coil models are built from functions which are provided for a finned tube, return bend and manifold. Geometric information about the tubes and fins are entered in an input file.

The throttling valve is modeled as a fixed orifice expansion device which is assumed to have two-phase Fanno flow (one-dimensional, adiabatic, compressible, with friction).

The equations for each of these components as well as a charge inventory must be solved simultaneously to find the steady-state operating point for the air conditioning unit. The

solution procedure involves the non-linear solution of three residual equations in the cycle. The effect of all five of the operating faults which are being studied can be simulated with ACMODEL.

Except for Rossi and Braun, the problem of developing a physical model for a rooftop air conditioning unit for FDD purposes has not been specifically addressed in the literature.

Stylianou and Nikanpour (1996) considered two different models for a reciprocating chiller to use with a model-based FDD technique. For the problem of fault detection, a gray-box model was used. This model, developed from first principles and first introduced by Gordon and Ng (1994), correlated the equipment COP with the condenser and evaporator inlet water temperatures. This performance index is used to decide when the impact of a fault is significant enough to warrant repair. The other model is a black-box model which will be discussed in the next section.

2.2 Black-box modeling

Since black-box models are easy to develop, accurately fit training data, and are computationally simple, they are popular for engineering use. Several kinds of black-box modeling approaches will be discussed here.

2.2.1 Polynomials

Linear regression polynomials are the easiest and most frequently used black-box models. Grimmeli et al. (1995) used steady-state linear models with three input variables to predict a number of output states of a vapor compression chiller. The predicted variables included the temperatures and pressures at the inlet and outlet of each component in the refrigeration cycle, suction superheat, liquid subcooling, oil pressure, temperature, and level, the pressure ratio across the compressor, temperature changes of the water across the evaporator and condenser, filter pressure drop, and compressor power. The three input variables were the chiller water inlet temperature, the cooling water temperature into the condenser, and the number of compressor cylinders in operation. The model form which was used is

$$y_i = \beta_{0,i} + \beta_{1,i}T_{chwi} + \beta_{2,i}T_{cwi} + \beta_{3,i}Z_1 + \beta_{4,i}Z_2 + \beta_{5,i}Z_3 + \beta_{6,i} \log(T_{chwi}) \\ + \beta_{7,i}(T_{chwi})^{-1} + \beta_{8,i} \log(T_{cwi}) + \beta_{9,i}(T_{cwi})^{-1}$$

where the i^{th} output variable y_i is the calculated value, $\beta_{0,i} - \beta_{9,i}$ are the regression coefficients, T_{chwi} is the chiller water inlet temperature, T_{cwi} is the cooling water temperature into the condenser, and Z are variables indicating the number of cylinders in operation. Regression coefficients were determined using a multivariate least-squares method applied to 8000 operating data points which were assumed to be fault-free. The R^2 statistic of the regression indicated that the fit to the data was quite accurate for almost all of the variables which were used in the FDD routine.

To create residuals to use in fault diagnosis, a black box model was used by Stylianou and Nikanpour (1996) to predict values for internal temperatures and pressures. The model uses two input variables, the water inlet temperature into the condenser and evaporator, and a simple linear equation for all of the output variables as given by

$$y_i = \beta_{0,i} + \beta_{1,i}T_{chwi} + \beta_{2,i}T_{cwi}$$

where the i^{th} output y_i is the calculated value, $\beta_0 - \beta_2$ are the regression coefficients, T_{chwi} is the chiller water inlet temperature, and T_{cwi} is the cooling water temperature into the condenser. The parameters of the model were determined using a multivariate least-squares analysis. The results showed an excellent fit to the experimental data, although the data only covered a relatively small range of evaporator inlet water temperatures (50°-59°F) and condenser inlet water temperatures (72°-93° F).

In addition to developing the FDD method considered in his thesis, Rossi (1995) also suggested some models for rooftop air conditioning units for use with his method. The performance of a rooftop air conditioner with fixed flow rates is a function of the condenser and evaporator inlet air temperatures and the moisture content of the evaporator inlet air. The moisture content can be represented using a relative humidity, dew point temperature, or wet bulb temperature. There are two modes of operation for a typical cooling coil, wet and dry. The coil is defined as wet when water is being removed from the air stream in addition to heat. When the coil is wet, the energy transfer to the coil is driven primarily by the difference between the temperature of the evaporating refrigerant and the wet bulb temperature of the air, independent of dry bulb temperature alone. When the coil is dry, the heat transfer is driven by the difference between the coil and the dry bulb temperature of the air,

independent of the moisture content in the air. Thus, if the operation between these two regimes can be separated, the problem of developing a model for the rooftop unit can be expressed as a function of two independent variables instead of three. To separate wet coil operation from dry coil operation, Rossi (1995) suggested using the following form for the models

$$f(T_{amb}, T_{ra}, T_{wb}) = f_{wet}(T_{dpt} - T_{evap}) * g_{wet}(T_{amb}, T_{wb}) \\ + (1 - f_{wet}(T_{dpt} - T_{evap})) * g_{dry}(T_{amb}, T_{ra})$$

where $f(T_{amb}, T_{ra}, T_{wb})$ is any state in the vapor compression cycle dependent on all three inputs, T_{dpt} is the dew point temperature of the evaporator inlet air, $f_{wet}(T_{dpt} - T_{evap})$ is a function which returns a value of 0 when the coil is dry and 1 when the coil is wet, and $g_{wet}(T_{amb}, T_{wb})$ and $g_{dry}(T_{amb}, T_{ra})$ are models for individual properties for the wet and dry operating regimes. Using data generated by the simulation model, Rossi found that the function $f_{wet}(T_{dpt} - T_{evap})$ can be approximated as a step function with a threshold value of 2.7° C. Thus, when T_{dpt} is greater than T_{evap} by more than 2.7° C, the coil is considered to be wet, and when this difference is less than 2.7° C the coil is considered to be dry.

Using this form, Rossi (1995) developed models for the total capacity of the rooftop unit as a function of the driving conditions. In the dry coil region, he found that the capacity could be approximated by a linear function of the two independent variables. In the wet region, a much more complex non-linear function was developed to fit the shape of the data which appeared to saturate at high wet bulb temperatures. Although Rossi did suggest that these model forms could be used to model the temperatures required by his FDD method, he did not attempt to fit any of the temperatures.

Breuker and Braun (1998) did extensive research on polynomial modeling for a rooftop unit with a fixed orifice expansion device. They examined the form of the experimental data over a range of driving conditions and compared different order polynomial models. The polynomial orders necessary to produce a satisfactory fit to both simulation and experimental data are given in table 2.1 shows. Three-inputs and two-inputs model were compared also. It was concluded that a polynomial model with three independent variables (three-inputs) provides the most accurate predictions of the test data, given a large set of training data.

Table 2.1 Best model orders for 3D polynomial fits for experimental data

Variable	Best Model to Use	RMS Error (F)	Maximum Error (F)
T_{evap}	1 st order	0.49	0.99
T_{sh}	3 rd order with cross terms	1.39	3.03
T_{hg}	3 rd order with cross terms	1.00	3.24
T_{cond}	1 st order	0.31	0.61
T_{sc}	2 nd order with cross terms	0.46	1.39
ΔT_{ca}	1 st order	0.18	0.48
ΔT_{ea}	2 nd order with cross terms	0.23	0.56

2.2.2 General Regression Neural Network

Donald [1991] described a memory-based network, general regression neural network (GRNN), which is a one-pass learning algorithm with a highly parallel structure. This approach eliminates the necessity of assuming a specific functional form of the model. Rather, it allows the appropriate form to be expressed as a probability density function (pdf) which is empirically determined from the observed data using nonparametric estimators. Thus, this approach is not limited to any particular form and requires no prior knowledge of the appropriate form. Secondly, the resulting regression equation can be implemented in a parallel, neural-network-like structure. Since the parameters of the structure are determined directly from examples rather than iteratively, the structure “learns” and can begin to generalize immediately. Considering that the idea and algorithm of GRNN is adopted in our FDD modeling, the derivation of GRNN is repeated and in order to better understand the original derivation some omitted intermediate derivation is added.

Assume that $f(X, y)$ represents the known joint continuous probability density function of a vector random variable, X , and a scalar random variable, y . The conditional mean of y given X (also called the regression of y on X) is given by

$$E[y | X] = \frac{\int_{-\infty}^{\infty} y f(X, y) dy}{\int_{-\infty}^{\infty} f(X, y) dy} \quad (1)$$

When the density $f(X, y)$ is not known, it should usually be estimated from a sample of observations of X and y . Here the consistent estimators proposed by Parzen (1962) are adopted. These estimators are a good choice for estimating the probability density

function, $f(X, y)$, if it can be assumed that the underlying density is continuous and that the first partial derivatives of the function evaluated at any X are small. The probability estimator $\hat{f}(X, y)$ is based upon sample values X^i and y^i of the random variables X and y , where n is the number of sample observations, p is the dimension of the vector variable X and σ is sample probability width:

$$\hat{f}(X, y) = \frac{1}{(2\pi)^{(p+1)/2} \sigma^{(p+1)}} \frac{1}{n} \sum_{i=1}^n \exp\left[-\frac{(X - X^i)^T (X - X^i) + (y - y^i)^2}{2\sigma^2}\right] \quad (2)$$

A physical interpretation of the probability estimate $\hat{f}(X, y)$ is that it assigns sample probability of width σ for each sample X^i and y^i , and the probability estimate is the sum of those sample probabilities. Substituting the joint probability estimate $\hat{f}(X, y)$ in equation (2) into the conditional mean, equation (1), gives the desired conditional mean of y given X . In particular, combining equations (1) and (2) and interchanging the order of integration and summation yields the desired conditional mean, designated $\hat{y}(X)$:

$$\hat{y}(X) = \frac{\sum_{i=1}^n \exp\left[-\frac{(X - X^i)^T (X - X^i)}{2\sigma^2}\right] \int_{-\infty}^{\infty} y \exp\left[-\frac{(y - y^i)^2}{2\sigma^2}\right] dy}{\sum_{i=1}^n \exp\left[-\frac{(X - X^i)^T (X - X^i)}{2\sigma^2}\right] \int_{-\infty}^{\infty} \exp\left[-\frac{(y - y^i)^2}{2\sigma^2}\right] dy} \quad (3)$$

Perform the following integration:

$$\begin{aligned} & \int_{-\infty}^{\infty} y \exp\left[-\frac{(y - y^i)^2}{2\sigma^2}\right] dy \\ &= \int_{-\infty}^{\infty} (y - y^i) \exp\left[-\frac{(y - y^i)^2}{2\sigma^2}\right] d(y - y^i) + \int_{-\infty}^{\infty} y^i \exp\left[-\frac{(y - y^i)^2}{2\sigma^2}\right] dy \\ &= -\sigma^2 \int_{-\infty}^{\infty} \exp\left[-\frac{(y - y^i)^2}{2\sigma^2}\right] d\left[-\frac{(y - y^i)^2}{2\sigma^2}\right] + y^i \int_{-\infty}^{\infty} \exp\left[-\frac{(y - y^i)^2}{2\sigma^2}\right] dy \\ &= -\sigma^2 \int_{-\infty}^{\infty} d \exp\left[-\frac{(y - y^i)^2}{2\sigma^2}\right] + y^i \int_{-\infty}^{\infty} \exp\left[-\frac{(y - y^i)^2}{2\sigma^2}\right] dy \\ &= 0 + y^i \int_{-\infty}^{\infty} \exp\left[-\frac{(y - y^i)^2}{2\sigma^2}\right] dy \\ &= y^i \int_{-\infty}^{\infty} \exp\left[-\frac{(y - y^i)^2}{2\sigma^2}\right] dy \end{aligned} \quad (4)$$

Define the scalar function D_i^2 ,

$$D_i^2 = (X - X^i)^T (X - X^i). \quad (5)$$

Substituting equations (4) and (5) into equation (3), yields the following:

$$\hat{y}(X) = \frac{\sum_{i=1}^n y^i \exp\left[-\frac{(X - X^i)^T (X - X^i)}{2\sigma^2}\right]}{\sum_{i=1}^n \exp\left[-\frac{(X - X^i)^T (X - X^i)}{2\sigma^2}\right]} = \frac{\sum_{i=1}^n y^i \exp\left(-\frac{D_i^2}{2\sigma^2}\right)}{\sum_{i=1}^n \exp\left(-\frac{D_i^2}{2\sigma^2}\right)} \quad (6)$$

Because the particular estimator, equation (3), is readily decomposed into X and y factors, the integrations were accomplished analytically. The resulting regression, equation (6), which involves summations over the observations, is directly applicable to problems involving numerical data. Parzen and Cacoullos (1966) have shown that density estimators of the form of equation (2) used in estimating equation (1) by equation (6) are consistent estimators (asymptotically converging to the underlying probability density function $f(X, y)$ at all points (X, y) at which the density function is continuous. Provided that $\sigma = \sigma(n)$ is chosen as a decreasing function of n such that

$$\lim_{n \rightarrow \infty} \sigma(n) = 0$$

and

$$\lim_{n \rightarrow \infty} n\sigma^p(n) = \infty \quad (7)$$

The estimate $\hat{y}(X)$ can be visualized as a weighted average of all of the observed values, y^i , where each observed value is weighted exponentially according to its Euclidean distance from X . When the smoothing parameter σ is made large, the estimated density is forced to be smooth and in the limit becomes a multivariate Gaussian with covariance $\sigma^2 I$. On the other hand, a smaller value of σ allows the estimated density to assume non-Gaussian shapes, but with the hazard that wild points may have too great an effect on the estimate. As σ becomes very large, $\hat{y}(X)$ assumes the value of the sample mean of the y^i and as σ goes to 0, $\hat{y}(X)$ assumes the value of the y^i associate with the observation closest to X . For intermediate values of σ , all values of y^i are taken into account, but those corresponding to points closer to X are given heavier weight.

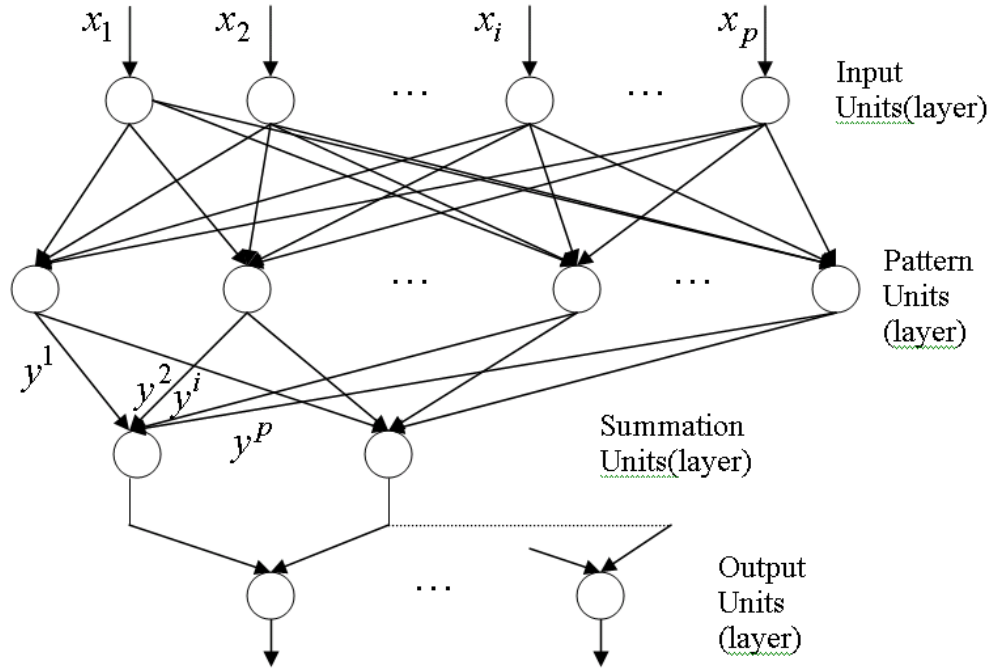


Figure 2.1 Neural-Network Implementation of GRNN

The above GRNN algorithm can be implemented in an artificial neural-network structure (shown as figure 2.1), which usually defined as a network composed of a large number of simple processors (neurons) that are massively interconnected, operate in parallel and learn from experience (training data). The input units are merely distribution units, which provide all of the (scaled) measurement variables X to all of the neurons on the second layer, the pattern units. The pattern unit is dedicated to on exemplar or one cluster center. The summation units perform a dot product between a weight vector and a vector composed of the signals from the pattern units. The output unit merely performs the operation of division to get the desired estimate of $\hat{y}(X)$.

When estimation of a vector Y is desired, each component is estimated using one extra summation unit, which uses as its multipliers sums of samples of the component of Y associated with each cluster center. There may be many pattern units (one for each exemplar or cluster center); however, the addition of one element in the output vector requires only one summation neuron and one output neuron.

2.2.3 Back-propagation neural network

Neural networks are composed of simple elements operating in parallel. These elements are inspired by biological nervous systems. As in nature, the network function is determined largely by the connections between elements. A neural network can be trained to perform a particular function by adjusting the values of the connections between elements. Commonly neural networks are adjusted, or trained, so that a particular input leads to a specific target output.

Back-propagation (BP) neural networks are used most often and were created by generalizing the Widrow-Hoff learning rule to multiple-layer networks and nonlinear differentiable transfer functions. Input vectors and the corresponding output vectors are used to train a network until it can approximate a function or associate input vectors with specific output vectors. Networks with biases, a sigmoid layer, and a linear output layer are capable of approximating any function with a finite number of discontinuities. Standard backpropagation is a gradient descent algorithm, as is the Widrow-Hoff learning rule. The term backpropagation refers to the manner in which the gradient is computed for nonlinear multilayer networks. Properly trained backpropagation networks tend to give reasonable answers when presented with inputs that they have never seen. Typically, a new input will lead to an output similar to the correct output for input vectors used in training that are similar to the new input being presented. This generalization property makes it possible to train a network on a representative set of input/output pairs.

The oldest algorithm is a gradient descent algorithm, for which the weights and biases are moved in the direction of the negative gradient of the performance function. However, this algorithm is often too slow for practical problems. So many improved algorithms such as variable learning rate, resilient backpropagation, conjugate gradient and reduced memory Levenberg-marquardt, have been proposed to increase training speed and reduce the memory requirements. Another problem that occurs during neural network training is called overfitting. The error on the training set is driven to a very small value, but when new data is presented to the network the error is large. The network has memorized the training examples, but it has not learned to generalize to new situations.

Since BP artificial neural networks can be used to build classifiers that directly classify input vectors, they are often used to build both the model and classifier as a whole for FDD use.

In a paper by Li, X., H. Hvaezi-Nejad (1996), an artificial neural network (ANN) prototype for fault detection and diagnosis (FDD) in complex heating systems was presented. The

prototype was developed by using the simulation data of a reference heating system. The prototype was then applied to four heating systems not used during the training phase. Six categories of fault modes and a reference normal mode were modeled. The paper demonstrated the feasibility of using ANNs for detecting and diagnosing faults in heating systems, provided that training data are available which are representative of the behavior of the system with and without faults. Although the ANN prototype was trained using only one simulated heating system, it showed good capacity for generalization. Two proposed structures of network were trained, tested and compared. In their study, a single artificial neural network performed better than multiple artificial neural networks. This is probably because a structure composed of a single network learns global knowledge easier than one composed of two multiple networks. So far, this FDD prototype has been studied only using simulation data. However, this paper gave no information about the severity of the faults detected.

Lee, House and Shin (1997) described the architecture for a two-stage artificial neural network for fault diagnosis in a simulated air handling unit (AHU), and the use of regression equations for sensor recovery of failed temperature sensors. To simplify the ANN, the AHU was divided into several subsystems. The stage-one ANN was trained to classify the subsystems in which faults occur, and the stage-two ANN was trained to diagnose the cause of faults at the subsystem level. The trained ANNs were applied to simulation data and shown to be able to identify eleven faults. A regression equation was used to recover the estimate for the supply air temperature when the supply air temperature sensor yielded erroneous measurements. The estimates of the sensor measurement could be used for control purposes during a fault.

2.2.4 Radial basis function

Another black-box modeling technique uses radial basis functions (RBF) that work directly from data as described by Mees [1992]. The main idea is as follows:

Suppose that by experiment, values y_1, \dots, y_m of y have been found at x_1, \dots, x_m . The radial basis approximation $f(x)$ fitting the experimental data is defined by

$$f(x) = \sum_{i=1}^m \lambda_i \phi(|x - x_i|) \quad (8)$$

where the radial basis function ϕ can be almost any scalar function of one variable we care to choose, and the λ_i 's are computed so that all the known values fit exactly. That is,

$$y_i = \sum_{j=1}^m \lambda_j \phi(|x_i - x_j|) \quad (9)$$

Writing the matrix Φ with elements

$$\Phi_{ij} = \phi(|x_i - x_j|) \quad (10)$$

we can rewrite equation (9) as m linear equations in m unknowns:

$$\Phi \lambda = y \quad (11)$$

where y and λ are the vectors with elements y_i and λ_i , $i = 1, \dots, m$. Solving equation (11), therefore, determines f completely.

Computationally, the significant part of the problem is that of solving the linear equations (11) for λ . The size of the matrix Φ is the number m of data points and so the computational effort, which is of order m^3 , may be large. Fortunately, this calculation is only performed once for a particular set of data points and ϕ . The work involved to interpolate for any given point is then considerably less, of order m .

As well as the difficulty of long computation time, there is a risk that as m grows, Φ will become ill-conditioned. Fortunately, Dyn and Levin (1983) found some well-conditioned Φ results from choices of ϕ .

3. Comparison of black-box modeling approaches using laboratory data

3.1 Laboratory experimental data

Breuker (1997) gathered data under controlled conditions in a laboratory on a test unit at a number of controlled operating conditions and used the data to test the ability of several model types to produce accurate estimates of unit performance. This test unit is a three ton packaged rooftop unit (Carrier Model 48DJE004610) which has a constant speed and hermetically-sealed reciprocating compressor (Copeland Model CRH3-0275-TFD) and uses fixed-orifice type expansion devices for refrigerant flow control. The grid of indoor conditions used in the testing is shown in figure 3.1. The larger set of data, labeled "Training Data" in the figure, was gathered at indoor dry bulb temperatures of 70, 73, 76, 79, and 82 F, indoor wet bulb temperatures of 55, 58, 61, 64, and 67 F, and ambient temperatures (not shown in figure) of 60, 70, 80, 90, and 100 F. The smaller set of data, or "Test Data", was gathered at indoor dry bulb temperatures of 71.5, 74.5, 77.5, and 80.5 F, indoor wet bulb temperatures of 56.5, 59.5, 62.5, and 65.5 F, and ambient temperatures of 65, 75, 85, and 95 F. As the figure shows, however, not all dry bulb conditions were simulated at all wet bulb conditions. A total of 40 distinct combinations were simulated in the "Test Data" and 94 combinations were simulated in the "Training Data" set. The conditions were selected because they completely cover the normal comfort region defined by ASHRAE (1993). The reason for gathering the data in two distinct sets was to allow for training and testing on separate sets of data. Training on the large set and testing on the small set of data tests the ability of the model to interpolate accurately. Training on the small set will test the ability of the model to extrapolate beyond the training data.

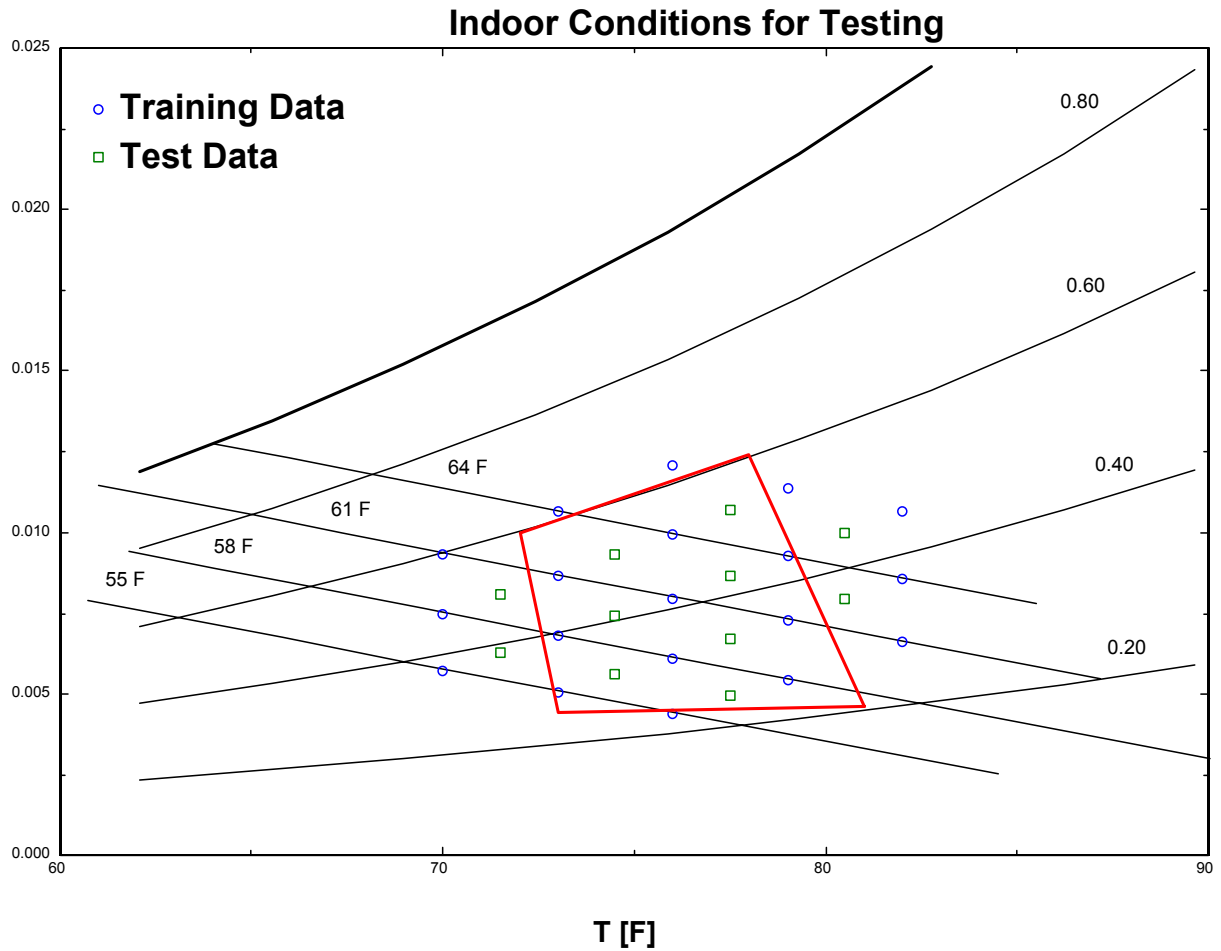


Figure 3.1 Indoor conditions simulated for training and testing steady-state models

The training data were gathered by running the rooftop unit with no faults. Data was gathered over the course of three weeks of testing. To ensure that there were no faults developing in the test unit over this time period and to test the experimental noise which is present in the operation of the test unit, a test condition at $T_{\text{amb}} = 85 \text{ F}$, $T_{\text{ra}} = 76 \text{ F}$, $\Phi_{\text{ra}} = 42\%$ was retested every few days. The results of this repeatability test for all of the measurements used by the FDD technique are shown in table 3.1. The most noisy measurements, as expected, are the suction superheat and hot gas temperatures. This level of experimental noise is already considerably above the measurement error levels which were used in the steady-state analysis of the FDD technique performed by Rossi. Figure 2.2 shows the level of suction superheat during the repeatability test. The fact that the graph is not increasing during the test indicates that the level of charge in the system is not decreasing, since suction superheat is particularly dependent on the charge level in the system. One cannot expect to develop a model

which is more accurate than the experimental noise of the measurements which are used in learning the model.

Table 3.1 Repeatability analysis during steady-state model testing

Property of Data (deg. F)	T_{evap}	T_{sh}	T_{hg}	T_{cond}	T_{sc}	ΔT_{ca}	ΔT_{ea}
Mean	43.76	8.42	195.11	108.69	7.05	11.72	19.14
Std. Dev.	0.39	1.73	1.25	0.40	0.25	0.09	0.17
Spread	1.21	4.80	4.04	1.28	0.60	0.26	0.64

Suction Superheat vs. Time During Repeatability Test

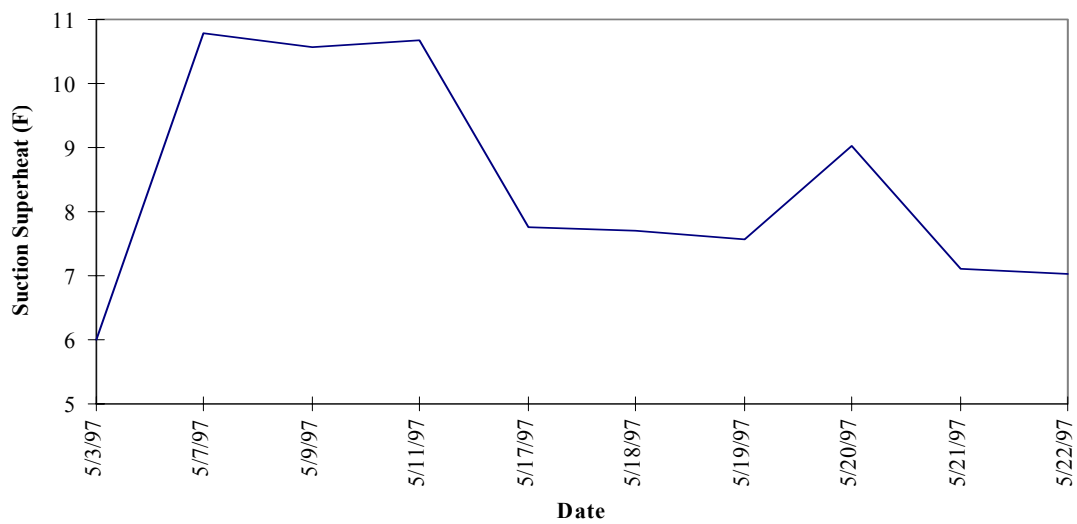


Figure 3.2 Suction superheat during repeatability test

3.2 Comparisons

Four black-box modeling approaches: polynomials, GRNN, RBF and BP neural networks were investigated using the laboratory data. Seven characteristic parameters (evaporating temperature T_{evap} , condensing temperature T_{cond} , compressor discharge temperature T_{dis} , suction line superheat T_{sh} , liquid line subcooling T_{sc} , condenser air temperature difference ΔT_{ca} , evaporator air temperature difference ΔT_{ea}) for FDD were modeled. Since the gathered data are very limited (94 points for large set data and 40 points for small set data), when testing interpolation, the large data set were used to train models and both the small and large data set were used to test models. When testing extrapolation, the core of the total data (T_{ra} from 73 to 79 F, T_{amb} from 70 to 90 F, T_{wb} from 58 to 64 F) were used to train models and the remaining data were used to test models.

To get a visual feeling of the modeling performance, figure 3.3 and figure 3.4 show the training performance and testing performance for evaporating temperature. Table 3.2 and figure 3.5 show the RMS error for the polynomial models. Polynomial models have good interpolating ability when the order is high enough (e.g. third order) and the interpolating performance increases as the order increases. However, low-order polynomial models have good extrapolating performance, while the extrapolating performance will be very poor when the polynomial order is too high (e.g. the third order). So there exists a conflict between interpolating and extrapolating performance.

Table 3.2 and figure 3.6 show that the GRNN models have very good interpolating ability but poor extrapolating performance. The spread has a significant influence on the interpolating performance but little influence on extrapolating performance. The smaller the spread, the better the interpolating performance. Another advantage of GRNN is that training is very fast. The disadvantage of GRNN is that large memory is required to record the nodes when the number of nodes is large.

From table 3.3, it can be seen that the BP neural network has very good interpolating ability when the number of neurons is appropriate, but extrapolating performance is poor. Also the performance is a little random, because the initial condition is random. The weakness of the BP neural network is that it takes a little long time to train.

Similar to GRNN, RBF has very good interpolating performance but poor extrapolating performance, which is shown in table 3.2. Table 3.4 summarizes the comparison among polynomial , GRNN, BP and RBF modeling approaches.

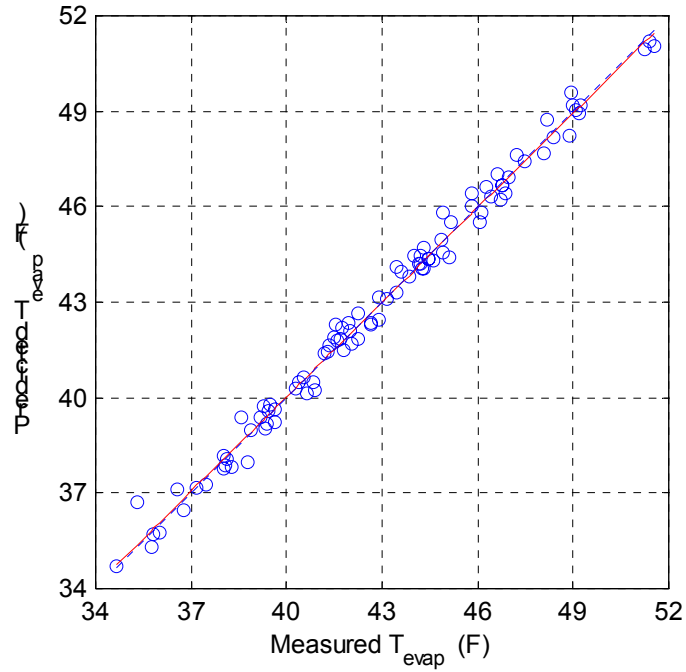


Figure 3.3 Training performance of third order polynomials for evaporating temperature

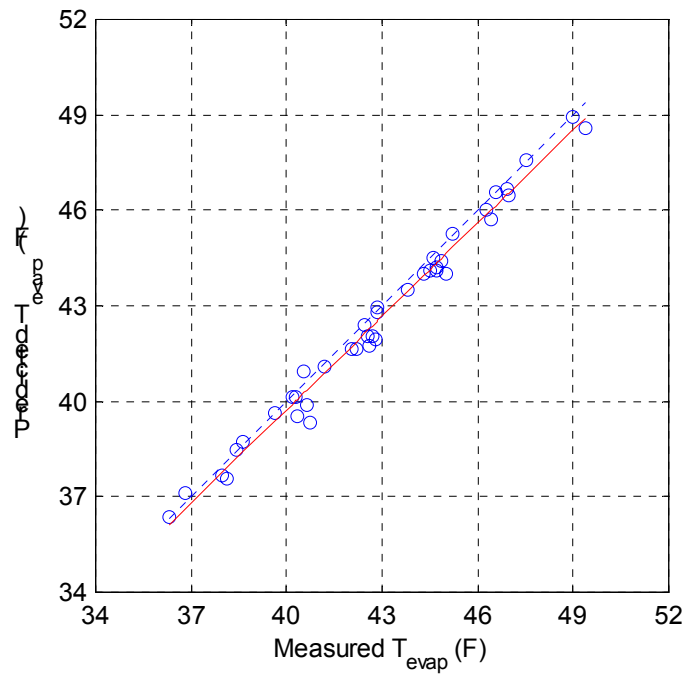


Figure 3.4 Testing interpolating performance of third-order polynomials for evaporating temperature

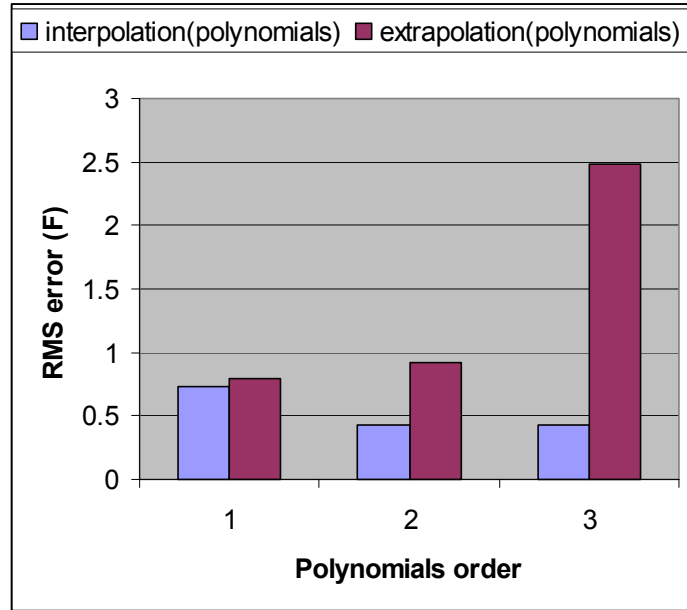


Figure 3.5 Polynomial regression performance (T_{evap} model)

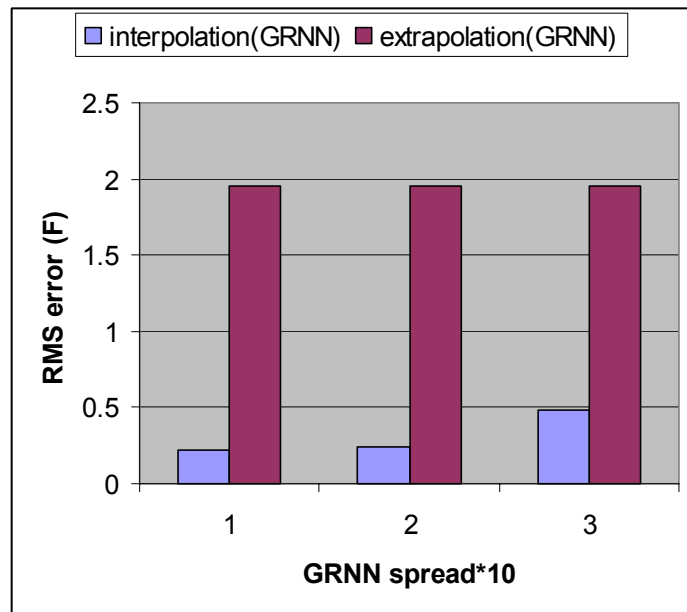


Figure 3.6 GRNN performance (T_{evap} model)

Table 3.2 RMS error (Polynomial,GRNN and RBF fitting for laboratory data)

RMS error (F)			Polynomial Order			GRNN Spread			RBF
			1	2	3	0.1	0.2	0.3	
T_{evap}	Interpolation	training	0.8002	0.4006	0.3944	0	0.1148	0.5034	0
		testing	0.7275	0.434	0.4301	0.2188	0.2393	0.4827	0.4717
	Extrapolation	training	0.6895	0.303	0.2734	0	0.0003	0.0541	0
		testing	0.7966	0.919	2.4865	1.9513	1.9518	1.9538	1.4375
T_{cond}	Interpolation	training	0.521	0.336	0.3252	0	0.269	1.2985	0
		testing	0.4877	0.3506	0.3449	0.2033	0.3047	1.1282	0.4366
	Extrapolation	training	0.5237	0.3136	0.2873	0	0.0006	0.1316	0
		testing	0.5186	0.6976	2.7911	6.5361	6.5393	6.5539	4.6993
T_{dis}	Interpolation	training	2.3693	1.3856	1.355	0	0.3035	1.3126	0
		testing	2.2856	1.3583	1.3092	0.5659	0.6217	1.2627	0.8922
	Extrapolation	training	2.0129	0.9145	0.9005	0	0.0005	0.113	0
		testing	2.6706	3.4217	5.2348	5.0263	5.0278	5.0333	3.7532
T_{sc}	Interpolation	training	0.8489	0.3926	0.384	0	0.0872	0.386	0
		testing	0.8237	0.4223	0.4238	0.2295	0.2409	0.4	0.4442
	Extrapolation	training	0.3856	0.2295	0.1653	0	0.0002	0.0375	0
		testing	1.2149	0.9543	3.8236	1.7216	1.7218	1.7233	1.4357
T_{sh}	Interpolation	training	2.4055	1.7555	1.7013	0	0.3005	1.1706	0
		testing	2.3956	1.7524	1.6646	0.7254	0.7699	1.2635	1.1423
	Extrapolation	training	2.1532	1.0286	1.0239	0	0.0007	0.1398	0
		testing	3.2821	4.7899	5.952	3.0436	3.0458	3.0514	2.1382
ΔT_{ca}	Interpolation	training	0.2204	0.1402	0.1353	0	0.0292	0.1165	0
		testing	0.2113	0.1525	0.1532	0.0828	0.0865	0.1306	0.1532
	Extrapolation	training	0.1516	0.1055	0.095	0	0.0001	0.0119	0
		testing	0.2406	0.334	0.9369	0.339	0.3389	0.3385	0.2981
ΔT_{ea}	Interpolation	training	0.8448	0.2197	0.2172	0	0.1193	0.5324	0
		testing	0.8066	0.2269	0.2278	0.1375	0.1711	0.4831	0.1666
	Extrapolation	training	0.6322	0.1067	0.1022	0	0.0002	0.0413	0
		testing	0.9553	0.858	1.1385	1.6797	1.6804	1.6819	1.1131

Table 3.3 RMS(BP fitting for laboratory data)

RMS error (F)			Number of Neurons(First trial)			Number of Neurons (Second trial)		
			6	12	18	6	12	18
T_{evap}	Interpolation	training	0.3514	0.2268	0.2283	0.2357	0.227	0.2043
		testing	0.4707	0.495	0.4956	0.4918	0.4933	0.5218
	Extrapolation	training	0.1925	0.6149	1.2108	0.1833	0.6151	0.615
		testing	1.4141	1.1559	2.1499	1.467	1.1528	1.1471
T_{cond}	Interpolation	training	0.3393	0.2643	0.2544	0.3537	0.2668	0.2621
		testing	0.3893	0.4555	0.4591	0.3483	0.4515	0.4549
	Extrapolation	training	0.2336	0.2285	0.2289	0.2336	0.2285	2.1229
		testing	2.3021	1.95	1.9041	2.302	1.9619	4.5249
T_{dis}	Interpolation	training	0.6026	0.5502	0.8923	0.6043	0.6319	0.7424
		testing	0.9934	0.9984	1.0172	0.9935	0.934	0.9473
	Extrapolation	training	0.4763	0.7584	0.4777	0.478	0.5168	1.9844
		testing	3.4367	3.5549	3.2618	3.4056	3.0524	3.0157
T_{sc}	Interpolation	training	0.3248	0.325	0.325	0.3543	0.3543	0.3542
		testing	0.4362	0.4363	0.4363	0.4646	0.4644	0.4643
	Extrapolation	training	0.1992	0.1992	0.2503	0.1992	0.1992	0.1992
		testing	1.2422	1.2416	0.9815	1.2423	1.2418	1.2414
T_{sh}	Interpolation	training	0.9975	1.0046	1.0024	0.9984	0.7823	1.0118
		testing	1.0464	1.0519	1.0422	1.045	1.0605	1.0531
	Extrapolation	training	0.7233	1.0792	0.7257	0.7248	0.8625	0.7276
		testing	2.1281	2.9464	2.1096	2.1216	2.0301	2.1055
ΔT_{ca}	Interpolation	training	0.0744	0.07	0.0768	0.0829	0.074	0.0716
		testing	0.1426	0.1408	0.1377	0.1412	0.1406	0.1459
	Extrapolation	training	0.0676	0.2028	0.1888	0.0676	0.2276	0.1767
		testing	0.2655	0.3352	0.3071	0.2656	0.3842	0.2809
ΔT_{ea}	Interpolation	training	0.1413	0.1389	0.1372	0.141	0.1375	0.1424
		testing	0.1867	0.1855	0.1824	0.1905	0.1831	0.1974
	Extrapolation	training	0.0635	0.062	0.0616	0.0635	0.063	0.1925
		testing	0.8058	0.7682	0.7589	0.8058	0.7922	0.4927

Table 3.4 Contrast of Black-box modeling approaches

	Characteristics	Advantages	Disadvantages
Polynomials	Assume polynomial functional form of the model	Easy to build Low-order model has reasonable extrapolating performance	Conflict between interpolation and extrapolation
GRNN	Memory-based network One-pass learning algorithm Parallel structure Free from the necessity of assuming a specific functional form of the model;	Very fast training Very good interpolating performance No conflict between interpolation and extrapolation Parallel ANN-like structure, not iterative, able to operate in parallel Takes noise and disturbances into account Easy to be adaptive Every additional output needs only two additional units	Need to cluster the data to reduce nodes and memory when data are large Poor extrapolating performance
Back-Propagation	Weights and biases are moved in the direction of minimizing the network error	Very good interpolating performance;	Need long time to train Poor extrapolating performance
Radial basis interpolation	Use radial basis function as basis function to interpolate	Very good interpolating performance	Poor extrapolating performance;

Strictly speaking, most real systems are nonlinear and can be expanded by Taylor series. Wide use of the first order approximation of Taylor series in engineering shows that most real systems have a low-order dominant component, so low-order polynomials which capture the system performance will have reasonable extrapolating performance far outside their training data range while high-order polynomials will extrapolate very poorly. However, the interpolating performance is normally proportional to the polynomial order.

So the interpolating performance of polynomials conflicts with their extrapolating performance.

Other black box modeling approaches such as GRNN, RBF and BP ANN can have very good interpolating performance and but can not be expected to extrapolate very well far outside the training data range.

3.3 Polynomial plus GRNN model

Low-order polynomials have good extrapolating ability but poor interpolating ability, whereas, GRNN, BP ANN and RBF have very good interpolating ability, so the combination of polynomials with one of GRNN, BP or RBF modeling approaches could have both good interpolating ability and good extrapolating ability. The result can be seen from the table 3.5.

GRNN was selected in ombination with polynomials since GRNN is easy to adapt. Nodes can be added to or deleted from the network to improve the accuracy.

First, a low-order polynomial model is regressed with the training data and then the residuals between the polynomial output and the training data are fit with a GRNN as shown in figure 3.7. After training, the model can be used to generalize as shown in figure 3.8.

The order of the low-order polynomial model depends on the characteristic of the system modeled. Different systems and different variables of the same system have a different “dominant order”. Usually the “dominant order” is not greater than two. Before modeling, the “dominant order” of the system is not known so the “dominant order” is determined by evaluating the extrapolating performance. Table 3.5 shows that first-order for T_{evap} , T_{cond} , T_{dis} and T_{sh} and second-order for T_{sc} , ΔT_{ca} and ΔT_{ea} work well and are best for polynomial models. The purpose of the low-order polynomial model is to optimize the extrapolating performance, whereas the GRNN compensates and improves the interpolating performance, which is sacrificed by the choice of a low-order polynomial model. The GRNN may improve also the extrapolating performance somewhat (figure 3.9). The interpolating and extrapolating performance of the various approaches are summarized in table 3.6.

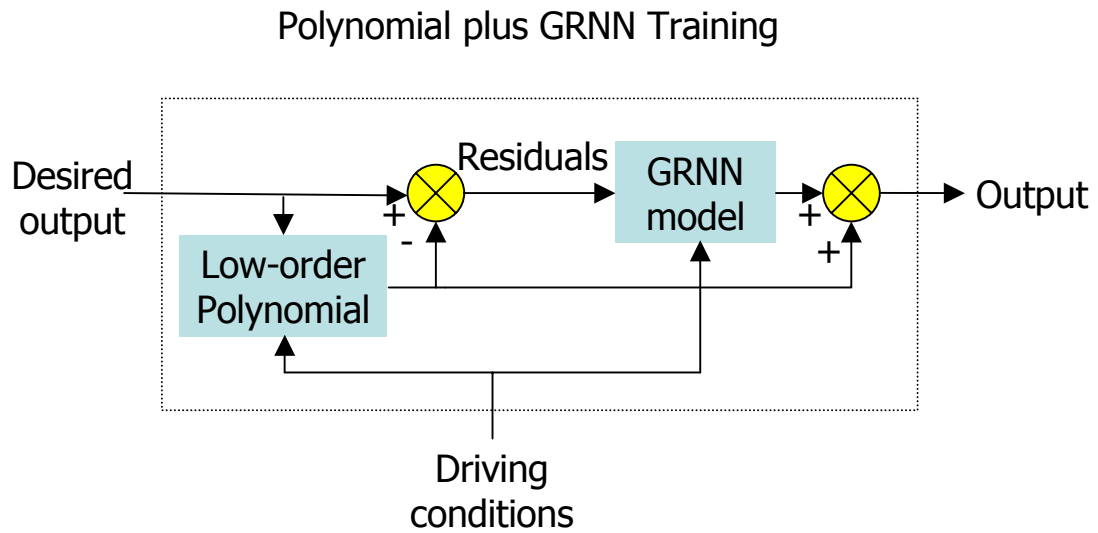


Figure 3.7 Polynomial plus GRNN training block diagrams

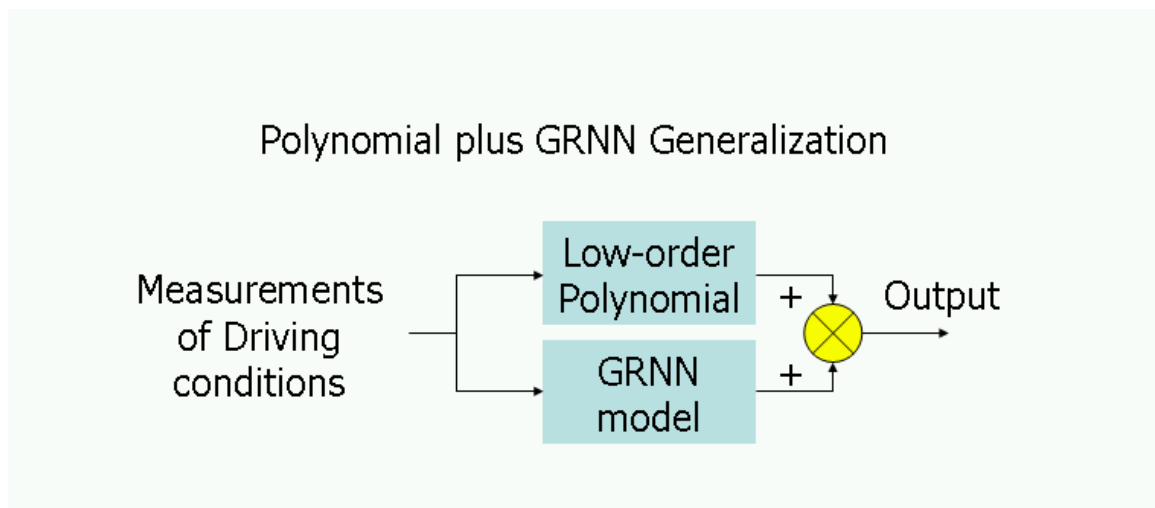


Figure 3.8 Polynomial plus GRNN generalization block diagrams

Table 3.5 RMS(Polynomial plus GRNN, BP and RBF fitting for laboratory data)

RMS error (F)			Polynomial+GRNN			Polynomial+BP		Polynomial+RBF	
			1	2	3	1	2	1	2
T_{evap}	Interpolation	training	0	0	0	0.8002	0.6931	0	0
		testing	0.2188	0.2233	0.2242	0.5152	0.4719	0.4858	0.4826
	Extrapolation	training	0	0	0	0.6895	0.579	0	0
		testing	0.8556	1.0658	2.532	0.7966	1.3864	0.6526	1.0958
T_{cond}	Interpolation	training	0	0	0	0.521	0.4269	0	0
		testing	0.2033	0.2059	0.2089	0.3974	0.3734	0.4241	0.4205
	Extrapolation	training	0	0	0	0.5237	0.4216	0	0
		testing	0.5789	1.0234	2.9342	0.5186	1.2049	0.5271	1.0129
T_{dis}	Interpolation	training	0	0	0	2.3693	2.2698	0	0
		testing	0.5659	0.582	0.5706	2.0733	2.0486	0.9199	0.941
	Extrapolation	training	0	0	0	2.0129	1.919	0	0
		testing	2.3344	2.341	4.6164	2.6706	3.3006	2.112	2.3815
T_{sc}	Interpolation	training	0	0	0	0.8489	0.6177	0	0
		testing	0.2295	0.2404	0.2447	0.7606	0.5903	0.4427	0.4519
	Extrapolation	training	0	0	0	0.3856	0.3443	0	0
		testing	1.1113	0.8034	3.7622	1.2149	0.8528	0.9775	0.83
T_{sh}	Interpolation	training	0	0	0	2.4055	2.2945	0	0
		testing	0.7254	0.7464	0.7331	2.3721	2.3807	1.1347	1.1524
	Extrapolation	training	0	0	0	2.1532	2.0576	0	0
		testing	3.0882	3.218	4.7116	3.2821	3.7127	2.7979	3.0393
ΔT_{ca}	Interpolation	training	0	0	0	0.2204	0.1846	0	0
		testing	0.0828	0.0823	0.0858	0.188	0.1647	0.1561	0.1574
	Extrapolation	training	0	0	0	0.1516	0.1463	0	0
		testing	0.2631	0.2418	0.8876	0.2406	0.2119	0.2423	0.2228
ΔT_{ea}	Interpolation	training	0	0	0	0.8448	0.6804	0	0
		testing	0.1375	0.1244	0.127	0.7076	0.5133	0.1925	0.2049
	Extrapolation	training	0	0	0	0.6322	0.5634	0	0
		testing	0.9729	0.545	0.9109	0.9553	0.9672	0.6272	0.6423

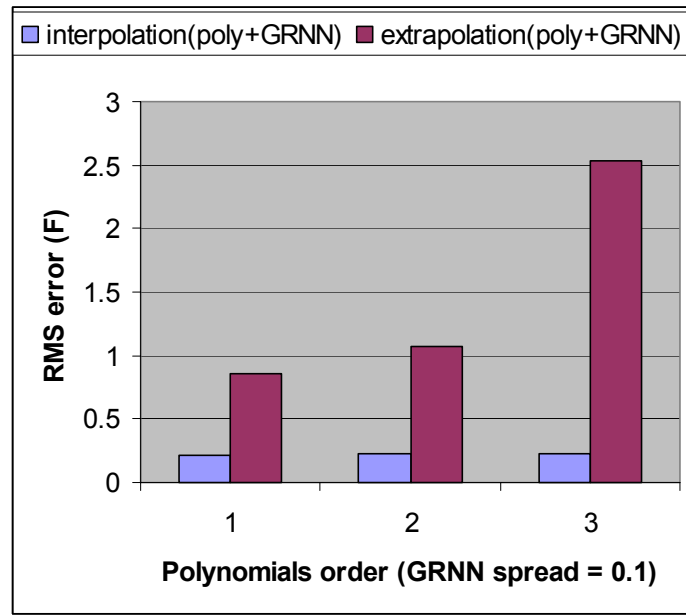


Figure 3.9 Polynomial plus GRNN modeling performance (Tevap Model)

Table 3.6 interpolating and extrapolating performance

Performance Method	fitting	interpolation	extrapolation
Polynomials	+++ ++++ +++++	+++ ++++ +++++	+++ ++ +
BP	+++++	+++++	++
BP+Polynomials	+++++	+++++	+++(+)
GRNN	+++++	+++++	++
GRNN+Polynomials	+++++	+++++	+++(+)
BRF	+++++	+++++	++
BRF+Polynomials	+++++	+++++	+++(+)

4. Modeling field site data

Polynomial plus GRNN models had good performance when tested with laboratory data. However, some factors, which will affect the actual field operations of rooftop units, were not considered in the experimental tests. Examples include unmeasured ambient weather conditions, such as solar radiation, rain, and strong wind on the condenser. Also the damper position changes the air flow rate. The laboratory experimental data was collected with a constant air flow rate. Since the mixing chamber is small, outdoor air and return air are not mixed well and different damper positions also have some impact on mixing. So it is necessary to investigate the impact on the model of these different factors.

4.1 Impact of unmeasured weather variables

4.1.1 Solar radiation impact on the system

Solar radiation has an impact on the whole system, which will absorb different amounts of radiation when the intensity of sunshine is varied. The most significant and direct impact is on the condenser. Fortunately, the solar radiation impact on the system is also reflected in the temperature sensor readings exposed to the solar radiation. However, whether the solar radiation impact on the whole system is properly reflected in the sensor's readings needs to be investigated. Solar radiation impact on the whole system will be analyzed inversely by modeling. It is necessary to investigate the impact on the sensor's reading before the data are used to build a model.

There are two temperature sensors, condenser inlet and outlet air temperature sensors, that are exposed to solar radiation. From the data gathered during August 13 to August 17 at Purdue field site (figure 4.1) when the solar radiation was not very intense, it is apparent that the solar radiation impact on the condenser inlet air temperature sensor is as much as 15F.

From figure 4.2, it is clear that the solar radiation impact on the condenser outlet air temperature sensor readings depends on whether the condenser fan is on or off. When the condenser fan is off, the solar radiation impact is up to 15 F. However, when the condenser fan is on, the solar radiation impact on the condenser outlet air temperature sensor readings is less than 1 F. Fortunately, the data when the condenser fan is off is not

used to build the steady-state model and the solar radiation impact on the condenser outlet air temperature sensor readings can be ignored.

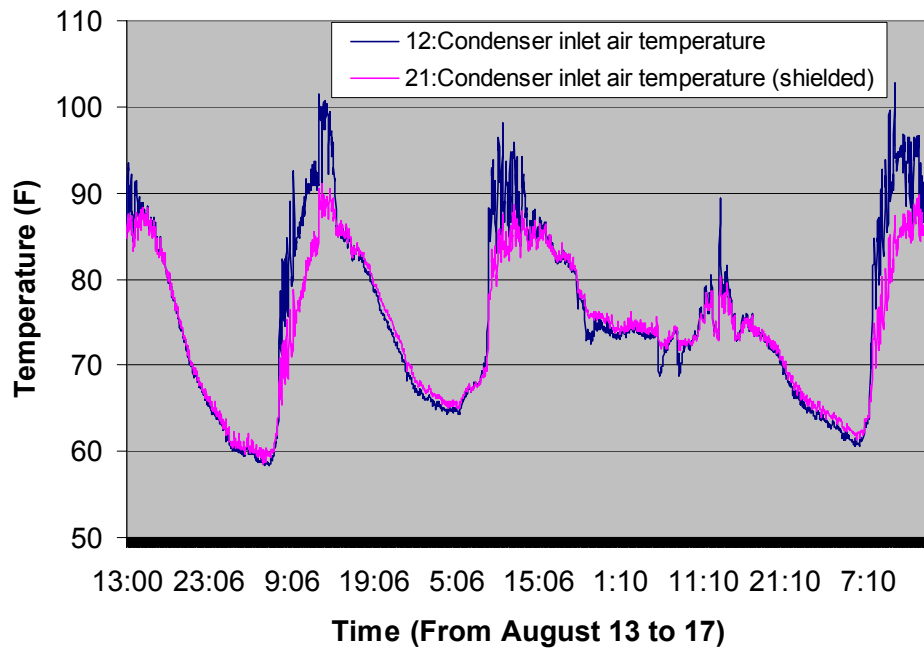


Figure 4.1 Solar radiation impact on condenser inlet air temperature readings (Purdue field site)

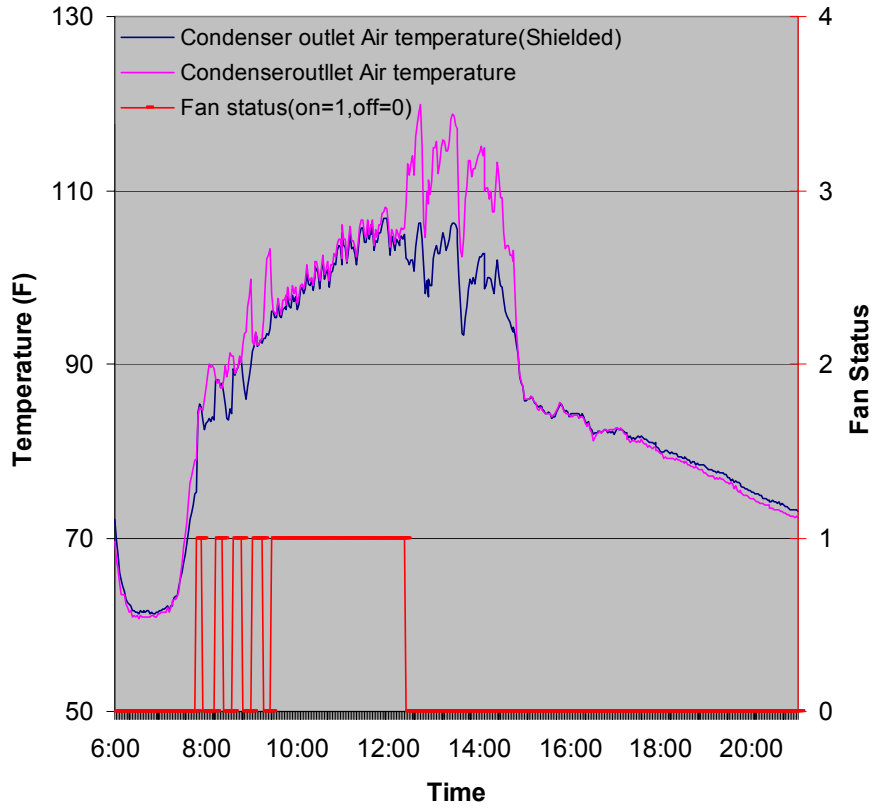


Figure 4.2 Solar radiation impact on condenser outlet air temperature readings (Purdue field site)

The process of solar-heat gain for the sensor is illustrated schematically in Figure 4.3. Since the sensor surface is opaque, transmittance τ is zero and a portion of the solar energy is reflected and the remainder absorbed. Since the sensor's thermal capacity is small it reaches steady-state very quickly.

According to steady-state energy balance on the sensor,

$$A\alpha I_t = Ah_o(t_s - t_a)$$

where, A =sensor surface area, α =absorptance, I_t =irradiation on sensor exterior surface, t_a =ambient air temperature, t_s =sensor surface temperature (sensor's reading), and

h_o =heat transfer coefficient between sensor and ambient air.

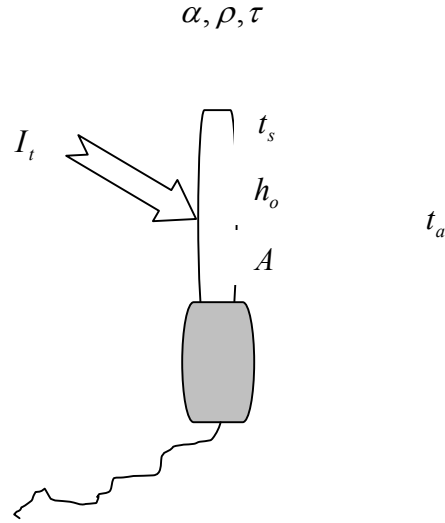
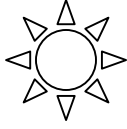


Figure 4.3 Solar radiation impact on the temperature sensor reading

Rearrange the above equation to get

$$t_s = \frac{\alpha I_t}{h_o} + t_a$$

Note that $\frac{\alpha I_t}{h_o} + t_a$ is also the sol-air temperature for any surface having the same α, I_t, h_o

and t_a . The sol-air temperature of HVAC equipment surfaces is an equivalent outside air temperature increased by an amount to account for the solar radiation when the heat transfer is calculated between outside air with the opaque HVAC equipment surfaces. However, only the form is the same, since different surfaces have different absorptances and incident radiation. HVAC equipment have surface absorptances that are different from the absorptance of temperature sensor and also different components of the HVAC equipment have different absorptances. The condenser can be considered a black body with an absorptance of 1. What's more, in deriving the above so called sol-air temperature, thermal balance is assumed and thermal storage is neglected, which is well satisfied by the temperature sensor but not by the HVAC equipment whose thermal storage is more significant. So the unshielded temperature sensor's reading is not exactly the sol-air temperature of the HVAC equipment.

For the condenser outlet air temperature sensor, the air flow rate is very high when the condenser fan is on, and thus h_o is large and $\frac{\alpha I_t}{h_o}$ is small.

As a result,

$$t_s \approx t_a$$

When condenser fan is off, the air flow rate is very low and h_o is very small and $\frac{\alpha I_t}{h_o}$ is relatively large.. However, the data when unit is off is not used to build the model.

In order to decide whether the unshielded or shielded sensor's reading should be used to build the HVAC system models, both options were evaluated.

4.1.2 Rainfall impact on the system

Rainfall on the condenser will cause evaporative cooling and will increase energy transfer rates. Rainfall will also influence the readings of exposed temperature sensor, Figure 4.4 shows that an unshielded sensor's reading will be about 2 F lower than a shielded temperature sensor in rainfall. The shielded sensor's reading is the dry bulb temperature of the ambient air and the unshielded sensor's reading approaches the wet bulb temperature of the ambient air, since the unshielded sensor is exposed to the rain and the rain water on the sensor will evaporate and cool the rain water on the sensor. Although, this temperature is not exactly the same as wet bulb temperature of the air, it is near to the wet bulb temperature. So the difference between the shielded sensor and unshielded sensor is dependent on the relative humidity of the air. However, normally the relative humidity of air in rain will be high enough to make the difference within 2-3 F.

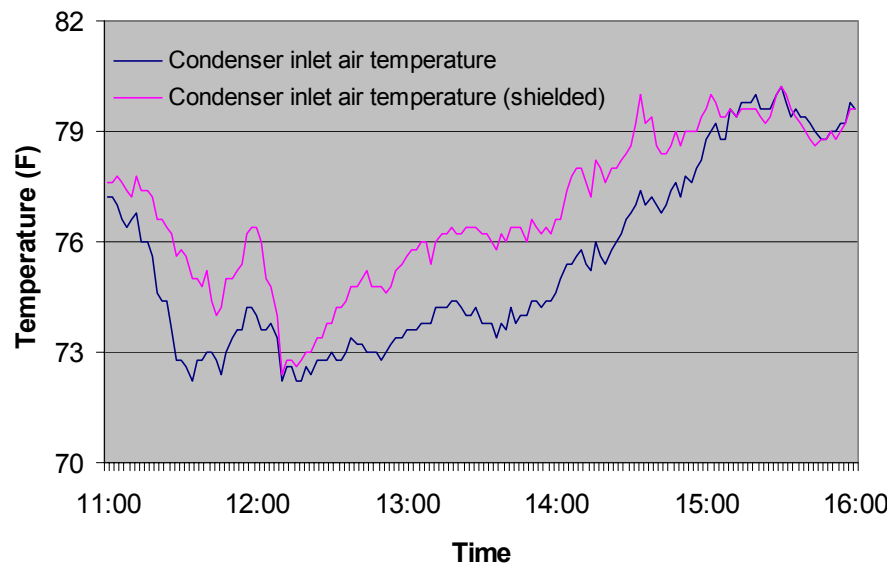


Figure 4.4 Rainfall impacts on temperature sensor readings (Purdue field site)

4.2 Data Processing

4.2.1 Driving condition problems

Of the three driving conditions, only outdoor air temperature and mixed air temperature are measured directly at the California field sites. One way to get mixed air humidity is to compute it from return air temperature and humidity and outdoor air temperature and humidity. The mixing process for outdoor air (oa) with return air (ra) is shown as figure 4.5.

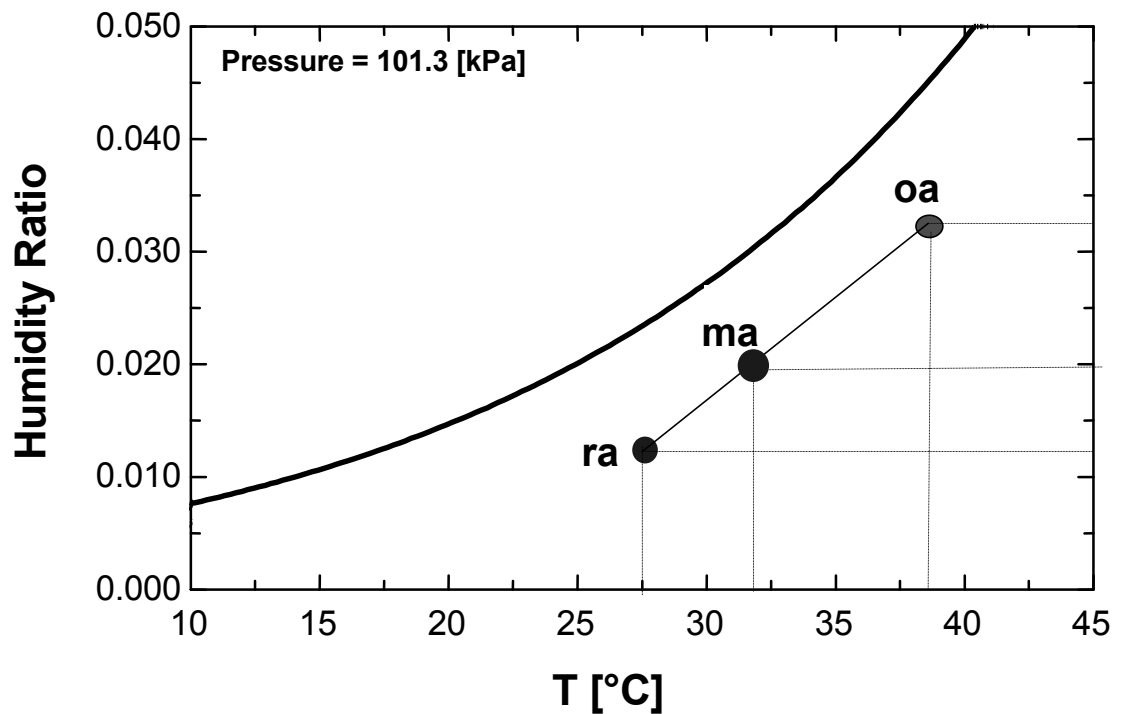


Figure 4.5 Outdoor air and return air mixing process

$$\frac{T_{ma} - T_{ra}}{T_{oa} - T_{ma}} = \frac{W_{ma} - W_{ra}}{W_{oa} - W_{ma}}$$

T_{ma} , T_{ra} , T_{oa} , W_{ra} and W_{oa} are knowns, from the above equation W_{ma} is obtained and thus the state of ma is settled. However, there are some problems with this scheme.

First, when T_{ra} and T_{oa} are equal (T_{ma} should be equal to T_{ra} and T_{oa}), the state of ma can not be determined, as depicted in figure 4.6.

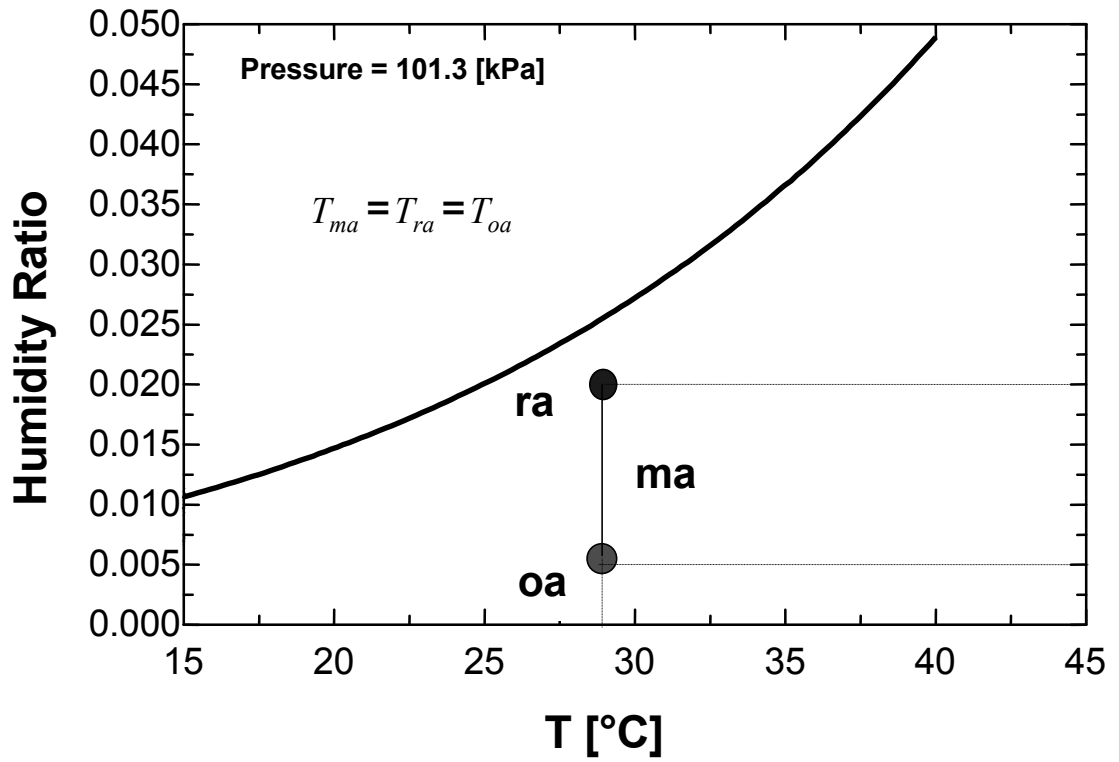


Figure 4.6 ma state cannot be determined when $T_{ra} = T_{oa}$

Second, when there is some uncertainty in the ra and oa states, the calculation according to the above equation will amplify the uncertainty in the mixed air state, which is shown in figure 4.7 schematically.

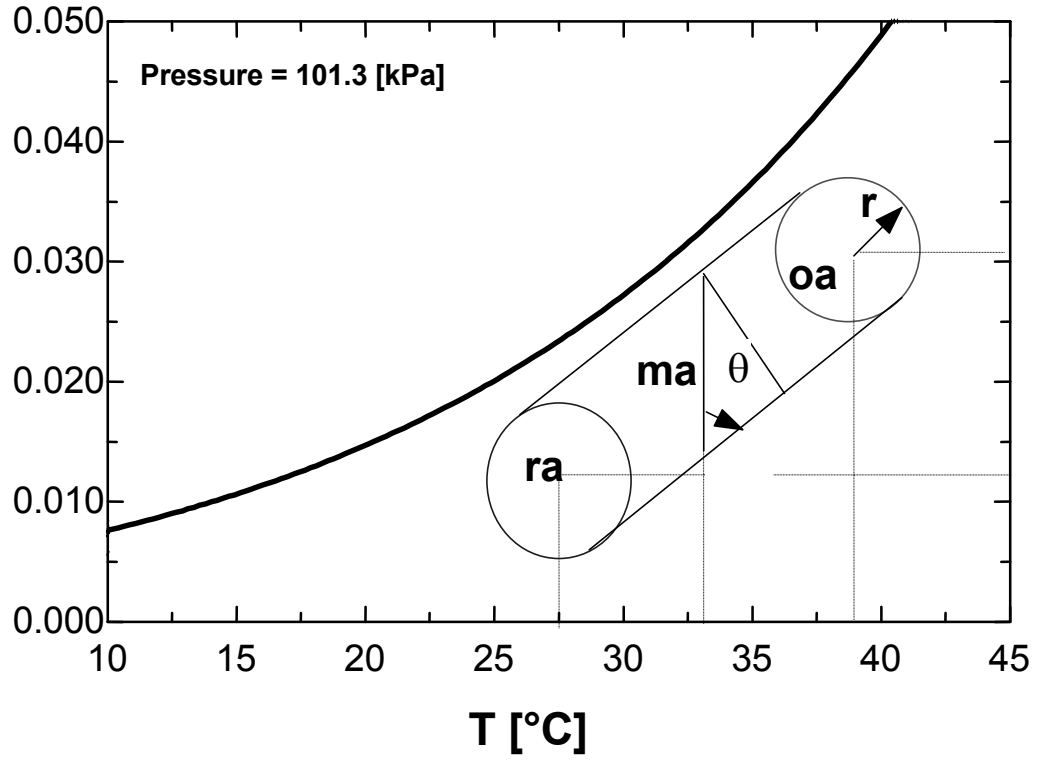


Figure 4.7 Uncertainty analysis for MAW

Assume that the oa and ra uncertainties are within a circle with radius r and there is no uncertainty in T_{ma} , then the uncertainty for W_{ma} propagated and amplified by the oa and ra uncertainties will be,

$$\Delta W_{ma} = \frac{2r}{\sin \theta} \geq 2r$$

It is obvious that the uncertainties will be propagated and amplified when θ is less than 90° .

So it is necessary to add a mixed air humidity sensor to fix the ma state and avoid uncertainty propagation and amplification.

However, there is another way to get mixed air humidity by computing it from return air temperature and humidity, outdoor air temperature and humidity and ratio of return and outdoor air mass flow rate f by following equation,

$$\frac{T_{ma} - T_{ra}}{T_{oa} - T_{ma}} = \frac{W_{ma} - W_{ra}}{W_{oa} - W_{ma}} = \frac{m_{oa}}{m_{ra}} = f$$

If the speed of the evaporator blower is constant, f approximates the ratio of return and outdoor air duct damper positions, which can be readily obtained from Honeywell DCV controllers. Although, unlike the first method, the ma state can be determined for any case, uncertainties will be propagated and amplified when θ is less than 90° .

In view of performance, it is still desirable to add a mixed air humidity sensor to avoid uncertainty propagation and amplification. However, since the humidity sensor is relatively expensive further work should be done to decide whether the extra expense is warranted by the improved accuracy.

4.2.2 Steady-State Detector

In order to apply a steady-state model to a system, which spends considerable time in transient operation, a steady-state detector is necessary. Thus, the error in the ability of the model to fit the training data is added to the error introduced by the fact that the system is almost never actually operating in steady-state. There are a number of desirable properties of a steady-state detector method. It should be computationally efficient, require a small amount of memory for storing values, be responsive to quick changes in operation, and be able to distinguish between changes in measurements caused by transient operation and measurement and system noise.

Three methods were studied by Davis (1995) through simulation for simple first-order responses with artificial noise introduced. The three steady-state detector methods all generate outputs which decrease as the system approaches steady-state. When the output of the steady-state preprocessor drops below a threshold value, the system is determined to be in steady-state. The first algorithm computes the slope of the best-fit line through a fixed-length sliding window of recent measurements. The other two algorithms compute the variance of recent measurements. One uses a fixed length sliding window of recent measurements. The other method, introduced by researchers at Landis and Gyr (Glass, 1995), recursively computes a weighted standard-deviation where more recent measurements are weighted more heavily. Based on his analysis, Davis concluded that the weighted standard-deviation method was the best of the three methods in terms of

efficiency and performance for the simulated data that he studied. These methods, however, have not been compared using real operating data. Breuker (1997) compared the performance of the methods using actual transient data recorded for the FDD demonstration shown in figure 4.8.

Each of the methods has design parameters that affect its performance. For the slope and variance methods based on measurements in a fixed-length sliding window of recent values, the number of measurements in the fixed-length window, the frequency with which new measurements are taken, and the steady-state detector threshold are the design parameters. Instead of using a fixed window length, the exponentially weighted variance method uses a forgetting factor to reduce the contribution of successively older measurements on the variance calculated at each step.

In order to compare the performance of the three methods, each was applied to a transient start-up profile for hot gas temperature from a rooftop air conditioning unit. This analysis used a fixed window length of 10 measurements and a forgetting factor of 0.7 with measurements being taken from the test unit every 5 seconds. The forgetting factor of 0.7 was chosen to give similar outputs between the variance calculated from the sliding window and the exponentially weighted variance. The first observation which can be made about the slope method with the two variance methods is that the slope can assume both positive and negative values, while the variance is only positive. This could lead to a problem with the slope method, since an overshoot could be interpreted as steady-state operation. For this reason, the methods which utilize variance rather than slope are more reliable. Figure 4.8 shows that the two methods which utilize variance as an indicator of steady-state operation have almost identical outputs during their transient startup. Since the exponentially weighted method is more computationally efficient than the fixed-window method, this method was selected for further study.

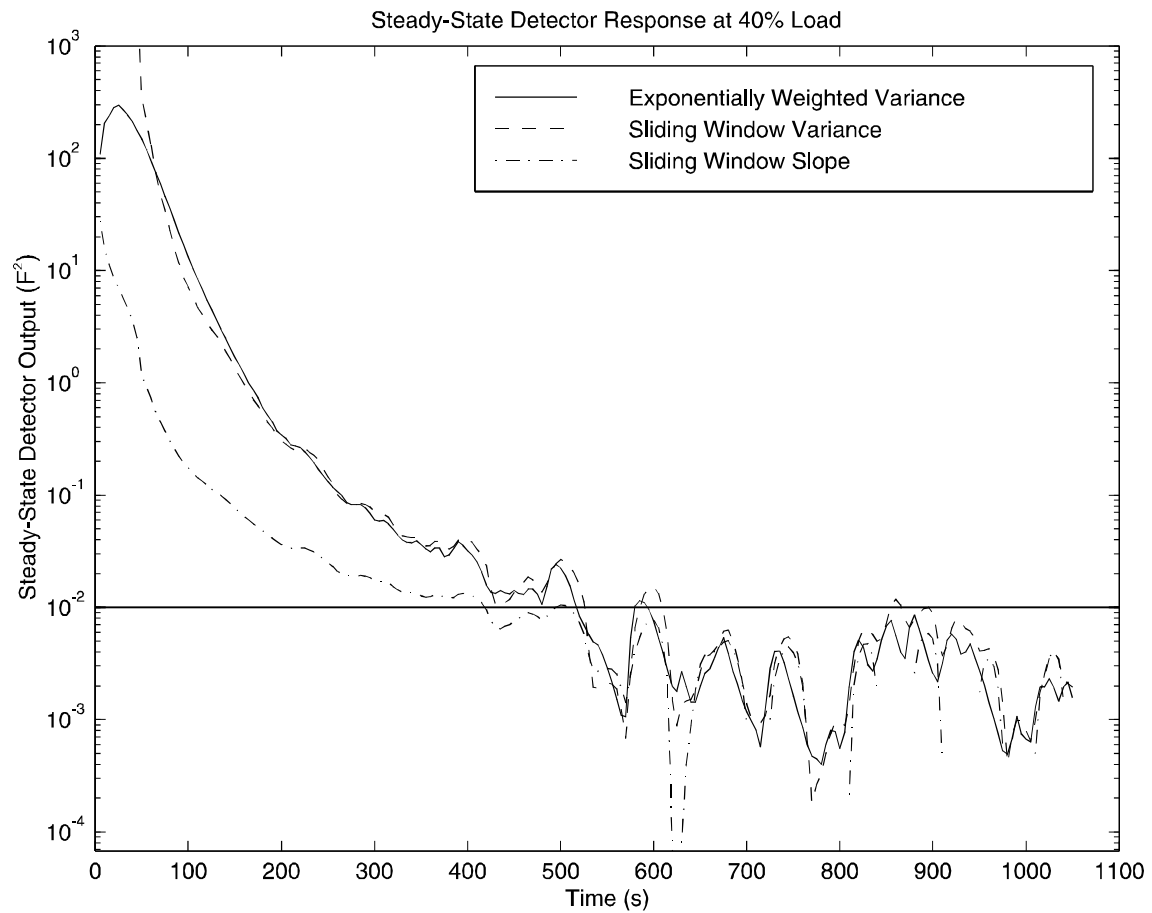


Figure 4.8 Output of three steady-state detectors on T_{hg} measurement (Breuker,1997)

Finding the right forgetting factor is important in tuning the exponentially weighted variance method for a particular application. As the forgetting factor increases, the response of the steady-state detector becomes more stable and more sluggish. It appears that a forgetting factor range of 0.6 - 0.8 provides reasonably quick response without introducing too much short-term noise.

Figure 4.9 shows transient data and output of a steady-state detector during August 21 to 24 for the Purdue field site. An exponentially weighted steady-state detector with a forgetting factor of 0.7 was used. The zero values of the detector output mean the system was not considered to be at steady state. The steady-state detector appears to work well.

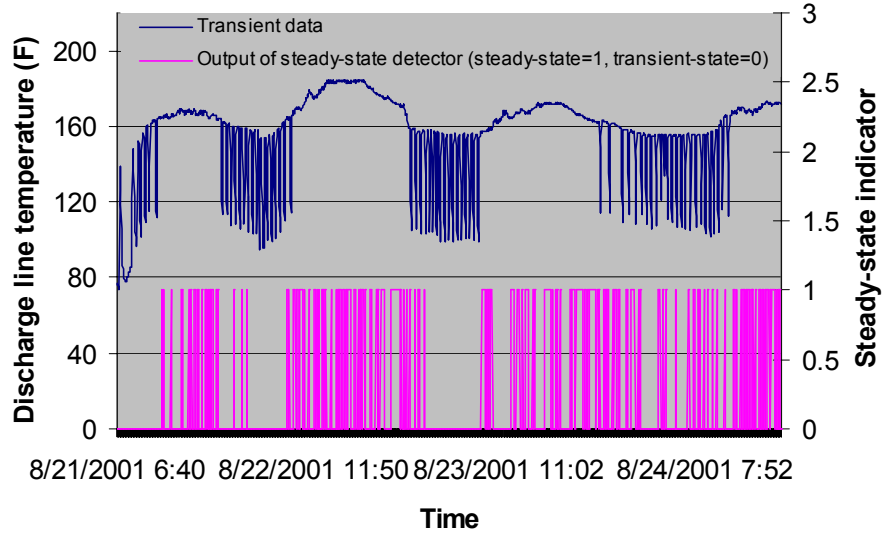


Figure 4.9 Steady-state detection

4.2.3 Clustering of steady-state data

For some problems, the number of data points may be small enough that all of the data available can be used directly in learning a model. In other problems, the number of data obtained can become sufficiently large that it is no longer practical to assign a separate node to each data. Clustering techniques can be used to group data so that the group can be represented by only one data point. Clustering of steady-state data is necessary for the following two reasons:

Firstly, there are measurement noise and system disturbances, so clustering will act as a filter.

Secondly, clustering will reduce the large number of steady state data to much a smaller set of steady state data. This will greatly reduce the nodes of the GRNN and memory to realize the GRNN algorithm.

First, establish a single radius of influence, r . Starting with the first point (X, Y) , establish a cluster center, X^i , at X . All future data for which the distance $|X - X^i|$ is less than the distance to any other cluster center and is also $\leq r$ would be grouped into cluster i . A data point for which the distance to the nearest cluster is larger than r would become the center for a new cluster. After clustering, the expectation (average) of each group data

will be calculated to represent the whole group. The radius r is an important parameter for the performance of clustering algorithm. For example, there are 256 of steady-state data points after steady-state detection for the data taken during August 13 to 17 at Purdue field site; there are 54 clusters after it is clustered.

4.3 Purdue Field Site Results

The interpolating performance of the polynomial plus GRNN model is very good, as shown with laboratory data. The interpolating performance for field site data (partially shielded condenser inlet air temperature) is also good, as shown in figures 4.10, 4.11 and 4.12.

To test extrapolating performance, three cases were considered, one using a partially shielded condenser inlet air temperature, one using a fully shielded condenser inlet air temperature and one using an unshielded condenser inlet air temperature. Since shields 1, 2 and 3 (figure 4.13) do not isolate the temperature sensors completely from solar radiation, rainfall and wind the way the outdoor air duct does, “partially shielded” refers to sensors shielded by shields 1, 2 and 3 and “full shielded” refers to the sensor in the outdoor air duct (figure 4.13) which is totally isolated from the environment. Figures 4.14 to 4.22 show that models built with partially shielded condenser inlet air temperature have reasonably good extrapolating ability which is the best among the three kinds of model. Models built using unshielded condenser inlet air temperature extrapolate poorly. The model that uses fully shielded condenser inlet air temperature data also extrapolates well but a little worse than the partially shielded condenser inlet air temperature model except that evaporating temperature is extrapolated better than with partially shielded model. So it can be concluded that the solar radiation impact on the whole system is not so significant as on the unshielded condenser inlet air temperature sensor. The readings of the unshielded condenser outlet air temperature sensor exaggerate the solar radiation impact on the system. In addition, the fully shielded sensor readings also underestimate the solar radiation impact on the whole system. The exception is for the evaporating temperature because the solar radiation and outdoor air temperature have very little impact on the evaporator, which is mainly driven by mixed air temperature and humidity. In summary, figure 4.23 shows an overview of the environmental factor impacts on modeling performance.

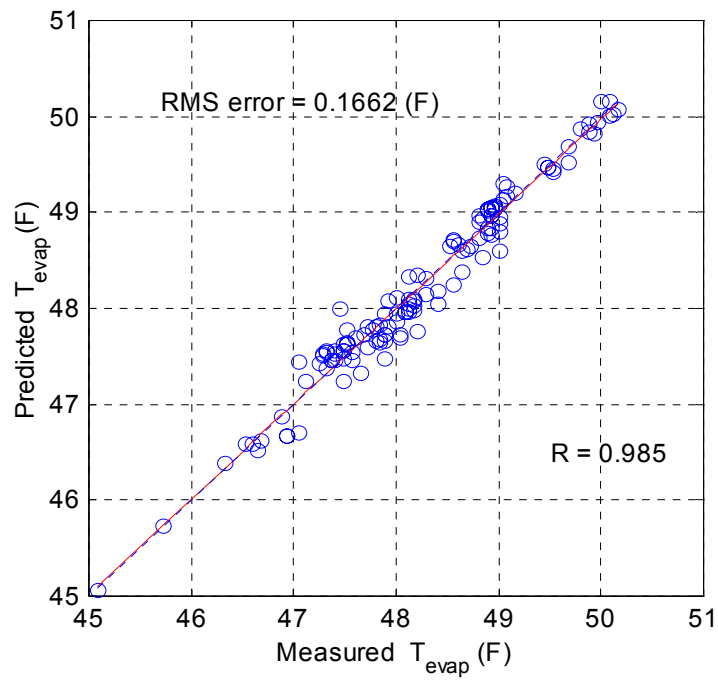
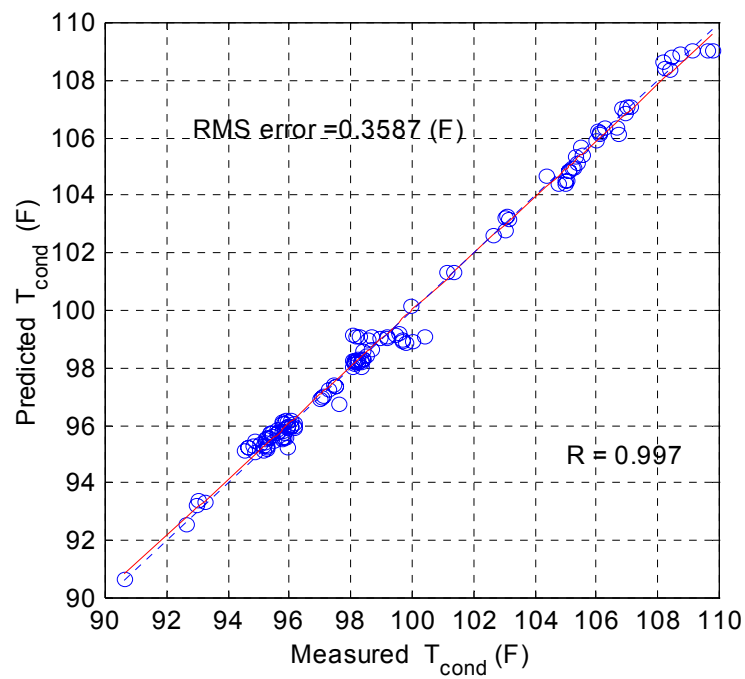


Figure 4.10 Interpolating performance for evaporating temperature



4.11 Interpolating performance for condenser temperature

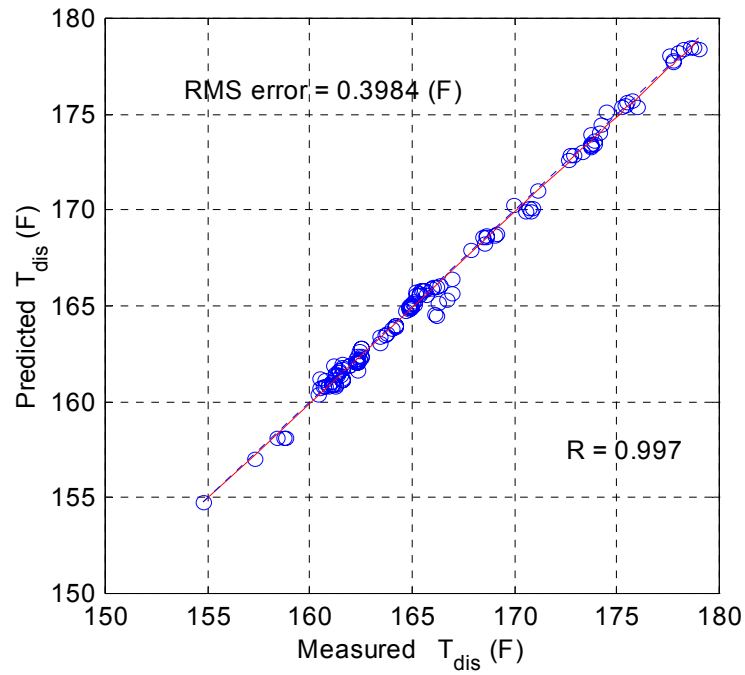


Figure 4.12 Interpolating performance for discharge temperature

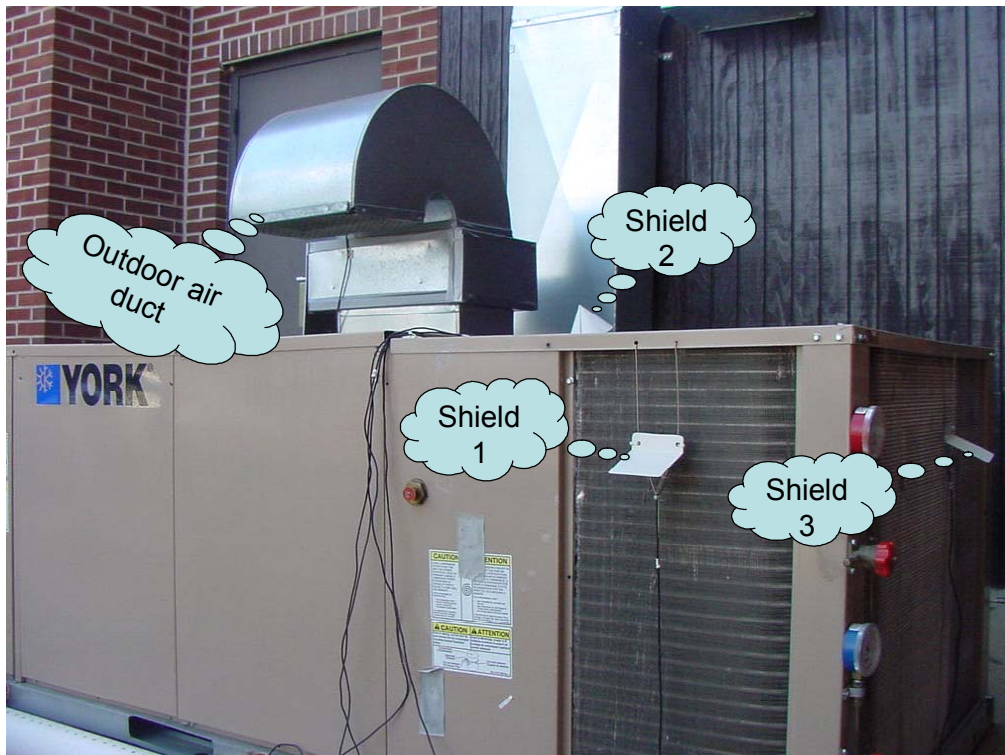


Figure 4.13 Purdue field site setup

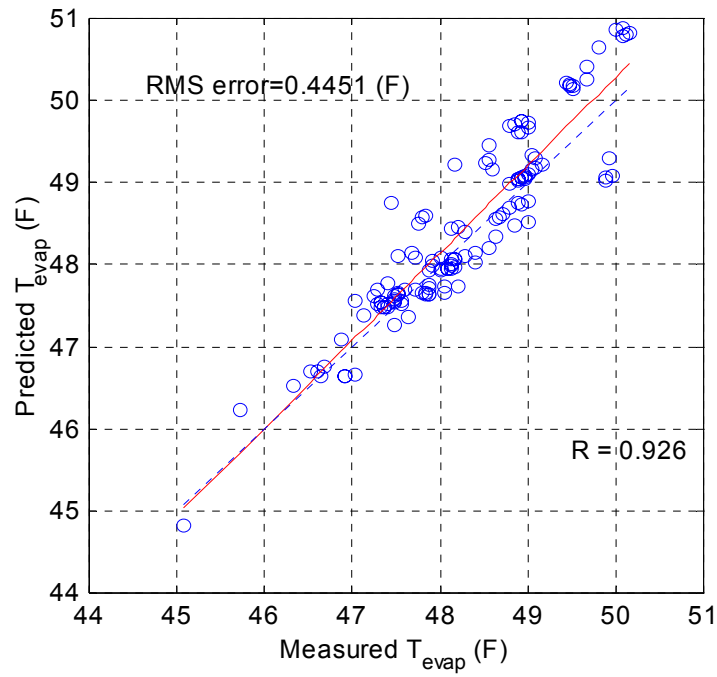


Figure 4.14 Extrapolation performance of evaporating temperature model using partially shielded data

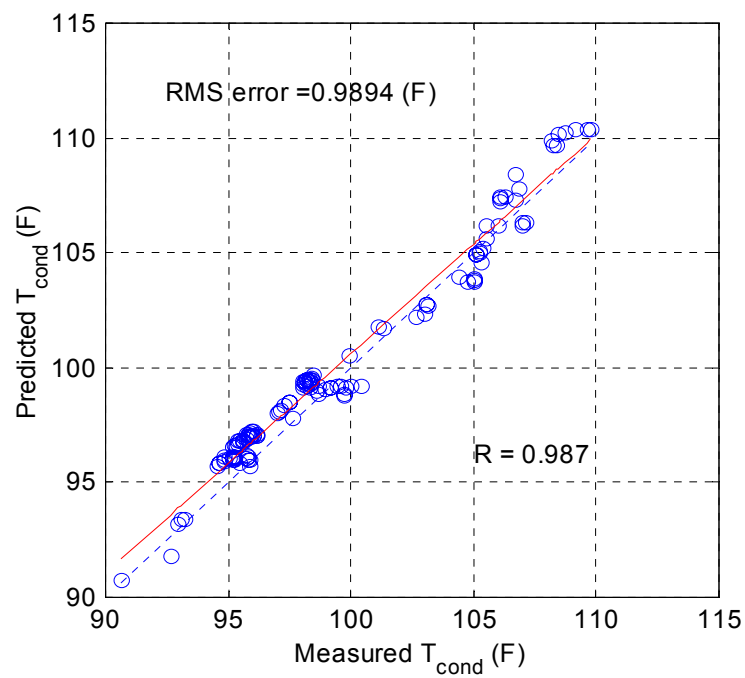


Figure 4.15 Extrapolation performance of condenser temperature model using partially shielded data

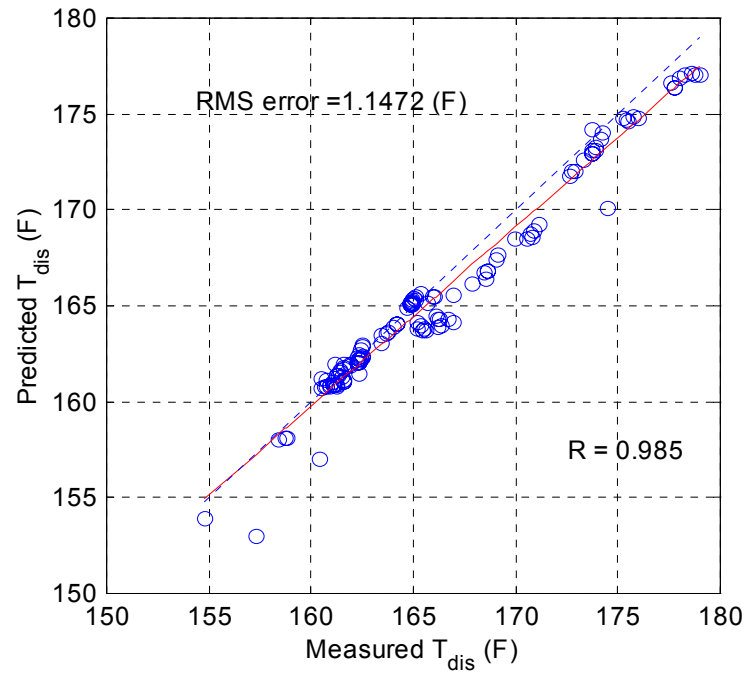


Figure 4.16 Extrapolation performance of discharge temperature model using partially shielded data

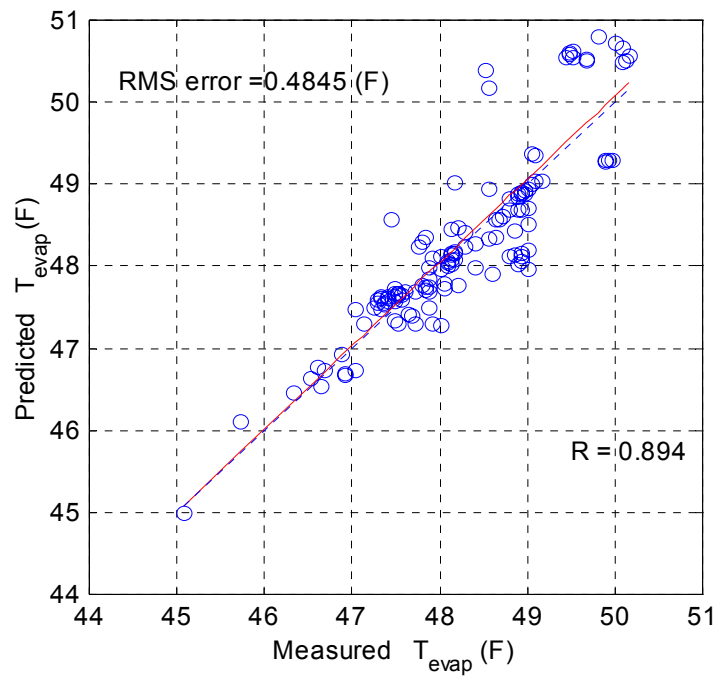


Figure 4.17 Extrapolation performance of evaporating temperature model using unshielded data

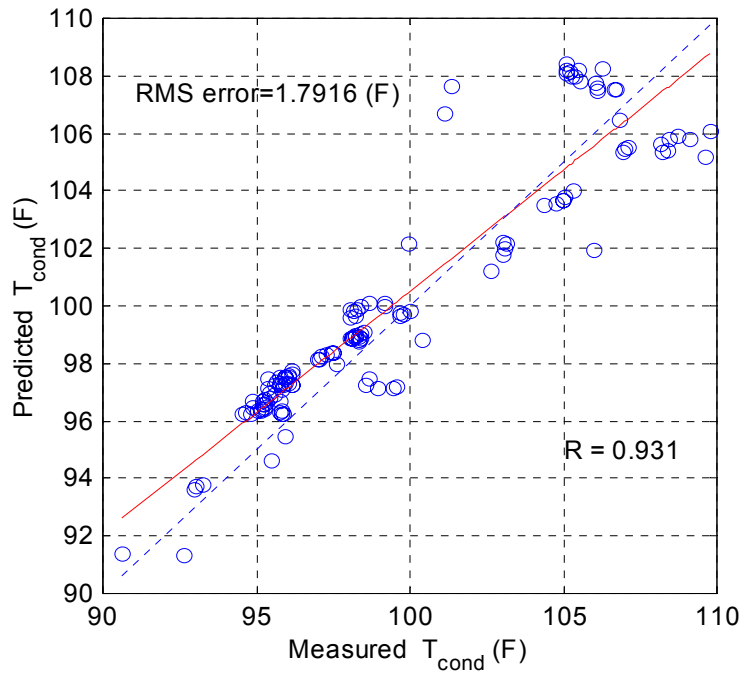


Figure 4.18 Extrapolation performance of condenser temperature model using unshielded data

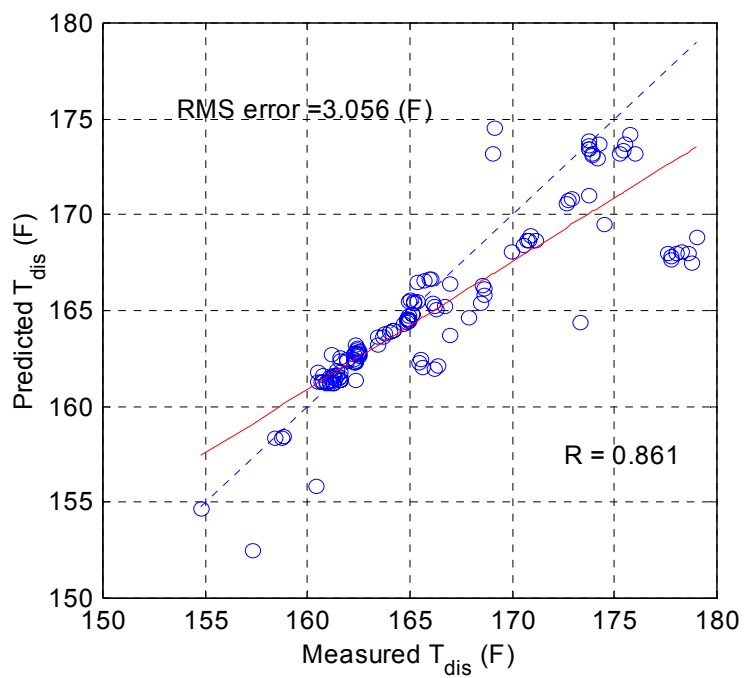


Figure 4.19 Extrapolation performance of discharge temperature model using unshielded data

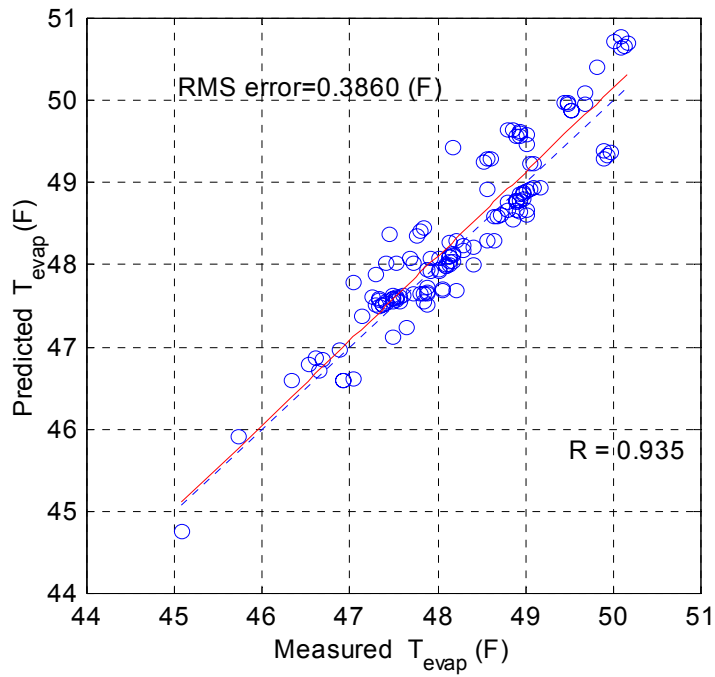


Figure 4.20 Extrapolation performance of evaporating temperature model using fully shielded data

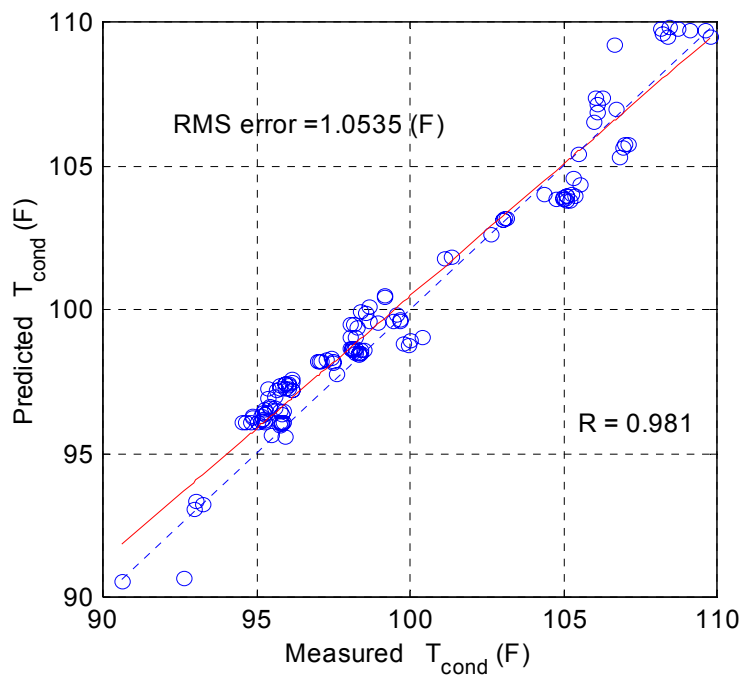


Figure 4.21 Extrapolation performance of condenser temperature model using fully shielded data

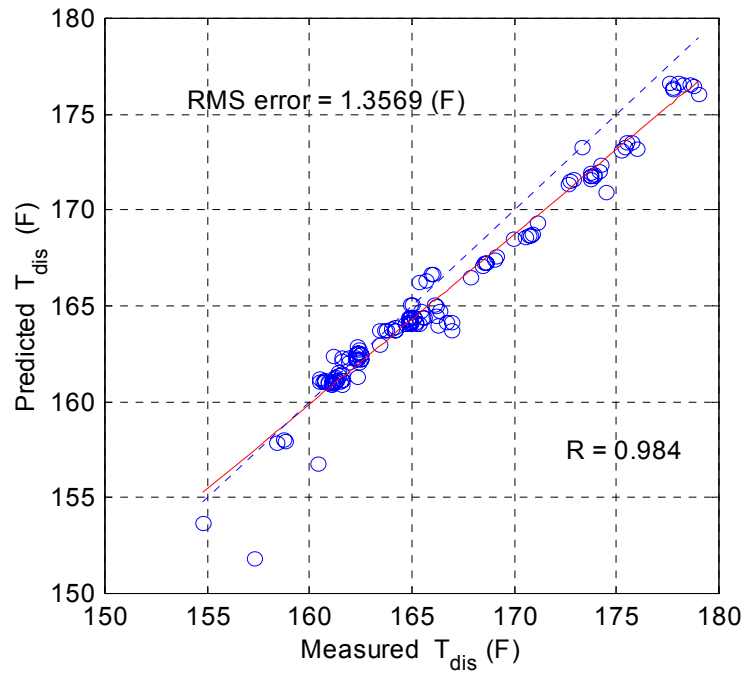
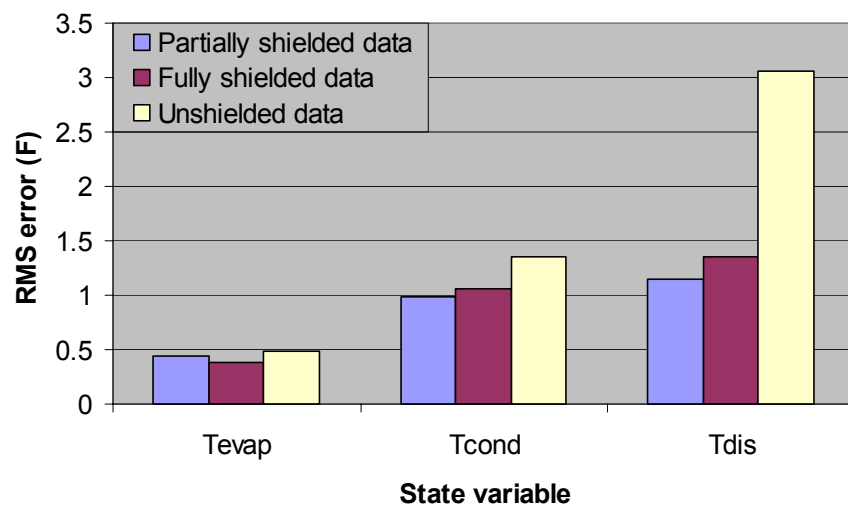


Figure 4.22 Extrapolation performance of discharge temperature model using fully shielded data



4.23 Environmental factor's impact on modeling

4.4 California field site results

Since there are some problems with data collection in California, there is not enough data to train models for every site. In this section, results are presented for one site, Milpitas. The rooftop unit has one stage and is installed in a McDonalds. This rooftop unit is a little different from the unit at Purdue field site. First, there is no mixed air humidity sensor available, so the damper position reading is used to calculate the mixed air humidity. Second, from the data collected during August 28 to September 26 (Figures 4.24 and 4.25), this unit kept cycling very frequently and seems that it never reached steady-state, so the steady-state detector parameters were modified to get some “steady-state” data (Figure 4.26). A moving window steady-state detector with a fixed window width of 2 was used. Figures 4.27 and 4.28 show the interpolation and extrapolation performance for condensing temperature, respectively. The interpolation performance was evaluated by randomly selecting two-thirds of the total data during August 28 to September 26 to train the model and one-third of the total data to test the model. For figure 4.28, the data collected during August 28 to September 15 was used to train the model and the data of September 15 to 26 was used to test the extrapolation performance. These two figures show that condensing temperature models worked reasonably well. Evaporating temperature models had RMS errors of 0.7528 F for interpolation and 1.1152 F for extrapolation. However, discharge line temperature models worked poorly and their RMS errors were 2.345 F for interpolation and about 4 F for extrapolation. The discharge line temperature takes the largest time to reach steady-state.

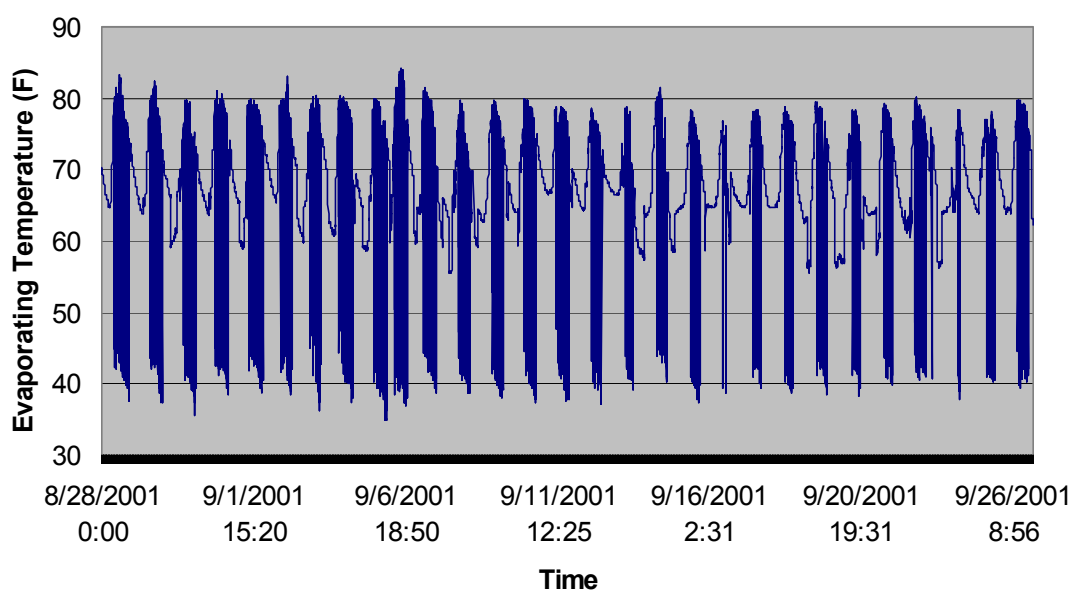


Figure 4.24 Frequent cycling of Milpitas site during August 28 to September 26

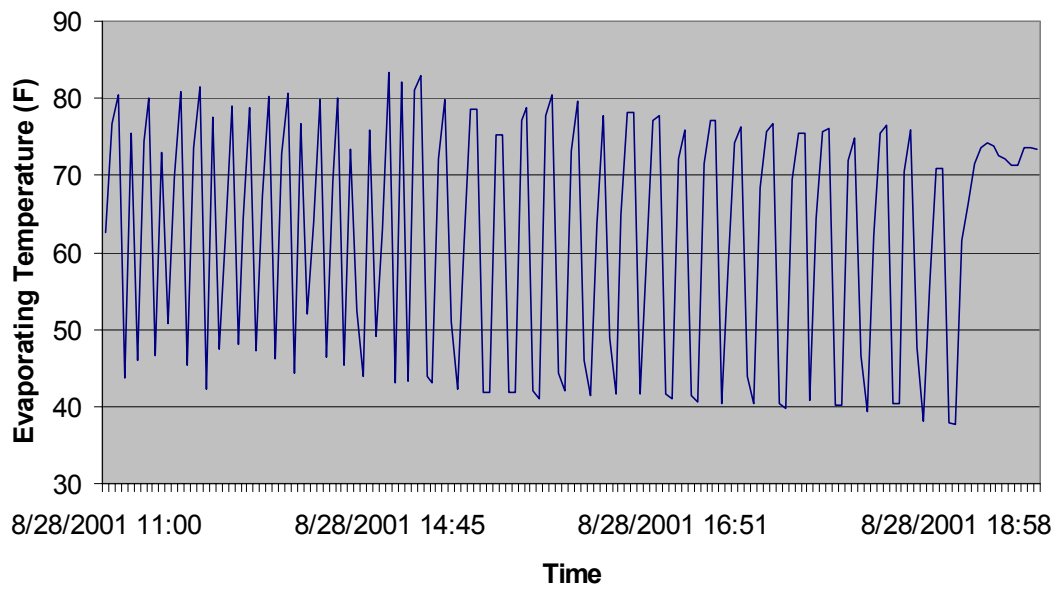


Figure 4.25 Frequent cycling of Milpitas site on August 28

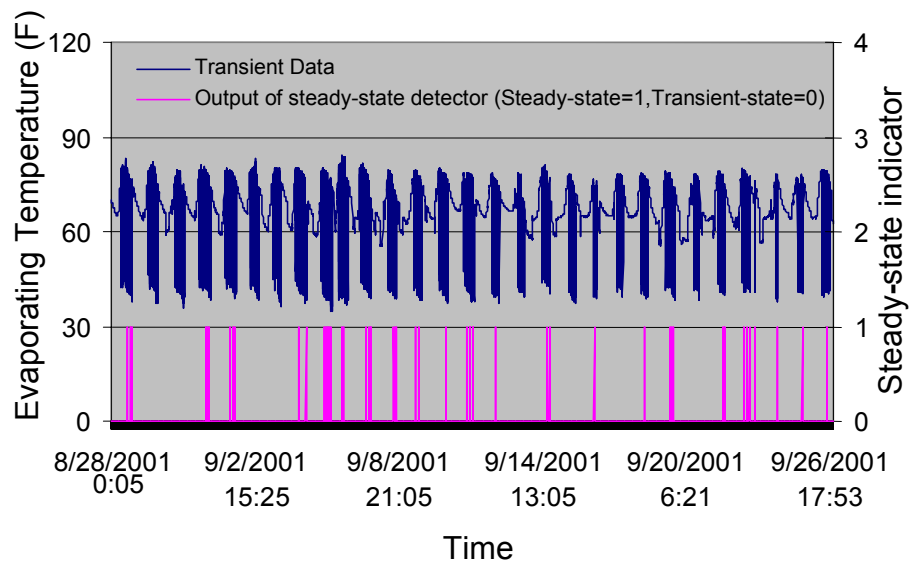


Figure 4.26 Steady-state detection for Milpitas site

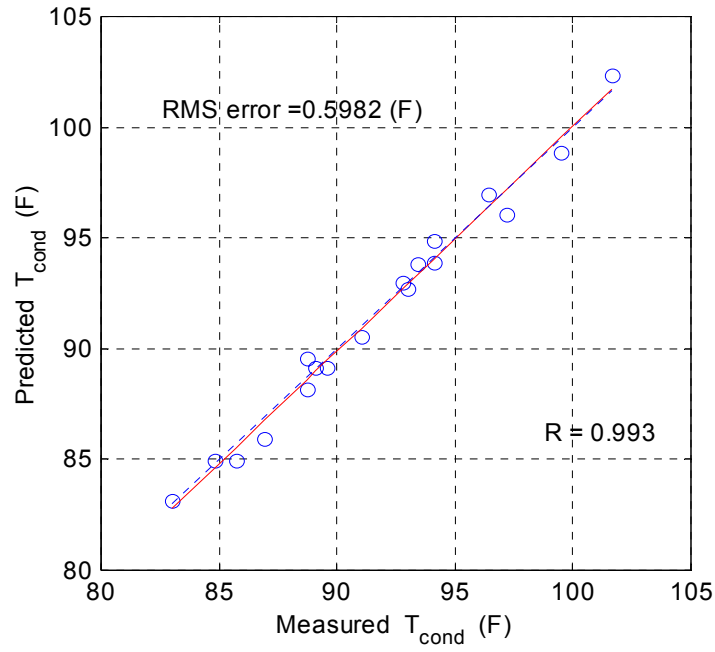


Figure 4.27 Interpolation performance of T_{cond} Model for Milpitas site

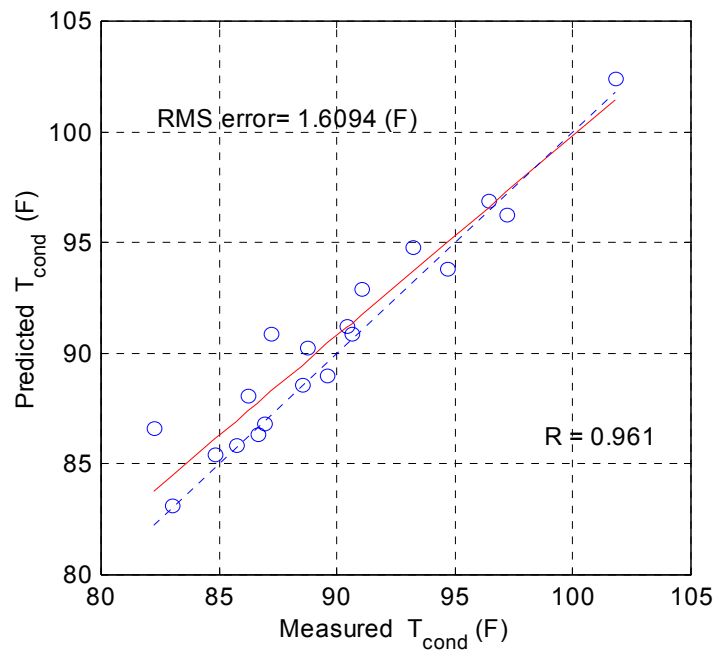


Figure 4.28 Extrapolation performance of T_{cond} model for Milpitas site

5. Adaptive Polynomial plus GRNN

Although the polynomial plus GRNN model has excellent interpolating performance and good extrapolating performance in the range of the training data, the extrapolating performance far outside the range of the training data is not guaranteed, especially for,

1. Noisy training data, which is a characteristic of measurement data
2. Sparse training data, which is normal when FDD is first commissioned
3. Range-limited training data, which is a normal case for field data
4. Strong nonlinear area where dry conditions change to wet conditions
5. Limited nodes, which will reduce memory greatly and reduce computing time

It is obvious that the interpolating ability is always far better than extrapolating ability. And the nearer the data to training data, the better the extrapolation ability. So the model performance can be improved greatly by enlarging the range of training data and changing the model extrapolation issue into an model interpolation issue, which can be realized by changing the fault free outside data into training data online. So it is advisable for a modeling approach to be adaptive to improve the robustness of the FDD method.

In addition to extrapolating performance improvement, adaptive modeling also will improve interpolating performance. The interpolating performance will be improved further if some more nodes are added when the training data is very sparse and where it is highly nonlinear, say, in the dry/wet area.

To realize the adaptability, modeling and FDD should be considered as a whole, because fault free data should be guaranteed in order to make use of the newly coming data. The adaptive modeling scheme is shown as figure 5.1. After the model is trained using limited original data, the model and the FDD system are commissioned. While the model and FDD system are being commissioned, the measurements will be processed as follows:

Firstly, measurements will be feeded into a steady-state detector to obtain steady state data. Secondly, steady state data are inputed to the preprocessor, where the model is embedded, to decide whether the data are “inside or near the training data” or not. If yes, the model will generalize the measurements, and then feed the expected value to the classifier to decide whether there is a fault or not, and if there is no fault, the new data will be recruited into new training data and used to refine the original model. If the data are not “inside or near the training data”, the incoming data will not be processed further but will be stored.

Since air conditioners always cycle, there is no doubt that some data which are “inside or near the range of training data” will appear. Using these coming “inside or near the training data” data, the FDD system can decide whether the system has a fault or not. If not, it can be said safely that the stored data also are free of a fault, so they can be recruited into the new training data and used to adapt the model.

Since so far the FDD is not developed, here only modeling adaptability is discussed and the combination of FDD and modeling will be not discussed here. The benefit of modeling adaptability can be simulated by adjusting the number of training data with the total number of data points being constant. The simulation results are shown in figure 5.2 using laboratory data collected by Breuker (1997) which are organized as table 5.1. Figure 5.2 shows that the model performance is improved considerably with the expanding range of training data.

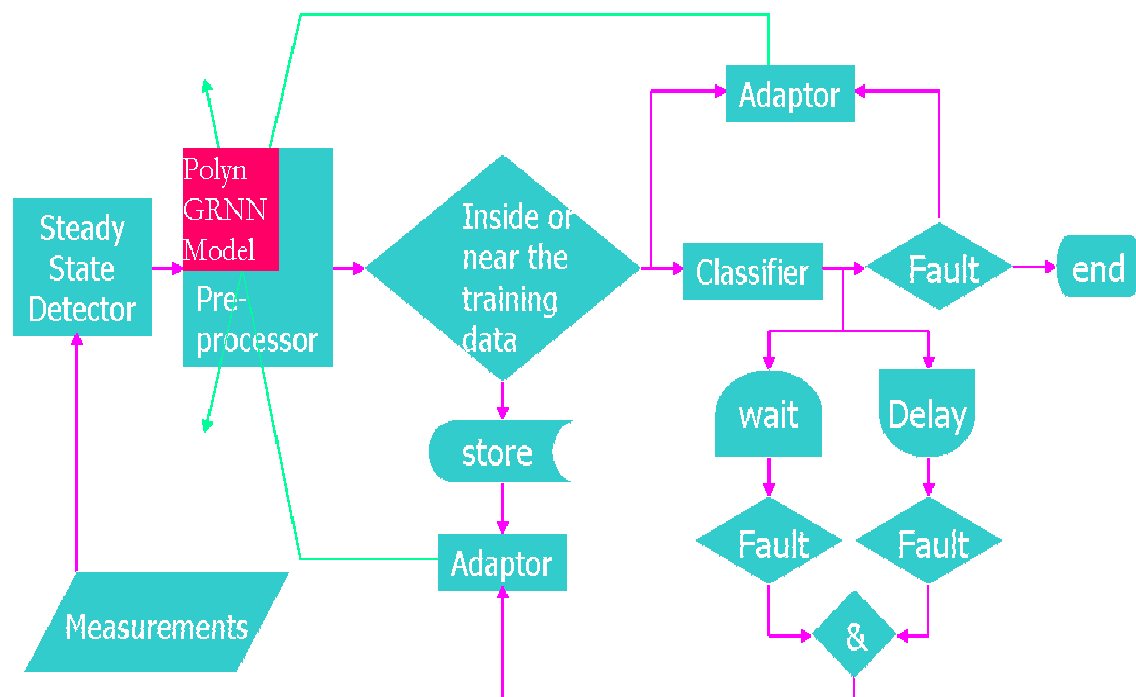


Figure 5.1 Adaptive modeling scheme block diagram

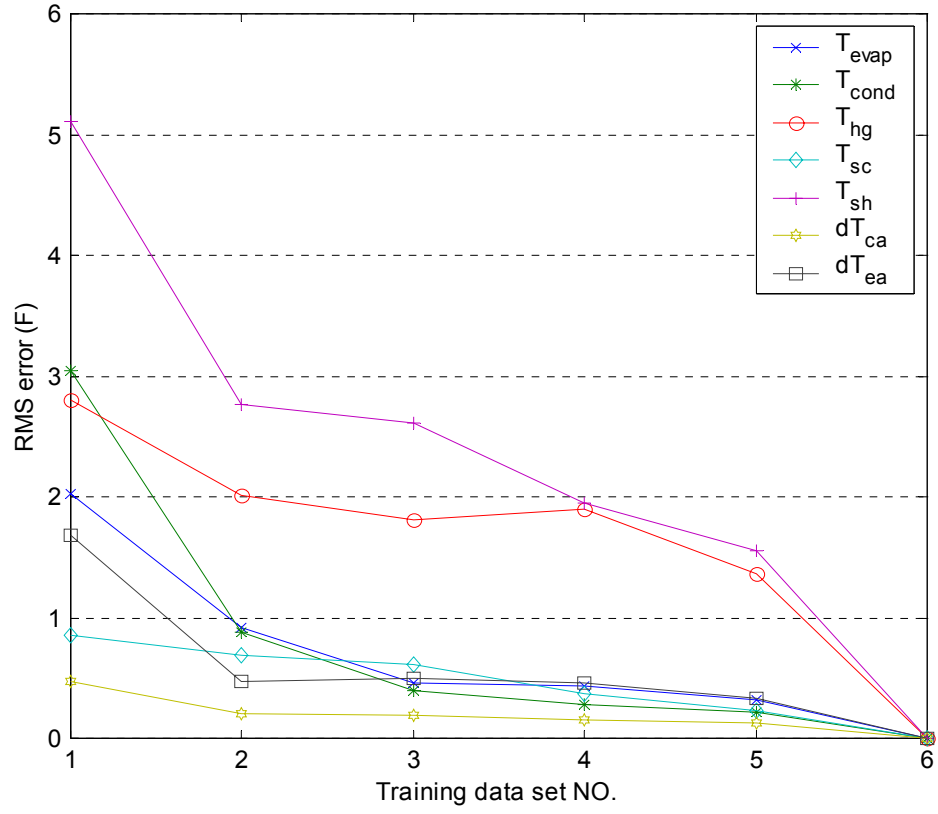


Figure 5.2 RMS error with different training data set

Table 5.1 Data organization for adaptive modeling

Training data set number	Driving conditions range			Training data amount
	T_{ra} (F)	T_{ai} (F)	T_{wb} (F)	
1	73-77.5	70-85	58-62.5	16
2	73-79	70-90	58-64	35
3	71.5-79	65-90	56.5-64	48
4	71.5-80.5	65-95	56.5-65.5	67
5	70-80.5	60-95	55-65.5	96
6	70-82	60-100	55-67	135

6. Conclusions and future work

So far,

- Some literature about FDD modeling has been reviewed
- Four black-box modeling approaches: polynomial, BP neural network, RBF and GRNN, were compared using laboratory data
- A polynomial plus GRNN modeling approach was proposed in order to improve modeling performance and was tested using Purdue field site and one California field site data. Some environmental factors have been investigated in field modeling,
- In order to further improve the robustness of FDD modeling, an idea of adaptive FDD modeling was proposed and was simulated using laboratory data

Future work will be to,

- Continue to complete the modeling work for California sites
- Develop and implement a prototype FDD System
- Develop an improved FDD method for handling multiple faults that occur simultaneously
- Implement improved FDD method in the field sites
- Perform an economic assessment of the FDD system for California

7. Reference

Alistair I. Mees, M. F. Jackson, and Leon O. Chua, 1992. Device Modeling by Radial Basis Functions. IEEE Transactions on Circuits and Systems-Fundamental Theory and Applications. 39 (1): 19-27.

ASHRAE. 1993. ASHRAE Handbook - 1993 Fundamentals, Atlanta: American Society of Heating, Refrigerating, and Air Conditioning Engineers, Inc., Atlanta, GA 30329.

Breuker, M.S. and Braun, J.E., 1997. Evaluation of a Statistical, Rule-based Detection and Diagnosis Method for Vapor Compression Air Conditioners, Master's Thesis, School of Mechanical Engineering, Purdue University.

Cacoullos, 1966. "Estimation of a multivariate density," Ann. Inst. Statist. Math, (Tokyo), Vol. 18, no. 2, pp.179-189.

Chen, B. and Braun, J.E., 2000. Evaluating the potential of on-line fault detection and diagnosis for rooftop air conditioners, Master's Thesis, School of Mechanical Engineering, Purdue University.

Davis, Coby. 1995. Comparison of steady state detection algorithms. ME 597 Report. Available from Professor Jim Braun, Herrick Labs, Purdue University, West Lafayette, IN

Donald F. Specht, 1991. A General Regression Neural Network. IEEE Transactions on Neural Networks. 2 (6): 568-576.

Dyn, N. and Levin, D., 1983. "Iterative solutions of systems originating from integral equations and surface interpolation." SIAM J. Numerical Analysis, vol. 20, pp. 377-390.

Glass, A.S., Gruber, P., Roos, and M., Todtli, J., 1995. Qualitative Model-based fault detection in air-handling units, IEEE control systems Magazine, 15(4): 11-22.

Gordon, J. M., and K. C. Ng. 1994. Thermodynamic modeling of reciprocating chillers. Journal of Applied Physics. 76(6):2769-2774.

Grimmelius, H. T., J. Klein Woud, and G. Been. 1995. On-line failure diagnosis for compression refrigeration plants. International Journal of Refrigeration 18(1):31-41.

Lee, W., House, J.M. and Shin, D.R., 1997. Fault diagnosis and Temperature Sensor Recovery for an Air-handling unit, ASHRAE Transaction, 103(1): 621-633.

Li, X., H. Hvaezi-Nejad, & J.C. Visier, 1996. Development of a fault diagnosis method for heating systems using neural networks. ASHRAE Transactions 102 (1): 607-614.

Parzen, 1962. On the estimation of a probability density function and the mode, Ann. Math. Stat., 33, pp. 1065-1076.

Rossi, T.M. and Braun, J.E., 1995. Detection, Diagnosis, and Evaluation of Faults in Vapor Compression Cycle Equipment, Ph.D. Thesis, School of Mechanical Engineering, Purdue University.

Stylianou, M. & D. Nikanpour. 1996. Performance monitoring, fault detection, and diagnosis of reciprocating chillers. ASHRAE Transactions 114 (4): 615-627.

DESCRIPTION AND EVALUATION OF AN IMPROVED FDD METHOD FOR ROOFTOP AIR CONDITIONERS

Deliverables 2.1.3 and 2.1.4

Progress report submitted to:
Architectural Energy Corporation

For the Building Energy Efficiency Program
Sponsored by:
California Energy Commission

Submitted By:
Purdue University

Principal Investigator: James Braun, Ph.D., P.E.
Research Assistant: Haorong Li

August 2002

Mechanical Engineering
1077 Ray W. Herrick Laboratories
West Lafayette, IN 47907-1077
(765) 496-6008
(765) 494-0787 (fax)

**RAY W. HERRICK
LABORATORIES
PURDUE ENGINEERING**



Table of Contents

<u>1</u>	<u>Introduction</u>	5
<u>2</u>	<u>Literature review of HVAC system FDD</u>	7
<u>2.1</u>	<u>Overview</u>	7
<u>2.2</u>	<u>Latest progress</u>	8
<u>2.2.1</u>	<u>Packaged air conditioning systems</u>	8
<u>2.2.2</u>	<u>Other HVAC systems</u>	11
<u>2.3</u>	<u>Future prospects</u>	14
<u>3</u>	<u>Description of FDD technique</u>	16
<u>3.1</u>	<u>Overview</u>	16
<u>3.2</u>	<u>Measurement Preprocessing</u>	18
<u>3.2.1</u>	<u>Measurement filter</u>	18
<u>3.2.2</u>	<u>Steady-state detector</u>	18
<u>3.3</u>	<u>Steady-state models</u>	20
<u>3.3.1</u>	<u>Normal state models</u>	21
<u>3.3.2</u>	<u>Overall performance models</u>	21
<u>3.4</u>	<u>Fault detection</u>	23
<u>3.4.1</u>	<u>Probability method</u>	25
<u>3.4.1.1</u>	<u>Independence assumption</u>	25
<u>3.4.1.2</u>	<u>Monte-Carlo (MC) simulation method</u>	27
<u>3.4.2</u>	<u>Normalized distance method</u>	28
<u>3.5</u>	<u>Fault diagnosis</u>	30
<u>3.5.1</u>	<u>Fault diagnosis rules</u>	31
<u>3.5.2</u>	<u>Fault diagnosis classification</u>	31
<u>3.5.2.1</u>	<u>Probability Method</u>	32
<u>3.5.2.2</u>	<u>Distance method</u>	34
<u>3.6</u>	<u>Fault evaluation and decision</u>	37
<u>4</u>	<u>Case study and method comparisons</u>	40
<u>4.1</u>	<u>Measurement preprocessing</u>	40
<u>4.2</u>	<u>Normal state and overall performance models</u>	41
<u>4.2.1</u>	<u>Normal state models</u>	41
<u>4.2.2</u>	<u>Overall performance models</u>	42
<u>4.3</u>	<u>Fault detection and diagnosis</u>	48
<u>4.3.1</u>	<u>Fault detection</u>	48
<u>4.3.2</u>	<u>Fault diagnosis rules</u>	48
<u>4.3.3</u>	<u>Fault diagnosis method</u>	49
<u>4.4</u>	<u>FDD results and comparisons with previous method</u>	49

<u>4.5</u>	<u>Fault Evaluation Results</u>	56
<u>5</u>	<u>Conclusions</u>	58
<u>6</u>	<u>References</u>	59
	<u>Appendix 1 Details Of Statistical Rule-Based Method By Rossi/Braun</u>	63
<u>1.1</u>	<u>Steady-state preprocessor</u>	64
<u>1.2</u>	<u>Steady-state model</u>	65
<u>1.3</u>	<u>Fault detection classifier</u>	65
<u>1.4</u>	<u>Diagnosis classifier</u>	66
<u>1.5</u>	<u>Evaluation of the statistical rule-based FDD</u>	68
	<u>Appendix 2 Proof for normalized distance method</u>	70
	<u>Appendix 3 Other load level and fault results</u>	71
	<u>Appendix 4 Fault diagnosis distance method</u>	76
	<u>Appendix 5 Introduction of faults</u>	78

NOMENCLATURE

AHU	= Air handling unit
α	= False alarm threshold
β	= Fault diagnosis threshold
d_i^2	= Normalized distance square
EER	= Equipment efficiency ratio
ΔT_{ca}	= Condenser air temperature difference
ΔT_{ea}	= Evaporator air temperature difference
η_v	= Compressor volumetric efficiency
FDD	= Fault detection and diagnosis
GRNN	= General regression neural network
HVAC	= Heating, Ventilating, and Air-Conditioning
M	= Mean vector of residuals
\dot{m}_r	= Refrigerant mass flow rate
μ	= Mean
N	= Number of suction strokes per unit time
ϕ_{ra}	= Relative humidity of return air
P_{dis}	= Discharge pressure
P_{suc}	= Suction pressure
\dot{Q}_{cap}	= Cooling capacity
RBF	= Radial basis function
RMS	= Root mean square
RTU	= Rooftop unit
σ	= Standard deviation
Σ	= Covariance matrix of residuals
T_{amb}	= Ambient temperature
T_{cond}	= Condensing temperature
T_{dis}	= Discharge line temperature
T_{evap}	= Evaporating temperature
T_{ll}	= Liquid line temperature
T_{ma}	= Mixed air temperature
T_{oa}	= Outdoor air temperature
T_{ra}	= Return air temperature
T_{sc}	= Sub-cooling
T_{sh}	= Superheat
v_1	= Specific volume of compressor inlet refrigerant
VAV	= Variable air volume
\dot{W}	= Compressor power consumption

1 Introduction

HVAC systems often do not function as well as expected due to faults introduced during initial installation or developed in routine operation. Rooftop air conditioners are used extensively throughout small commercial and institutional buildings, but compared to larger systems, they tend to be not well maintained. As a result, widespread application of automated fault detection and diagnosis (FDD), which has been used widely in critical systems, will significantly reduce energy use & peak electrical demand, down time and maintenance costs.

Unlike critical systems, FDD for HVAC systems, especially for rooftop air conditioners, is subject to economic constraints. Economic constraints bring special difficulties and issues, which do not need to be considered in critical systems.

First, since a rooftop AC is relatively inexpensive, the cost to realize FDD for HVAC systems in terms of software and hardware should be low. Therefore some relatively expensive measurements such as flow rate, pressure or even humidity, cannot be used. This is a particular problem in fault diagnosis since some faults may have similar symptoms and more sensors can help in distinguishing them. On the one hand, features as sensitive as possible should be extracted from limited available measurements, and on the other hand, the diagnosis method should be as sensitive as possible to isolate several faults with similar symptoms and insensitive features. Computation should be small enough to be implementable within a microprocessor.

Second, since HVAC equipment are used in diverse weather and climates, the behavior of the HVAC plant will vary drastically. In addition, since single-point sensor placement is generally used, many measurements often are biased and noisy. So the FDD should be able to handle biased measurements and be robust to different operating modes and against noise and disturbances.

Third, unlike critical systems in which faults have zero tolerance, a fault evaluation and decision step should be added to assess the impact of a fault on overall system performance and make a decision whether the benefit of servicing the fault justifies its expense.

Finally, unlike a critical FDD system which is engineered for a specific large system, FDD for HVAC systems needs to be adaptive and generic to the same type of system, or at least to similar models from the same product family. This would reduce the per-unit costs, which need to be low compared to the HVAC equipment price.

So, FDD for HVAC systems should have analytical redundancy. That means the information from system measurements should be preprocessed extensively before it is used to detect and diagnose fault. In addition, the characteristic of being adaptive and generic should be emphasized when developing FDD for HVAC systems.

This progress report first presents a literature review about FDD for HVAC systems, especially for rooftop air conditioners, and then describes an improved FDD prototype for rooftop air conditioning systems. Finally, the performance of the improved FDD method is evaluated and compared with results of Breuker and Braun (1998b).

2 Literature review of HVAC system FDD

2.1 Overview

In the late of 1980's, some researchers investigated common faults and methods for fault detection and diagnosis in simple vapor compression cycles, such as a household refrigerator. With the growing realization of the benefits brought by FDD, many more papers about HVAC FDD have appeared in the recent ten years. Figures 2-1 and 2-2 show the paper statistics in HVAC FDD over the past 15 years.

From these two figures, it can be seen that the number of papers significantly increased since 1996 and most of the papers focused on variable air volume (VAV) air handling units (AHU). Since Comstock, Chen, and Braun (1999) did a very detailed and comprehensive literature review in 1999, the next section of this report will briefly refer to some significant contributions before 1999 and concentrate on up-to-date progress after that.

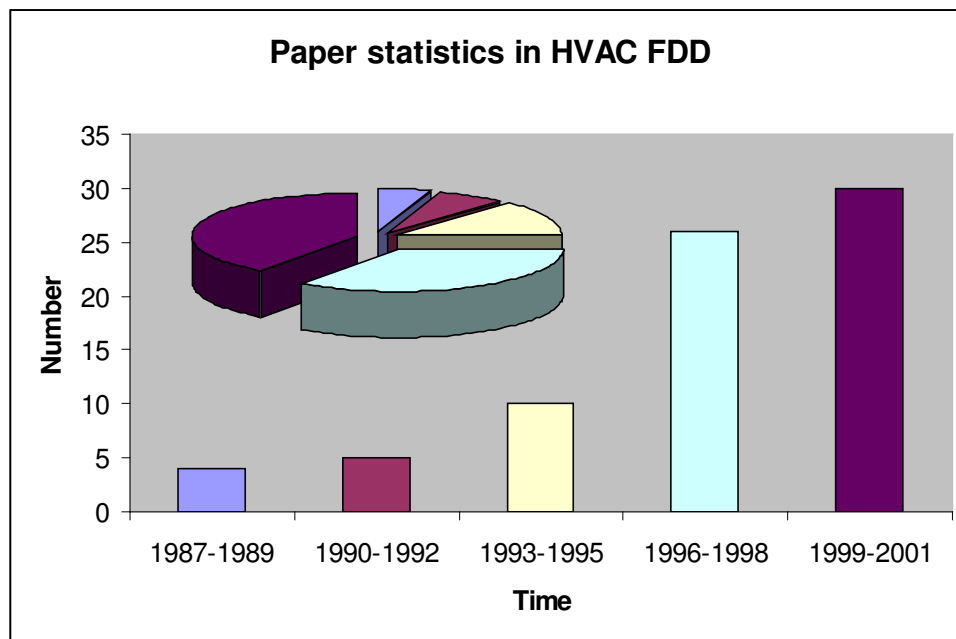


Figure 2-1 Paper statistics in HVAC FDD with time

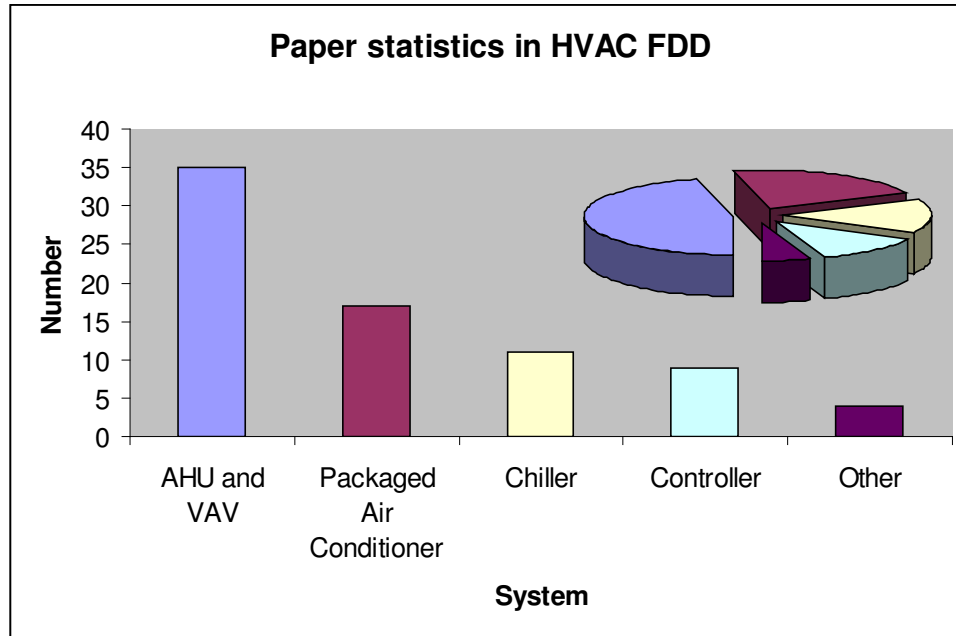


Figure 2-2 Paper statistics in HVAC FDD with system

2.2 Latest progress

Since 1999, about 30 papers have been published. According to IEA ANNEX 34 edited by Dexter and Pakanen (2001),

- Twenty-three prototype FDD performance monitoring tools and three validation tools have been developed.
- Thirty demonstrations have been taken place in twenty buildings.
- Twenty-six FDD tools have been tested in real buildings.
- Four performance monitoring schemes have been jointly evaluated on three documented data sets from real buildings.
- A test shell has been developed to simplify the comparative testing of the FDD tools.

2.2.1 Packaged air conditioning systems

Rossi and Braun (1995, 1997) modified the general FDD supervision methodology first described by Isermann (1984) for non-critical HVAC system as shown in Figure 2-1 and developed a statistical rule-based FDD technique for vapor compression air conditioners. This technique uses only nine temperatures and one relative humidity. Among the ten measurements, ambient air temperature T_{amb} , return air temperature T_{ra} , and return air

relative humidity Φ_{ra} (or wet-bulb temperature T_{wb}) are considered to be driving conditions. The other seven measurements (evaporating temperature T_{evap} , condensing temperature T_{cond} , suction line superheat T_{sh} , liquid line subcooling T_{sc} , compressor discharge temperature T_{dis} , air temperature rise across the condenser ΔT_{ca} , and air temperature drop across the evaporator ΔT_{ea}) are used to specify the system operating state. A steady-state model is used to describe the relationship between the driving conditions and the expected output states in a normally operating condition. By comparing the measurements of the output states with those predicted by the steady-state model, residuals are generated. These residuals are statistically evaluated to perform fault detection and compared with a set of rules based on directional changes to identify the most likely cause of the faulty behavior (diagnosis). In addition, fault impact evaluation criteria based upon economic and operational constraints were developed. This research laid a blueprint for later research, whose strengths and weaknesses will be discussed in a later part of the report.

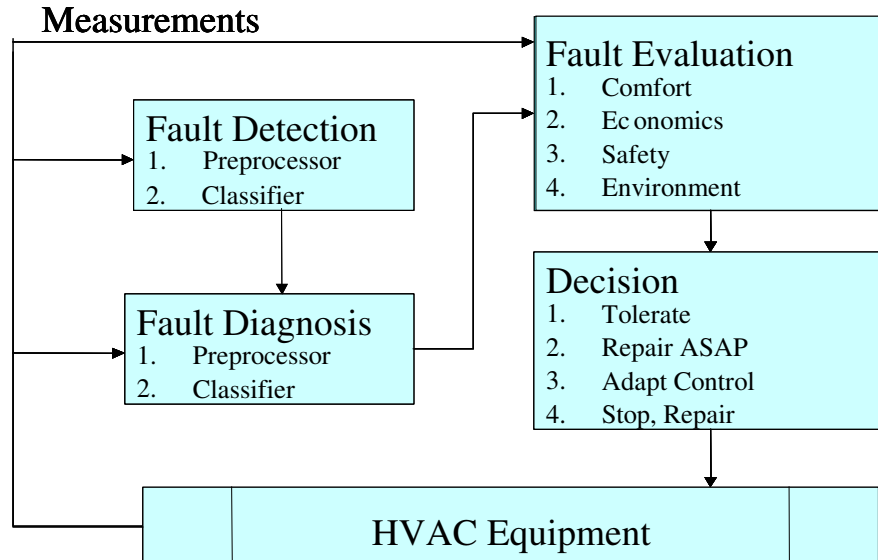


Figure 2-1 Supervision approach of HVAC&R equipment.

Following this research, Breuker and Braun (1997, 1998a, 1998b) first identified important faults and their impacts on rooftop air conditioners through interactions with industry personnel, and then did a detailed evaluation of the performance of the FDD technique

presented by Rossi and Braun (1997). It was found that by the frequency of occurrence, approximately 40% of the failure incidents of "No air conditioning" were electrical or controls related and the other 60% were mechanical. By the service occurrences, refrigerant leakage (12%) dominated among the mechanical faults while the occurrences of faults relating to condenser (7%), air handling (7%), evaporator (6%), and compressor (5%) are similar. By the service costs, the faults related to compressor failure dominated with 24% of total service costs. Controls related faults were the second-rated class of high cost fault, accounting for 10% of total service costs. Further analysis showed that, although most failures in hermetic compressors are diagnosed as a failure in the motor, those failures usually result from mechanical problems such as overload or liquid refrigerant in the compressor. Based on their survey and analysis, Breuker and Braun concluded that five fault types should be considered for systems with fixed expansion devices: (1) refrigerant leakage; (2) condenser fouling; (3) evaporator filter fouling; (4) liquid line restriction; and (5) compressor valve leakage.

To evaluate the FDD technique presented by Rossi and Braun, the above five faults were introduced within a 3-ton fixed orifice air conditioner in well-controlled environmental chambers under various fault levels and cooling load levels. Results showed that refrigerant leakage, condenser fouling, and liquid line restriction faults could be detected and diagnosed before an 8% reduction in COP occurred; compressor valve leakage was detected and diagnosed before a 12% reduction occurred; and the least sensitivity was evaporator fouling at 20%. These results are compared with the improved FDD technique later in the report.

To keep track of the up-to-date research, Comstock, Chen, and Braun (1999) performed an exhaustive literature review of FDD in HVAC. This review provided a solid background and guide for later research.

The fault characteristics on a system with a TXV are different from those with a fixed orifice for which Rossi and Braun originally developed the statistical rule-based technique. Chen and Braun (2000, 2001) modified and evaluated the original FDD technique for a 5-ton rooftop unit with a TXV as the expansion device. To simplify the FDD method, two innovative and easy-to-implement methods were proposed. The first method, termed the "Sensitivity Ratio Method", used measurements and model predictions of temperatures for

normal system operation to compute ratios that are sensitive to individual faults. The second method, termed the “Simple Rule-Based Method”, dispensed with any on-line model but used performance indices computed from raw measurements that are relatively independent of operating state but are sensitive to faults. Both methods were tested using experimental data for different fault types and fault levels at different operation conditions. Also, a 7.5-ton unit from the same product family as the 5-ton unit was used for a robustness test.

Ghiaus (1999) presented a bond graph method for a packaged air conditioning system. The bond graph is a graph in which nodes represent conservation of energy equations, and terminal nodes represent either system elements (such as resistance, capacitance, inertia) or sources. A bond is a power connection between two parts of the system: A and B. The power is the product of power variables: effort and flow. Effort represents force, torque, pressure, voltage, or absolute temperature, while flow represents velocity, rotational frequency, volume flow rate, current, or entropy flow rate. For the air conditioning system, a thermal bond graph used temperature as effort and entropy flow rate as flow. Two faults: reducing the heat removed by the evaporator (by slowing the evaporator fan) and reducing the heat rejected by the condenser (by slowing the condenser fan) were considered. The advantage of the method is that it could diagnose a fault without any a priori knowledge of the possible faults and implementation of the fault inference algorithm is fast and simple due to its recursive nature. However, there are several drawbacks for this method. Firstly, the method does not consider impact of variation in driving conditions on the bond graph, so it cannot tell driving condition effects from faulty effects. Secondly, only two simple faults were considered. If there is a refrigerant fault such as leakage or flow restriction, the technique described in the paper could not make the correct diagnosis, due to the assumption of constant refrigerant flow rate.

2.2.2 Other HVAC systems

There is a large body of literature on other HVAC systems, especially variable air volume (VAV) air handling units (AHU) and chillers. Since this project is focused on rooftop air conditioners, only recent and representative research is discussed here.

Shaw and Norford (2002) presented two techniques for using electrical power data for detecting and diagnosing a number of faults in AHUs. One technique relies on gray-box correlations of electrical power with such exogenous variables as airflow or motor speed. This technique was developed to detect and diagnose a limited number of air handler faults and was shown to work well with data taken from a test building. The other method relies on physical models of the electromechanical dynamics that occur immediately after a motor is turned on. This technique has been demonstrated with sub-metered data for a pump and for a fan. Tests showed that several faults could be successfully detected from motor startup data alone. While the method relies solely on generally stable and accurate voltage and current sensors, thereby avoiding problems with flow and temperature sensors used in other fault detection methods, it requires electrical data taken directly at the motor, down-stream of variable-speed drives, where current sensors would not normally be installed for control or load-monitoring purposes. Later Norford and Wright (2002) presented some results from controlled field tests and concluded that: the first-principles-based method misdiagnosed several faults and required a larger number of sensors than the electrical power correlation models, while the latter method demonstrated greater success in diagnosis (limited number of faults addressed in the tests may have contributed to this success) but required power meters that were not typically installed.

Yoshida and Kumar (1999) presented a model-based methodology for online fault detection for VAV HVAC systems. Two models, Auto Regressive Exogenous (ARX) and Adaptive Forgetting Through Multiple Models (AFMM), were trained and validated on data obtained from a real building. Based on the results, it was concluded that the variation of parameters rather than the difference between the predicted and actual output is more prominent and reflective of a sudden fault in the system. The AFMM could detect any change in the system but required a long window length and therefore may not detect faults of low magnitude. The ARX model, on the other hand, could be used with very short window length and was more robust. Yoshida and Kumar (2001a) further put forth an off-line analysis based on ARX method. It was concluded that off-line analysis of data by this model was likely to detect most of the faults. To evaluate the robustness of this technique, Yoshida and Kunmar (2001b) developed a recursive autoregressive exogenous algorithm (RARX) to build the

frequency response dynamic model for VAV AHUs. It was concluded that the method was quite robust against sensor error and could detect and diagnose several types of faults.

Carling (2002) presented a comparison of three fault detection methods for AHUs. The three methods were: a qualitative method that compares controller outputs and model-based predictions, a rule-based method that examines measured temperatures and controller outputs, and a model-based method that analyzes residuals based on steady-state models. The author concluded that the first method was easy to set up and generated few false alarms. However, it detected only a few faults of those introduced. The second method is straightforward and detected more faults while requiring some analysis during setup. The third method also detected more faults but it also generated more false alarms and demanded considerably more time for setup. The third method may have generated more false alarms because of poor steady-state detector performance and a bad detection and diagnosis threshold. In this paper, an exponentially weighted variance steady-state detector was used. Our investigation, which will be discussed in a later part of the report shows that the variance method, either the exponentially weighted method or fixed moving window method, is not robust enough and should be used together with a slope method for steady-state detection.

Dexter and Ngo (2001) proposed a multi-step fuzzy model-based approach to improve their earlier diagnosis results for AHUs. A computer simulation study demonstrated that a more precise diagnosis can be obtained and experimental results also showed that the proposed scheme does not generate false alarms. This method was based on the use of two kinds of reference models, the fault-free reference model and one of the reference models describing faulty behavior, to perform multiple-diagnosis. Although this new technique overcame some weaknesses of the fuzzy method, the difficulty to summarize or generate fuzzy rules when the number of fault types and levels and load levels increased could not be eliminated.

In addition to fuzzy methods, several investigators (Lee & Park, 1996, Li & Vaezi 1997) attempted to use artificial neural network (ANN) directly to do FDD for AHUs. The common feature of ANN FDD is to use an ANN to map the symptoms to the fault indicators. The network must first be trained to recognize the symptoms of the possible faults, which requires tremendous data for different load levels, fault levels and types. For

complicated problems with many fault types and levels and operating conditions, it is difficult, if not possible, to gather so much data. So recently there seems to be no research on ANN for HVAC FDD. It should be clarified that although it is difficult to directly use ANN to do FDD, it is very useful to use ANN to build fault-free reference models for model-based FDD.

Finally, in the literature of HVAC FDD, some researchers (Salsbury & Diamond 2001, Liu & Dexter 2001) attempted to deal with the FDD in control loop problems or use the information from the controller to do FDD.

2.3 Future prospects

So far, FDD is at the laboratory or field demonstration stage, with most of the effort on improving FDD performance with little concern about how to reduce the cost of FDD techniques and at the same time to improve performance. Commercialization of FDD is a big challenge, since many practical and economical issues should be addressed. The goal of keeping the costs low while improving performance has guided the development of the improved FDD method presented in this report. The only literature to address multiple simultaneous faults in HVAC equipment was presented by Breuker (1997), who investigated two simultaneous faults using simulation. However multiple simultaneous faults are possible. For instance, evaporators and condensers foul at the same time. Breuker found that the FDD technique of Rossi and Braun (1997) would detect and diagnose one of the two faults that were implemented. However, in general, the presence of multiple simultaneous faults could change the system behavior: produce compensated or exaggerated effects or even trigger another symptom, which is normally not covered by existing rules. Existing diagnostic classifiers are not capable of making multiple diagnoses. So the ability of the system to respond to multiple simultaneous faults warrants further investigation. This issue will be addressed at a later stage of this project.

There are two kinds of investigators conducting FDD research in the HVAC field, mechanical and electrical engineers. Most of the research in HVAC FDD has been conducted by the former, who have addressed the problem mainly from a physical point of

view. The electrical engineering investigators normally lack physical knowledge about the HVAC system and often approach the problem from a mathematical or empirical point of view (such as fuzzy logic, neural network, wavelet, and etc.). Both kinds of investigators claim their own methods are better than those of others. So it would be a good contribution to attempt to make some contrasts and comparisons between these two kinds of methods. Later research may address this issue.

3 Description of FDD technique

3.1 Overview

The statistical rule-based FDD method, developed by Rossi and Braun (1997) and evaluated by Breuker and Braun (1998b), is the basis for the method presented in this report and is reviewed in Appendix 1. The method only uses low-cost temperature measurements to do automated FDD, which is important for commercialization. The paper also introduced fault evaluation to HVAC equipment FDD and developed four fault evaluation criteria.

One of the difficulties in applying the method is evaluating the probabilities associated with the different faults that are possible. The method requires evaluation and integration of a 7-dimensional probability distribution for the detection and diagnostic steps. In order to simplify the calculations, the 7 temperature residuals are assumed to be independent. However, our recent research indicates that it is possible to sacrifice fault detection sensitivity and introduce false alarms with this independence assumption. So we have improved on this technique by eliminating the independence assumption and developing an improved FDD technique, which does not utilize a probability distribution for fault detection or diagnosis. The improved FDD technique also incorporates an improved steady-state detector, and improved models for the normal states used to calculate residuals and overall performance models useful in the evaluation step.

To make the supervision approach for HVAC equipment clearer, Figure 2-1 is detailed and modified as Figure 3-1. In Figure 3-1, there are two kind of signals, one indicated by bold (red) lines and the other indicated by regular (black) lines, both of which begin and end at the HVAC equipment. Bold (red) lines trigger the processing blocks, while the signals associated with regular (black) lines are necessary for processing the blocks. The signals associated with dotted (red) lines are used to adapt the model. The processing procedures start from the HVAC equipment and follow the bold (red) lines.

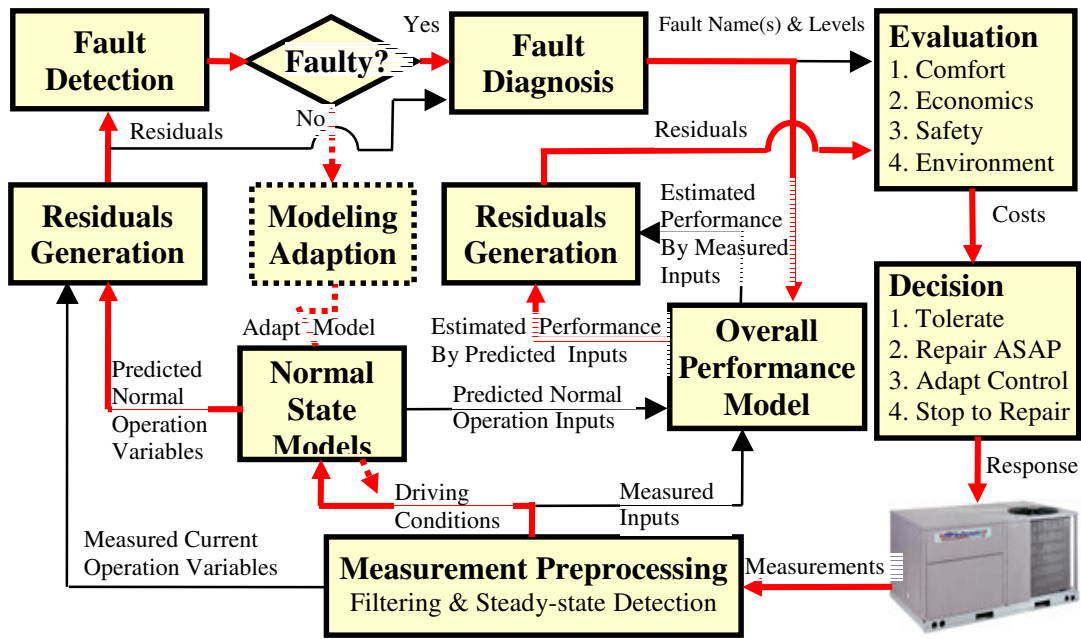


Figure 3-1 A generalized HVAC FDD system scheme

Data (including system driving conditions and state variables) gathered from HVAC equipment are fed into the preprocessor, which includes at least two parts: a filter and steady-state detector. The filter detects the HVAC equipment operating status and eliminates the data when the HVAC equipment is off, and reduces some measurement noise. The steady-state detector determines whether the system is considered to be at steady-state and thus filters the transient data.

After preprocessing, measurements are split into driving conditions and measured current operating variables. Driving conditions are first fed into the normal state models to produce predictions of normal operating state variables. The residuals between current measured and predicted normal operating states are used to detect whether the system is operating with a fault. If the system operation is normal, the current measurements are used to adapt and refine the normal state models. However, if the system is operating with a fault, residuals are further used to diagnose the fault.

Using driving conditions and fault information, the overall performance models estimate the cooling capacity and power consumption associated with both the current and normal

operating states. The residuals of these performance indices are used in the fault evaluation step.

According to the fault name and level and performance residuals, a fault evaluation algorithm evaluates the impact of the fault according to comfort, economic, safety, and environmental criteria. Using estimated impacts, the FDD system will make a decision on how to respond to the fault: tolerate, repair ASAP, adapt control, or stop to repair.

The next five sections discuss various aspects of the technique: measurement preprocessing, steady-state models for normal states and overall performance, fault detection classifiers, diagnostic classifiers, and fault evaluator and decision-maker. The focus is on the development and evaluation of improvements in these elements. For the most part, the evaluation has occurred using laboratory data obtained by Breuker (1998b).

3.2 Measurement Preprocessing

Because the proposed FDD systems are based on steady-state data with the compressor on, the first step is to abstract steady-state measurements from real-time sampling data.

3.2.1 Measurement filter

The measurement filter is used to filter out data when the compressor is off or when there is a communication error. The pressure difference between the compressor suction line and discharge line can be used to detect whether the compressor is on or not. Sometimes there is electrical noise or a disturbance in the data acquisition equipment, which makes the collected data meaningless. This data cannot be used to do FDD and should be filtered out.

3.2.2 Steady-state detector

If there is no drift in the driving conditions, no noise and no other disturbances, all the state variables will be constant. In practice, driving condition drift will make state variables vary deterministically while noise and other disturbances will make state variables have random variations. Two kinds of detection methods, a slope method and two variance methods, have

been proposed to decide whether the system has approached steady-state (see Breuker (1998b)). If the variance threshold is set low enough, variance methods can filter out data with both deterministic and random variations. Although the slope method can filter out data with deterministic variations, it has difficulty distinguishing data with pure large oscillating magnitude from those with pure small oscillating magnitude. The combination of the slope and variance methods can improve the overall performance.

Figure 3-2 shows example behavior for three steady-state detectors using suction line superheat as the measurement. Suction line superheat increases very quickly after the compressor turns on. After reaching a peak, it drops slowly for a while and then oscillates with decreased amplitude. For overall FDD, only those data after 450 seconds work well. There would be false alarms if data before 450 second were used for FDD.

If only the moving window slope was used for detection and the slope threshold was set at $0.02 \text{ } F/s$, data at the beginning would be filtered out and all the oscillating data, with large and small amplitude, would be classified as steady-state data. Consequently, this steady-state detector cannot distinguish data with small oscillating amplitude from that with large oscillating amplitude. If all oscillating data were used for FDD, false alarms or even wrong detection and diagnosis would arise. So a moving window slope method itself cannot guarantee good performance.

It is obvious from Figure 3-2 that the outputs of the exponentially weighted variance method and moving window variance method are almost identical. If the variance threshold were set at $0.3 \text{ } F^2$, either of these two methods would filter out the data before 620 second and thus the overall FDD system would have no false alarms and wrong diagnosis. However, the cost to set the variance threshold at $0.3 \text{ } F^2$ is too high, because it filters out the steady-state data between 450 second and 620 second. Thus, the overall FDD system would delay its decision for 3 minutes. However, if the variance threshold were set at $0.7 \text{ } F^2$, all the good performance data between 450 and 620 would be kept but the bad performance data between 50 second and 200 second would be introduced. The combination of the variance and slope methods is more robust. If the variance threshold were set at $0.7 \text{ } F^2$ and

the slope threshold at $0.02 F/s$, then the use of both criteria would filter out all bad performance data and keep all good performance data.

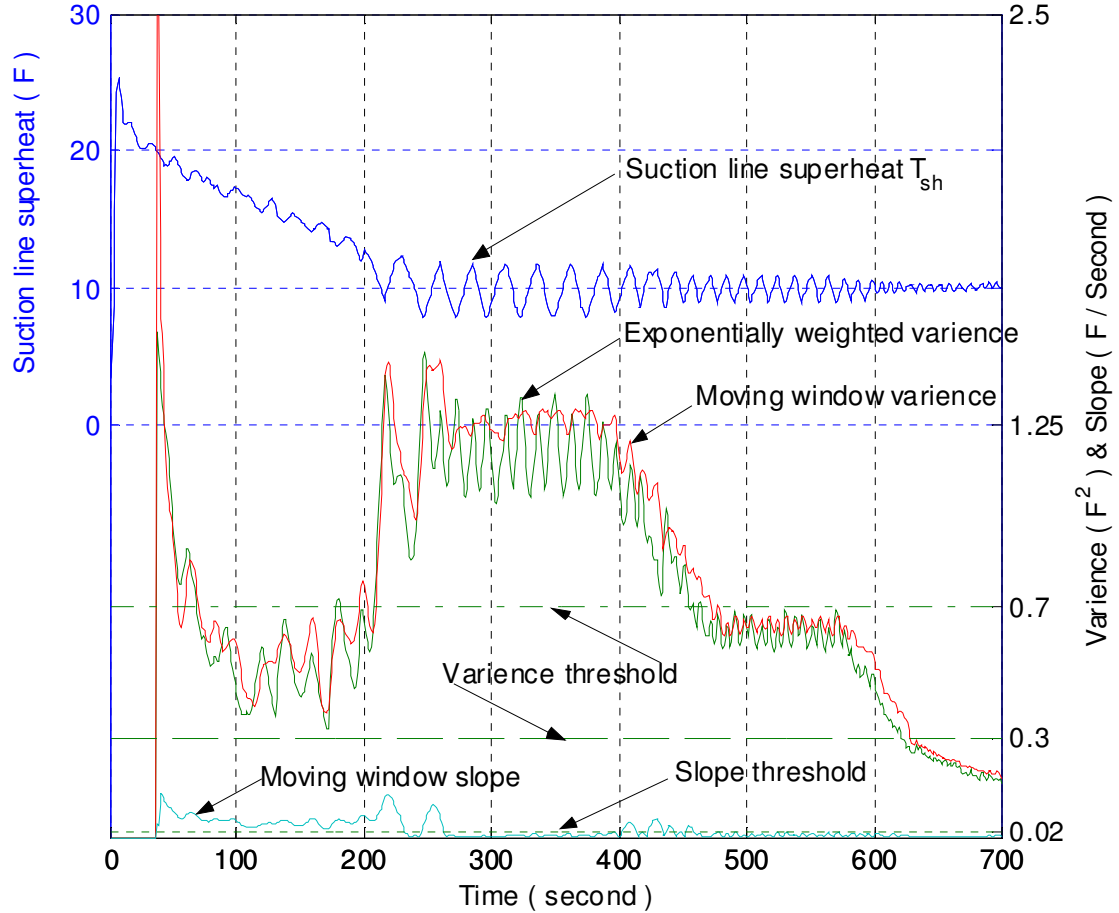


Figure 3-2 Three steady-state detectors' performance

3.3 Steady-state models

The proposed automated FDD technique relies on the use of steady-state models for expected values of operating states under hypothetically normal operating conditions. Furthermore, some on-line measurements such as power consumption and some overall performance indices such as cooling capacity and EER are useful in evaluating whether faults are severe enough for service to be performed. Calculation of cooling capacity involves refrigerant or air flow rate. However, it is not economic to directly measure power

consumption and flow rate. So a model (virtual sensor) for estimating refrigerant flow rate, compressor power consumption and cooling capacity is very useful.

3.3.1 Normal state models

The last deliverable described a modeling approach for operating temperatures that combines a low-order polynomial with a general regression neural network (GRNN) to achieve both good interpolating and extrapolating performance.

3.3.2 Overall performance models

Overall system performance indices such as EER, power and capacity are useful for monitoring and making decisions regarding the need for service. Direct online determination of these indices requires flow rate and power measurements and would be too expensive for a commercial product. However, it is possible to estimate these quantities using low-cost on-line measurements and a compressor map, which is available from the compressor manufacturer.

Compressor maps give refrigerant mass flow rate and compressor power consumption as functions of suction and discharge pressures (or temperatures) for a specified suction superheat. These data can be correlated and used with on-line suction and discharge measurements to estimate cooling capacity and EER. Since the compressor map covers almost all the operating conditions, this model should be reasonably accurate unless the compressor is not operating properly.

The compressor map can be obtained from the manufacturer. Rather than correlating mass flow rate directly, the compressor map data are used to calculate the volumetric efficiency of the compressor and then volumetric efficiency is correlated. Volumetric efficiency (η_v) is defined as the ratio of volumetric flow rate at the suction of the compressor to the volumetric displacement rate of the compressor. With this definition, the mass flow rate is

$$\dot{m}_r = \eta_v \frac{NV}{v_1}$$

where N is the number of suction strokes per unit time, V is the displacement volume, and v_1 is the inlet specific volume. After several trials, the following form for correlating volumetric efficiency was adopted

$$\eta_v = a_0 + a_1 \frac{P_{dis}}{P_{suc}} + a_2 \left(\frac{P_{dis}}{P_{suc}} \right)^2 + a_3 (T_{amb} - T_{suc})^{a_4}$$

where a_0 , a_1 , a_2 , a_3 , a_4 are empirical coefficients, P_{suc} is suction pressure, P_{dis} is discharge pressure, T_{amb} is compressor ambient temperature, T_{suc} is suction temperature. The cooling capacity of the unit is estimated according to

$$\dot{Q}_{cap} = \dot{m}_r (h_1 - h_3)$$

where h_1 is refrigerant enthalpy leaving the evaporator and h_3 is the refrigerant enthalpy entering the evaporator. The refrigerant enthalpy entering the evaporator is assumed to be the same as the enthalpy exiting the condenser and is calculated using refrigerant property correlations with pressure and temperature as inputs. The refrigerant enthalpy leaving the evaporator is evaluated with pressure and temperature as inputs.

Similar to mass flow rate, compressor power consumption, \dot{W} , is correlated using the following equation

$$\dot{W} = \frac{NV}{v_1} \left(b_0 + b_1 \frac{P_{dis}}{P_{suc}} + b_2 \left(\frac{P_{dis}}{P_{suc}} \right)^2 + b_3 (T_{amb} - T_{suc})^{b_4} \right)$$

where b_0 , b_1 , b_2 , b_3 , and b_4 are empirical coefficients.

EER is calculated from the estimated cooling capacity and power as

$$EER = \frac{\dot{Q}_{cap}}{\dot{W}}$$

where the units of EER are Btu/h-W.

3.4 Fault detection

With the statistical rule-based FDD technique, faults can be detected and separated in one step by calculating the probabilities that the current operating mode belongs to different fault modes. However, to simplify the diagnosis procedure and improve the overall performance, it is advisable to separate fault detection from fault diagnosis.

The fault detection classifier uses the residuals between the measurements and the model expectation to detect the possible presence of faults in the system. When the system is running under normal conditions (no faults), the residual(s) are assumed to be normally distributed with a mean of zero (see two-dimensional example in Figure 3-3). When a fault becomes severe, the distribution of the residual(s) should drift from the zero mean (see Figure 3-4). A fault is detected if a significant difference in the residual distribution is detected. That is, when the overlap of the actual distribution and the expected distribution of the residual(s) decreases to a preset value (the classification error threshold), a fault is considered to be at present.

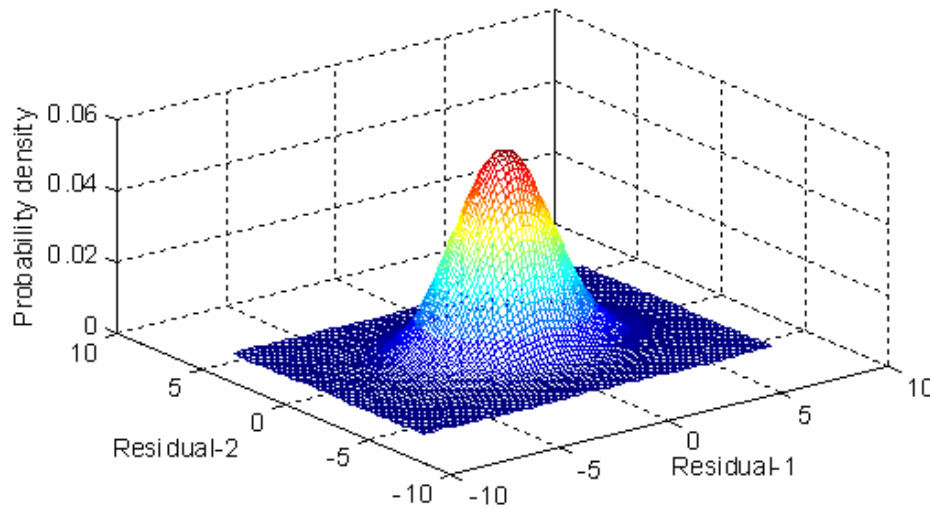


Figure 3-3 2-dimensional residual distribution when system is running in a normal mode

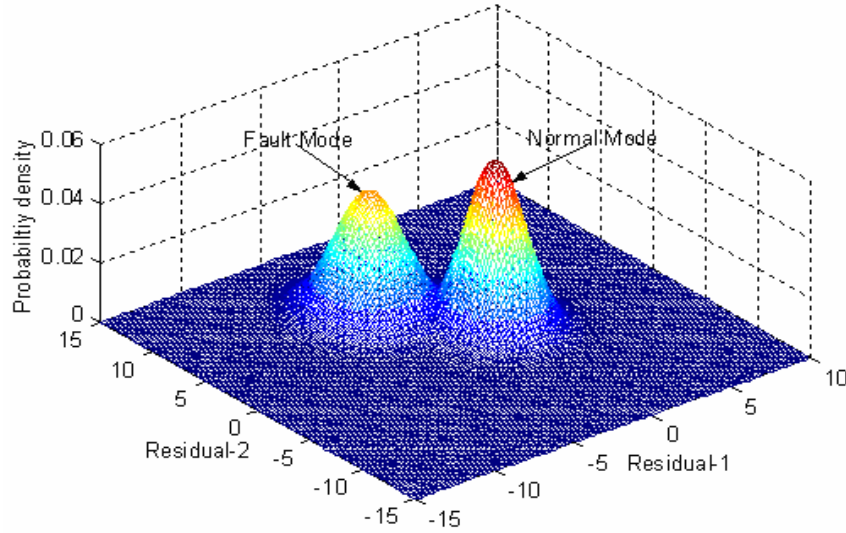


Figure 3-4 2-dimensional residual distribution when system is running in a fault mode

The residual distributions can be characterized in terms of the covariance matrix Σ_{normal} and mean vector M_{normal} and depicted in the residual space plane as in Figure 3-5. In the residual space plane, any operating state (point) outside the normal operating region is classified as faulty. The normal operating ellipse is the fault detection boundary.

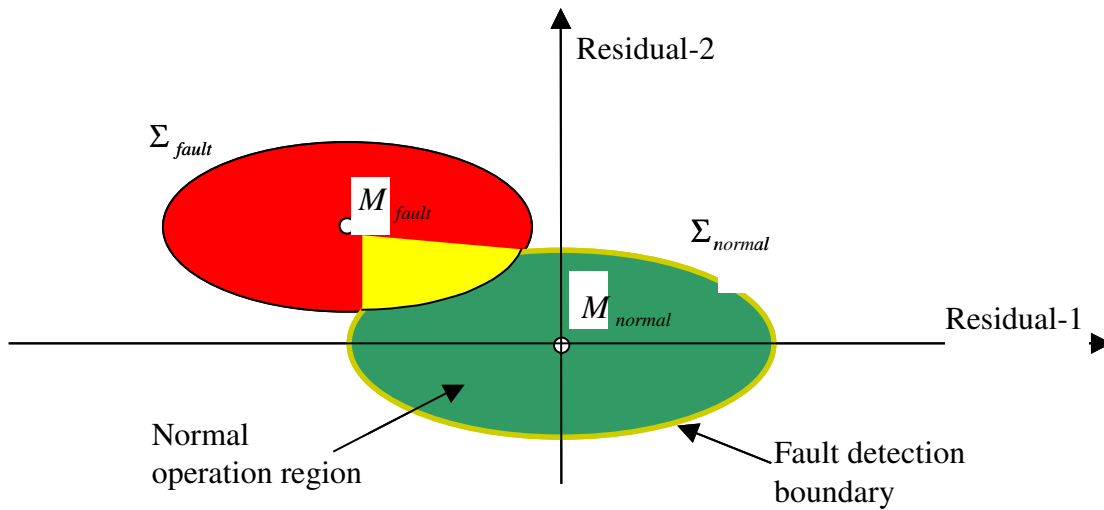


Figure 3-5 2-dimensional residual distribution

The probability that the current operation is normal can be estimated by calculating the overlapping area between the current and normal residual distributions. Direct calculation of this overlap for high dimensional (e.g., 7-dimensional for our case) probability distributions cannot be performed in real time on a microcomputer. Therefore, some simplifications are necessary. The following sections consider simplifications to calculate fault probabilities and a new method that does not require probability calculations.

3.4.1 Probability method

3.4.1.1 Independence assumption

The proposed FDD technique uses 7 temperature residuals to detect and diagnose 5 possible faults for systems with a fixed expansion device. To calculate the overlap of two 7-dimensional distributions, a seven-dimensional integral should be computed. Rossi and Braun (1997) simplified the calculation by assuming that each dimension is independent. However, by checking the normal operation data gathered by Breuker (1997), it has been found that the covariance matrix in normal operation is far from diagonal (see Figure 3-6).

$$\begin{bmatrix} \underline{0.0185} & 0.0115 & 0.0556 & -0.0041 & 0.0271 & 0.0005 & -0.0100 \\ 0.0115 & \underline{0.0120} & 0.0185 & 0.0021 & -0.0068 & 0.0016 & -0.0113 \\ 0.0556 & 0.0185 & \underline{1.0544} & 0.1108 & 0.9209 & 0.0106 & -0.1390 \\ -0.0041 & 0.0021 & 0.1108 & \underline{0.0596} & 0.1794 & 0.0001 & -0.0530 \\ 0.0271 & -0.0068 & 0.9209 & 0.1794 & \underline{1.6472} & -0.0086 & -0.2350 \\ 0.0005 & 0.0016 & 0.0106 & 0.0001 & -0.0086 & \underline{0.0025} & -0.0021 \\ -0.0100 & -0.0113 & -0.1390 & -0.0530 & -0.2350 & -0.0021 & \underline{0.0700} \end{bmatrix}$$

Figure 3-6 Covariance matrix Σ_{normal} of residuals at normal operation

Although Rossi and Braun (1997) and Breuker and Braun (1998b) obtained some good results using this assumption, in theory, it is possible to sacrifice fault detection sensitivity (see Figure 3-7) or introduce false alarms (see Figure 3-8) with this assumption.

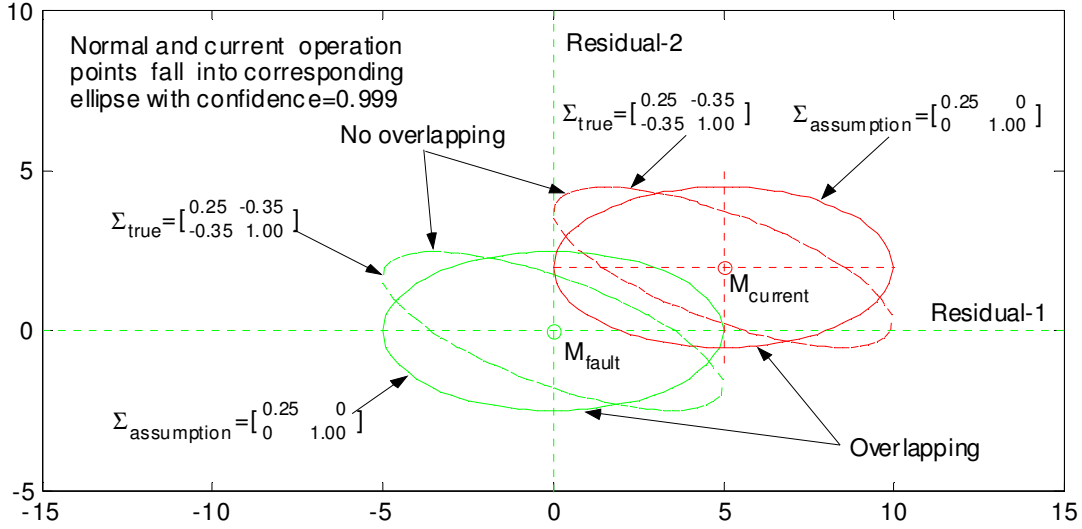


Figure 3-7 Fault detection sensitivity sacrificed by independence assumption

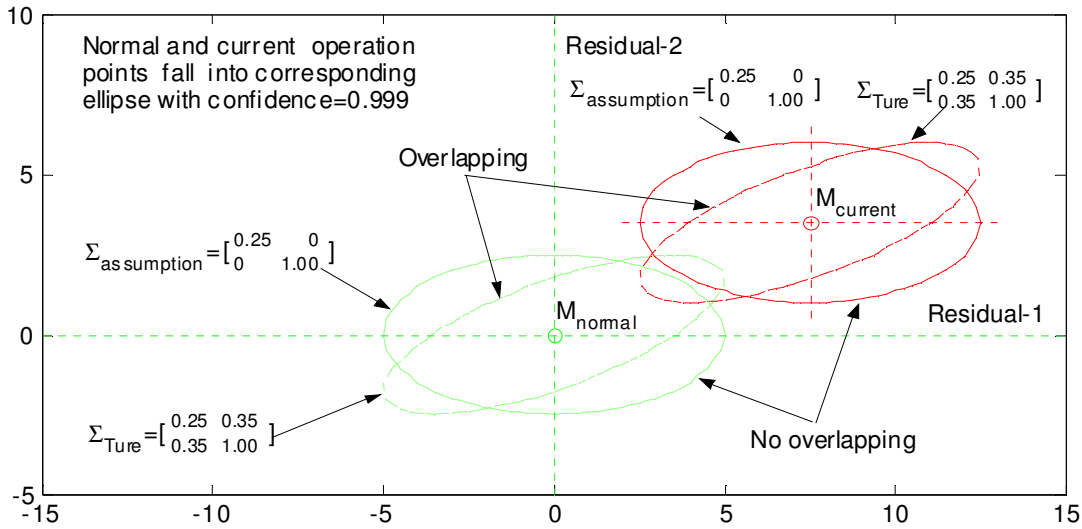


Figure 3-8 False alarm introduced by independence assumption

Figure 3-7 illustrates a situation where fault detection sensitivity will be sacrificed if independence is assumed. In this case, there is no overlap between the current and normal operating modes with confidence of 0.999 (using the “true” covariance matrix), so the current operation is indicated as faulty if the detection threshold is set at 0.001. However if independence is assumed (using the “assumed” covariance matrix), there is a large

overlapping region, about a quarter of the ellipse (probability equal to 0.25), between the current and normal operating mode. The fault detection classifier will consider the current operating mode as normal with the same threshold of 0.001. Consequently, fault detection sensitivity is sacrificed (later calculation results in chapter 4 show this also).

In Figure 3-8, there is a small overlapping region between the normal and current distributions, whose probability is more than 0.001, so that the current operation would be considered as normal. However, the assumption of independence would lead to classification of a fault and a false alarm. Although false alarms can be avoided by setting a high threshold, this will reduce sensitivity.

3.4.1.2 Monte-Carlo (MC) simulation method

An alternative to the independence assumption is to use Monte-Carlo simulation to calculate overlapping areas for high-dimensional probability distributions.

Given a general normal distribution $N_X(M_X, \Sigma_X)$, whose characteristic parameters are mean vector M_X and covariance matrix Σ_X , the probability P_Ω within area Ω_X is calculated with the following steps:

1. From the given Σ_X of X - *space*, find the whitening transformation of $Y = \Lambda^{-1/2} \Phi X$, where X is any point in the original space, Λ and Φ are the eigenvalue matrix and eigenvector matrix of Σ_X , respectively, and Y is the corresponding point in the transformed space.
2. In the transformed Y - *space* with $\Sigma_Y = I$, generate N (>10.000) independent and normally distributed samples, Y_1, Y_2, \dots, Y_N , with zero expected vector and unit covariance matrix.
3. Transform back the generated samples to the X - *space* by $X_i = \Phi \Lambda^{1/2} Y_i \quad (i = 1, 2, \dots, N)$.
4. Add M_X to the samples in the X - *space* as $X_i + M \quad (i = 1, 2, \dots, N)$.

5. Calculate the number of points N_{Ω} within Ω_x and then calculate the frequency of

$$f = \frac{N_{\Omega}}{N}.$$

6. Repeat previous five steps K (>10) times and approximate the probability P_{Ω} by averaging the frequencies f_j ($j = 1, 2, \dots, K$).

This method cannot only approximate the theoretical value at any accuracy but can also be implemented using a microcomputer. Although the Monte-Carlo simulation method is accurate and provides a good way to check other probability methods, it requires relatively large memory and computation time. So it is a good off-line analysis tool but still not computationally efficient enough for on-line fault detection and diagnosis. Section 4 compares results of the Monte-Carlo simulation and the independence assumption methods.

3.4.2 Normalized distance method

This section presents a simpler approach, termed the normalized distance method, to do fault detection.

For a 1-dimensional normal distribution $N_x(\mu_{normal}, \sigma_{normal})$, it is well-known that

$$prob(|x - \mu_{normal}| < 3\sigma_{normal}) \approx 99.73\% \quad or \quad prob\left(\frac{|x - \mu_{normal}|}{\sigma_{normal}} < 3\right) \approx 99.73\%$$

where, $\frac{|x - \mu_{normal}|}{\sigma_{normal}}$ can be seen as the distance between x and the mean μ_{normal} normalized by the standard deviation σ_{normal} . The probability for all x whose normalized distance from the mean μ_{normal} is less than 3 is about 99.73%. This can be used for fault detection with the following procedure:

1. Set a threshold α for false alarms. Normally α is a very small value, say 0.0027, which means the probability for false alarm is 0.0027.

2. Calculate the maximum normalized distance d_{\max} corresponding to the given false alarming threshold α by referring to a normal distribution table. For $\alpha = 0.0027$, the corresponding maximum normalized distance d_{\max} is equal to 3.
3. Given a measurement x_i , calculate the normalized distance by $d_i = \frac{|x_i - \mu_{normal}|}{\sigma_{normal}}$. If $d_i \leq d_{\max}$, the supervised system is considered to be normal with a confidence of $1 - \alpha$. On the contrary, if $d_i > d_{\max}$, then a fault is assumed with a false alarm probability of α .

This method eliminates the need for the probability calculation and requires very little computation and memory.

Inspired by the 1-dimensional case, the idea for one dimension can be extended to the multi-dimensional case. The condition for normal operation can be rewritten as

$$\begin{aligned}
 \text{prob}\left(\frac{|x - \mu_{normal}|}{\sigma_{normal}} < d_{\max}\right) &= 1 - \alpha \\
 \Rightarrow \\
 \text{prob}((x - \mu_{normal})(\sigma_{normal}^2)^{-1}(x - \mu_{normal}) < d_{\max}^2) &= 1 - \alpha
 \end{aligned}$$

For a multi-dimensional case, the statistical parameters became vectors or matrices: x becomes a vector X , μ_{normal} becomes vector M_{normal} , and σ_{normal}^2 becomes matrix Σ_{normal} . Therefore,

$$\text{prob}((X - M_{normal})^T \Sigma_{normal}^{-1} (X - M_{normal})) < d_{\max}^2 = 1 - \alpha$$

The key to generalizing from the 1-dimensional to a multi-dimensional case is determining d_{\max}^2 for given $1 - \alpha$. It can be proven that $(X - M_{normal})^T \Sigma_{normal}^{-1} (X - M_{normal})$ satisfies a $\chi^2(n)$ distribution (see Appendix 2), where n is the dimension of the given distribution. So the procedure to apply the normalized distance method to a multi-dimensional case is almost identical to the 1-dimensional case:

1. Set a threshold α for false alarms.
2. Calculate d_{\max}^2 by referring to a $\chi^2(n)$ distribution table or some software for a given $1-\alpha$ and dimension n . Table 3-1 shows some α and corresponding d_{\max}^2 values for dimension $n = 7$.
3. Given a measurement X_i , calculate the normalized distance squared by $d_i^2 = (X_i - M_{\text{normal}})^T \Sigma_{\text{normal}}^{-1} (X_i - M_{\text{normal}})$. If $d_i^2 \leq d_{\max}^2$, then the supervised system is assumed normal with a confidence of $1-\alpha$. On the contrary, if $d_i^2 > d_{\max}^2$, then a fault is assumed with a false alarming probability of α .

Table 3-1 α and corresponding d_{\max}^2 for dimension $n = 7$

α	0.1	0.01	0.001	0.0001	0.00001	0.000001
$1-\alpha$	0.9	0.99	0.999	0.9999	0.99999	0.999999
d_{\max}^2	12.0170	18.4753	24.3219	29.8775	35.2585	40.5218

3.5 Fault diagnosis

After a fault is detected it is important to determine which component of the system is faulty.

3.5.1 Fault diagnosis rules

To identify the detected fault from known fault types, it is important to know the characteristics of each fault type expressed as a set of diagnostic rules. For example, when a system with a fixed expansion device has a refrigerant leak,

- evaporating temperature will decrease;
- suction line superheat will increase;
- condensing temperature will decrease;
- liquid line subcooling will decrease;
- discharge line temperature will increase;
- the temperature difference between condenser inlet and outlet air will decrease;
- the temperature difference between evaporator inlet and outlet air will decrease.

When a fault is detected and the above phenomena appear, it can be concluded that the system has a refrigerant leakage fault. The evaluation of whether the states increase or decrease must be done relative to the values under normal operation, which depend upon the driving conditions. The normal state models provide the estimates of the normal states as a function of driving conditions. However, there is uncertainty in both the current measurements and the model predictions. Therefore, it is necessary to utilize a classifier to identify which rule has the greatest probability of being correct and to evaluate whether the evidence is strong enough to make a diagnosis.

3.5.2 Fault diagnosis classification

The diagnostic rules are expressed as positive and negative changes in residuals, so that each fault type corresponds to a unique quadrant of a multi-dimensional residual space. To decide which fault is the most probable is equivalent to identifying which quadrant the current measurement belongs to. Combined with the normal operating ellipse, coordinate axes form the fault diagnosis boundary (see Figure 3-9).

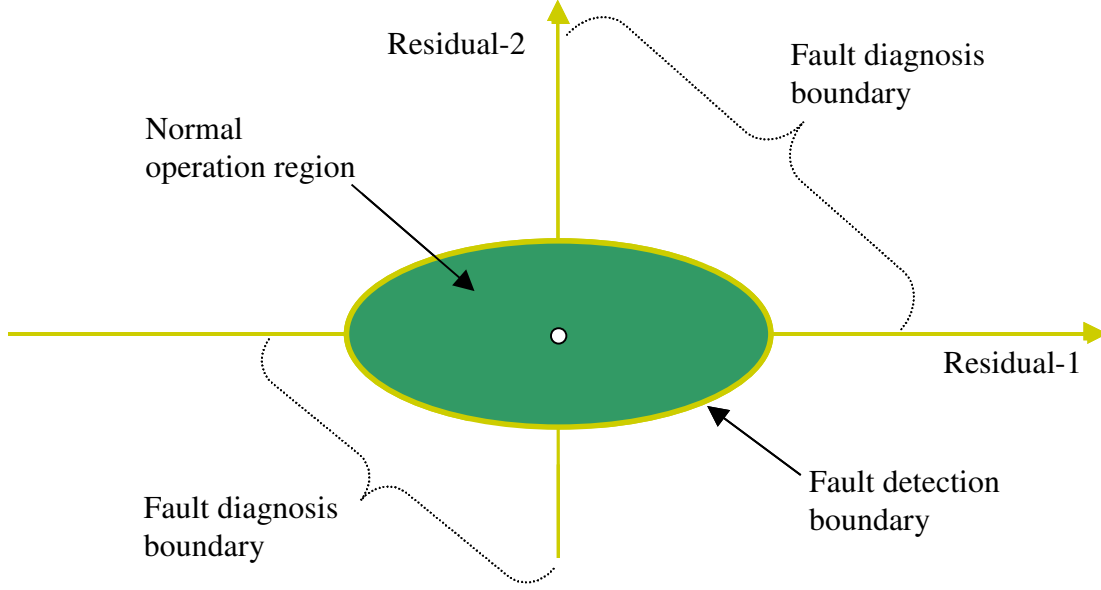


Figure 3-9 Fault Detection and Diagnosis boundaries

Two methods were considered in this study: the probability and distance methods.

3.5.2.1 Probability Method

The probability method is based on statistical parameters associated with current operation. According to the sampling data, the covariance matrix $\Sigma_{current}$ and mean $M_{current}$ are estimated. The probabilities of different faults occurring is then estimated by calculating the overlap of the probability distribution within each fault quadrant.

Ideally, the residuals reside at the origin of the multi-dimensional space at normal operating states. As the fault develops, the probability of the current distribution within each fault quadrant is calculated. To simplify calculation of probability within each fault quadrant, Rossi and Braun (1997) assumed that the distributions of all measurements are independent. The following equation was re-derived by Chen (2000):

$$w_j = \prod_{k=1}^m \frac{1}{2} \left[1 + C_{jk} \operatorname{erf} \left(\frac{M_{current}(k) - M_{normal}(k)}{\sqrt{2\Sigma_{current}(k,k)}} \right) \right]$$

where

j is the index of fault type j,

w_j is the probability of fault type j ,

M is the sample mean vector,

Σ is the covariance matrix,

$C_{jk} = 1$ if $M_{current}(k) - M_{normal}(k)$ has the same sign as d_{jk} ; $C_{jk} = -1$, otherwise.

Subscript *normal* is for normal distribution

Subscript *current* is for current distribution

k is the index of the measurement.

When the probability of the most likely fault class exceeds that of the second most likely class by a preset threshold (fault probability ratio threshold), a diagnosis is made.

It has been shown that the 7 residuals are not truly independent. So it is necessary to validate the assumption of independence. Similar to fault detection, Monte-Carlo simulation can be used to evaluate the probability for each fault. Table 3-2 shows the results of the two different methods for refrigerant leakage at 20% load using the data collected by Breuker (1997). Appendix 3 lists all the other results. From the results, it can be seen that the probability values are different but the trends are the same. The probability of refrigerant leakage increases with the level of this fault. At low fault levels, a liquid-line restriction has the highest probability for both methods. However, the fault detection threshold would not be sufficient to allow diagnosis at this level. Both methods would diagnose the correct fault at higher levels. However, the evidence for refrigerant leakage is much stronger when the probabilities are estimated with the Monte-Carlo approach. This leads to better FDD sensitivity and a lower risk of false alarms.

Table 3-2 Refrigerant Leak at 20% load

Fault Level	Method	Refrigerant Leak	Comp. Valve Leak	Liquid Line Restriction	Cond. Foul	Evap. Foul
Normal	Monte-Carlo	0	0.0010	0	0	0
	Independent	0.0008	0.0007	0.0015	0.0009	0.0004
3.5%	Monte-Carlo	0	0	0.0034	0	0
	Independent	0.0016	0.0004	0.0028	0.0004	0.0002
7%	Monte-Carlo	0.0318	0.	0.0135	0	0
	Independent	0.0039	0.0002	0.0027	0.0002	0.0001
10%	Monte-Carlo	0.0803	0	0.0041	0	0
	Independent	0.0067	0.0001	0.0017	0	0
14%	Monte-Carlo	0.1037	0	0.0004	0	0
	Independent	0.0023	0.0001	0.0008	0.0001	0.0001

3.5.2.2 Distance method

The probability methods require estimates of the covariance matrices for normal and current operation, Σ_{normal} and $\Sigma_{current}$, and integration of the overlapping areas within each of the fault quadrants. To perform these calculations without the assumption of independence is not practical within a microprocessor controller. Figure 3-10 depicts a 2-dimensional example of a simpler approach to fault diagnosis that does not require integration of the probability distributions.

This method is called the simple distance method. In figure 3-10, there are two Cartesian coordinates: one for the residual space with dashed coordinate axes and the other for the double residual space with solid coordinate axes. This is because residuals, the difference between measurements and model predictions, are not distributed with zero mean value when the system operates normally because of modeling error. Assuming that the residual mean value of normal operation is M_{normal} , which can be calculated before the FDD system is commissioned, the residual of current operation can be denoted in the double residual space by subtracting M_{normal} from it. Later discussion is based on the double residual space. As shown in Figure 3-10, there are two possible faults occupying two different quadrants in the 2-dimensional space with 4 quadrants (this assumption will make FDD more difficult because in our case there are only 5 faults for a 7-dimensional space with 128 quadrants).

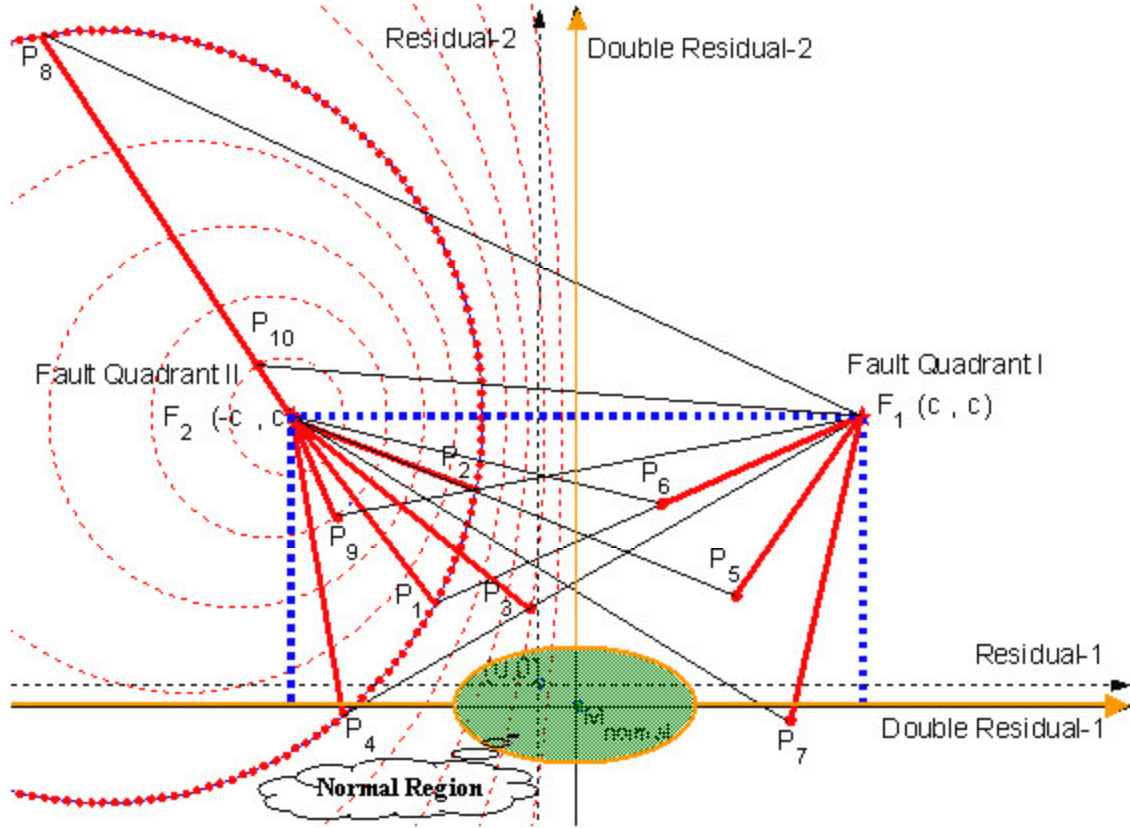


Figure 3-10 Distance method for fault diagnosis

The distance method can be described as follows:

1. Predefine a fault point for each fault quadrant. All the distances of the fault point from all the axes should have the same magnitude and the magnitude should not be less than the largest expected residual (e.g., 20 F). In Figure 3-10, F_1 and F_2 represent fault quadrant I and fault quadrant II, respectively.
2. Calculate the distance from the current operating point to each fault point, for example, the distance from P_1 to F_1 , $\|P_1 F_1\| = \|F_1 - P_1\|$ and from P_1 to F_2 , $\|P_1 F_2\| = \|F_2 - P_1\|$.
3. Find the two lines with the smallest distance ($\|P_1 F_2\|$ in Figure 3-10) and the second smallest distance ($\|P_1 F_1\|$ in Figure 3-10).

4. Calculate the distance ratio of the smallest distance to the second smallest distance

$$(ratio_{dist} = \frac{\|P_1 F_2\|}{\|P_1 F_1\|}, \text{ in Figure 3-10}).$$

5. When the distance ratio is less than a preset threshold β , then a fault corresponding to the minimum distance will be indicated. In Figure 3-10, the fault point with the minimal distance for P_1 is F_2 , and if the distance ratio is lower than a preset threshold, fault II would be indicated.

Establishing a fault point at the largest expected residual makes the distance ratio inversely related to fault level. For a 2-dimensional space, appendix 4 proves that all the points with the same distance ratio, $ratio_{dist}$, are on a circle characterized with:

$$(x + \frac{c(1 + ratio_{dist}^2)}{1 - ratio_{dist}^2})^2 + (y - c)^2 = (\frac{2ratio_{dist}c}{1 - ratio_{dist}^2})^2$$

where x and y are the coordinates in the double residual space and c is the distance of the fault point from each of axes. Given a value of c , a distance ratio corresponds to a circle in a cluster of circles (see Figure 3-10), whose centers have the same y coordinate, c . Since $ratio_{dist}$ is always less than 1, the scale of the magnitude of x coordinates of the center is larger than c and increases with increasing distance ratio, and the radius of the circles will increase with increasing distance ratio but with larger magnitude than the former. In Figure 3-10, points P_1 , P_2 and P_4 are on the same circle and thus have the same distance ratio, while their distance ratios are smaller than that of point P_3 . It is obvious that the fault associated with point P_3 is less serious than those of points P_1 , P_2 and P_4 .

It is important, but not critical, to have a reasonable estimate of the largest expected residual in order to locate the fault points. For the example of Figure 3-10, point P_8 has a significantly higher fault level than points P_1 , P_2 , P_3 , P_4 , P_9 and P_{10} , and yet has the same distance ratio as points P_1 , P_2 and P_4 , and a lower distance ratio than points P_9 and P_{10} . However, if only correct diagnosis of fault type is necessary and diagnosis of relative fault

level is not strictly considered, the standard of selecting the parameter c associated with the largest expected residual can be loosened. The choice for c is not critical and the actual fault level can be more severe without any loss in accuracy for diagnosing a particular fault type. For example, in Figure 3-10, if fault point P_{10} is the most severe fault level expected, F_1 and F_2 will be reasonably good fault points.

From Figure 3-10, it can be seen that points P_3 , P_6 and P_7 will be classified to fault type I. Points P_4 and P_7 are two special cases. They are actually not in any fault quadrant but considering the statistical uncertainty, point P_4 would be classified to fault type II and point P_7 to fault type I. It should be pointed out that there is a risk of classifying points in other non-fault quadrants to some predefined fault type, but the risk to make wrong diagnoses is very low because of the following reasons: 1) The fault detection classifier filters all the normal operating points. In Figure 3-10, although the ellipse normal region covers all 4 quadrants, it is classified as normal through the fault detection step; 2) The probability of faulty operation appearing in other non-fault quadrants is very small, if the important faults are considered and predefined by corresponding quadrants. It is very important to consider as many faults as possible, at least those occurring frequently.

The risk of making wrong diagnoses for non-defined faults is not unique to the distance diagnosis method. The only way to avoid this risk is to calculate the probability or distance in all quadrants, fault and non-fault quadrants. For the probability method, it is not economical to consider all 128 quadrants for a 7-dimensional case. Although probably not necessary, all quadrants could be considered for the distance method because of low memory and computational requirements.

3.6 Fault evaluation and decision

Fault evaluation is particularly important when the performance of a component is degrading slowly over time, such as occurs for heat exchanger fouling. In this case, it is possible to detect a fault well before it is severe enough to justify the service expense. In

contrast, abrupt failures such as broken belts would not require the evaluation step when it is obvious that the fault should be repaired (e.g., the system no longer maintains comfort).

In principle, fault evaluation could be achieved by minimizing lifetime operating costs. An optimal service scheduler would purchase service when it contributes to reducing overall costs. Important costs to consider are: maintenance, energy, equipment down time (i.e. the cost of not maintaining comfort or refrigeration set point), premature component wear (avoidable service costs), and liability costs associated with injury to people, damaged facilities, or pollution of the environment. With the exception of maintenance and energy, the other costs are difficult to quantify. The optimization problem could be simplified by assuming that the comfort, premature wear, and liability costs are much larger than the service cost to repair them. This is equivalent to assigning an infinite economic penalty for these conditions (i.e. treating them as constraints) and minimizing the combined costs of energy and service. With these considerations in mind, the following four fault evaluation criteria are proposed for HVAC systems.

1. ECONOMIC CRITERIA - Service is required when it contributes to the reduction of the combined costs of energy and service over the lifetime of the unit.
2. COMFORT CRITERIA - Service is required when the equipment is not capable of maintaining building comfort.
3. SAFETY CRITERIA - Service is required when the operating state of the equipment could lead to damage or injury (e.g. liquid entering a compressor or head pressure above the tube burst pressure).
4. ENVIRONMENTAL CRITERIA - Service is required when the equipment is polluting the environment. This criteria is included for refrigerant leaks.

Criteria 3 and 4 are relatively straightforward to apply. Service should be performed whenever a fault within these categories is detected and diagnosed. The second criteria could be handled in the same fashion: wait until the equipment could not maintain comfort conditions and use the output of the diagnostic classifier to identify the required service. However, this approach would lead to some loss in productivity. A better approach would

be to evaluate the cooling capacity online and compare it to the peak required cooling capacity. Using this information, service could be scheduled in advance of a loss in comfort.

The first criterion is based upon trading off service and energy costs. Rossi and Braun (1996) developed a method for determining optimal service times for cleaning condensers and replacing evaporator filters that balances service and energy costs. The method requires a measurement of power and is relatively straightforward to apply. Inputs to the method are the residual between the current power and power associated with normal operation and the ratio of service cost to the unit energy cost.

Online cooling capacity and power measurements are expensive and not practical for implementation within an FDD system for HVAC&R at this time. However, these measurements can be estimated using the approach described earlier in this report.

4 Case study and method comparisons

The last report (2001) described normal operating data gathered by Breuker (1997) under controlled conditions in a laboratory and described their use in training the normal state models. In addition, five types of artificial faults were introduced at different fault levels and the unit was tested at different load levels in order to evaluate the performance of the FDD technique. The five types of faults are refrigerant leakage, compressor valve leakage, condenser fouling, evaporator fouling and liquid line restriction. Each fault was introduced at four or five different levels and tested at five different load levels: 20%, 40%, 60%, 80% and 100%. In all, there are 120 sets of fault data available to test the proposed FDD method. Appendix 5 describes how the faults were introduced. For each of the different load levels, the unit was on for different amounts of time. The total cycle time was held constant at 45 minutes and the on time was varied for the different load levels. For example at 20% load, the unit ran for 9 minutes and was off for 36 minutes. Two consecutive transient start-up responses were generated and data were recorded at 5-second intervals at each of the conditions and fault levels. Measurements from the second transient were used to evaluate the FDD performance.

Since transient states were recorded when the faults were introduced, data was fed to the FDD prototype at the sampling frequency in order to imitate on-line FDD.

4.1 Measurement preprocessing

Since only transient-state data with the compressor on were recorded, there was no need to use a measurement filter to detect whether the compressor is on or not. The steady-state detector uses both the slope and variance methods. The length of the moving window was set at 24 sampling data points (sampling time of 5 seconds). To make sure the system reaches steady state, all the three driving conditions and 7 state variables were used for steady state detection. The detector thresholds for the 10 variables are listed in table 4-1.

Table 4-1 Thresholds for steady-state detector's variables

	T_{ai}	T_{ra}	ϕ_{ra}	T_{evap}	T_{cond}	T_{hg}	T_{sc}	T_{sh}	ΔT_{ca}	ΔT_{ea}
Slope Threshold (F / s)	0.028	0.028	0.0025	0.028	0.028	0.055	0.058	0.095	0.025	0.025
Variance Threshold (F^2)	0.28	0.28	0.05	0.58	0.28	0.58	0.58	1.085	0.25	0.25

4.2 Normal state and overall performance models

4.2.1 Normal state models

Inputs of the normal state models are ambient air temperature T_{ai} , return air temperature T_{ra} , and return air relative humidity ϕ_{ra} . As outlined in a previous report, the polynomial plus GRNN approach is used to predict evaporating temperature T_{evap} , condensing temperature T_{cond} , discharge line or hot gas temperature T_{hg} , liquid line subcooling T_{sc} , suction line superheat T_{sh} , condenser air temperature increase ΔT_{ca} , and evaporator air temperature decrease ΔT_{ea} . In addition, another four variables: discharge line pressure P_{hg} , suction line pressure P_{suct} , suction line temperature T_{suct} and liquid line temperature T_{ll} were added in order to provide inputs for the overall performance (cooling capacity and power consumption). The parameters of polynomial plus GRNN are listed in Table 4-2. Steady-state training data with 95 normal operating conditions were used to train the model and steady-state testing data with 35 normal operating conditions were used to test the model. Results of the model performance were presented in the last report for this project.

Table 4-2 Polynomial plus GRNN model parameters

	T_{evap}	T_{cond}	T_{hg}	T_{sc}	T_{sh}	ΔT_{ca}	ΔT_{ea}	T_{suct}	T_{ll}	P_{hg}	P_{suct}
Polynomial order	1	1	2	2	1	1	2	1	2	2	2
GRNN Spread	0.1	0.1	0.1	0.1	0.1	0.1	0.1	0.1	0.1	0.1	0.1

4.2.2 Overall performance models

Overall performance models (virtual sensors) include refrigerant flow rate, cooling capacity, compressor power consumption and EER. The compressor map data for the test unit are shown in Table 4-3. The models for volumetric efficiency and power were fit using the manufacturer's compressor maps and then used to estimate mass flow rate, cooling capacity, power consumption, and EER for test conditions with the system operating normally. Direct measurements of flow rate and compressor power consumption were also available for these test conditions and used to evaluate the performance of this simple estimation approach. Figures 4-1 and 4-2 show comparisons between measurements and estimates for mass flow rate and cooling capacity. Predictions of mass flow rate and cooling capacity based upon the compressor map were about 8% higher than those determined directly from measurements. This difference may be within the normal range of expected performance of this compressor model or possibly, this compressor deteriorated after extensive laboratory testing.

As shown in Figure 4-3, the agreement between measured and estimated power consumption was somewhat better and the overall bias in the predictions was much smaller. The model overpredicts compressor power for high values and underpredicts for low values. This could result from compressor deterioration. A deteriorated compressor would produce lower mass flow rate with a lower isentropic efficiency. However, power consumption is proportional to flow rate and inversely proportional to efficiency. Thus, there is a tradeoff between these two factors. Furthermore, mass flow rate and efficiency depend upon the

operating conditions so that the tradeoffs vary between conditions associated with low and high power consumption.

Figure 4-4 shows comparisons of EER, where EER is the ratio of cooling capacity to power consumption. At conditions associated with high values of EER (cooler ambients), the model overpredicts cooling capacity and underpredicts compressor power leading to relatively large errors in EER. For lower values of EER (warmer ambients), the cooling capacity and power consumption error have the same sign and are of similar magnitude, resulting in smaller errors in EER.

Other results for system performance when the system operates at fault conditions are given in a later section (see evaluation section).

Table 4-3 Compressor map data

Condensing Temperature °F (°C)	CAPACITY (BTU/HR)					Evaporating Temperature			
	-10 (-23.3)	0 (-17.8)	10 (-12.2)	20 (-6.7)	30 (-1.1)	40 (4.4)	45 (7.2)	50 (10.0)	55 (12.8)
80 (26.7)	23700	30000	37300	45900	55900	67700	74200	81300	89000
90 (32.2)	22500	28700	35900	44200	53800	65100	71500	78300	85600
100 (37.8)	21000	27200	34100	42200	51500	62400	68500	75000	82100
110 (43.3)	.	25400	32200	40000	49000	59500	65300	71600	78300
120 (48.9)	.	.	30100	37600	46300	56400	62000	68000	74500
130 (54.4)	.	.	.	35100	43500	53200	58500	64300	70500
140 (60.0)	40600	49900	55000	60600	66500
150 (65.6)	46500	51500	56700	62400

Condensing Temperature °F (°C)	EER (BTU/WATT-HR)					Evaporating Temperature			
	-10 (-23.3)	0 (-17.8)	10 (-12.2)	20 (-6.7)	30 (-1.1)	40 (4.4)	45 (7.2)	50 (10.0)	55 (12.8)
80 (26.7)	8.7	11.0	13.6	16.7	20.5	24.8	27.2	29.8	32.5
90 (32.2)	7.2	9.2	11.5	14.3	17.5	21.3	23.4	25.7	28.1
100 (37.8)	5.9	7.7	9.7	12.0	14.8	18.1	20.0	21.9	24.1
110 (43.3)	.	6.3	8.0	10.1	12.5	15.3	16.8	18.5	20.4
120 (48.9)	.	.	6.6	8.3	10.4	12.8	14.1	15.6	17.1
130 (54.4)	.	.	.	6.8	8.6	10.6	11.7	13.0	14.3
140 (60.0)	7.0	8.8	9.7	10.8	11.9
150 (65.6)	7.2	8.0	8.9	9.9

Condensing Temperature °F (°C)	POWER (WATTS)					Evaporating Temperature			
	-10 (-23.3)	0 (-17.8)	10 (-12.2)	20 (-6.7)	30 (-1.1)	40 (4.4)	45 (7.2)	50 (10.0)	55 (12.8)
80 (26.7)	2720	2740	2740	2740	2730	2730	2730	2730	2730
90 (32.2)	3110	3110	3110	3090	3080	3060	3050	3050	3040
100 (37.8)	3550	3540	3530	3500	3470	3450	3430	3420	3410
110 (43.3)	.	4040	4010	3980	3940	3900	3880	3860	3840
120 (48.9)	.	.	4570	4520	4470	4420	4390	4370	4350
130 (54.4)	.	.	.	5140	5080	5020	4980	4950	4930
140 (60.0)	5770	5690	5660	5620	5590
150 (65.6)	6460	6420	6380	6340

Condensing Temperature °F (°C)	CURRENT (AMPS)					@ 230 Volts			
	-10 (-23.3)	0 (-17.8)	10 (-12.2)	20 (-6.7)	30 (-1.1)	40 (4.4)	45 (7.2)	50 (10.0)	55 (12.8)
80 (26.7)	9.5	9.5	9.5	9.5	9.5	9.5	9.5	9.5	9.5
90 (32.2)	10.3	10.3	10.2	10.2	10.2	10.2	10.2	10.2	10.2
100 (37.8)	11.2	11.2	11.1	11.1	11.1	11.1	11.1	11.1	11.1
110 (43.3)	.	12.3	12.2	12.1	12.1	12.0	12.0	12.0	12.0
120 (48.9)	.	.	13.5	13.4	13.3	13.2	13.2	13.2	13.1
130 (54.4)	.	.	.	14.8	14.7	14.6	14.5	14.5	14.4
140 (60.0)	16.3	16.2	16.1	16.0	16.0
150 (65.6)	18.0	17.9	17.8	17.7

Condensing Temperature °F (°C)	MASS FLOW (LBS/HR)					Evaporating Temperature			
	-10 (-23.3)	0 (-17.8)	10 (-12.2)	20 (-6.7)	30 (-1.1)	40 (4.4)	45 (7.2)	50 (10.0)	55 (12.8)
80 (26.7)	280	356	443	543	658	792	866	947	1030
90 (32.2)	275	353	441	542	657	790	864	944	1030
100 (37.8)	266	347	436	537	653	786	859	939	1020
110 (43.3)	.	336	427	529	646	779	853	931	1020
120 (48.9)	.	.	416	519	636	770	844	922	1010
130 (54.4)	.	.	.	507	625	759	833	912	996
140 (60.0)	612	747	821	900	984
150 (65.6)	733	808	887	971

Nominal Performance Values (±5%) based on minimum 24 hours run-in. Subject to change without notice.

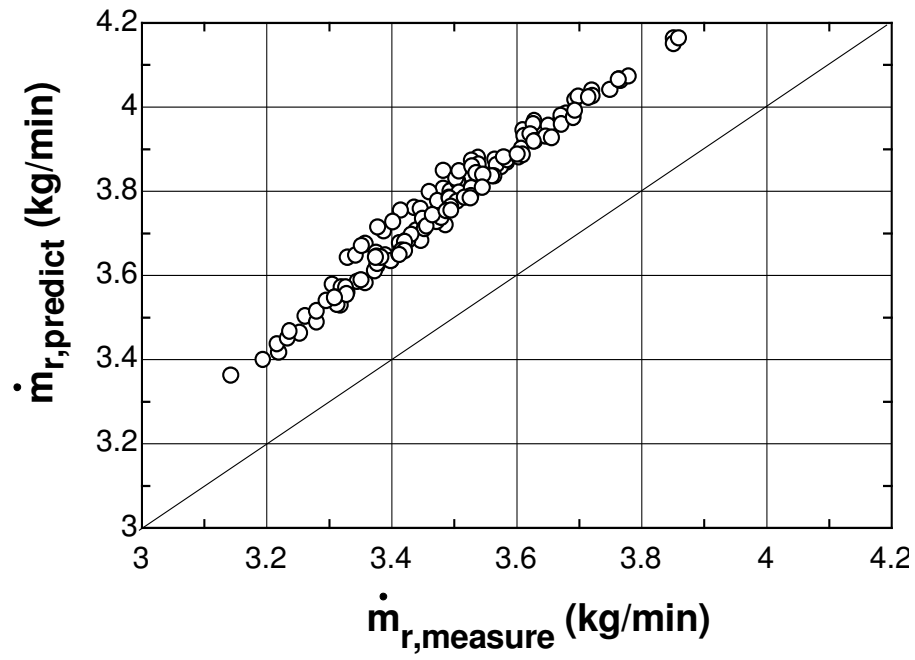


Figure 4-1 Refrigerant flow rate prediction and measurement

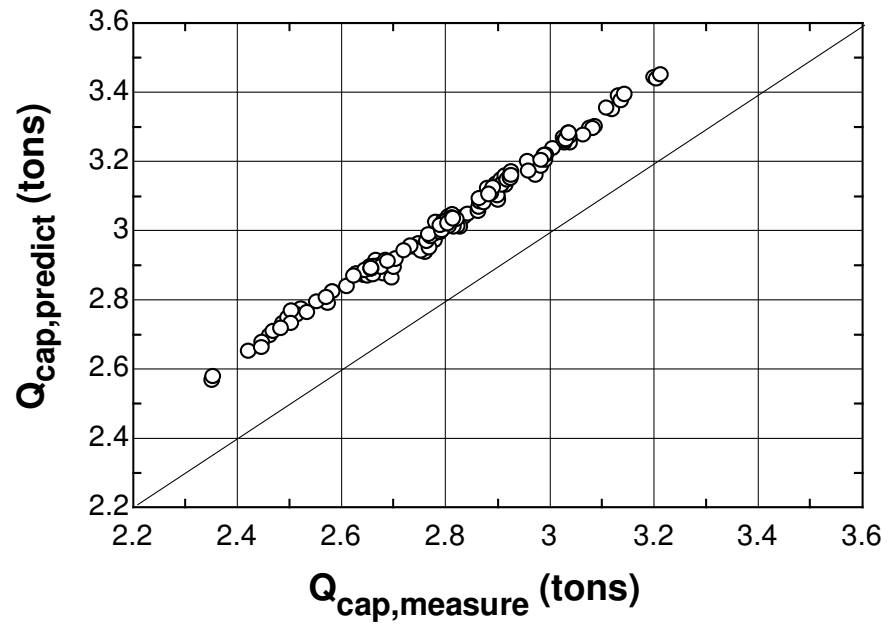


Figure 4-2 Cooling capacity prediction and measurement

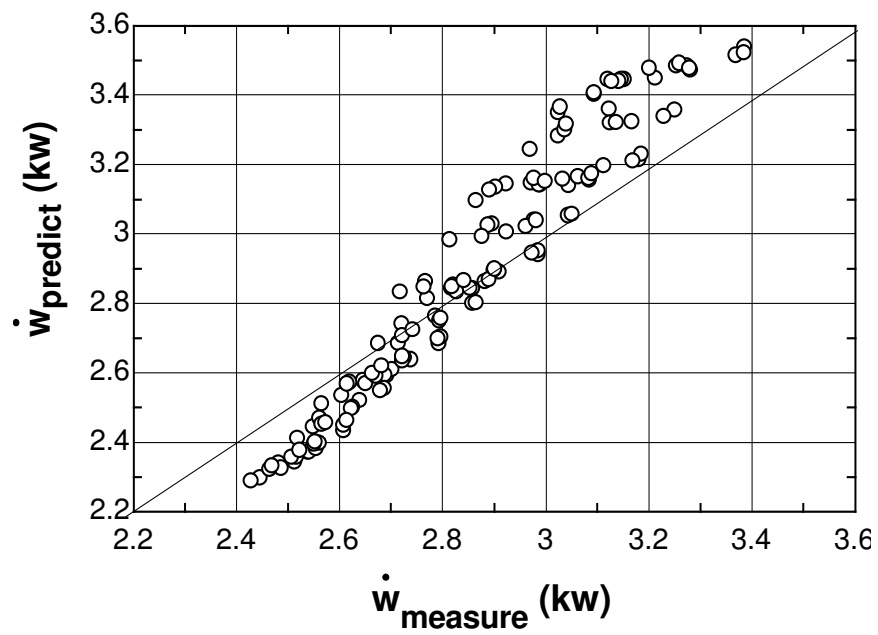


Figure 4-3 Compressor power consumption prediction and measurement

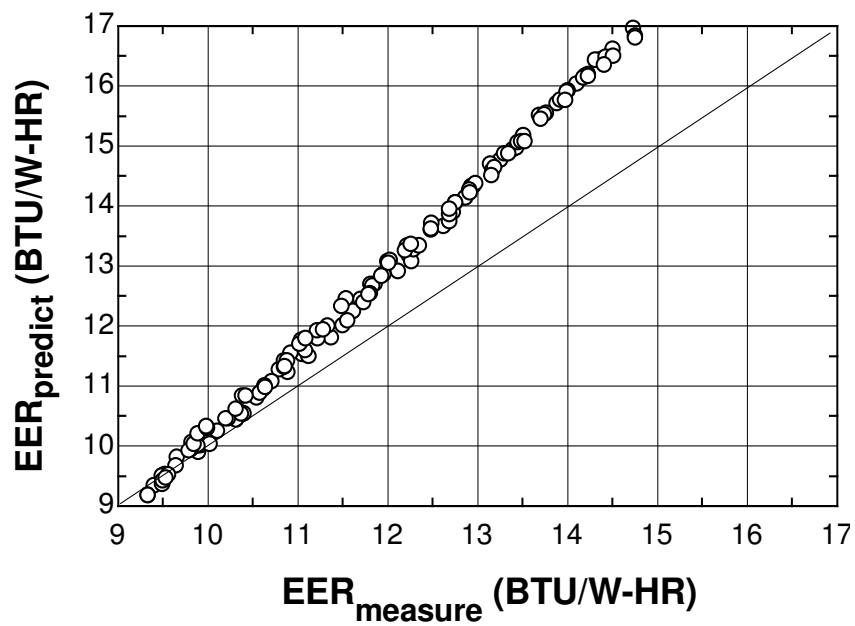


Figure 4-4 EER prediction and measurement

4.3 Fault detection and diagnosis

4.3.1 Fault detection

The technique used for fault detection is the normalized distance method. Three necessary parameters are the covariance matrix and mean vector associated with normal operation, Σ_{normal} and M_{normal} , and the false alarm threshold α . The former two parameters are calculated from normal operating residuals. The covariance matrix Σ_{normal} was shown in Figure 3-5 for the test unit and M_{normal} is

$$M_{normal} = [0.6255 \quad 0.6963 \quad -1.3140 \quad 0.6544 \quad -1.1815 \quad 0.1798 \quad -0.1060]^T$$

To make the false alarm rate as small as possible, the false alarm threshold α was set at 0.0000001.

4.3.2 Fault diagnosis rules

Based on theoretical analysis, Rossi and Braun (1995) summarized the residual direction change of five faults. Breuker and Braun (1997) confirmed all rules using laboratory tests except for the compressor valve leakage fault rule. These modified rules are summarized in Table 4-4 (+ indicates an increase in the residual, - decrease). The modification made was that the hot gas temperature should increase with the occurrence of compressor valve leakage. The simulation model Rossi and Braun used to generate the diagnostic rules did not consider the energy of the refrigerant which leaks back into the suction line from the discharge side when a compressor valve leaks. This refrigerant increases the compression chamber temperature and tends to increase the discharge temperature. These rules were intended to be generic for all similar types of air conditioners and should not require on-line learning.

Ideally, the residuals reside at the origin of the multi-dimensional space at normal operating states. However, practically there is measurement noise, system disturbances and modeling error. Typically, residuals will be distributed with non-zero M_{normal} and Σ_{normal} even at

normal operating conditions. The set of rules, M_{normal} and Σ_{normal} define a multi-dimensional space where each class (fault type) occupies a unique fault space. This means that the Cartesian axes and normal operation ellipse form the classification boundaries.

Table 4-4 Fault diagnosis rules

Fault type	T_{evap}	T_{sh}	T_{cond}	T_{sc}	T_{hg}	ΔT_{ca}	ΔT_{ea}
Refrigerant leakage	-	+	-	-	+	-	-
Comp. Valve Leak	+	-	-	-	-	-	-
Liquid Restriction	-	+	-	+	+	-	-
Condenser Fouling	+	-	+	-	+	+	-
Evaporator Fouling	-	-	-	-	-	-	+

4.3.3 Fault diagnosis method

The distance method is used to do fault diagnosis. The only two parameters are the distance of fault points from the axes (c) and the diagnosis threshold (β). For this case study, c was set at 10 F and β was set at 0.99 to avoid wrong diagnosis.

4.4 FDD results and comparisons with previous method

The FDD results are shown in Tables 4-5 to 4-20. For each fault, there are three tables. The first table contains information about the detection results. Each entry in these tables gives three pieces of data: the number of data points for each transient when the unit is on, the number of points that were considered normal, and the number of points that were classified as a fault. The number of data points increases with load level because the unit is on a longer portion of the total cycle time. The second table in each set of three gives diagnostic results. Each entry in these tables also gives three pieces of data: the number of steady state points, the number of correct diagnoses, and the number of false diagnoses. The third table in each set of three gives average diagnostic ratios for both the correct and incorrect diagnoses.

In reviewing the results of Tables 4-5 through 4-20, it is apparent that all faults, except refrigerant leakage, were detected and diagnosed correctly at all fault levels for all the load levels. Refrigerant leakage was detected and diagnosed at all fault levels greater than the lowest level and at all load levels. There were no incorrect diagnoses for any faults. If the diagnosis threshold were set at 0.9995, refrigerant leakage would be detected and diagnosed at the lowest fault level and all load levels. However, this change would lead to two incorrect diagnoses for liquid line restriction at the lowest fault level with the 20% and 40% load levels. The only difference between the rules for refrigerant leakage and liquid line restriction is associated with liquid line subcooling. Furthermore, liquid line subcooling is very noisy and experiences a relatively small change when there is a fault. To avoid incorrect diagnoses, the diagnosis threshold should be set to 0.99.

Compared with the previous results obtained by Breuker and Braun (1998b), the proposed FDD prototype has superior performance. Breuker and Braun (1998b) presented results in terms of a “1st Detected” and “All Detected” level. The “1st Detected” level is the level at which the fault was first successfully detected and diagnosed throughout the data set. The “All Detected” level is the level at which the fault was detected and diagnosed during all steady-state operating conditions. Table 4-21 gives comparative results for the two methods in terms of these performance indices. As an example, the “1st Detected” refrigerant leakage fault level is 3.5% for this proposed prototype and 7.8% for Breuker and Braun’s result, and “All Detected” refrigerant leakage fault level is 7% for the proposed prototype and 9.5% for Breuker and Braun’s result. Similar results occur for the other faults. The results of Breuker and Braun do show some “1st Detected levels” that are below the lowest level of fault that was introduced. This is because their results were calculated by interpolating the impact of the fault level. This was not done for the current study.

Table 4-5 Detected (**normal**, **fault**) points/ total operation points @ compressor valve leakage fault

		Load Level				
		20%	40%	60%	80%	100%
Fault Level	Normal	(11,0)/98	(70,0)/147	(186,0)/277	(208,0)/335	(229,0)/359
	7%	(0,31)/108	(0,80)/191	(0,56)/324	(0,319)/401	(0,336)/396
	14%	(0,2)/72	(0,49)/143	(0,88)/216	(0,222)/288	(0,544)/593
	19%	(0,21)/108	(0,33)/190	(0,220)/304	(0,340)/423	(0,511)/569

	28%	(0,19)/108	(0,90)/164	(0,229)/324	(0,341)/432	(0,717)/782
--	-----	------------	------------	-------------	-------------	-------------

Table 4-6 (**Right**, **wrong**) diagnosed points/ total detected steady-state points @ compressor valve leakage fault

		Load Level				
		20%	40%	60%	80%	100%
Fault Level	Normal	(11,0)/11	(70,0)/70	(186,0)/186	(208,0)/208	(229,0)/229
	7%	(31,0)/31	(80,0)/80	(56,0)/56	(319,0)/319	(336,0)/336
	14%	(2,0)/2	(49,0)/49	(88,0)/88	(222,0)/222	(554,0)/554
	19%	(21,0)/21	(33,0)/33	(220,0)/220	(340,0)/340	(511,0)/511
	28%	(19,0)/19	(90,0)/90	(229,0)/229	(341,0)/341	(717,0)/717

Table 4-7 Average (**right**, **wrong**) fault diagnosis ratio @ compressor valve leakage fault

		Load Level				
		20%	40%	60%	80%	100%
Fault Level	Normal	(N/A, N/A)	(N/A, N/A)	(N/A, N/A)	(N/A, N/A)	(N/A, N/A)
	7%	(0.9613, N/A)	(0.9418, N/A)	(0.9379, N/A)	(0.9260, N/A)	(0.9367, N/A)
	14%	(0.9163, N/A)	(0.9157, N/A)	(0.9080, N/A)	(0.9075, N/A)	(0.9190, N/A)
	19%	(0.8813, N/A)	(0.8877, N/A)	(0.8887, N/A)	(0.8716, N/A)	(0.8806, N/A)
	28%	(0.7747, N/A)	(0.7794, N/A)	(0.7630, N/A)	(0.7358, N/A)	(0.7260, N/A)

Table 4-8 Detected (**normal**, **fault**) points/ total operation points @ refrigerant leakage fault

		Load Level				
		20%	40%	60%	80%	100%
Fault Level	Normal	(11,0)/98	(70,0)/147	(186,0)/277	(208,0)/335	(229,0)/359
	3.5%	(0,30)/104	(0,67)/145	(0,137)/216	(0,245)/329	(0,67)/175
	7%	(0,7)/108	(0,121)/215	(0,160)/279	(0,251)/334	(0,164)/224
	10%	(0,24)/107	(0,62)/166	(0,170)/324	(0,255)/336	(0,731)/780
	14%	(0,6)/72	(0,11)/145	(0,120)/322	(0,314)/394	(0,581)/646

Table 4-9 (**Right**, **wrong**) diagnosed points/ total detected steady-state points @ refrigerant leakage fault

		Load Level				
		20%	40%	60%	80%	100%
Fault Level	Normal	(11,0)/11	(70,0)/70	(186,0)/186	(208,0)/208	(229,0)/229
	3.5%	(7,23)/30	(5,62)/67	(137,0)/137	(245,0)/245	(67,0)/67

7%	(7,0)/7	(121,0)/121	(160,0)/160	(251,0)/251	(164,0)/164
10%	(24,0)/24	(62,0)/62	(170,0)/170	(255,0)/255	(731,0)/731
14%	(6,0)/6	(11,0)/11	(120,0)/120	(314,0)/314	(581,0)/581

Table 4-10 Average (right, wrong) fault diagnosis ratio @ refrigerant leakage fault

		Load Level				
		20%	40%	60%	80%	100%
Fault Level	Normal	(N/A, N/A)	(N/A, N/A)	(N/A, N/A)	(N/A, N/A)	(N/A, N/A)
	3.5%	(0.9973, 0.9974)	(0.9994, 0.9968)	(0.9814, N/A)	(0.9924, N/A)	(0.9779, N/A)
	7%	(0.9800, N/A)	(0.9858, N/A)	(0.9772, N/A)	(0.9884, N/A)	(0.9776, N/A)
	10%	(0.9404, N/A)	(0.9779, N/A)	(0.9481, N/A)	(0.9665, N/A)	(0.9582, N/A)
	14%	(0.9095, N/A)	(0.9508, N/A)	(0.9404, N/A)	(0.9855, N/A)	(0.9693, N/A)

Table 4-11 Detected (normal, fault) points/ total operation points @ condenser fouling fault

		Load Level				
		20%	40%	60%	80%	100%
Fault Level	Normal	(11,0)/98	(70,0)/147	(186,0)/277	(208,0)/335	(229,0)/359
	14.6%	(0,20)/108	(0,110)/216	(0,230)/319	(0,35)/431	(0,650)/712
	29.2%	(0,34)/108	(0,107)/190	(0,126)/216	(0,196)/288	(0,435)/480
	41.4%	(0,2)/90	(0,80)/173	(0,211)/309	(0,344)/418	(0,207)/265
	56.1%	(0,14)/108	(0,133)/216	(0,232)/311	(0,333)/410	(0,484)/544

Table 4-12 (Right, wrong) diagnosed points/ total detected steady-state points @ condenser fouling fault

		Load Level				
		20%	40%	60%	80%	100%
Fault Level	Normal	(11,0)/11	(70,0)/70	(186,0)/186	(208,0)/208	(229,0)/229
	14.6%	(20,0)/20	(110,0)/110	(230,0)/230	(35,0)/35	(650,0)/650
	29.2%	(34,0)/34	(107,0)/107	(126,0)/126	(196,0)/196	(435,0)/435
	41.4%	(2,0)/2	(80,0)/80	(211,0)/211	(344,0)/344	(207,0)/207
	56.1%	(14,0)/14	(133,0)/133	(232,0)/232	(333,0)/333	(484,0)/484

Table 4-13 Average (**right**, **wrong**) fault diagnosis ratio @ condenser fouling fault

		Load Level				
		20%	40%	60%	80%	100%
Fault Level	Normal	(N/A , N/A)	(N/A , N/A)	(N/A , N/A)	(N/A , N/A)	(N/A , N/A)
	14.6%	(0.9329, N/A)	(0.9542, N/A)	(0.9373, N/A)	(0.9544, N/A)	(0.9555, N/A)
	29.2%	(0.8197, N/A)	(0.8345, N/A)	(0.8266, N/A)	(0.8366, N/A)	(0.8594, N/A)
	41.4%	(0.6598, N/A)	(0.6834, N/A)	(0.6924, N/A)	(0.7060, N/A)	(0.7323, N/A)
	56.1%	(0.5135, N/A)	(0.5606, N/A)	(0.5521, N/A)	(0.5438, N/A)	(0.5757, N/A)

Table 4-14 Detected (**normal**, **fault**) points/ total operation points @ evaporator fouling fault

		Load Level				
		20%	40%	60%	80%	100%
Fault Level	Normal	(11 , 0)/98	(70 , 0)/147	(186 , 0)/277	(208 , 0)/335	(229 , 0)/359
	12%	(0 , 38)/108	(0 , 122)/199	(0 , 192)/316	(0 , 111)/313	(0 , 136)/188
	24%	(0 , 39)/105	(0 , 77)/157	(0 , 217)/323	(0 , 314)/429	(0 , 330)/405
	35%	(0 , 6)/96	(0 , 98)/211	(0 , 23)/216	(0 , 200)/288	(0 , 71)/128

Table 4-15 (**Right**, **wrong**) diagnosed points/ total detected steady-state points @ evaporator fouling fault

		Load Level				
		20%	40%	60%	80%	100%
Fault Level	Normal	(11 , 0)/11	(70 , 0)/70	(186 , 0)/186	(208 , 0)/208	(229 , 0)/22 2
	12%	(38 , 0)/38	(122 , 0)/122	(192 , 0)/192	(111 , 0)/111	(136 , 0)/136
	24%	(39 , 0)/39	(77 , 0)/77	(217 , 0)/217	(314 , 0)/314	(330 , 0)/33 0
	35%	(21 , 0)/21	(33 , 0)/33	(220 , 0)/220	(340 , 0)/340	(511 , 0)/511

Table 4-16 Average (**right**, **wrong**) fault diagnosis ratio @ evaporator fouling fault

		Load Level				
		20%	40%	60%	80%	100%
Fault Level	Normal	(N/A , N/A)	(N/A , N/A)	(N/A , N/A)	(N/A , N/A)	(N/A , N/A)
	12%	(0.9843, N/A)	(0.9400, N/A)	(0.8950, N/A)	(0.8497, N/A)	(0.8302, N/A)
	24%	(0.8252, N/A)	(0.7929, N/A)	(0.7888, N/A)	(0.7615, N/A)	(0.7485, N/A)
	35%	(0.7352, N/A)	(0.6988, N/A)	(0.6604, N/A)	(0.6639, N/A)	(0.6550, N/A)

Table 4-17 Detected (**normal**, **fault**) points/ total operation points @ liquid-line restriction fault

		Load Level				
		20%	40%	60%	80%	100%
Fault Level	Normal	(11,0)/98	(70,0)/147	(186,0)/277	(208,0)/335	(229,0)/359
	5%	(0,21)/108	(0,119)/216	(0,44)/324	(0,183)/400	(0,156)/479
	10%	(0,5)/72	(0,73)/162	(0,171)/277	(0,281)/432	(0,87)/371
	15%	(0,15)/108	(0,111)/215	(0,184)/294	(0,244)/360	(0,231)/440
	20%	(0,12)/105	(0,91)/216	(0,283)/301	(0,314)/424	(0,538)/630

Table 4-18 (**Right**, **wrong**) diagnosed points/ total detected steady-state points @ liquid-line restriction fault

		Load Level				
		20%	40%	60%	80%	100%
Fault Level	Normal	(11,0)/11	(70,0)/70	(186,0)/186	(208,0)/208	(229,0)/229
	5%	(21,0)/21	(119,0)/119	(44,0)/44	(183,0)/183	(156,0)/156
	10%	(5,0)/5	(73,0)/73	(171,0)/171	(281,0)/281	(87,0)/87
	15%	(15,0)/15	(111,0)/111	(184,0)/184	(244,0)/244	(231,0)/231
	20%	(12,0)/12	(91,0)/91	(183,0)/183	(314,0)/314	(538,0)/538

Table 4-20 Average (**right**, **wrong**) fault diagnosis ratio @ liquid-line restriction fault

		Load Level				
		20%	40%	60%	80%	100%
Fault Level	Normal	(N/A , N/A)	(N/A , N/A)	(N/A , N/A)	(N/A , N/A)	(N/A , N/A)
	5%	(0.9107, N/A)	(0.9035, N/A)	(0.9318, N/A)	(0.9243, N/A)	(0.9450, N/A)
	10%	(0.8095, N/A)	(0.8125, N/A)	(0.8525, N/A)	(0.8685, N/A)	(0.8980, N/A)
	15%	(0.7030, N/A)	(0.7105, N/A)	(0.7607, N/A)	(0.7945, N/A)	(0.8232, N/A)
	20%	(0.6325, N/A)	(0.6512, N/A)	(0.7155, N/A)	(0.7743, N/A)	(0.8272, N/A)

Table 4-21 Performance comparison of previous and improved FDD method

FDD results	Refrigerant leakage (3.5,7,10,14)%		Liquid-line restriction (5,10,15,20)%		Compressor valve leakage (7,14,19,28)%		Condenser fouling (14.6,29.2,41.4,56.1)%		Evaporator fouling (12,24,35)%	
	1 st	All	1 st	All	1 st	All	1 st	All	1 st	All
Breuker	7.8	9.5	6.2	8.1	6.5	14.2	11.6	15.1	11.1	30.9
Improved	3.5	7	5	5	7	7	14.6	14.6	12	12

To evaluate the impact of parameter c on the performance of the FDD method, the results with c equal to 20 F and 1 F were calculated. The results show that the difference between c equal to 20 F and 10 F is very small, while the difference between c equal to 10 F and 1 F is very significant (see Figure 4-5 and Figure 4-6). From Figure 4-5, it can be seen that the distance ratio monotonously decreases with increasing fault level if parameter c is either 10 F or 20 F. However, the distance ratio behavior is different when parameter c is set to 1 F.

From Figure 4-6, it can be seen that the distance ratio is relatively constant with increasing cooling load level for the same fault level if parameter c is set to 10 F or 20 F but has a different behavior when parameter c is set at 1 F. These results illustrate that it is not necessary to have an accurate determination of the largest expected residual, c , as long as it is large enough (e.g, 10 to 20 F).

In summary, the distance method has several following good characteristics. The performance of the method is good (good sensitivity for detecting/diagnosing faults) and is relatively insensitive to the choice of parameters and different operating conditions.

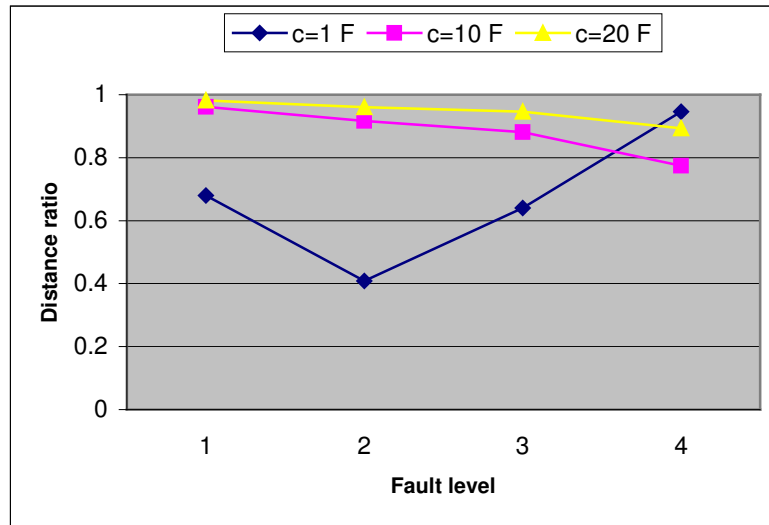


Figure 4-5 Impact of parameter c on the performance of FDD for different compressor valve leakage fault levels with 20% cooling load

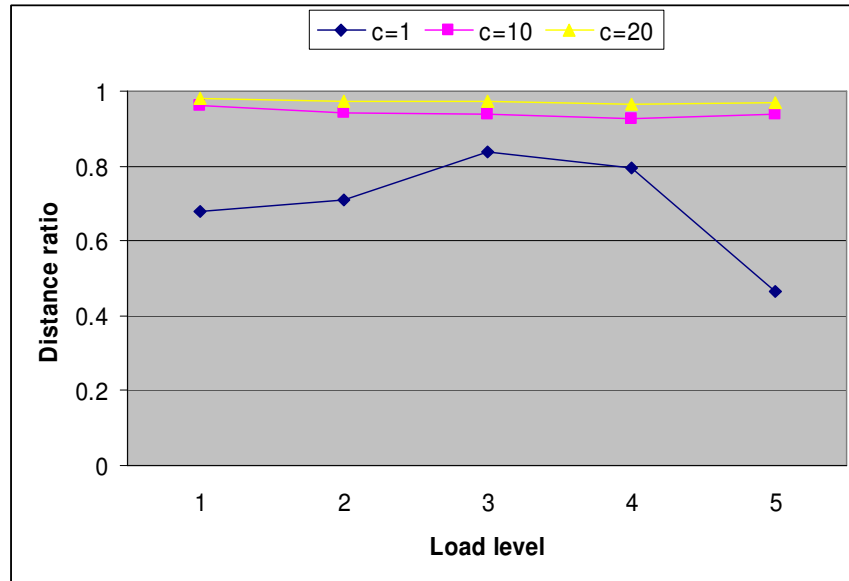


Figure 4-6 Impact of parameter c on the performance of FDD for 3.5% compressor valve leakage fault with different cooling load

4.5 Fault Evaluation Results

The data for the test unit includes refrigerant flow rate, cooling capacity, and power consumption. As a result, it is possible to compare the impact of the different faults on these actual performance indices and those calculated using the compressor maps. Tables 4-22, 4-23 and 4-24 give the actual percent change of system performance and estimated percent change of system performance for different faults.

Except for compressor valve leakage, the trend and magnitude of performance changes with respect to fault levels are similar for the actual and estimated flow rate, cooling capacity and power consumption. Compressor valve leakage has a significant effect on refrigerant flow rate (up to -15%) and thus cooling capacities and compressor power consumption. Refrigerant leakage at the levels considered had a small effect on refrigerant flow rate, cooling capacities, and compressor power consumption. Condenser fouling also had a relatively small effect on refrigerant flow rate and capacities, but had a significant effect on power consumption. Evaporator fouling had a small effect on refrigerant flow rate, compressor power consumption, and cooling capacity. Liquid line restriction had a

significant effect on refrigerant flow rate, and thus cooling capacities and compressor power consumption.

The overall performance models (virtual sensors) do not provide accurate estimates of refrigerant flow rate and cooling capacity when the compressor operates abnormally since they are based upon correlated compressor data obtained for normal operation. When the compressor has a fault, the volumetric and isentropic efficiencies will be reduced.

Table 4-22 Actual /estimated per cent change of compressor power consumption

Fault name	Fault level				
	normal	1	2	3	4
compnv	1/1.3	2/2.4	3/3	4/3.5	7/5.6
refleak	1/1.2	1/-0.7	1/-0.25	-1/-5	-2.5/-6
condfoul	1/1.2	2.5/2.7	4/5.8	7/9.6	10/13.8
evapfoul	1/1.2	1/1.2	-1/0.6	-2/-0.6	
llrestr	1/1.2	1/-2	-0.5/-3.8	-3/-7	-8/-13

Table 4-23 Actual /estimated per cent change of cooling capacity on refrigerant side

Fault name	Fault level				
	normal	1	2	3	4
compnv	1.5/1	-4/7.5	-5/10	-7/12	-15/22
refleak	1/1	1/-0.2	1/-1.6	-1/-3.6	-3/-6.5
condfoul	1/1	1/0.2	-1.5/-0.5	-3.5/-2	-6/-5
evapfoul	1.5/1	0.6/-0.2	-2/-2.5	-4/-3.8	
llrestr	1.5/1	1/-1	-1/-2	-3.5/-6	-12/-12

Table 4-24 Actual /estimated per cent change of refrigerant flow rate

Fault name	Fault level				
	normal	1	2	3	4
compnv	1.5/1.5	-3/8	-5/9.5	-7/12.5	-15/22
refleak	1.5/1.5	-0.2/-1	-1.5/-3	-3/-6	-6/-9
condfoul	1.5/1.5	2/1.5	3/3	3/4	4/5
evapfoul	1.5/1.5	0.5/0.5	-1/-0.4	-2/-2	
llrestr	1.5/1.5	-1.5/-3	-4/-6	-9/-12	-22/-24

5 Conclusions

Following the literature review by Comstock et. al (1999), up-to-date literature on HVAC FDD was reviewed. FDD techniques developed by previous investigators were studied. An improved FDD prototype and a case study were presented. The new FDD technique improves on previous methods in the following aspects:

- ✓ Incorporates a new steady-state detector, which is a combination of the slope and variance methods. This new steady-state detector has better robustness for filtering transient data and thus improves overall FDD performance.
- ✓ Incorporates a new modeling approach for predicting normal operation variables, which was documented in the last report.
- ✓ Incorporates a novel fault detection classifier called the normalized distance method, which eliminates the probability calculation and requires very small memory and computation.
- ✓ Incorporates a new fault diagnosis classifier called the simple distance method. This method also does not require multi-dimensional probability calculations or online estimation of the current covariance matrix.
- ✓ Incorporates overall performance models, which act as virtual sensors to estimate some system performance variables that cannot be economically measured. These system variables can be used to access the impact of the fault on the system performance in order to evaluate whether service should be performed.

6 References

- ASHRAE. 1993. ASHRAE Handbook - 1993 Fundamentals, Atlanta: American Society of Heating, Refrigerating, and Air Conditioning Engineers, Inc., Atlanta, GA 30329.
- Braun, J.E. and Li, Haorong. 2001. Description of FDD modeling approach for normal performance expectation. Progress report submitted to Architectural Energy Corporation.
- Breuker, M.S., 1997. Evaluation of a Statistical, Rule-based Detection and Diagnosis Method for Vapor Compression Air Conditioners, Master's Thesis, School of Mechanical Engineering, Purdue University.
- Breuker, M.S. and Braun, J.E., 1998. Common Faults and Their Impacts for Rooftop Air Conditioners, HVAC&R Research, Vol. 4, No. 3, pp.303-318.
- Breuker, M.S. and Braun, J.E., 1998. Evaluating the performance of a Fault Detection and Diagnostic System for Vapor Compression Equipment, International Journal of Heating, Ventilating, and Air Conditioning and Refrigerating Research, Vol. 4, No. 4, pp.401-425.
- Cacoullos, 1966. "Estimation of a multivariate density," Ann. Inst. Statist. Math, (Tokyo), Vol. 18, no. 2, pp.179-189.
- Carling, P., 2002. Comparison of Three Fault Detection Methods Based on Field Data of an Air-Handling Unit, ASHRAE Transactions 2002, V. 108, Pt.1.
- Chen, B., 2000. Evaluating the potential of on-line fault detection and diagnosis for rooftop air conditioners, Master's Thesis, School of Mechanical Engineering, Purdue University.

Chen, Bin and Braun, J.E, 2000. Simple fault detection and diagnostics methods for packaged air conditioners, Proceedings of the 8th international refrigeration conference, Purdue University.

Chen, Bin and Braun, J.E, 2001. Simple rule-based methods for fault detection and diagnostics applied to packaged air conditioners, ASHRAE Trans., vol. 107, part 1, paper No. AT-01-14-2, 847-857.

Comstock, M.C., J.E. Braun, and B. Chen, 1999, *Literature Review for Application of Fault Detection and Diagnostic Methods to Vapor Compression Cooling Equipment*, Purdue University, Ray W. Herrick Laboratories, Report # HL99-19.

Davis, Coby. 1995. Comparison of steady state detection algorithms. ME 597 Report. Available from Professor Jim Braun, Herrick Labs, Purdue University, West Lafayette, In.

Dexter, Arthur; Pakanen, Jouko (ed.). Demonstrating Automated Fault Detection and Diagnosis Methods in Real Buildings. Espoo. VTT Building Technology, 2001. VTT Symposium 217. 381 p. + app. 13 p.

Dexter, A.L. and Ngo, D., 2001. Fault Diagnosis in Air-Conditioning Systems: A Multi-Step Fuzzy Model-Based Approach, International Journal of Heating, Ventilating, and Air Conditioning and Refrigerating Research, Vol. 7, No. 1, pp.83-102.

Donald F. Specht, 1991. A General Regression Neural Network. IEEE Transactions on Neural Networks. 2 (6): 568-576.

Dyn, N. and Levin, D.,1983. "Iterative solutions of systems originating from integral equations and surface interpolation." SIAM J. Numerical Analysis, vol. 20, pp. 377-390.

Ghiaus, C. 1999. Fault diagnosis of air conditioning systems based on qualitative bond graph, Energy and Buildings 30 (1999) 221-132.

Glass, A.SI, Gruber, P.,Roos, and M., Todtli, J., 1995. Qualitative Model-based fault detection in air-handling units, IEEE control systems Magazine, 15(4): 11-22.

Gordon, J. M., and K. C. Ng. 1994. Thermodynamic modeling of reciprocating chillers. Journal of Applied Physics. 76(6):2769-2774.

Grimmelius, H. T., J. Klein Woud, and G. Been. 1995. On-line failure diagnosis for compression refrigeration plants. International Journal of Refrigeration 18(1):31-41.

Isermann, R. 1984. Process Fault Detection Based on Modeling and Estimation - A Survey, *Automatica*, 20(4): 387-404.

Lee, W., House, J.M. and Shin, D.R., 1997. Fault diagnosis and Temperature Sensor Recovery for an Air-handling unit, ASHRAE Transaction, 103(1): 621-633.

Lee, W.Y. & House, J.M., etc., 1996. Fault diagnosis of an Air-Handling Unit Using Artificial Neural Networks, AHRAE Transactions V.102, Pt.1, pp.540-549,1996

Li, X., H. Hvaezi-Nejad, & J.C. Visier, 1996. Development of a fault diagnosis method for heating systems using neural networks. ASHRAE Transactions 102 (1): 607-614.

Norford, L.K., Wright, J.A., etc., 2002. Demonstration of Fault Detection and Diagnosis Methods for Air-Handling Units, International Journal of Heating, Ventilating, and Air Conditioning and Refrigerating Research, Vol. 8, No. 1, pp.41-71.

Parzen, 1962. On the estimation of a probability density function and the mode, Ann. Math. Stat., 33, pp. 1065-1076.

Rossi, T.M., 1995. Detection, Diagnosis, and Evaluation of Faults in Vapor Compression Cycle Equipment, Ph.D. Thesis, School of Mechanical Engineering, Purdue University.

Rossi, T.M. and Braun, J.E., “Minimizing Operating Costs of Vapor Compression Equipment with Optimal Service Scheduling,” International Journal of Heating,

Ventilating, Air-Conditioning and Refrigerating Research, Vol. 2, No. 1, pp. 23 - 47, 1996.

Rossi, T.M. and Braun, J.E., 1997. A Statistical, Rule-Based Fault Detection and Diagnostic Method for Vapor Compression Air Conditioners, International Journal of Heating, Ventilating, and Air Conditioning and Refrigerating Research, Vol. 3, No. 1, pp.19-37.

Shaw, S.R., Norford, L.K., Luo, D., etc., 2002. Detection and Diagnosis of HVAC Faults Via Electrical Load Monitoring, International Journal of Heating, Ventilating, and Air Conditioning and Refrigerating Research, Vol. 8, No. 1, pp.13-40.

Stylianou, M. & D. Nikanpour. 1996. Performance monitoring, fault detection, and diagnosis of reciprocating chillers. ASHRAE Transactions 114 (4): 615-627.

Yoshida, H. & Kumar, S. 1999. ARX and AFMM model-based on-line real-time data base diagnosis of sudden fault in AHU of VAV system, Energy Conversion & Management 40 (1999) 1191-1206.

Yoshida, H. & Kumar, S. 2001. Development of ARX model based off-line FDD technique for energy efficient buildings, Energy Conversion & Management 22 (2001) 53-59.

Yoshida, H. & Kumar, S. 2001. Online fault detection and diagnosis in VAV air handling unit by RARX modeling, Energy Conversion & Management 33 (2001) 391-401.

Appendix 1 Details Of Statistical Rule-Based Method By Rossi/Braun

The structure of the FDD technique developed by Rossi and Braun (1997) is depicted in Figure 1. The technique requires the measurement of nine temperatures and one relative humidity on the rooftop unit. If the supply voltage to the air conditioner and the supply airflow rate can be assumed constant, the driving conditions (input U) for the vapor compression cycle are the ambient temperature (T_{amb}), return air temperature (T_{ra}) and the return air relative humidity (RH_{ra}). Given those inputs, the performance of the vapor compression cycle is determined. That's, in a normally operating, simple rooftop air conditioning unit (on/off compressor control, fixed speed fans), all the output states (Y) in the system are assumed to be functions of only these three driving conditions. The output state measurements used by this technique are five refrigerant temperatures and two air temperatures. They include: 1) evaporating temperature (T_{evap}), 2) suction line superheat (T_{sh}), 3) condensing temperature (T_{cond}), 4) liquid line subcooling (T_{sc}), 5) hot gas line or compressor outlet temperature (T_{hg}), 6) air temperature rise across the condenser (ΔT_{ca}), and 7) air temperature drop across the evaporator (ΔT_{ea}). A steady-state model is used to describe the relationship between the driving conditions and the expected output states in a normally operating system. By comparing the measurements of the output states (Y_{meas}) with those predicted by the steady-state model (Y_{exp}), residuals (ΔY) are generated. These residuals are used to perform detection and diagnosis. The detection classifier uses the residuals to determine a binary “fault” or “no-fault” output. The diagnostic classifier also uses the residuals to identify the most likely cause of the faulty behavior.

Since a steady-state model is used to predict normal operating states, a steady-state detector must be used to distinguish between transient and steady state operation. The next four sections discuss the various aspects of the technique: a steady-state preprocessor, a steady-state model, a fault detection classifier and a diagnostic classifier.

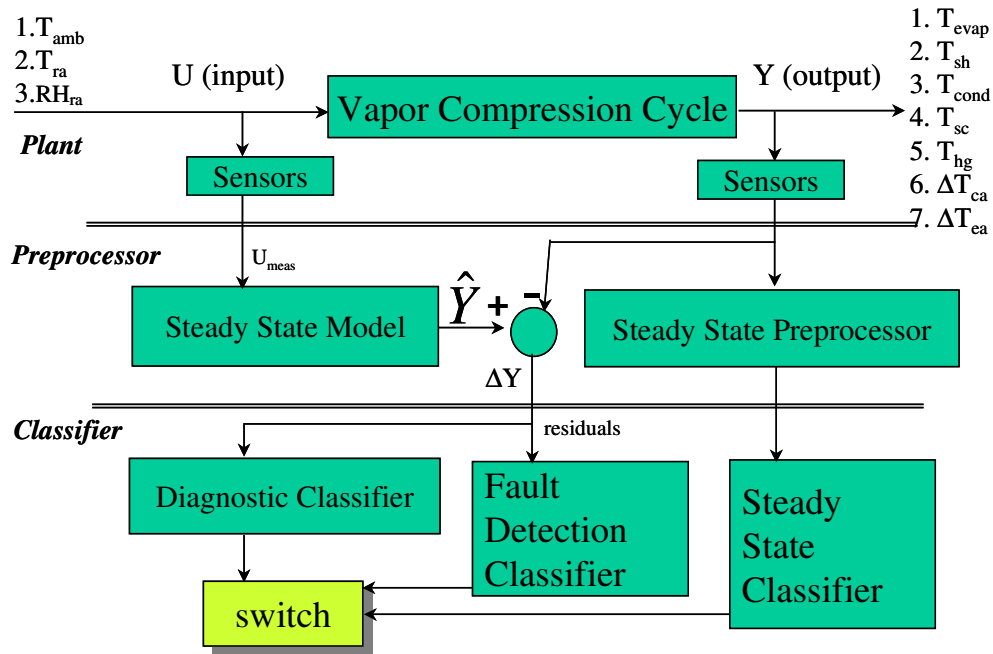


Figure 1 Summary of Rossi/Braun statistical FDD method.

1.1 Steady-state preprocessor

Usually rooftop air conditioners use on/off control for the indoor temperature control. Because of the many on and off cycles, they spend a lot of time in the start up and shut down transient states. However, they also spend a considerable time near steady state. To incorporate a steady-state model in the FDD method, a steady-state detector is used to determine whether the system is operating near steady state. When the output of the steady-state preprocessor is below a preset threshold value, the system is regarded to be in steady state such that the application of a steady-state model is reasonable. Breuker and Braun (1998b) analyzed three different algorithms for the determination of steady-state conditions. They were the slope of the best-fit line through a fixed-length sliding window of recent measurements, the variance of a fixed-length sliding window of recent measurements, and the exponentially weighted variance of a sliding time window. Breuker concluded that the exponentially weighted variance method is the best to use on the transient response of the rooftop air conditioning unit. Compressor discharge temperature was used as the steady-state detection

measurement because it was found to take the longest time to reach steady state among all the measurements.

1.2 Steady-state model

Since a rooftop unit spends much of the time near steady state and the faults will affect the steady-state operation, a steady-state model is appropriate to identify the expected performance. Breuker and Braun (1998b) investigated two model types: linear regression polynomial models and look-up tables. They found that refrigerant suction superheat, hot gas temperature and refrigerant liquid subcooling are best modeled using third-order polynomials. T_{sc} and ΔT_{ea} are best modeled using second-order polynomials. First-order polynomial models perform well for other measurements. A set of 80 training points appeared to be the least amount of data appropriate for training.

A comparison of the linear regression polynomials and look up tables with linear interpolation showed that they result in similar accuracy given the same 80 training points. The difficulty with the look-up table model is that it is hard to get the uncertainty information, which is important for statistical analysis.

The number of inputs required is also important in deciding which type of model to use. Models that used three inputs (return air dry bulb temperature, return air wet bulb temperature and the ambient temperature) generate the most accurate predictions. A two-input model (return wet bulb temperature and ambient temperature) may give similar results, but eliminating the humidity measurement as an input could greatly sacrifice model accuracy in some situations.

1.3 Fault detection classifier

The detection classifier uses residuals to determine whether the current equipment behavior is normal or faulty. The residuals are calculated by comparing the current output measurements with the expected output values generated by a steady-state model. When the current residuals are statistically different than the expected residuals (zero mean), a fault is identified. Figure 2 shows a one-dimensional example of the detection classifier, with the Tsh residual plotted on the x-axis and the output of the probability density function for the Tsh residual plotted on the y-axis. The two curves represent the probabilities $[P(Tsh)]$ of obtaining specific residuals for normal and faulty measurements. The uncertainty of the

residuals is assumed to follow a Gaussian distribution. The integrated overlap of the two distributions, which indicates the likelihood that the faulty distribution of residuals represents normal operation, is termed the classification error. A fault in the system will cause a difference in the mean values and/or standard deviations of the residuals. As the fault becomes progressively worse, the difference between the mean values increases and the classification error decreases. Once the classification error drops below a threshold value, a fault is indicated by the detection classifier. In order to compare the current behavior with expected behavior using all seven output state measurements, an optimal linear classifier (Fukunaga 1990) is used. The residuals for the current and expected operation are fitted to a Gaussian model which can be completely described by the mean vector and covariance matrix (Rossi and Braun, 1997). A value of 10^{-3} has been used as the threshold for classification error for all quantitative analyses published by Rossi and Braun.

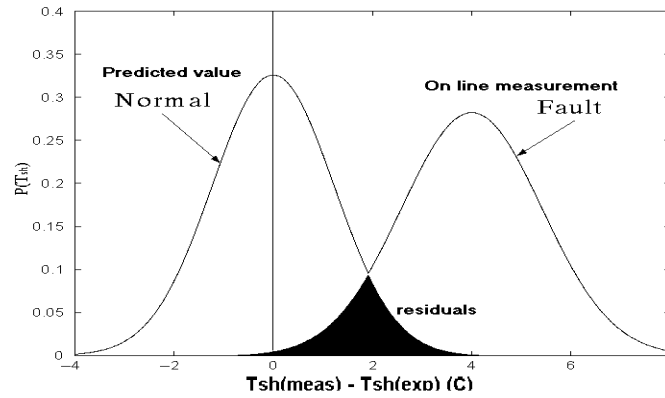


Figure 2 Residual in 1-D.

1.4 Diagnosis classifier

The role of the diagnostic classifier in the FDD system is to determine the most likely explanation of the faulty behavior occurring in the system using a set of diagnosis rules. Rossi and Braun (1997) developed a set of rules related to the faults of interest through simulation modeling and tested the rules using experiments at a single point. Breuker and Braun (1998b) confirmed this set of rules using experiment data, although one rule was modified. These rules are summarized in table 1(+ indicates an increase in the residual, - decrease). The modification made was that the hot gas temperature should increase with the

occurrence of compressor valve leakage. The simulation model Rossi and Braun used to generate the diagnostic rules did not consider the energy of the refrigerant which leaks back into the suction line from the discharge side when a compressor valve leaks. This refrigerant increases the compression chamber temperature and tends to increase the discharge temperature. These rules were intended to be generic for all similar types of air conditioners and should not require on-line learning.

Table 1 Diagnosis rules for rooftop air conditioners (with a fixed orifice as the expansion valve).

Fault	T _{evap}	T _{sh}	T _{cond}	T _{sc}	T _{hg}	ΔT _{ca}	ΔT _{ea}
Refrigerant leakage	-	+	-	-	+	-	-
Comp. Valve Leak	+	-	-	-	+	-	-
Liquid Restriction	-	+	-	+	+	-	-
Condenser Fouling	+	-	+	-	+	+	-
Evaporator Fouling	-	-	-	-	-	-	+

The set of rules defines a multi-dimensional space where each class (fault type) occupies a unique quadrant. This means that the Cartesian axes form the classification boundaries. Ideally, the residuals reside at the origin of the multi-dimensional space at normal operating states. By integrating the overlap of the current distribution with each of the fault classes described by the set of rules, the probability that the current behavior can be explained by each of the fault classes can be calculated and compared (Rossi and Braun 1997). The following equation shows how this probability is calculated:

$$w_j = \prod_{k=1}^m \frac{1}{2} \left[1 + C_{jk} \operatorname{erf} \left(\frac{M_c(k) - M_N(k)}{\sqrt{2 \sum_c(k,k)}} \right) \right]$$

where

j is the index of fault type j,

w_j is the probability of fault type j,

M is the sample mean vector,

\sum is the covariance matrix,

C_{jk} = 1 if $M_c(k) - M_N(k)$ has the same sign as d_{jk}; C_{jk} = -1, otherwise.

Subscript N is for normal distribution

Subscript c is for current distribution

k is the index of the measurement.

While calculating the overlap within each class, the distributions of all measurements are assumed to be independent. When the most likely fault class exceeds the second most likely class by a preset threshold (fault probability ratio threshold), a diagnosis is made.

1.5 Evaluation of the statistical rule-based FDD

Breuker and Braun tested the statistical FDD technique on a 3-ton rooftop unit with a fixed orifice as the expansion device. They presented two prototype designs chosen for evaluation whose parameters are summarized in Table 2. By interpolating the experimental data, their performances were evaluated. Tables 3 and 4 summarize the sensitivity of the two prototypes for the FDD technique applied to a fixed orifice system. Two indices were used to quantify the sensitivity of the technique, the “First Detected” level and the “All Detected” level. “First Detected” level is the level at which the fault is first successfully detected and diagnosed. “All Detected” level is the level at which the fault can be detected and diagnosed during all steady-state conditions.

Table 2 Statistical FDD method parameters used by Breuker and Braun (1998b).

FDD Design Parameter	“Low-Cost” Design	“High-Performance” Design
Steady-state model	T_{wb} / T_{amb} polynomial, 1 st order polynomial	$T_{ra} / T_{wb} / T_{amb}$ polynomial. T_{sh}, T_{hg} 3 rd order polynomial, $T_{sc}, \Delta T_{ea}$ 2 nd order polynomial, others 1 st order polynomial
Measurements	$T_{evap}, T_{sh}, T_{hg}, T_{cond}, T_{sc}$	$T_{evap}, T_{sh}, T_{hg}, T_{cond}, T_{sc}, \Delta T_{ea}, \Delta T_{ca}$
Steady-state detector (SSD) threshold	$0.04 F^2$	$0.04 F^2$
Forgetting factor for SSD method	0.7	0.7
Fault probability ratio threshold	2.0	2.0
Confidence interval for model uncertainty	68%	68%
FDD buffer size / frequency	30 measurements @ 5 second intervals	30 measurements @ 5 second intervals
Detection error safety factor	10	10
Detection error threshold (calculated)	0.0029	0.0029

Table 3 Sensitivity of Statistical FDD method (low-cost design) on a rooftop unit with a fixed orifice.

Performance Index	Refrigerant		Liquid Line		Compressor		Condenser		Evaporator	
	Leakage (% Leakage)		Restriction (% ΔP)		Valve Leak (% $\Delta \eta_v$)		Fouling (% Lost area)		Fouling (% Lost flow)	
	1st	All	1st	All	1st	All	1st	All	1st	All
Fault Level (%)	9.7	12.5	9.0	10.5	17.5	20.0	16.4	19.5	27.2	Max
% Loss Capacity	5.5	7.1	4.6	5.4	10.7	12.2	3.2	3.6	15.3	>19.4
% Loss COP	3.2	4.1	3.3	3.8	11.9	13.6	4.6	6.2	13.5	>17.4
ΔT_{sh}	9.2	10.5	7.8	8.9	-5.9	-6.8	-1.9	-3.0	-4.6	<-5.5
ΔT_{hg}	7.6	9.3	7.9	9.0	0.0	0.4	2.3	2.4	-3.8	<-5.1

Table 4 Sensitivity of Statistical FDD method (high-performance) on a rooftop unit with a fixed orifice.

Performance Index	Refrigerant		Liquid Line		Compressor		Condenser		Evaporator	
	Leakage (% Leakage)		Restriction (% ΔP)		Valve Leak (% $\Delta \eta_v$)		Fouling (% Lost area)		Fouling (% Lost flow)	
	1st	All	1st	All	1st	All	1st	All	1st	All
Fault Level (%)	5.4	Max	2.1	4.1	3.6	7.0	11.2	17.4	9.7	20.3
% Loss Capacity	3.4	> 8	1.8	3.4	3.7	7.3	2.5	3.5	5.4	11.5
% Loss COP	2.8	> 4.6	1.3	2.5	3.9	7.9	3.4	5.1	4.9	10.3
ΔT_{sh}	5.4	> 11	2.3	4.8	-1.8	-3.6	-0.6	-1.6	-1.7	-2.7
ΔT_{hg}	4.8	> 10	2.4	4.8	0.0	0.0	1.8	2.3	-1.2	-2.7

Appendix 2 Proof for normalized distance method

Given a general normal distribution $N_x(M, \Sigma)$, whose characteristic parameters are mean vector M and covariance matrix Σ . From the given Σ of X -space, find the diagonalized transformation of $Y = \Phi^T X$, where X is any point in the original space, Φ is eigenvector matrix of Σ , and Y is the corresponding point in the transformed space.

$$\begin{aligned} D &= E\{Y\} = \Phi^T E\{X\} = \Phi^T M \\ \Lambda &= E\{(Y - D)(Y - D)^T\} \\ &= \Phi^T E\{(X - M)(X - M)^T\} \\ &= \Phi^T \Sigma \Phi \end{aligned}$$

$$\text{where } D = \begin{bmatrix} d_1 \\ d_2 \\ \vdots \\ d_{n-1} \\ d_n \end{bmatrix} \text{ and } \Lambda = \begin{bmatrix} \lambda_1 & & & & \\ & \lambda_2 & & & \\ & & \ddots & & \\ & & & \lambda_{n-1} & \\ & & & & \lambda_n \end{bmatrix} \text{ are the expected vector in the}$$

diagonalized space and eigenvalue matrix of Σ , respectively.

The normalized distance from any point X to mean vector is,

$$\begin{aligned} d_x^2 &= (X - M)^T \Sigma^{-1} (X - M) \\ &= (\Phi Y - \Phi D)^T (\Phi \Lambda \Phi^T)^{-1} (\Phi Y - \Phi D) \\ &= (Y - D)^T \Phi^T (\Phi^T)^{-1} \Lambda^{-1} \Phi^{-1} \Phi (Y - D) \\ &= (Y - D)^T \Lambda^{-1} (Y - D) \\ &= \sum_i^n \frac{(y_i - d_i)^2}{\lambda_i} \\ &= \sum_i^n \left(\frac{y_i - d_i}{\sqrt{\lambda_i}} \right)^2 \end{aligned}$$

It is obvious that,

$$\left(\frac{y_i - d_i}{\sqrt{\lambda_i}} \right) \sim N(0,1).$$

$$\text{So, } d_x^2 = \sum_i^n \left(\frac{y_i - d_i}{\sqrt{\lambda_i}} \right)^2 \sim \chi^2(n)$$

Appendix 3 Other load level and fault results

The following 5 tables list probability computation results using Monte-Carlo simulation and simple independence assumption. At each load level, numbers on the first line are calculated using Monte-Carlo simulation and those on the second line using independence assumption.

Refrigerant leakage fault results at other load levels

Load	Fault Level	Refrigerant Leak	Comp. Valve Leak	Liquid Line Restriction	Cond. Foul	Evap. Foul
40%	Normal	0	0	0	0	0
		0	0	0.0035	0	0
	1	0.0004	0	0.0164	0	0
		0.0010	0	0.0071	0.0001	0.0001
	2	0.0213	0	0.0597	0	0
		0.0063	0	0.0163	0	0
	3	0.0634	0	0.0768	0	0
		0.0081	0	0.0109	0	0
	4	0.1517	0	0.0488	0	0
		0.0113	0	0.0061	0	0
60%	Normal	0.	0.0040	0	0.0001	0
		0.0001	0.0002	0.0055	0.0003	0.0001
	1	0.0064	0.0009	0.0121	0.0006	0
		0.0040	0.0008	0.0056	0.0013	0.0005
	2	0.0759	0	0.0496	0	0
		0.0142	0	0.0100	0	0
	3	0.2388	0	0.0255	0	0
		0.0464	0	0.0044	0	0
	4	0.3412	0	0.0255	0	0
		0.0755	0	0.0044	0	0
80%	Normal	0	0	0	0	0
		0	0	0.0043	0	0
	1	0.0039	0	0.0543	0	0
		0.0004	0	0.0187	0	0
	2	0.0669	0	0.1683	0	0
		0.0045	0	0.0276	0	0
	3	0.2874	0	0.0867	0	0
		0.0427	0	0.0145	0	0
	4	0.1621	0	0.3133	0	0
		0.0105	0	0.1078	0	0
100%	Normal	0	0.0010	0	0.0002	0.0003
		0	0	0	0	0
	1	0.0016	0	0.0048	0.0010	0
		0.0026	0.0004	0.0027	0.0007	0.0004
	2	0.0807	0	0.0815	0	0
		0.0050	0	0.0065	0	0

	3	0.4284	0	0.0563	0	0
		0.1285	0	0.0030	0	0
	4	0.4382	0	0.1120	0	0
		0.1624	0	0.0262	0	0

Compressor valve leakage fault results

Load	Fault Level	Refrigerant Leak	Comp. Valve Leak	Liquid Line Restriction	Cond. Foul	Evap. Foul
20%	Normal	0	0.0009	0	0	0
		0.0008	0.0007	0.0015	0.0009	0.0004
	1	0	0.1821	0	0.0010	0
		0.0022	0.0033	0.0012	0.0017	0.0013
	2	0	0.1950	0	0.0083	0
		0.0006	0.0011	0.0004	0.0007	0.0006
	3	0	0.3200	0	0.0520	0
		0.0010	0.0078	0.0003	0.0027	0.0021
	4	0	0.4560	0	0.0261	0
		0.0009	0.0154	0.0001	0.0020	0.0019
40%	Normal	0	0	0	0	0
		0.	0.	0.0035	0.	0.
	1	0	0.1210	0	0.0088	0
		0.0017	0.0068	0.0039	0.0021	0.0015
	2	0	0.1267	0	0.0015	0
		0.0010	0.0042	0.0021	0.0015	0.0013
	3	0	0.2589	0	0.0013	0
		0.0025	0.0142	0.0034	0.0017	0.0014
	4	0	0.5018	0	0.0005	0
		0.	0.0433	0.	0.0008	0.0009
60%	Normal	0	0.0042	0	0.0001	0
		0.0001	0.0002	0.0055	0.0003	0.0001
	1	0	0.2646	0	0.0284	0
		0.0038	0.0414	0.0022	0.0058	0.0029
	2	0	0.2359	0	0.0120	0
		0.0007	0.0194	0.0007	0.0040	0.0027
	3	0	0.3796	0	0.0038	0
		0.0001	0.0628	0.0001	0.0014	0.0007
	4	0	0.5551	0	0.0002	0
		0.	0.1418	0.	0.	0.
80%	Normal	0	0.0002	0	0.	0
		0.	0.	0.0043	0.	0.
	1	0	0.0447	0.	0.0005	0
		0	0.0008	0.	0.	0.
	2	0	0.0460	0	0.0001	0
		0	0.0011	0	0.0001	0
	3	0	0.3026	0	0.0002	0
		0	0.0418	0	0.	0.
	4	0	0.4446	0	0	0
		0	0.173	0	0.	0.
100%	Normal	0.0013	0	0.0003	0.0005	0
		0.	0.	0.	0.	0.
	1	0	0.0837	0	0.0139	0
		0.	0.0019	0.	0.0004	0.0001
	2	0	0.2135	0	0.0133	0
		0.	0.0188	0.	0.0004	0.

	3	0	0.3440	0	0.0261	0.
		0.	0.1559	0.	0.0003	0.
	4	0	0.2125	0	0.	0
		0	0.2605	0	0	0

Liquid-line restriction fault

Load	Fault Level	Refrigerant Leak	Comp. Valve Leak	Liquid Line Restriction	Cond. Foul	Evap. Foul
20%	Normal	0	0.0010	0	0	0
		0.0008	0.0007	0.0015	0.0009	0.0004
	1	0	0	0.0107	0	0
		0	0	0.0054	0	0
	2	0	0	0.0517	0	0
		0	0	0.0025	0	0
	3	0	0	0.1318	0	0
		0	0	0.0120	0	0
	4	0	0	0.2728	0	0
		0	0	0.0185	0	0
40%	Normal	0	0	0	0	0
		0	0	0.0035	0	0
	1	0	0	0.0453	0	0
		0.	0.	0.0199	0.	0.
	2	0	0	0.1144	0	0
		0.	0.	0.0159	0.	0.
	3	0	0	0.2264	0	0
		0.	0.	0.0512	0	0
	4	0	0	0.3884	0	0
		0.	0.	0.0834	0.	0.
60%	Normal	0	0.0039	0	0.0001	0
		0.0001	0.0002	0.0055	0.0003	0.0001
	1	0.0001	0	0.1175	0	0
		0.	0.	0.0247	0.	0.
	2	0	0	0.1911	0	0
		0.	0.	0.0324	0.	0.
	3	0	0	0.1833	0	0
		0.	0.	0.0034	0.	0.
	4	0	0	0.4476	0	0
		0.	0.	0.1179	0.	0.
80%	Normal	0	0.0002	0	0	0
		0.	0.	0.0043	0.	0.
	1	0.	0	0.2369	0	0
		0.	0.	0.0322	0.	0.
	2	0	0	0.3390	0	0
		0.	0	0.0554	0	0
	3	0	0	0.3362	0	0
		0.	0.	0.0220	0.	0.
	4	0	0	0.5134	0	0
		0.	0.	0.1780	0.	0.
100%	Normal	0	0.0011	0	0.0002	0.0005
		0	0	0	0	0
	1	0.0007	0	0.1834	0	0
		0.	0.	0.0165	0	0
	2	0.0001	0.	0.3195	0	0
		0.	0.	0.0256	0.	0.

	3	0	0	0.4360	0	0
		0.	0.	0.0750	0.	0.
	4	0	0	0.5160	0	0
		0	0	0.2725	0	0

Condenser fouling fault

Load	Fault Level	Refrigerant Leak	Comp. Valve Leak	Liquid Line Restriction	Cond. Foul	Evap. Foul
20%	Normal	0	0	0	0	0
		0.0008	0.0007	0.0015	0.0009	0.0004
	1	0	0.0036	0	0.0085	0
		0.0010	0.0010	0.0012	0.0016	0.0005
	2	0	0	0	0.2660	0
		0.0007	0.0020	0.0001	0.0061	0.0010
	3	0	0	0	0.3090	0
		0.0001	0.0008	0	0.0060	0.0004
	4	0	0	0	0.3874	0
		0	0.0002	0	0.0121	0.0001
40%	Normal	0	0	0	0	0
		0	0	0.0035	0	0
	1	0	0	0	0	0
		0.0002	0.0002	0.0061	0.0004	0.0001
	2	0	0	0	0.1459	0
		0.0006	0.0033	0.0002	0.0173	0.0011
	3	0	0	0	0.3325	0
		0.0001	0.0006	0	0.0264	0.0002
	4	0	0	0	0.4713	0
		0	0	0	0.0673	0
60%	Normal	0	0.0039	0	0.0001	0
		0.0001	0.0002	0.0055	0.0003	0.0001
	1	0	0.0188	0	0.0597	0
		0.0010	0.0067	0.0013	0.0160	0.0020
	2	0	0	0	0.2499	0
		0.0001	0.0041	0	0.0332	0.0015
	3	0	0	0	0.3925	0
		0	0	0	0.0958	0
	4	0	0	0	0.3925	0
		0	0	0	0.9580	0
80%	Normal	0	0	0	0	0
		0	0	0.0043	0	0
	1	0	0.0041	0	0.0216	0
		0.0002	0.0007	0.0050	0.0018	0.0001
	2	0	0	0	0.2959	0
		0	0.0037	0	0.0606	0.0008
	3	0	0	0	0.4842	0
		0	0	0	0.1513	0
	4	0	0	0	0.6731	0
		0	0	0	0.1944	0
100%	Normal	0	0.0012	0	0.0002	0.0004
		0	0	0	0	0
	1	0	0.0094	0	0.0906	0
		0	0.0187	0	0.0418	0.0036
	2	0	0	0	0.2785	0
		0	0.0020	0	0.1188	0.0002

	3	0	0	0	0.4503	0
		0	0.0003	0	0.0735	0
	4	0	0	0	0.7896	0
		0	0	0	0.2815	0

Evaporator fouling fault

Load	Fault Level	Refrigerant Leak	Comp. Valve Leak	Liquid Line Restriction	Cond. Foul	Evap. Foul
20%	Normal	0	0.0011	0	0	0
		0.0008	0.0007	0.0015	0.0009	0.0004
	1	0E-3	0.0550 E-3	0 E-3	0.0300 E-3	0.3800 E-3
		0.0007	0.0007	0.0015	0.0008	0.0007
	2	0	0	0	0.0014	0.1890
		0.0007	0.0017	0.0004	0.0015	0.0028
	3	0	0	0	0	0.3387
		0.0006	0.0015	0.0002	0.0010	0.0035
	4					
40%	Normal	0	0	0	0	0
		0	0	0.0035	0	0
	1	0	0	0	0	0.0064
		0.0002	0.0003	0.0028	0.0004	0.0005
	2	0	0	0	0	0.1535
		0.0002	0.0008	0.0006	0.0005	0.0028
	3	0	0	0	0	0.4560
		0.0002	0.0014	0.0001	0.0004	0.0247
	4					
60%	Normal	0	0.0040	0	0.0001	0
		0.0001	0.0002	0.0055	0.0003	0.0001
	1	0	0.0001	0	0	0.1169
		0.0003	0.0010	0.0011	0.0014	0.0039
	2	0	0	0	0	0.3757
		0.0001	0.0013	0	0.0006	0.0353
	3	0	0	0	0	0.4784
		0.0001	0.0007	0	0.0002	0.0348
	4					
80%	Normal	0	0	0	0	0
		0	0	0.0043	0	0
	1	0	0	0	0	0.0599
		0	0.0002	0.0009	0.0001	0.0009
	2	0	0	0	0	0.2675
		0	0	0	0	0.0145
	3	0	0	0	0	0.4546
		0	0.0001	0	0	0.0543
	4					
100%	Normal	0.	0.0011	0	0.0003	0.0004
		0	0.	0.0001	0.0001	0.0001
	1	0	0	0	0	0.1947
		0	0	0	0	0.3991
	2	0	0.0001	0	0	0.0590
		0	0.0001	0	0	0.0590

	3	0	0	0	0	0.4173
		0	0.0010	0	0.0005	0.0109
	4					

Appendix 4 Fault diagnosis distance method

Assume c is the largest expected magnitude of residuals and as shown in following figure, $F_1(c, c)$ and $F_2(-c, c)$ represent fault quadrant I and fault quadrant II respectively. $P(x, y)$ is a point in the double residual space.

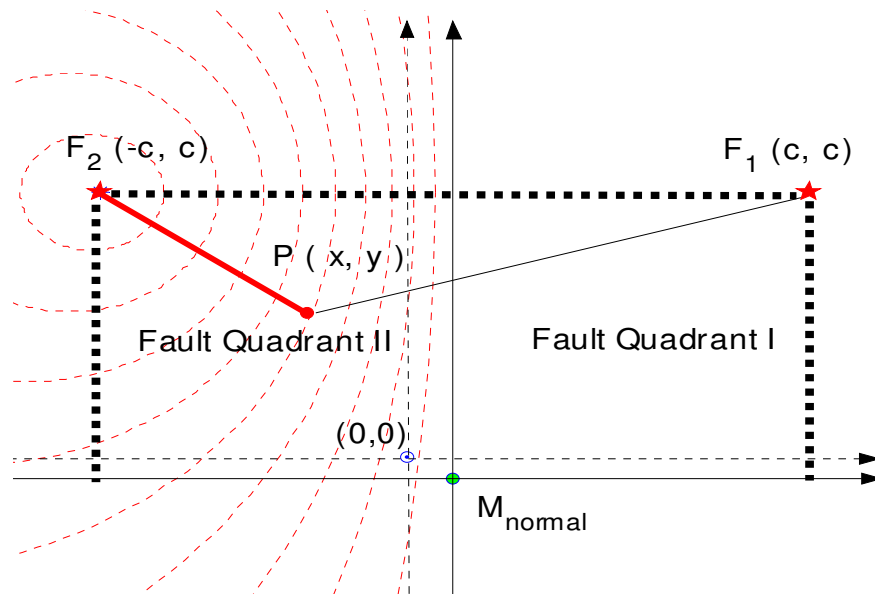


Illustration of distance ratio method for FDD

$$\underbrace{\left\{ \begin{array}{l} \|PF_1\| = \sqrt{(x-c)^2 + (y-c)^2} \\ \|PF_2\| = \sqrt{(x+c)^2 + (y-c)^2} \end{array} \right\} \Rightarrow ratio_{dist} = \frac{\|PF_2\|}{\|PF_1\|} = \frac{\sqrt{(x+c)^2 + (y-c)^2}}{\sqrt{(x-c)^2 + (y-c)^2}}}_{\Downarrow}$$

$$\underbrace{\frac{(x+c)^2 + (y-c)^2}{(x-c)^2 + (y-c)^2}}_{\Downarrow} = ratio_{dist}^2$$

$$\underbrace{(1 - ratio_{dist}^2)x^2 + 2c(1 + ratio_{dist}^2)x + (1 - ratio_{dist}^2)(y-c)^2 + (1 - ratio_{dist}^2)c^2}_{\Downarrow} = 0$$

$$\underbrace{\left(x + \frac{c(1 + ratio_{dist}^2)}{1 - ratio_{dist}^2} \right)^2 + (y-c)^2 + c^2 - \frac{c^2(1 + ratio_{dist}^2)}{(1 - ratio_{dist}^2)^2}}_{\Downarrow} = 0$$

$$\underbrace{\left(x + \frac{c(1 + ratio_{dist}^2)}{1 - ratio_{dist}^2} \right)^2 + (y-c)^2}_{\Downarrow} = \left(\frac{2ratio_{dist}c}{(1 - ratio_{dist}^2)} \right)^2$$

$$x_o = -\frac{c(1 + ratio_{dist}^2)}{1 - ratio_{dist}^2} = -\left(\frac{c(1 - ratio_{dist}^2)}{1 - ratio_{dist}^2} + \frac{2ratio_{dist}c}{1 - ratio_{dist}^2} \right) = -\left(\frac{c(1 - ratio_{dist}^2)}{1 + ratio_{dist}^2} + \frac{2ratio_{dist}c}{1 - ratio_{dist}^2} \right)$$

$$y_o = c$$

$$r = \frac{2ratio_{dist}c}{1 - ratio_{dist}^2}$$

From this equation, it can be seen that given a constant magnitude of fault points a distance ratio corresponds to a circle in a cluster of circles whose centers have the same y coordinate, the constant magnitude of c .

Since $ratio_{dist}$ is always less than 1, the magnitude of x coordinates of the center is larger than c and increases with increasing distance ratio, and the radius of the circles will increase with increasing distance ratio but with the larger magnitude than the former.

Appendix 5 Introduction of faults

The proper method for simulating operating faults in a system is a very important part of the evaluation of any fault detection method. If the faults are simulated in a way which does not accurately represent how a fault occurs it is not likely that the technique will make correct decisions in a real operating situation. The methods for simulating faults in the test unit are explained in this section.

Condenser fouling results in the loss of the ability to transfer heat from the condenser coil to the surrounding air stream. It may occur in a few different ways. For instance, condenser fouling might occur as a build-up of a "scale" on the condenser fins resulting from substances in the air or rain such as dust, minerals, etc. This would result in an increased resistance to heat transfer, but a negligible change in the mass flow of air across the coil. Condenser fouling may also be the result of a build-up of debris on the face of the condenser coil. This build-up will cause a net loss of condenser surface area available for heat transfer and will reduce the total mass flow rate of air across the coil. For the research performed in this thesis, the "area blockage" method was chosen for the simulation of condenser fouling.

A blockage of air flow through the condenser coil may be uniform or non-uniform. For example, if the coil is located on the ground, one might expect the fouling to be more severe near the bottom of the coil than the top. However, it could be uniformly distributed throughout the condenser coil since air is drawn through the coil at a uniform velocity. The location of the coil fouling could change the effect of the fouling on the internal refrigerant states in some condenser coils. The condenser coil on the test unit contains two parallel condensing sections and a subcooling section as shown in Figure 1.

Fouling in the subcooling section of the coil, after the refrigerant has already condensed into a liquid, could have a different effect on the refrigeration cycle than fouling in the condensing section. Some initial studies have showed that it is difficult to detect a fouled condenser if the fouling occurs only in the subcooling section of the coil. Possible future work might investigate this effect more closely. The uniformly fouled approach was chosen for the work in this thesis because it is the most likely type to occur and is the most easily

repeatable and quantifiable. Uniform condenser fouling was introduced by blocking the condenser coil with uniformly spaced, vertical strips of either paper or duct tape. The level of fouling is expressed as a total % reduction in the surface area of the condenser coil.

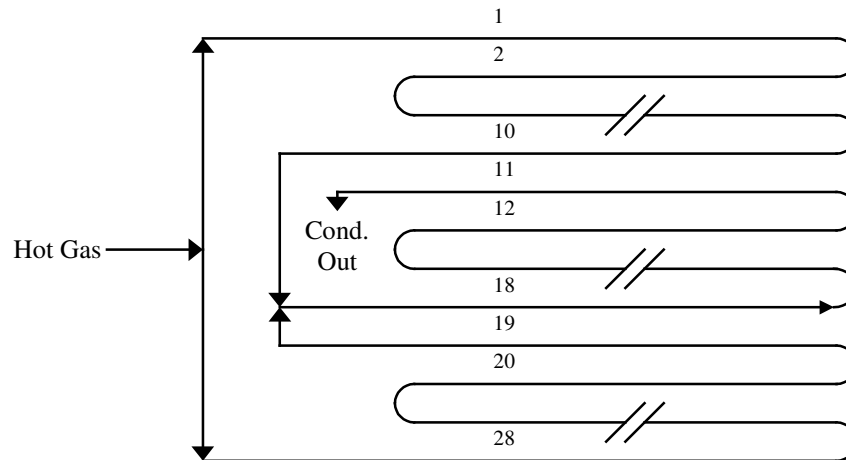


Figure 1 Test unit condenser coil circuitry

Evaporator fouling is generally the result of a plugged air filter or a blocked return air vent. Both of these cause a restriction in the air flow path, resulting in a decrease in the flow of air over the evaporator coil. For tests which were performed before the air measurement system was operational, evaporator fouling was simulated by partially blocking the air flow upstream of the evaporator coil. By measuring the change in differential pressure across the evaporator fan as a result of the blockage, a reduction in air flow rate was calculated from the fan curve. Once the air measurement system was commissioned, evaporator fouling was simulated by simply reducing the speed of the variable speed fan in the air measurement circuit. The change in air flow was measured using the air flow measurement system. Fouling in both cases is expressed as a % reduction from the nominal air flow rate.

A liquid line restriction can be caused by a plugged filter/dryer or some debris lodged in the fixed orifice expansion device. In either case, it results in an increased pressure drop in the liquid line. It was simulated in the experiments by partially closing a globe valve placed in the liquid line. The level of fault is characterized by the following ratio:

$$\text{Restriction Level} = 100\% \cdot \frac{\Delta P_{\text{res}}}{\Delta P_{\text{sys}}} \quad (1)$$

where ΔP_{res} is the pressure drop across the restriction valve and ΔP_{sys} is the difference between high side (condensing) and low side (evaporating) pressures in the system before a restriction fault is introduced.

A compressor valve leakage is one cause of a reduction in the capacity of a compressor. It is typically caused by slugs of liquid refrigerant which damage the suction valve in the compressor, causing it to lose an effective seal. When this happens, some of the high pressure refrigerant in the compression cylinder leaks back into the suction line across the suction valve. This results in a reduction in the volumetric efficiency of the compressor. A compressor valve leakage was simulated by opening a globe valve which allows gas from the discharge line to recycle into the suction line. The % reduction in the net volumetric efficiency of the compressor is calculated using the known compressor specifications, the inlet refrigerant state, and the mass flow measurement as shown in Equations 2 and 3 below.

$$\eta_v = \frac{\dot{m}_{\text{actual}}}{\dot{m}_{\text{ideal}}} \quad (2)$$

$$\dot{m}_{\text{ideal}} = n \cdot V \cdot \rho \quad (3)$$

where \dot{m}_{actual} is the measured mass flow rate of refrigerant from the compressor, n is the rotational speed of the compressor, V is the volume displaced with each compressor cycle, and ρ is the density of the inlet refrigerant.

Refrigerant leakage is simply the loss of refrigerant from the system. It was simulated by discharging a fixed amount of refrigerant from the rooftop unit into a receiving vessel and weighing the vessel before and after the discharge. The level of refrigerant leakage is quantified as the % reduction in the total charge in the system.

A DECOUPLING-BASED FDD APPROACH FOR MULTIPLE - SIMULTANEOUS FAULTS

Deliverable 2.1.5

Progress report submitted to:
Architectural Energy Corporation

For the Building Energy Efficiency Program
Sponsored by:
California Energy Commission

Submitted By:
Purdue University

Principal Investigator: James Braun, Ph.D., P.E.
Research Assistant: Haorong Li

June 2003

Mechanical Engineering
1077 Ray W. Herrick Laboratories
West Lafayette, IN 47907-1077
(765) 496-6008
(765) 494-0787 (fax)

RAY W. HERRICK
LABORATORIES
PURDUE ENGINEERING



TABLE OF CONTENTS

TABLE OF CONTENTS.....	2
LIST OF FIGURES	5
LIST OF TABLES.....	8
NOMENCLATURE	9
ABSTRACT.....	11
1 The Fault Detection and Diagnosis Methodology	13
1.1 Mathematical Formulation of Model-Based FDD Problem	13
1.1.1 Fault Detection.....	15
1.1.1.1 Original SRB Fault Detection Classifier.....	15
1.1.1.2 Normalized Distance Fault Detection Classifier.....	17
1.1.2 Fault Diagnosis	19
1.1.2.1 Original SRB Fault Diagnosis Method	20
1.1.2.1.1 Original SRB Fault Diagnosis Classifier	23
1.1.2.1.2 Simple Distance Fault Diagnosis Classifier.....	23
1.1.2.2 Decoupling-Based Fault Diagnosis Method	24
1.1.2.3 Unilateral Decoupling Case	26
1.2 Strategy for Decoupling Rooftop Unit System.....	28
1.2.1 Taxonomy of Faults	29
1.2.2 Interactions.....	32
1.2.3 Decoupling of Component Faults	34
1.2.3.1 Compressor Valve Leakage Fault	34
1.2.3.2 Condenser-Related Faults	36
1.2.3.2.1 Non-Condensable Gas Fault	36
1.2.3.2.2 Condenser Fouling Fault	40
1.2.3.3 Liquid-line Restriction Fault	42

1.2.3.4 Evaporator Fouling Fault	45
1.2.3.5 Summary of Decoupling Component-Level Faults	47
1.2.4 Decoupling System-Level Faults	49
1.2.5 Summary of Decoupling Schemes for Rooftop Unit System Faults	52
2 Case Studies	53
2.1 Case Study of Decoupling Rooftop Unit Faults	53
2.1.1 Compressor Valve Leakage	53
2.1.2 Condenser Fouling Decoupling	55
2.1.3 Evaporator Fouling Decoupling	56
2.1.4 Liquid-Line Restriction Decoupling	58
2.1.5 Refrigerant Leakage Decoupling	60
2.2 Purdue Field Emulation Site's Demonstration	61
2.2.1 Field Fault Simulation Window	62
2.2.2 Fault Detection and Diagnosis Window	64
2.2.3 System Performance & Safety Degradation Window	65
2.2.4 FDD Report Window	66
2.2.5 Output of the FDD Demonstration	66
2.3 Results for California Field Sites	75
2.3.1 Milpitas McDonalds Field Site	75
2.3.2 Summarized Results for Other Sites	82
3 Conclusions and Recommendations	84
Reference	85
Appendix 1 Physical Models of Expansion Device.....	90
A1.1 Fixed-Area Expansion Device Models	90
A1.1.1 Orifice Models	90
A1.1.2 Short-Tube Models	92
A1.1.2 Capillary-Tube Models	93
A1.2 Adjustable Throat-Area Expansion Valve Models	93
A2.2.1 Model Format Validation Using Manufacturers' Rating Data	94
A1.2.2 Derivation of Throat-Area A Expression.....	97

A1.2.3 Valve Position Expression	99
A1.2.4 Overall Mass Flow Rate Model of TXV	100
A1.2.5 Parameter Estimation Method.....	102
A1.3.2.5.1 Global Linear Assumption Method.....	102
A1.2.5.2 Nonlinear Parameter Estimation Without Specification Data	103
A1.2.5.3 Validation Using Harms' Data.....	104
Appendix 2 RTD Temperature Sensor Measuring Issue	109

LIST OF FIGURES

Figure 1-1 System after being incorporated with a normal operation model	14
Figure 1-2 2-dimensional residual distribution when system is running in a fault mode ..	14
Figure 1-3 Fault detection classifier scheme for a 2-dimensional case	18
Figure 1-4 Fault detection and diagnosis boundaries	22
Figure 1-5 Taxonomy of Rooftop Faults	30
Figure 1-6 Interactions of Rooftop Unit System.....	33
Figure 1-7 Compressor Valve Leakage Decoupling Scheme	35
Figure 1-8 Condenser Fouling and Non-Condensable Gas Faults Decoupling Scheme ..	42
Figure 1-9 Liquid-line restriction illustration	43
Figure 1-10 Vapor Compression Cycle Illustration.....	44
Figure 1-11 Liquid-Line Restriction Decoupling Scheme.....	45
Figure 1-12 Evaporator Fouling Decoupling Scheme	46
Figure 1-13 Ideal Decoupling Scheme of Component-Level Faults with Refrigerant mass flow measurement	47
Figure 1-14 Actual Decoupling Scheme of Component-Level Faults without Refrigerant Mass Flow Measurement	49
Figure 1-15 The Decoupling Scheme for System Level Faults	50
Figure 1-16 ΔT_{sh-sc} with different refrigerant charge levels	51
Figure 1-17 The Decoupling Scheme of All Rooftop System Faults	52
Figure 2-1 Decoupling compressor valve leakage fault using estimated compressor power measurement and estimated refrigerant mass flow rate	54
Figure 2-2 Decoupling condenser fouling fault using measured refrigerant mass flow rate	55
Figure 2-3 Decoupling condenser fouling fault using estimated refrigerant mass flow rate	56
Figure 2-4 Decoupling evaporator fouling fault using measured evaporator air mass flow rate.....	57
Figure 2-5 Decoupling evaporator fouling fault using measured refrigerant mass flow rate	58
Figure 2-6 Decoupling evaporator fouling fault using estimated refrigerant mass flow rate	58
Figure 2-7 Decoupling liquid-line restriction using measured pressure drop.....	59
Figure 2-8 Decoupling liquid-line restriction using estimated pressure P_{up} and measured P_3	59
Figure 2-9 Decoupling liquid-line restriction using estimated pressure drop.....	60

Figure 2-10 Decoupling refrigerant leakage faults using ΔT_{sh-sc}	61
Figure 2-12 Timeline of the fault simulation in minutes.	63
Figure 2-13 Outputs of the FDD demonstration after introduction of low refrigerant charge fault.....	67
Figure 2-14 Outputs of the FDD demonstration after introduction of condenser fouling fault	68
Figure 2-15 Outputs of the FDD demonstration after introduction of liquid line restriction fault	69
Figure 2-16 Outputs of the FDD demonstration after introduction of compressor leakage fault	70
Figure 2-17 Outputs of the FDD demonstration after removal of condenser fouling fault	71
Figure 2-18 Outputs of the FDD demonstration after removal of liquid line restriction fault	72
Figure 2-19 Outputs of the FDD demonstration after removal of compressor leakage fault	73
Figure 2-20 Outputs of the FDD demonstration after removal of low refrigerant low charge fault.....	74
Figure 2-21 Histogram bar plot of the normalized fault indicator for liquid line restriction	76
Figure 2-22 Histogram bar plot of the normalized fault indicator for refrigerant low charge	76
Figure 2-23 Histogram bar plot of the normalized fault indicator for condenser fouling ..	77
Figure 2-24 Histogram bar plot of the normalized fault indicator for compressor valve leakage	78
Figure 2-25 Histogram bar plot of the normalized fault indicator for cooling capacity degradation.....	79
Figure 2-26 Histogram bar plot of the return air temperature	79
Figure 2-27 Histogram bar plot of the continuous running time between off-cycles of the RTU.....	80
Figure 2-28 Histogram bar plot of the normalized fault indicator for EER degradation...	81
Figure 2-29 System power consumption reduction	81
Figure A1-1 The CA value of an ALCO EXV of manufacturer rating conditions.....	95
Figure A1-2 The CA value of a SPORLAN TXV of manufacturer rating conditions	95
Figure A1-3 P-T saturation curve for R22.....	96
Figure A1-4 Three types of valve geometry	97
Figure A1-5 Geometric model of type I and II valve	98
Figure A1-6 Throat-area curves of different valve types.....	98
Figure A1-7 Geometric model of valve type III	99
Figure A1-8 Valve position curve	100
Figure A1-10 The $C_d A$ value of the 5-ton Trane RTU TXV as a function of superheat	106
Figure A1-11 Comparison of TXV modeling error	107
Figure A1-12 Illustration of the three parameter estimation methods	108

Figure A2-1 RTD measuring scheme	109
Figure A2-2 Thermocouple measuring scheme	110
Figure A2-3 Equivalent thermal circuit	110

LIST OF TABLES

Table 1-1 Fault diagnosis rules	22
Table 1-2 c_{ref} and $\Delta T_{cond,abnorm}$ with compressor off and nominal charge and 1% non-condensable gas	39
Table 1-3 c_{ref} and $\Delta T_{cond,abnorm}$ with compressor off and ambient temperature=30°C and 1% non-condensable gas	40
Table 2-1 FDD results of Modular School sites	82
Table 2-2 FDD results of McDonalds Restaurant Sites	83
Table 2-3 FDD results of Walgreen Retail Store Sites at Rialto	83
Table A1-1 TXV rating settings	103
Table A1-2 Comparison of TXV modeling error	107
Table A2-1 Thermal resistance distribution of thermocouple measuring scheme	111
Table A2-2 Thermal resistance distribution of RTD measuring scheme	111
Table A2-3 Thermal resistance distribution of RTD for measuring cold water	112
Table A2-4 Thermal resistance distribution of RTD for measuring refrigerant vapor	112

NOMENCLATURE

AHU	= Air handling unit
\mathbf{a}	= Thermal resistance portion
\mathbf{a}	= False alarm threshold
\mathbf{b}	= Fault diagnosis threshold
c	= Distance from fault point to axes
$\mathbf{c}^2(n)$	= Chi-square distribution
d_i^2	= Normalized distance square
d_{\max}	= Maximum normalized distance
ΔT_{ca}	= Condenser air temperature difference
ΔT_{ea}	= Evaporator air temperature difference
EER	= Equipment efficiency ratio
\mathbf{h}_v	= Compressor volumetric efficiency
FDD	= Fault detection and diagnosis
F_i	= Fault points
f_i	= Frequency
GRNN	= General regression neural network
h_o	= Heat transfer coefficient between sensor and ambient air
HVAC	= Heating, Ventilating, and Air-Conditioning
IA	= Independence Assumption
\mathbf{I}_i	= Eigenvalue of Σ
Λ	= Eigenvalue matrix
\mathbf{M}	= Mean vector of residuals
\mathbf{M}_{normal}	= Mean vector for normal operation
$\mathbf{M}_{current}$	= Mean vector for current operation
MCS	= Monte-Carlo Simulation
\dot{m}_r	= Refrigerant mass flow rate
\mathbf{m}	= Mean
\mathbf{m}_{normal}	= Mean value for normal operation
\mathbf{M}_X	= Mean vector for sample X
\mathbf{M}_Y	= Mean vector for sample Y

N	= Number of generated sample points
N_X	= Normal distribution for sample X
Ω_X	= Area for probability evaluation
P_{dis}	= Discharge pressure
Φ	= Eigenvector matrix
P_i	= Data points
P_Ω	= Probability within area Ω_X
f_{ra}	= Relative humidity of return air
P_{dis}	= Discharge pressure
P_{suc}	= Suction pressure
\dot{Q}_{cap}	= Cooling capacity
$ratio_{dist}$	= Distance ratio
SRB	= Statistical rule-based
RTU	= Rooftop unit
\mathbf{S}	= Standard deviation
\mathbf{S}_{normal}	= \mathbf{S} for normal operation
Σ	= Covariance matrix
$\Sigma_{assumption}$	= Σ with independence assumption
$\Sigma_{current}$	= Σ for current operation
Σ_{normal}	= Σ for normal operation
Σ_X	= Covariance matrix for X
T_{amb}	= Ambient temperature
T_{cond}	= Condensing temperature
T_{dis}	= Discharge line temperature
T_{evap}	= Evaporating temperature
T_{ll}	= Liquid line temperature
T_{ma}	= Mixed air temperature
T_{oa}	= Outdoor air temperature
T_{ra}	= Return air temperature
T_{sc}	= Sub-cooling
T_{sh}	= Superheat
T_{wb}	= Wet bulb temperature
VAV	= Variable air volume
v_1	= Specific volume of compressor inlet refrigerant
X_i	= Sample point in original space
Y_i	= Sample point in transformed space

ABSTRACT

Although the statistical rule-based (SRB) fault detection and diagnosis (FDD) method developed by Rossi and Braun (1997) has good performance for individual faults, it requires measurements over a wide range of conditions for training reference models. The development of these models can be time consuming and costly. Furthermore, SRB FDD methods can only handle individual faults. This report presents new methods that reduce engineering and installed costs for FDD and handle multiple-simultaneous faults. The methods were evaluated using both laboratory and field data.

Inspired by a mathematical formulation for a general FDD methodology, a decoupling-based FDD approach was developed to handle multiple-simultaneous faults. To decouple different faults, all faults are categorized according to two criteria: scope of the fault impact and fault cause. The fault impact scope separates faults into system-level and component-level faults. The fault cause criterion classifies faults into service and operational faults. After decoupling, features are identified that uniquely depend on each fault. The other advantage of the mathematical formulation is that the previously developed SRB FDD method can be cast within the general mathematical framework, which guides the improvement and provides a better understanding of the SRB FDD.

In the proposed FDD approach, normal operation models and virtual sensors play a very important role. So, various models and virtual sensors are proposed to generate decoupled features. Wherever possible, physical or gray-box models are proposed that exploit manufacturers' performance rating data and only require very limited experimental or field data to train model parameters.

Finally, three case studies are presented in this document. One case study provides initial validation of the decoupling-based FDD approach using laboratory data where single faults were artificially introduced into a 3-ton Trane rooftop unit (RTU)

with a fixed-orifice as the expansion device. The second case study demonstrates the whole FDD methodology by artificially introducing multiple-simultaneous faults into the Purdue field emulation site, where a 5-ton York RTU with a TXV as the expansion device is installed. Finally, the decoupling-based FDD approach was applied to California field sites.

1 THE FAULT DETECTION AND DIAGNOSIS METHODOLOGY

One of the drawbacks of the SRB method presented by Rossi and Braun (1997) is that it can not handle multiple-simultaneous faults. From the control point of view, decoupling is an efficient way to deal with complicated interactions among multiple inputs and multiple outputs. From the mathematical point of view, transformation is the key to decoupling a system. Section 1.1 first formulates the FDD methodology in a mathematical way. And then, from a mathematical perspective, a decoupling-based FDD scheme is proposed to deal with multiple-simultaneous faults efficiently. The mathematical decoupling approach leads to infinite decoupling cases, but only those which have physical meaning are practical for low-cost FDD use. To find the physical decoupling, section 1.2 describes a way to analyze the system from a component point of view.

1.1 Mathematical Formulation of Model-Based FDD Problem

The (thermodynamic) states of a (RTU) system are functions of external driving conditions and various faults, as is shown in Figure 1-1. It is important for fault detection and diagnosis (FDD) not to misinterpret variations in (thermodynamic) state-variables caused by changes in the driving conditions for faults. If measurements are classified directly, the classification has to be complicated to consider the effect of external driving conditions. In order to simplify classification and improve overall FDD performance, normal operation models are used to predict expected values for these measurements under normal operation in terms of measured external driving conditions. For any steady-state measurement, the difference between expected and actual measurement values

(residuals) should have a zero mean when there are no faults (see Figure 1.2) and a probability distribution that is a weak function of driving conditions but dominantly dependent on faults.

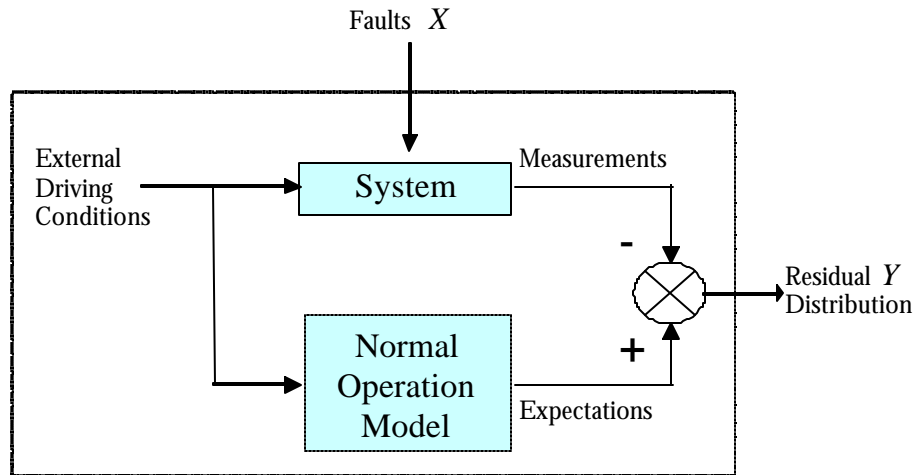


Figure 1-1 System after being incorporated with a normal operation model

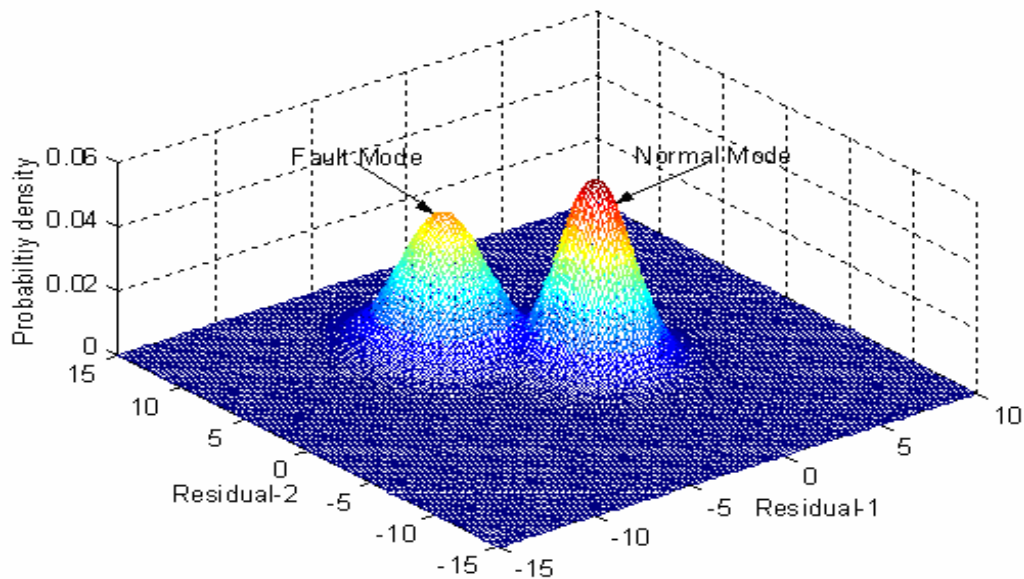


Figure 1-2 2-dimensional residual distribution when system is running in a fault mode

So, the input-output relationship of the system after being incorporated with a normal operation model can be described approximately as follows,

$$Y = F(X) \quad (1-1)$$

where,

$$X = \begin{bmatrix} x_1 \\ x_2 \\ \vdots \\ x_n \end{bmatrix}, Y = \begin{bmatrix} y_1 \\ y_2 \\ \vdots \\ y_m \end{bmatrix}, \text{ and } F(X) = \begin{bmatrix} f_1(x_1, x_2, \dots, x_n) \\ f_2(x_1, x_2, \dots, x_n) \\ \vdots \\ f_m(x_1, x_2, \dots, x_n) \end{bmatrix}.$$

X is the fault vector with each entry x_i representing a measure of the fault level for fault i (for example x_1 could characterize the level of compressor valve leakage, say, 20%). Y is the state variable residual vector, with each entry y_i representing a particular state-variable residual (for example y_1 is discharge line temperature residual ΔT_{dis} and its value is temperature variation, say, 10 F). $F(X)$ is a nonlinear function vector with each individual nonlinear function $f_i(x_1, x_2, \dots, x_n)$ defining the relationship between different faults at different levels and the state-variable residuals Y . n is the number of fault types considered, and m is the number of chosen state variables.

1.1.1 Fault Detection

Fault detection, which is to indicate whether the system is normal or not, can be done by evaluating whether the resulting Y in equation (1-1) is zero or not in a statistical sense.

1.1.1.1 Original SRB Fault Detection Classifier

Rossi & Braun (1997) proposed a way to evaluate whether Y is zero indirectly by evaluating the overlap (see Figure 1-2) of the actual distribution and the expected distribution of the residual(s). When the overlap of the actual distribution and the

expected distribution of the residual(s) decreases to a preset value (the classification error threshold), a fault is considered to be at present.

The direct numerical integration of this overlap for high dimensional (e.g., 7-dimensional for our case) probability distributions cannot be performed in real time on a microprocessor. Therefore, Rossi & Braun (1997) cleverly employed the concept of Bayes classifier to obtain the analytical solution of overlap, also known as Bayes error (Fukunaga, 1990).

The other merit of this classifier is that it cleverly converted the classification of an individual observation Y among infinite predefined classes $\mathbf{w}_1, \mathbf{w}_2, \dots, \mathbf{w}_n, \dots$ inversely into identification of whether any class \mathbf{w}_i deviating from the normal operation appears using a series of observations Y_1, Y_2, \dots, Y_n with certain overlap and let the fault diagnosis classifier separate different faults.

Since it is impracticable, if not impossible, to estimate the high-dimensional covariance matrix of current operation online, an identical covariance matrix with that of normal operation is assumed. However, if this assumption is not well grounded it may undermine the fault detection performance, because the overlap is highly dependent on the covariance matrix. It is really difficult to evaluate the identical covariance matrix assumption because a large data set is necessary to estimate a high-dimensional covariance matrix at reasonable accuracy. However, it can be evaluated indirectly by checking the variance of individual variables. According to the experimental data collected by Breuker (1997),

1. Faults have significant impact on the variance of state variables. For example, variances of subcooling, superheat and evaporating temperature increase when the system has refrigerant leakage fault.
2. Different faults have different impacts. For example, refrigerant leakage has a larger impact on the variance of subcooling than evaporator fouling.

As a result of these considerations, a new fault detection classifier, which does not require a faulty operation covariance matrix, was developed and is described in the next section.

1.1.1.2 Normalized Distance Fault Detection Classifier

The attached ASHRAE paper (Li & Braun, 2003) and Deliverables 2.1.3 & 2.1.4 (2002) present details of a normalized distance fault detection classifier that can be used for both individual and multiple-simultaneous faults simply. The classifier evaluates the following inequality.

$$(Y - M_{normal})^T \Sigma_{normal}^{-1} (Y - M_{normal}) \underset{w_2: Faulty}{\overset{w_1: Normal}{\leq}} (\mathbf{c}^2)^{-1} \{(1 - \mathbf{a}), m\} \quad (1-2)$$

where $(Y - M_{normal})^T \Sigma_{normal}^{-1} (Y - M_{normal})$ is the normalized distance, $(\mathbf{c}^2)^{-1} \{(1 - \mathbf{a}), m\}$ is the threshold of normalized distance for normal operation, $(\mathbf{c}^2)^{-1} \{, \}$ is the inverse of the chi-square cumulative distribution function, \mathbf{a} is the false alarm rate, and m is the degree of freedom or dimension which is equal to the number of chosen state variables. Due to modeling error M_{normal} is not exactly zero, so equation (1-2) takes modeling error into account to statistically evaluate whether Y is zero or not.

The above fault detection scheme can be illustrated using Figure 1-3. The residual distribution of normal operation can be characterized in terms of the covariance matrix Σ_{normal} and mean vector M_{normal} and depicted in the residual space plane as in Figure 1-3. In the residual space plane, any operating states (points) outside the normal operating region are classified as faulty while those inside the normal operation region are classified as normal. The normal operating ellipse is the fault detection boundary.

Practically, normal operation information, such as the mean and covariance matrix, is more accessible and more reliable, compared to faulty operation data. In addition, this scheme is intuitive in that the opposite of normal operation is abnormal operation. If the current operation point is not inside the normal operation region at a certain confidence according to reliable prior information, it should be classified as faulty

operation. Another advantage is that the fault detection decision is based on individual points rather than on a distribution, so it is more computational efficient for online application.

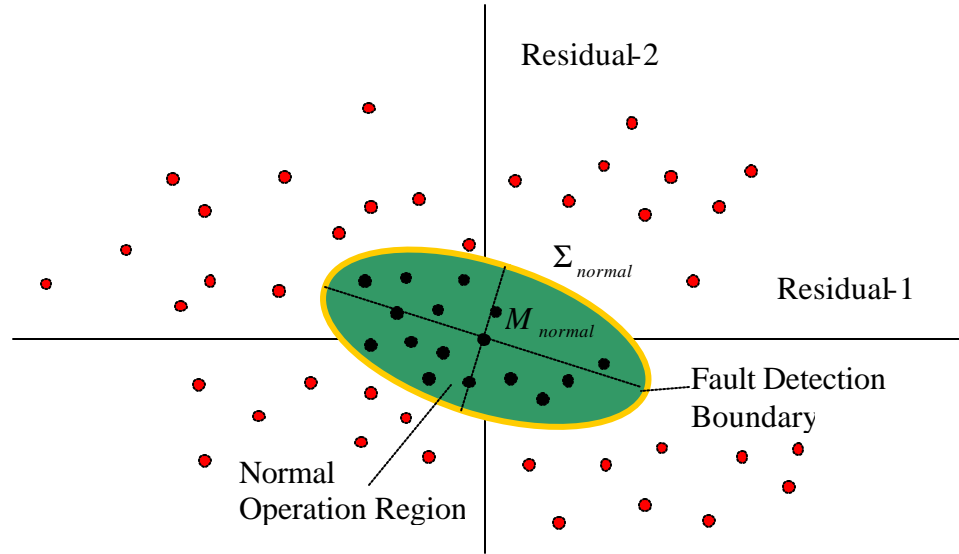


Figure 1-3 Fault detection classifier scheme for a 2-dimensional case

Although some quantitative fault diagnosis techniques can also do fault detection at the same time, implementing fault detection prior to attempting any diagnosis is recommended for following reasons:

1. Fault detection is much easier than fault diagnosis and the probability for abnormal operation is lower than normal operation. Therefore, advance fault detection would save considerable computation by eliminating the costly fault diagnosis step under normal operation.
2. Fault detection can take statistical analysis into account easily, which makes the fault diagnosis method more flexible.

1.1.2 Fault Diagnosis

Fault diagnosis, which entails the determination of the kind and location of the detected fault from a list of possibilities, needs to use the resulting Y (knowns) to find the causes X (unknowns) qualitatively or quantitatively. The nonlinear equation (1-1) can not get unique solutions for X for a given Y if $m < n$ and may result in inconsistencies if $m > n$, but it would not lose any generality to assume $m = n$. If $F(X)$ is known, multiple-simultaneous fault diagnosis becomes easy. However, it is very difficult, if not impossible, to find $F(X)$. To simplify equation (1-1), the first two items of Maclaurin's series can be used to linearize the nonlinear equations.

$$Y = F(0) + \frac{\partial F}{\partial X}(0)(X - 0) = JX \quad (1-3)$$

where,

$$F(0) = 0, \quad J = \frac{\partial F}{\partial X}(0) = \begin{bmatrix} \frac{\partial f_1}{\partial x_1} & \frac{\partial f_1}{\partial x_2} & \dots & \frac{\partial f_1}{\partial x_n} \\ \frac{\partial f_2}{\partial x_1} & \frac{\partial f_2}{\partial x_2} & \dots & \frac{\partial f_2}{\partial x_n} \\ \vdots & \vdots & \ddots & \vdots \\ \frac{\partial f_n}{\partial x_1} & \frac{\partial f_n}{\partial x_2} & \dots & \frac{\partial f_n}{\partial x_n} \end{bmatrix}$$

is the Jacobian matrix of $F(X)$ evaluated at 0. Compared to $F(X)$, J is much easier to estimate by experiment, which requires n^2 tests. After J is estimated, diagnosis can be done more easily by,

$$X = J^{-1}Y \quad (1-4)$$

It should be pointed out that a nonsingular matrix J is a necessary and sufficient condition for the above equation. For a practical engineering problem, this condition is readily guaranteed if the given set of state variables Y can be used to uniquely describe the system under the possible fault vector X . It is not difficult at all to find such a set of state variables Y with the help of physical knowledge.

1.1.2.1 Original SRB Fault Diagnosis Method

Although J can be estimated approximately by experiment, it is still not generic because different units of the same type may have different values of J . Estimation of J for individual systems is only practical for large or critical systems. Instead of estimating J , the rule-based FDD method proposed by Rossi and Braun is equivalent to using the sign of J to do fault diagnosis,

$$J_{sign} = sign(J) = sign \left(\begin{bmatrix} \frac{\partial f_1}{\partial x_1} & \frac{\partial f_1}{\partial x_2} & \dots & \frac{\partial f_1}{\partial x_n} \\ \frac{\partial f_2}{\partial x_1} & \frac{\partial f_2}{\partial x_2} & \dots & \frac{\partial f_2}{\partial x_n} \\ \vdots & \vdots & \ddots & \vdots \\ \frac{\partial f_n}{\partial x_1} & \frac{\partial f_n}{\partial x_2} & \dots & \frac{\partial f_n}{\partial x_n} \end{bmatrix} \right)$$

If faults occur individually, for example, only individual fault i happens at some time and

$$X_{sign} = sign(X) = sign \left(\begin{bmatrix} 0 \\ \vdots \\ x_i \\ \vdots \\ 0 \end{bmatrix} \right) = \begin{bmatrix} 0 \\ \vdots \\ 1 \\ \vdots \\ 0 \end{bmatrix}$$

and then

$$Y_{sign} = J_{sign} X_{sign} = sign \left(\begin{bmatrix} \frac{\partial f_1}{\partial x_i} \\ \frac{\partial f_2}{\partial x_i} \\ \vdots \\ \frac{\partial f_n}{\partial x_i} \end{bmatrix} \right).$$

So, if a fault happens individually, for a given matrix J_{sign} , Y_{sign} is determined uniquely by X_{sign} and vice versa. Inversely, this can be used to do fault diagnosis by comparing Y_{sign} with the column of J_{sign} in the statistical sense or mathematically by,

$$X_{sign} = \text{sign} \left(J_{sign}^T Y_{sign} - \begin{bmatrix} n \\ n \\ \vdots \\ n \end{bmatrix} \right) \quad (1-5)$$

By determining which entry of vector X_{sign} is 1, the fault diagnosis classifier can make a decision. The advantages of this method are that:

1. It is very easy to infer the J_{sign} accurately by n simple tests or from experience, compared to n^2 well- designed tests to estimate J roughly.
2. Although this method is derived from a linearization operation and driving-condition-independence assumption, it applies without these two assumptions. Actually there is no linearization approximation necessary for the sign of J_{sign} .
3. J_{sign} is generic at least for the same type of system, compared to different J 's for different systems.
4. This diagnosis method cleverly uses direction change pattern (sign) to convert an infinite classification problem (infinite number of fault levels for an individual type of fault) into a multiple classification one.

The drawback is that it can only handle individual faults.

It also should be pointed out that the above deduction only involves a matrix transposition operation instead of a matrix inverse operation, so the conclusion can be obtained without the assumption of $m = n$. This is because the SRB fault diagnosis method uses “sign” to do fault diagnosis qualitatively instead of quantitatively. The “possible inconsistencies” in the case of $m > n$ are impossible. Mathematically the maximum number of faults can be diagnosed by m state variables is up to $n = 2^m$, which can be either larger or smaller than m . Practically, in order to simplify the process of extracting rules, more state variables ($m > n$) are often adopted. For example, Rossi and Braun (1997) use seven state variables to deal with five faults.

Corresponding to the SRB fault diagnosis terminology, J_{sign} is equivalent to the fault diagnosis rules (see Table 1-1), which are expressed as positive and negative changes in residuals, so that each fault type corresponds to a unique quadrant of a multi-dimensional residual space. To decide which fault is the most probable is equivalent to identifying which quadrant the current measurement belongs to. Combined with the normal operating ellipse, coordinate axes form the fault diagnosis boundary (see Figure 1-4).

Table 1-1 Fault diagnosis rules

Fault type	T_{evap}	T_{sh}	T_{cond}	T_{sc}	T_{hg}	ΔT_{ca}	ΔT_{ea}
Refrigerant leakage	-	+	-	-	+	-	-
Comp. Valve Leak	+	-	-	-	-	-	-
Liquid Restriction	-	+	-	+	+	-	-
Condenser Fouling	+	-	+	-	+	+	-
Evaporator Fouling	-	-	-	-	-	-	+

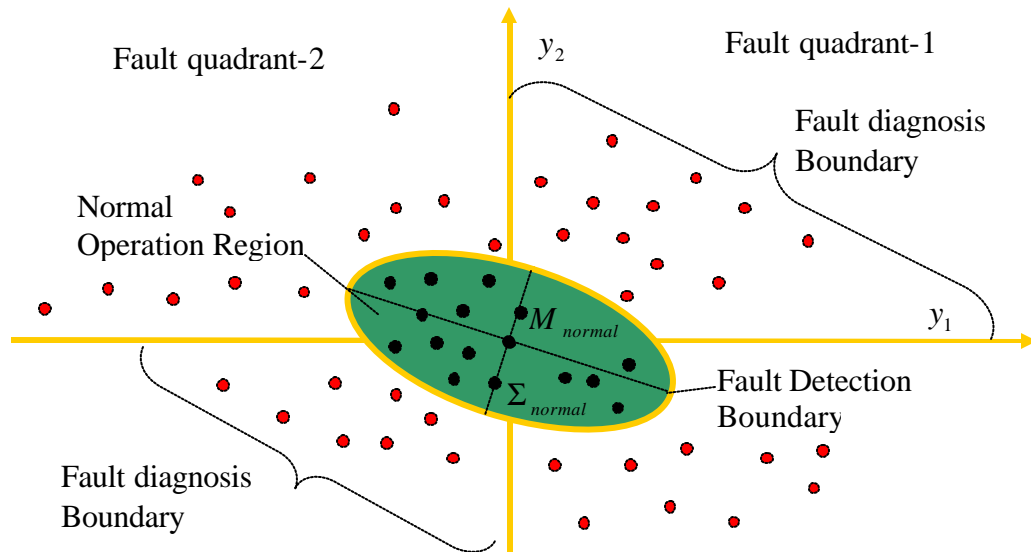


Figure 1-4 Fault detection and diagnosis boundaries

There are many good classifiers in the literature to handle finite classes (especially two classes) with regular patterns, which can be parameterized using covariance matrix and mean vector. However, for this problem, boundaries of each class

or pattern are coordinate axes, and can not be parameterized using a covariance matrix and mean vector. So, a fault diagnosis classifier to realize this diagnosis method is the key.

1.1.2.1.1 Original SRB Fault Diagnosis Classifier

Similar to the fault detection classifier, Rossi & Braun (1997) proposed a fault diagnosis classifier that involves evaluating the probability of the current distribution within each fault quadrant. When the probability of the most likely fault class exceeds that of the second most likely class by a preset threshold (fault probability ratio threshold), a diagnosis is made.

The merit of this classifier is that it maintains the SRB fault diagnosis method's merit, converting an infinite classification problem into a multi-classification one. However, similar to the fault detection classifier, direct numerical integration of the high dimensional (e.g., 7-dimensional for this case) probability distributions cannot be performed in real time using a microprocessor. However, unlike the detection classifier, it is impossible to find an analytical solution. Therefore, Rossi & Braun (1997) made an assumption that each dimension of the 7-dimensional density function is independent. In other words, the cross terms of the current operation covariance matrix are removed. This assumption simplified the 7-dimensional integration into a multiplication of seven 1-dimensional integrations.

However, experimental data show that the covariance matrix in normal operation is far from diagonal. The impact of the independence assumption on FDD performance was evaluated through comparison with a classifier that utilizes Monte-Carlo simulation and was shown to degrade fault diagnosis sensitivity. The results of this analysis appear in the attached ASHRAE paper (Li & Braun, 2003) and Deliverable 2.1.3 & 2.1.4 (2002).

1.1.2.1.2 Simple Distance Fault Diagnosis Classifier

To eliminate the independence assumption and improve fault diagnosis performance, a simple distance fault diagnosis classifier, which does not require

integration of the probability distributions, was developed and validated (see the attached ASHRAE paper (Li & Braun, 2003)). The performance of the method is good (good sensitivity for detecting/diagnosing faults) and is relatively insensitive to the choice of parameters and different operating conditions over a wide range (Li & Braun, 2003).

1.1.2.2 Decoupling-Based Fault Diagnosis Method

In order to extend the easily-implemented SRB fault diagnosis idea to handle multiple-simultaneous faults, equation (1-3) can be further transformed as follows,

$$PY = PJX$$

$$Z = \Lambda X = \begin{bmatrix} \mathbf{I}_1 x_1 \\ \mathbf{I}_2 x_2 \\ \vdots \\ \mathbf{I}_n x_n \end{bmatrix}$$

where

$$\Lambda = PJ = \begin{bmatrix} \mathbf{I}_1 & & & \\ & \mathbf{I}_2 & & \\ & & \ddots & \\ & & & \mathbf{I}_n \end{bmatrix}$$

$Z = PY$ is the transformed feature vector, and $P = \Lambda J^{-1}$ is the transformation matrix to make Λ diagonal. There exists infinite number of transformation combinations of Λ , P and Z by arbitrarily choosing a diagonal Λ if matrix J is non-singular (this can be guaranteed by proper choice of Y physically). This transformation decouples interactions among the different faults and makes each entry of the feature vector Z only correspond to unique fault entries of the fault vector X and vice versa.

$$X = \Lambda^{-1}Z = \begin{bmatrix} \frac{z_1}{\mathbf{I}_1} \\ \frac{z_2}{\mathbf{I}_2} \\ \vdots \\ \frac{z_n}{\mathbf{I}_n} \end{bmatrix} \quad (1-6)$$

To eliminate impacts of the linearization operation and driving-condition-independence assumption on diagnosis, the signum operation is applied to both sides of equation (1-6). Since Z , based on actual measurement or virtual estimate, is corrupted by measurement noise, system disturbance and modeling error, it should be statistically evaluated by the signum operation. So, the n -dimensional FDD problem has been decoupled to be $n-1$ -dimensional SRB FDD problems.

$$\text{sign}(X) = \text{sign}(\Lambda^{-1})\text{sign_stat}(Z)$$

where, $\text{sign_stat}(z)$ is a signum operation in a statistical sense, such that

$$\text{sign_stat}(z) = \begin{cases} -1, & \text{if } (z < -c\mathbf{s}_z) \\ 0, & \text{if } (|z| < c\mathbf{s}_z) \\ 1, & \text{if } (z > c\mathbf{s}_z) \end{cases}$$

where, c is a constant, say, 3.

$$X_{\text{sign}} = \begin{bmatrix} \frac{\text{sign_stat}(z_1)}{\text{sign}(\mathbf{I}_1)} \\ \frac{\text{sign_stat}(z_2)}{\text{sign}(\mathbf{I}_2)} \\ \vdots \\ \frac{\text{sign_stat}(z_n)}{\text{sign}(\mathbf{I}_n)} \end{bmatrix} \quad (1-7)$$

Equation (1-7) can be easily used to do multiple-simultaneous fault diagnosis. Although the impacts of the linearization operation and driving-condition-independence assumption on diagnosis are eliminated and multiple-simultaneous faults diagnosis can be handled, P and Z depend on J . If J is not known, P and Z can not be determined mathematically. Since there exists infinite number of transformation combinations of Λ , P and Z , from the mathematical viewpoint, it can be supposed without proof that there exists at least one Z which has physical meaning. So, if some Z can be found physically or empirically, the sign of Λ can also be decided empirically. Consequently, the methodology to physically find the decoupled feature vector Z becomes the key point of this approach, which will be discussed in next section 1.2.

In addition to the previous advantages listed for the SRB fault diagnosis method, the decoupling-based diagnosis method:

1. Simplifies fault detection from a high-D problem to n 1-D ones. Equation (1-2) boils down to following n 1-D equations,

$$sign_stat(|z_i|) = \left\{ \frac{(z_i - \mathbf{m}_{i,normal})^2}{\mathbf{s}_{i,normal}^2} > (\mathbf{c}^2)^{-1} \{(1-\mathbf{a}), 1\} \right\} \quad (1-8A)$$

or

$$= \left\{ \frac{|z_i - \mathbf{m}_{i,normal}|}{\mathbf{s}_{i,normal}} > N^{-1} \{(1-\mathbf{a}), 0, 1\} \right\} \quad (1-8B)$$

where, $i = 1, 2, \dots, n$.

2. Automatically achieves fault diagnosis without any extra computation immediately after fault detection is finished, because equations (1-8) have obtained what equation (1-7) needs. So the fault diagnosis classifier is not required.

$$x_{i,sign} = \frac{sign_stat(z_i)}{sign(\mathbf{I}_i)} = \frac{sign(z_i)sign_stat(|z_i|)}{sign(\mathbf{I}_i)} = sign_stat(|z_i|)$$

3. Overcomes the drawback of the SRB diagnosis method and handles multiple-simultaneous faults diagnosis.
4. Becomes more generic and system-independent and does not require complicated rules, which depend on the system.

1.1.2.3 Unilateral Decoupling Case

The above methodology based on full decoupling can handle multiple-simultaneous faults easily, but the criterion of full decoupling is not a necessary condition and can be lowered. To lower the full decoupling criterion has practical application. Although a physically decoupled feature vector Z can be found for a fault vector X , some features may be too expensive to be used for a non-critical FDD application. For example, condenser air flow rate, which is independent of any other faults, could be the decoupled feature for condenser fouling, but its measurement is too expensive. An alternative way to obtain this kind of feature is to estimate it using a virtual sensor, which may be corrupted by other faults. In other words, although fault i may not impact other

faults' features z_j 's ($j \neq i$), its feature z_i would be contaminated by another fault j ($j \neq i$). For example, the condenser air flow rate can be estimated from an energy balance with refrigerant mass flow rate estimated from a compressor performance map. However, the air flow rate estimate can be corrupted by a compressor valve leakage fault. Therefore, only the coupling from i to j is broken while the one from j to i is not. The worse case which can be handled is described in equation (1-9), in which the feature z_i would be impacted by faults j 's ($< i$) but not by those ($> i$).

$$Z = LX = \begin{bmatrix} l_{11} & & & \\ l_{21} & l_{22} & & \\ \vdots & \vdots & \ddots & \\ l_{n1} & l_{n2} & \cdots & l_{nn} \end{bmatrix} \begin{bmatrix} x_1 \\ x_2 \\ \vdots \\ x_n \end{bmatrix} \quad (1-9)$$

A sequential FDD method, which is contrasted with the above simultaneous FDD technique, can be used to solve this case.

Step 1 Do FDD on fault 1. Because feature z_1 is independent of any other faults, fault 1 can be detected and diagnosed independently. If fault 1 does not exist, go to the next step. Otherwise, don't go to the next step until either fault 1 is fixed if it is severe enough or the features, which have been corrupted by this fault, are modified according to this diagnosed fault in the virtual sensor.

$$z_1 = l_{11}x_1 \quad \Rightarrow \quad x_1 = \frac{z_1}{l_{11}} \quad \Rightarrow \quad x_{1,sign} = \frac{sign_stat(z_1)}{sign(l_{11})}$$

Step 2 Do FDD on fault 2. After step 1 has been done, either $x_1 = 0$ (if fault 1 does not exist or is fixed) or $l_{21} = 0$ (after modification according to fault 1) can be guaranteed. So,

$$z_2 = l_{21}x_1 + l_{22}x_2 = l_{22}x_2 \quad \Rightarrow \quad x_2 = \frac{z_2}{l_{22}} \quad \Rightarrow \quad x_{2,sign} = \frac{sign_stat(z_2)}{sign(l_{22})}$$

If it exists, fix fault 2 if it is severe enough, or otherwise modify the infected features.

$$\vdots \qquad \qquad \qquad \vdots$$

Step i Do FDD on fault i . After steps $1, 2, \dots, i-1$ have been done, either $x_k = 0$ or $l_{ik} = 0$ (for $k < i$) is guaranteed.

$$z_i = l_{i1}x_1 + l_{i2}x_2 + \dots + l_{ii}x_i = l_{ii}x_i \quad \Rightarrow \quad x_{i,sign} = \frac{sign_stat(z_i)}{sign(l_{ii})}$$

If it exists, fix fault i if it is severe enough, or otherwise modify the infected features.

\vdots \vdots

Step n Do FDD on fault n . After steps $1, 2, \dots, n-1$ have been done, either $x_k = 0$ or $l_{nk} = 0$ (for $k < n$) is guaranteed.

$$z_n = l_{n1}x_1 + l_{n2}x_2 + \dots + l_{nn}x_n = l_{nn}x_n \quad \Rightarrow \quad x_{n,sign} = \frac{sign_stat(z_n)}{sign(l_{nn})}$$

Fix fault n , if it exists and is severe enough.

1.2 Strategy for Decoupling Rooftop Unit System

The approach proposed in the previous section is based on decoupled features. Mathematically, there exists an infinite number of decoupled features, but for HVAC systems only those with intuitive physical meaning and those that are readily available (low-cost) are practical. This section develops a methodology or guidelines to find these kinds of features.

Philosophically, any problem could be approached microscopically or macroscopically or both to obtain required results with different details. A macroscopic approach uses external and overall information to interpret the observed phenomenon or predict a coming phenomenon, while a microscopic approach uses internal and component information to interpret or predict the phenomenon. In some situations, a macroscopic approach is preferred and unnecessary details are often ignored to simplify a complicated problem to be a manageable one at the cost of losing some information. For example, statistical thermodynamics considers physical models at the level of particles

while classical thermodynamics focuses on macroscopic and overall behavior of the particle system. FDD is not an exception. The original SRB method approaches the FDD problem from the overall system point of view. It considers the thermodynamic impact of different faults on overall system state variables, and uses models to predict normal operation state variables according to the overall system driving conditions, and then statistically evaluates the overall system state residuals to do FDD. The merit of this method is that it is simple and systematic, while the drawback is that it has difficulty in handling multiple-simultaneous faults and also depends on components which constitute the system. Multiple-simultaneous faults have almost infinite combinations with different fault types and levels and each combination has an overall impact on the overall system behavior. So it is almost impossible to extract so many system-level rules to do FDD with multiple-simultaneous faults. In addition, system-level rules depend on the composition or structure of the system. So these two drawbacks are inherent. To overcome these two drawbacks, an approach is developed that is based on individual components, which leads to identification of decoupled features.

1.2.1 Taxonomy of Faults

Taxonomy always is based on and also conversely contributes to the understanding of a subject. For the SRB FDD method, all the faults are treated equally and only the overall impacts of them on the overall system state variables are discriminated. For example, from the macroscopic and overall system point of view, the only discrimination among the 7 faults of refrigerant leakage, compressor valve leakage, condenser fouling, evaporator fouling, liquid-line restriction, refrigerant overcharge and non-condensable gas is the directional change of the overall system state variables' residuals. However, from microscopic and macroscopic points of view, the seven faults can be divided into two classes: component-level and system-level faults, which are shown in Figure 1-5. If classified from the view of fault cause, they can be divided into: operational and service faults.

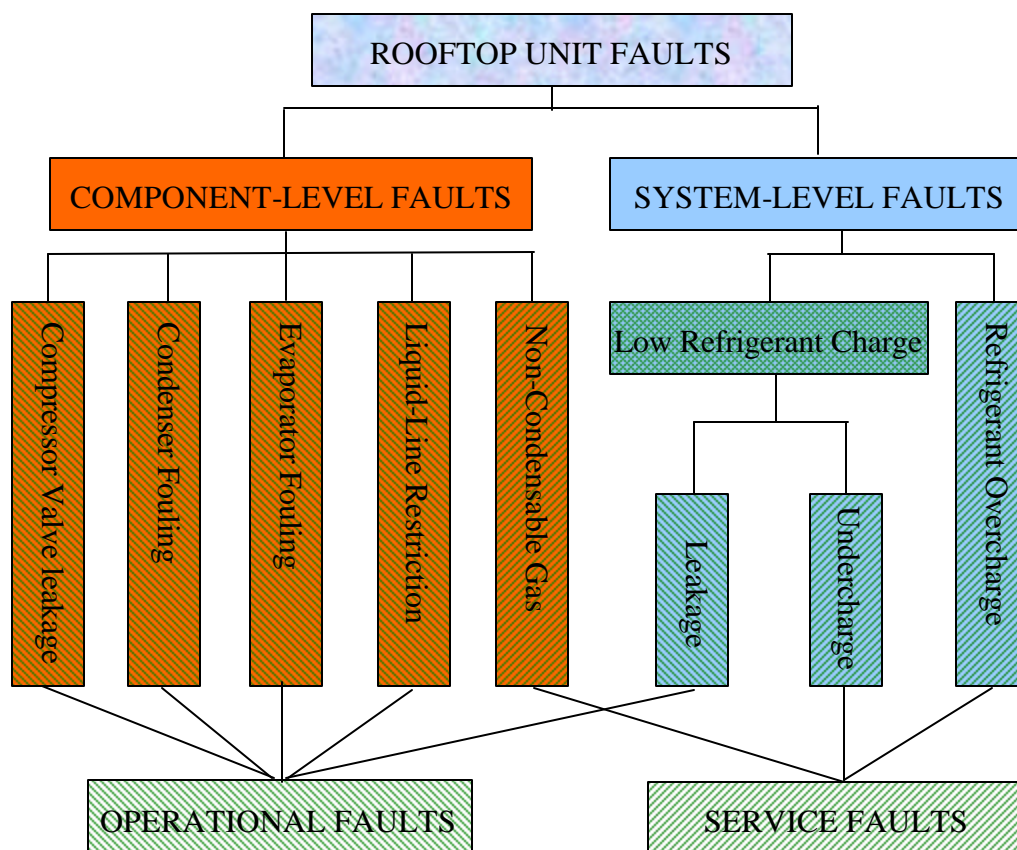


Figure 1-5 Taxonomy of Rooftop Faults

Compressor valve leakage is a component-level and operational fault. Although it impacts the overall system performance such as discharge temperature and condensing temperature, these impacts are indirectly related to a compressor volumetric efficiency reduction, which is directly impacted by valve leakage. A loss of compressor volumetric efficiency results in the reduction of refrigerant flow rate and increasing power consumption per refrigerant flow rate and discharge pressure and temperature, and other changes of system variables, whose direction and intensity depend on the expansion device used. Physically, this source impact can be confined to the compressor component. Since a compressor valve is normally damaged when the system is running, it is classified to be an operational fault.

Condenser fouling is also a component-level fault. For a rooftop unit, a direct impact of condenser fouling is the reduction of condenser air flow rate. A reduction of

condenser air flow rate results in a heat transfer penalty that causes changes in state variables, whose direction and intensity depend on the expansion device used. For example, evaporator temperature would increase significantly for fixed orifice systems but it would be unchanged for a TXV system until the fouling became very. A condenser fouling fault develops slowly when the system is running, so it is classified to be an operational fault.

Similar to condenser fouling, evaporator filter and/or coil fouling is a component-level fault. For a rooftop unit, a direct impact of evaporator fouling is the reduction of evaporator air flow rate. The reduction of evaporator air flow rate results in poorer heat transfer performance and causes changes of state variables, whose direction and intensity also depend on the expansion device used. For example, condenser temperature would decrease significantly for fixed orifice systems but it would be unchanged for a TXV system until the fouling became severe level. Evaporator fouling is classified as an operational fault.

A liquid-line restriction fault often occurs in a dryer or a filter and can be classified as a component-level fault. This fault has a direct impact of increasing the pressure and possibly temperature difference between the inlet and outlet of the dryer or filter. The increased pressure drop also results in a series of changes in state variables, whose direction and intensity are highly dependent on the expansion device used. For example, for a system with a fixed orifice as the expansion device, a liquid-line restriction will result in a significant reduction of refrigerant flow rate, while a moderate liquid-line restriction will not result in noticeable reduction of refrigerant flow rate when a TXV is used as the expansion device. This is because a TXV, an automatic control device, can compensate for an increased pressure drop resulting from a liquid-line restriction by increasing the opening of the TXV. Filter-driers continuously absorb water and dirt and become restricted over time, so a liquid line restriction fault is classified as an operational fault.

Low or high refrigerant charge is a system-level fault because it can occur anywhere and its direct impact cannot be confined to a particular location. Refrigerant overcharge only happens during service, so it is a service fault. Low refrigerant charge

has two possible causes: refrigerant is undercharged when service was done or there is a refrigerant leakage. Therefore, low charge can be a system-level operational or service fault.

Since the rooftop unit is under positive gage pressure system when charged, non-condensable gases can only be introduced during service. Non-condensable gases tend to accumulate in the condenser. Its primary impact is to increase heat transfer resistance and results in high condensing pressures and temperatures. So, non-condensable gas is considered to be a component-level service fault.

In summary, the characteristic of a component-level fault is that its source impact is confined to a specific location or component and all the other impacts on the system originate from this source impact. On the contrary, the source impact of a system-level fault cannot be confined to a specific location or component. Operational faults usually develop through running and occur randomly or gradually, while service faults are introduced with service.

1.2.2 Interactions

As depicted in Figure 1-6, a rooftop unit can be represented as a black-box, which is driven by faults, disturbances and overall system driving conditions, including T_{aoc} , T_{aie} , and f_{aie} , and outputs overall system state variables. It is difficult to tell which factors contribute to the current operation state directly from overall state variables. The SRB method uses normal state models to predict the normal operation states according to the overall driving conditions and generates residuals to decouple the interactions between driving conditions and faults, and further uses statistical analysis to further decouple the actions from disturbances, but leaves the couplings among the different faults untouched. This is the reason why the SRB FDD methods cannot handle multiple-simultaneous faults.

To handle multiple-simultaneous faults, the interactions among different faults should be decoupled. That is, if one independent feature, which is impacted only by one fault, can be found for each individual fault, then multiple-simultaneous faults are decoupled. For a linear system or some special nonlinear systems, a transformation can be found to diagonalize a transfer function matrix to decouple the system if a detailed system physical model is available. However, to obtain such a detailed physical model taking faults into account for a rooftop unit system is extremely difficult. Even so, an objective is to decouple the interactions between faults. Another way to decouple the system is to unfold the black-box representing the rooftop unit system to view it from a microscopic point of view and find some independent features with physical meaning for component-level faults, and isolate service faults from operation faults immediately after service is done and when the system stops. There is an important and practical restriction for the independence features. They should be able to be expressed as functions of low-cost measurements such as temperature and pressure.

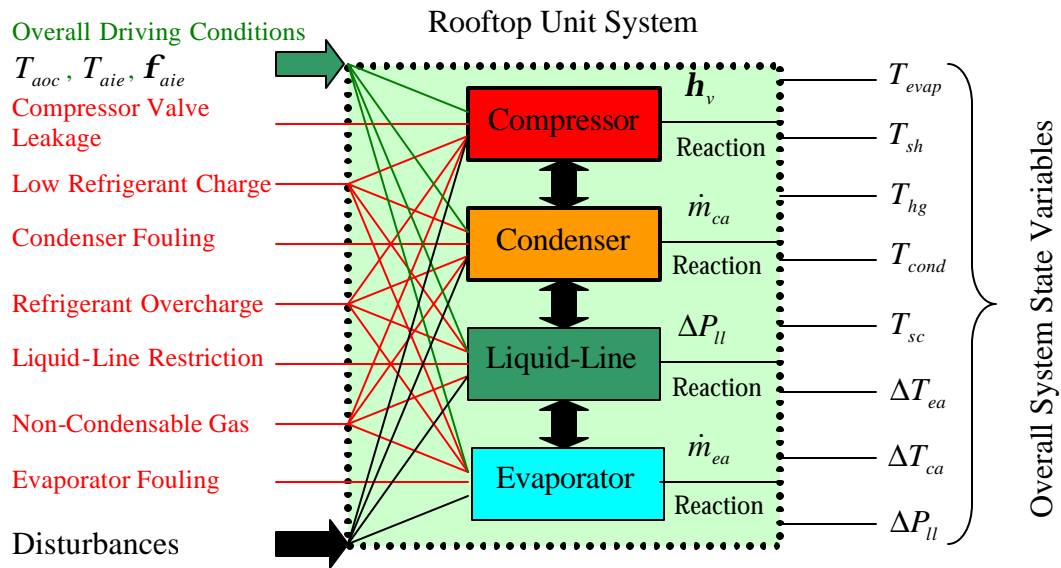


Figure 1-6 Interactions of Rooftop Unit System

1.2.3 Decoupling of Component Faults

In section 1.2.1, rooftop unit faults were divided into two classes according to two different criteria: component-level or system-level faults according to fault impact scope, and service or operational faults according to fault cause criterion. The characteristic of component-level faults is that their source impact can be confined to a component and this source impact is independent of other faults locally. So, the independence features for individual component-level faults can be found by investigating their source impacts. The independence features for service faults can be found by investigating their impact when the system stops.

1.2.3.1 Compressor Valve Leakage Fault

A compressor pumps a certain flow rate of refrigerant with certain thermodynamic state to the whole system. At steady state, the compressor is mainly driven by three conditions: any two independent thermodynamic parameters of the compressor inlet conditions, say pressure P_{suc} and temperature T_{suc} , and compressor outlet pressure P_{dis} . These three driving conditions determine all the outlet thermodynamic parameters and refrigerant mass flow rate $\dot{m}_{ref,pred}$. For a certain set of driving conditions: P_{suc} , T_{suc} and P_{dis} ,

$$T_{dis,pred} = ref(P_{dis}, h_{dis,pred}) \quad (1-10)$$

$$h_{dis,pred}(P_{suc}, T_{suc}, P_{dis}) = h_{suc}(P_{suc}, T_{suc}) + w_{pred}(P_{suc}, T_{suc}, P_{dis}) - Q_{loss} \quad (1-11)$$

where,

$$w_{pred}(P_{suc}, T_{suc}, P_{dis}) = \frac{\dot{W}_{pred}(P_{suc}, T_{suc}, P_{dis})}{\dot{m}_{ref,pred}(P_{suc}, T_{suc}, P_{dis})}$$

is the compressor specific power consumption, $h_{dis,pred}$ is the predicted discharge line refrigerant enthalpy, T_{dis} is discharge line temperature, h_{suc} is suction line refrigerant enthalpy.

When a compressor valve has leakage, the compressor volumetric efficiency η_v decreases compared to the given set of driving conditions. The decrease of volumetric efficiency η_v causes the refrigerant mass flow rate \dot{m}_{ref} to decrease compared to the normal value for the given set of driving conditions. Although the power consumption \dot{W} may increase or decrease, w , power consumption per mass flow rate, would increase compared to the normal value. As a result, the compressor discharge line enthalpy h_{dis} would increase significantly. Since, at a given pressure P_{dis} , the discharge line temperature T_{dis} monotonically increases with h_{dis} , the discharge line temperature would increase significantly due to a compressor valve leakage fault.

Using a compressor map, $w_{pred}(P_{suc}, T_{suc}, P_{dis})$ can be predicted and then $T_{dis,pred}$ can be calculated. Using this model, the residual ΔT_{dis} between predicted $T_{dis,pred}$ and measured $T_{dis,meas}$ would be a function of compressor valve leakage independent of operating conditions and faults in other components. Figure 1-7 shows the decoupling scheme. It can be seen that the residual ΔT_{dis} is only impacted by compressor faults and all the other factors including other component faults and overall system driving conditions have been taken into account by P_{suc} , T_{suc} and P_{dis} .

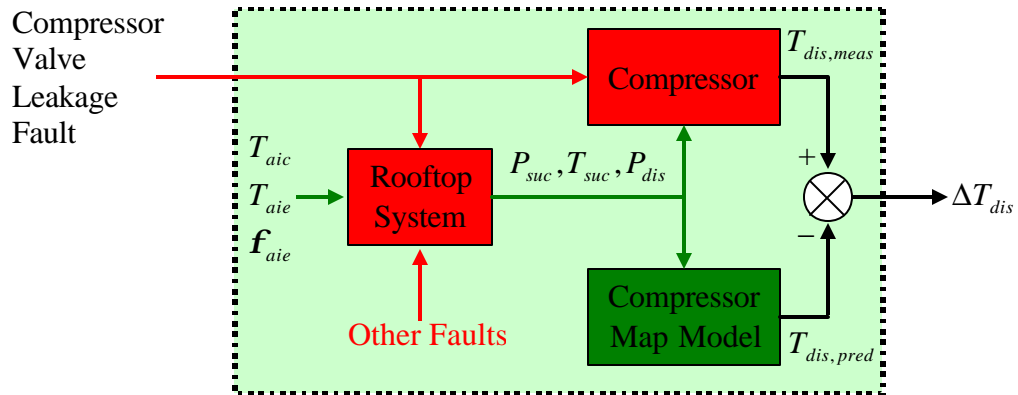


Figure 1-7 Compressor Valve Leakage Decoupling Scheme

1.2.3.2 Condenser-Related Faults

Usually, one component-level fault corresponds to one component, so the decoupling can easily be achieved. However, it is possible for one component to have more than one component-level fault. The condenser is such a case. There are two possible component-level faults related to condensers: non-condensable gas and condenser fouling faults. Although the SRB method can handle low-dimensional cases such as 2-D without decoupling, it is still advisable to find an independence feature to further decouple them. Fortunately, these two condenser-related faults can be decoupled further.

1.2.3.2.1 Non-Condensable Gas Fault

As discussed in section 1.2.1, a non-condensable gas fault is not only a component-level fault but also a service fault and can only be introduced through service. In addition, its impact influences not only the performance of a running system but also the state of a stopped system. When a system is stopped, the non-condensable gas tends to accumulate in the condenser (it can possibly to accumulate in other components such as evaporator, but this will not impact final the result). The non-condensable gas fault can be detected and diagnosed immediately after the service was done and the system is stopped. For a given system, the condenser pressure at any point can be related to the compressor discharge according to

$$P_{cond} = P_{dis} - G^2 \left(\frac{1}{2D} \int_0^L f v dx + v_2 - v_1 \right) \quad (1-12)$$

where P_{cond} and P_{dis} are condenser pressure and discharge line pressure, G is mass flux, D is tube diameter, f is Darcy friction factor, L is tube length, and v , v_1 and v_2 are specific volume.

After the system stops, it will take some time for the system to balance high-side and low-side pressures. During pressure balancing, the flow rate is quite small ($G \approx 0$) so,

$$P_{cond} = P_{dis} - 0^2 \left(\frac{1}{2D} \int_0^L f v dx + v_2 - v_1 \right) = P_{dis}$$

After the system stops, at least one of the condenser and evaporator coils will be filled with two-phase refrigerant and the refrigerant will not be subcooled anywhere. For a TXV system, since the TXV has the ability to shut off the refrigerant flow when the compressor stops, the refrigerant in both coils could remain in a two-phase condition. For a fixed-orifice system, after the system has been off for a long time in the daytime, the refrigerant in the condenser will normally be superheated. However, it takes some time for the high and low sides to reach a balance and for the refrigerant to become superheated. In addition, in the nighttime at many locations the outdoor temperature is normally lower than the indoor temperature, so the refrigerant in the condenser will be two-phase mixture when the system is off. Consequently, it is safe to assume that the refrigerant in the condenser would be saturated at some time when the system is off and the following derivation holds.

$$T_{cond,pred} = T_{sat}(P_{cond}) = T_{sat}(P_{dis}) \quad (1-13)$$

$$\Delta T_{cond,norm} = T_{cond,meas} - T_{cond,pred} = T_{cond,meas} - T_{sat}(P_{dis}) = 0 \quad (1-14)$$

However, when there is non-condensable gas in the system and according to Dalton's law,

$$P_{ref,vapor} = P_{dis} - P_{ncg} = (1 - y_{ncg})P_{dis}, \quad y_{ncg} \gg 0 \quad (1-15)$$

$$\begin{aligned} y_{ncg} &= \frac{P_{ncg}}{P_{dis}} = \frac{N_{ncg}}{N_{ncg} + N_{ref,vapor}} = \frac{(N_{ncg}/N_{ref,total})}{(N_{ncg}/N_{ref,total}) + (N_{ref,vapor}/N_{ref,total})} \\ &= \frac{1}{1 + \frac{(N_{ref,vapor}/N_{ref,total})}{(N_{ncg}/N_{ref,total})}} \\ &= \frac{1}{1 + \frac{c_{ref}}{r_{ncg}}} \end{aligned}$$

where, $P_{ref,vapor}$ is the refrigerant partial pressure, P_{ncg} is non-condensable gas partial pressure, y_{ncg} is the mole fraction of non-condensable gas in the refrigerant vapor-gas

mixture, c_{ref} is known as the quality or the mole fraction of vapor refrigerant in the refrigerant liquid-vapor mixture, r_{ncg} is the mole ratio of non-condensable gas over total refrigerant, and N_{ncg} , $N_{ref-vapor}$, and $N_{ref,total}$ are the numbers of moles of non-condensable gas, vapor refrigerant, and total refrigerant.

According to the Clapeyron equation,

$$\left(\frac{dP}{dT}\right)_{sat} = \frac{h_{fg}}{Tv_{fg}}$$

$$\Rightarrow \Delta T \approx \Delta P \frac{Tv_{fg}}{h_{fg}}$$

where, h_{fg} is the enthalpy of vaporization, v_{fg} is specific volume change, and T is absolute temperature for vaporization. So, equation (1-14) can be modified to,

$$\begin{aligned} \Delta T_{cond,abnorm} &= T_{cond,meas} - T_{cond,pred} = T_{cond,meas} - T_{sat}(P_{dis}) \\ &= \{T_{cond,meas} - T_{sat}(P_{ref,vapor})\} + \{T_{sat}(P_{ref,vapor}) - T_{sat}(P_{dis})\} \\ &= T_{sat}(P_{ref,vapor}) - T_{sat}(P_{dis}) \\ &= (P_{ref,vapor} - P_{dis}) \frac{T_{cond,meas} v_{fg}}{h_{fg}} \\ &= -(1 - y_{ncg}) \frac{P_{dis} v_{fg}}{h_{fg}} T_{cond,meas} \\ &= \left(1 - \frac{1}{1 - y_{ncg}}\right) \frac{P_{ref,vapor} (T_{cond,meas}) v_{fg}}{h_{fg}} T_{cond,meas} \quad (1-16) \\ &= \frac{-r_{ncg}}{c_{ref}} \frac{P_{ref,vapor} (T_{cond,meas}) v_{fg}}{h_{fg}} T_{cond,meas} \end{aligned}$$

For an air conditioning application, $\frac{P_{ref,vapor} (T_{cond,meas}) v_{fg}}{h_{fg}}$ can be approximated as

a constant, 0.125, and if the Celsius scale is used, equation (1-16) can be reduced to be,

$$\begin{aligned} \Delta T_{cond,abnorm} &= -\frac{r_{ncg}}{c_{ref}} (0.125)(273.15 + T_{cond,meas}) \\ &= \left(-\frac{r_{ncg}}{c_{ref}}\right) (34.14 + 0.125 T_{cond,meas}) \end{aligned}$$

$$\Delta T_{cond,abnorm} < -34.14 \frac{r_{ncg}}{c_{ref}} \text{ } ^\circ C \quad (1-17)$$

Suppose that there is 1% (in mole sense) non-condensable gas in the whole system, and refrigerant quality is 0.03

$$r_{ncg} = \frac{1}{99} \text{ and } c_{ref} = 0.05$$

then,

$$y_{ncg} = \frac{1}{1 + \frac{c_{ref}}{r_{ncg}}} = \frac{1}{1 + \frac{0.05}{1/99}} \approx 0.17$$

It is obvious that although the mole fraction of the non-condensable gas in the whole system is very small, say 1%, the refrigerant partial pressure $P_{ref,vapor}$ is considerably less than the total pressure P_{dis} (83%). According to equation (1-17),

$$\Delta T_{cond,abnorm} < -34.14 \frac{r_{ncg}}{c_{ref}} = -34.14 \frac{1/99}{0.05} = -6.90 \text{ } ^\circ C = -12.41 \text{ } F$$

So, $\Delta T_{cond,abnorm}$ is a very sensitive FDD feature. From equation (1-17), it is obvious that $\Delta T_{cond,abnorm}$ is inversely dependent on the refrigerant quality, c_{ref} . If the refrigerant quality approaches to 1, the sensitivity would be low. However, the high quality case is not possible when the system is stopped and immediately after the service. Table 1-2 lists the refrigerant quality at different ambient temperature for a 3-ton rooftop unit with the compressor off and nominal charge. From Table 1-2, it can be seen that refrigerant quality is very low when the system is stopped and fully charged, so the sensitivity would be very high.

Table 1-2 c_{ref} and $\Delta T_{cond,abnorm}$ with compressor off and nominal charge and 1% non-condensable gas

$T_{amb} (^\circ C)$	20	30	40	30
c_{ref}	0.031	0.040	0.032	0.063
$\Delta T_{cond,abnorm} (^\circ C)$	-11.12	-8.62	-6.63	-3.31

Table 1-3 also lists the refrigerant quality for different refrigerant charge levels with an ambient temperature of 30°C. From Table 1-3, it can be seen that refrigerant overcharge would raise the non-condensable FDD sensitivity, whereas refrigerant undercharge would reduce the non-condensable FDD sensitivity. Even at an unrealistic worst case of 20% of nominal charge, this feature would provide sufficient FDD sensitivity.

Table 1-3 c_{ref} and $\Delta T_{cond,abnorm}$ with compressor off and ambient temperature=30°C and 1% non-condensable gas

Charge Level	20%	40%	60%	80%	90%	100%	110%	120%	140%
c_{ref}	0.384	0.169	0.098	0.062	0.030	0.040	0.033	0.026	0.016
$\Delta T_{cond,abnorm}$ (°C)	-0.90	-2.04	-3.32	-3.36	-6.90	-8.62	-10.3	-13.3	-21.6

In summary, although refrigerant charge has some influence on the sensitivity of $\Delta T_{cond,abnorm}$ to detect and diagnose a non-condensable gas fault, the influence would not change the fault pattern and the sensitivity is high enough over a very large range of ambient and charge conditions. So, the non-condensable gas fault could be detected and diagnosed independently. In a broad sense, $\Delta T_{cond,abnorm}$ could be considered as an independent feature to detect and diagnose a non-condensable gas fault and the coupling between non-condensable gas fault and condenser fouling can be broken when the system stops. Since it is not a real decoupling, it is termed pseudo-decoupling to distinguish it from real decoupling.

1.2.3.2.2 Condenser Fouling Fault

A rooftop unit system typically uses a constant-speed fan to force ambient air to cool condenser coils. Fouling mainly develops on the air side and affects heat transfer in two ways. On the one hand, it increases the thermal resistance mainly by small-scale dirt particles attached to the coils, and on the other hand, it reduces the air flow area by large-scale dirt and results in a reduction of air flow rate. Since a rooftop air conditioner is normally installed outside, there can be a lot of large-scale dirt such as paper and leaves.

Also, high velocity air makes it difficult for small-scale dirt to attach to the condenser coils. Therefore, the condenser air flow rate reduction can be chosen as an independent feature for condenser fouling. Applying the first thermodynamic law to the condenser,

$$\dot{m}_{ca} C_{p,air} (T_{aoc} - T_{aic}) = \dot{m}_{ref} (h_{dis}(P_{dis}, T_{dis}) - h_{ll}(P_{ll}, T_{ll})) \quad (1-18)$$

$$\dot{m}_{ca} = \frac{\dot{m}_{ref} (h_{dis}(P_{dis}, T_{dis}) - h_{ll}(P_{ll}, T_{ll}))}{C_{p,air} (T_{aoc} - T_{aic})} \quad (1-19)$$

where, \dot{m}_{ca} is condenser air mass flow rate, $C_{p,air}$ is air specific heat, T_{aoc} is condenser outlet air temperature, T_{aic} is condenser inlet air temperature, \dot{m}_{ref} is refrigerant mass flow rate, h_{dis} is discharge line refrigerant enthalpy, P_{dis} is discharge line pressure, T_{dis} is discharge line temperature, h_{ll} is liquid line refrigerant enthalpy, and T_{ll} is the liquid line temperature.

Normally the refrigerant is subcooled at the outlet of condenser. If it is not subcooled, then a fault is most likely present, which the FDD system should detect and diagnose. So, the enthalpy $h_{ll}(P_{ll}, T_{ll})$ can be approximated by $h_{ll}(P_{dis}, T_{ll})$ very accurately.

$$\dot{m}_{ca} \approx \frac{\dot{m}_{ref} (h_{dis}(P_{dis}, T_{dis}) - h_{ll}(P_{dis}, T_{ll}))}{C_{p,air} (T_{aoc} - T_{aic})} \quad (1-20)$$

Since all the parameters on the right side of equation (1-20) are measured directly or estimated from measurements by virtual sensors, equation (1-20) offers a virtual sensor or observer for measured air mass flow rate $\dot{m}_{ca,meas}$. The normal model for \dot{m}_{ca} would be constant value for a fixed-speed condenser fan. Practically, the normal value of \dot{m}_{ca} would be learned when the FDD scheme is implemented assuming that there is no fouling.

In order to evaluate refrigerant properties in equation (1-20), it is necessary that there be no non-condensable gas in the system. This assumption is reasonable, because the non-condensable gas fault can be excluded immediately after service is done. Figure 1-8 illustrates the decoupling scheme for condenser fouling and non-condensable gas faults.

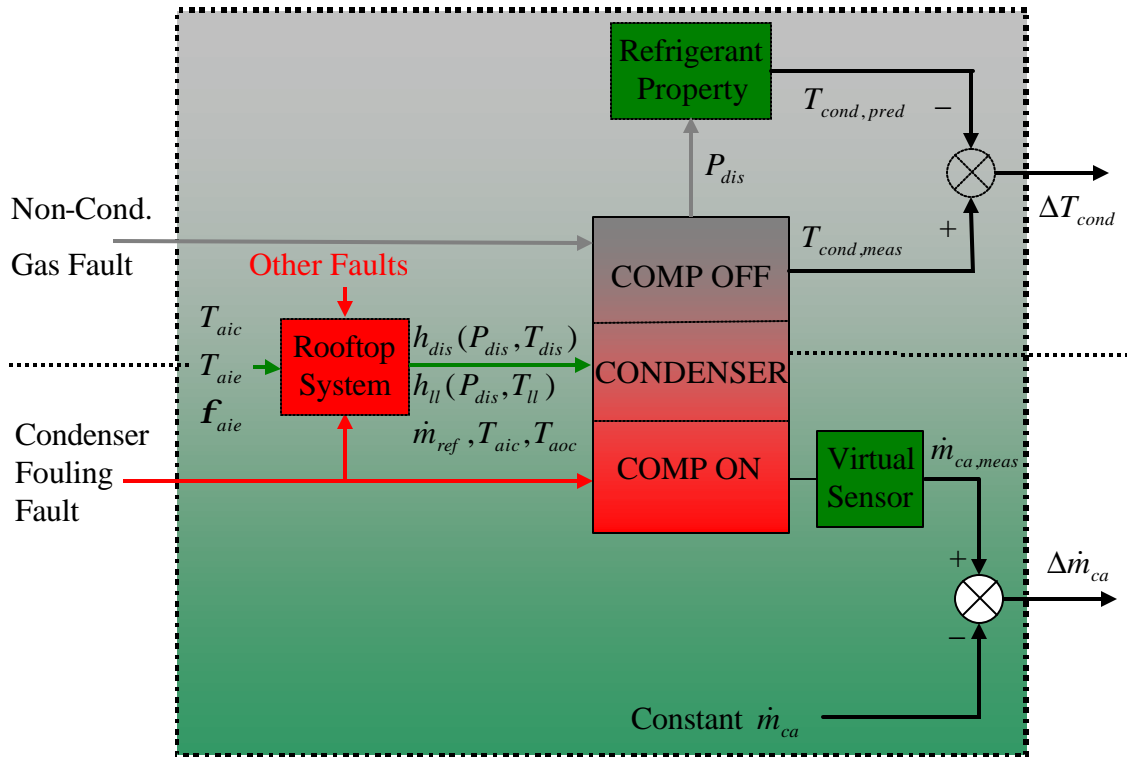


Figure 1-8 Condenser Fouling and Non-Condensable Gas Faults Decoupling Scheme

1.2.3.3 Liquid-line Restriction Fault

Because water dissolved in the refrigerant would result in clogging of the expansion device and dirt such as carbon and rust in the system would wear the compressor valve and cylinder, rooftop units usually include dryer/filters to absorb water and filter the dirt. When the dryer/filter is saturated with too much water and dirt, it would result in significant pressure loss and need to be replaced.

The source and direct impact of a restriction is significant pressure drop ΔP_{ll} , but a temperature drop ΔT_{ll} is not a sufficient feature. Only when the restriction is large enough to cause the refrigerant to change phase, would the temperature begin to drop.

Figure 1-9 illustrates the liquid-line restriction on a P-h diagram. Normally the refrigerant at the condenser outlet (3) has about 15 F subcooling. For the conditions of Figure 1-9, the pressure drop resulting from a restriction would need to be larger than 49.2 psi for the temperature to drop and 14.9 psi more pressure drop would cause a 5 F temperature drop. Consequently, if temperature drop is used to do FDD, any restriction lower than 49.2 psi is not detectable and to get 5 F temperature drop, a total pressure drop of 64.1 psi is necessary. In addition, when there is a liquid-line restriction, the actual subcooling would become even larger (say 20 F at 3') and more pressure drop (64.1 psi) is needed to trigger the temperature drop.

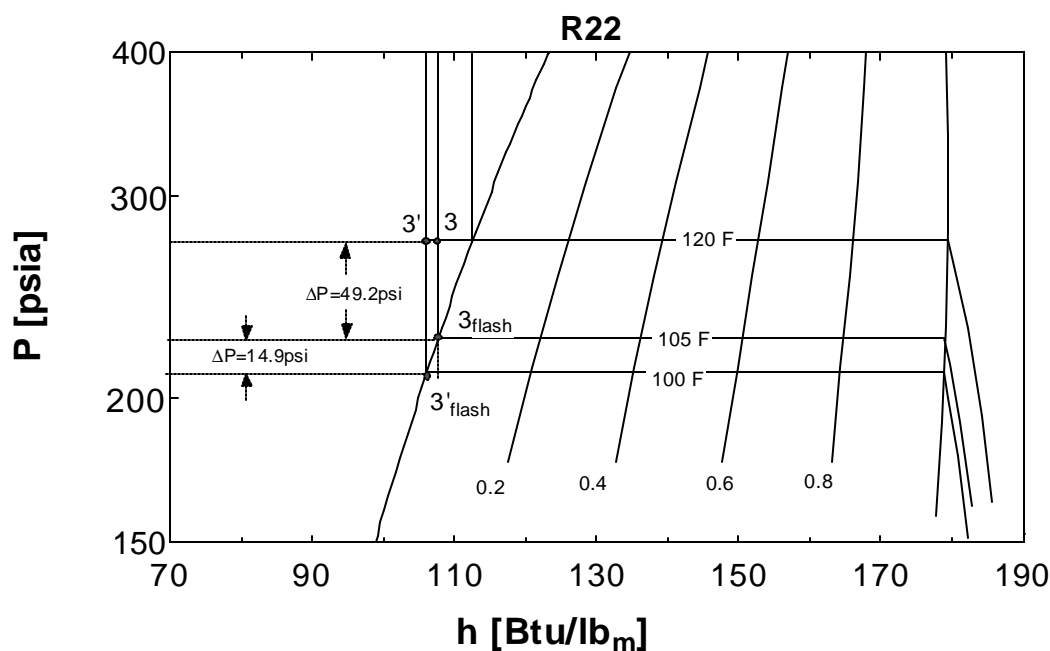


Figure 1-9 Liquid-line restriction illustration

It also should be pointed out that a large restriction may be necessary to obtain a phase change but once the phase change occurs the pressure drop rate would increase significantly with the restriction size because two-phase flow is more sensitive to flow area than pure liquid refrigerant flow. The dryer/filter with a restriction acts as an expansion device, which can result in a significant pressure and temperature drop between the inlet and outlet of the dryer/filter. Therefore, the temperature drop can serve

as an independent feature only for very large liquid-line restriction faults. However, low-cost is an advantage of using temperature drop as the feature.

To detect small liquid-line restriction faults, the pressure drop could be used. However, pressure measurements are relatively expensive. Therefore, an approximate scheme should be developed. Figure 1-10 illustrates the relevant components and state variables.

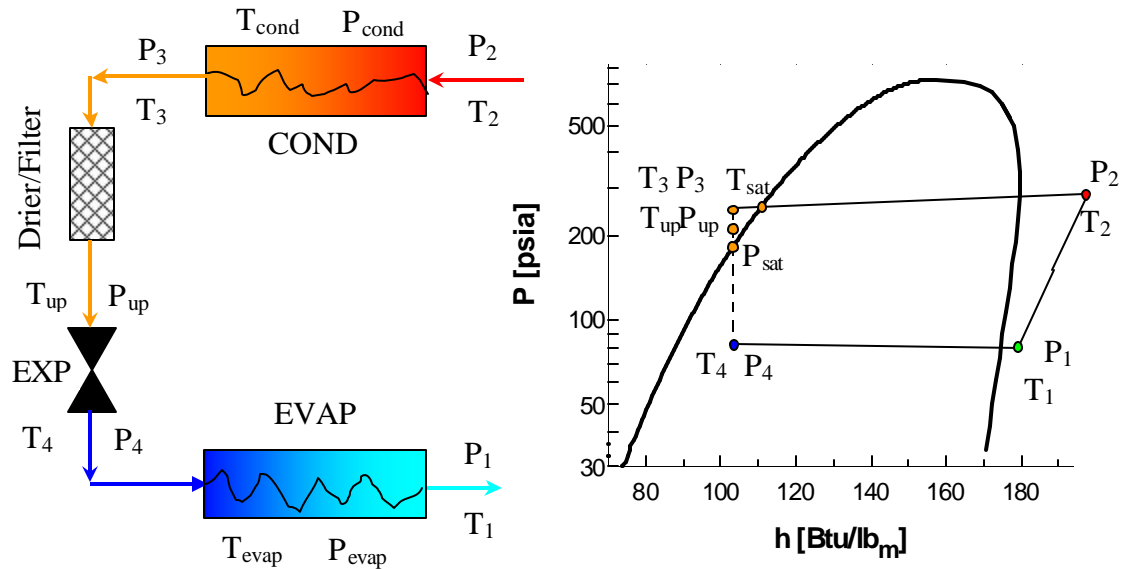


Figure 1-10 Vapor Compression Cycle Illustration

Using the nomenclature defined in Figure 1-10, the pressure drop across the filter/dryer is

$$\Delta P_{ll} = P_3 - P_{up}$$

P_3 can be approximated very well by $P_{cond} = P_{sat}(T_{cond})$ if T_{cond} can be measured properly because the condenser pressure drop resulting from liquid refrigerant flow is small (less than 3 psi). The key point for this technique is placement of the condenser temperature sensor, because a non-saturated temperature would result in large estimation error, especially if a superheated temperature were measured. A relatively safe approach is to place the temperature sensor at the point where different condensing circuits are combined, where the refrigerant is almost never superheated unless the refrigerant charge

is extremely low. However, it is possible for the refrigerant at this point to have a small degree of subcooling if there is a severe liquid line restriction or a refrigerant overcharge fault. Even so, a small subcooling would not have a big impact. On the contrary, 1-2 F subcooling would compensate for the error resulting from neglecting the pressure drop in the liquid-line and condenser subcooling section. 4 F subcooling may result in around a -3 psi error. Another more approximate approach to estimating P_3 is to assume constant pressure drop across condenser, which may result in a ± 10 psi error.

An estimate of P_{up} can be obtained by modeling the expansion device. There are rather mature techniques available for modeling fixed orifices including short tube and capillary tube (see Appendix 1). For a TXV or EXV system, Appendix 1 develops a practical and useful modeling approach to estimate the upstream pressure using factory performance map data. The models for estimating pressures work as a virtual sensor for pressure drop. The decoupling scheme is shown in Figure 1-11.

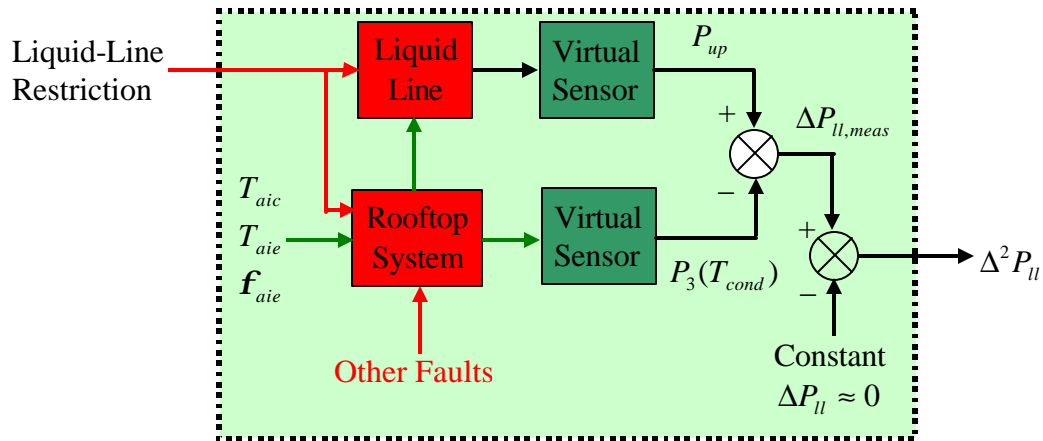


Figure 1-11 Liquid-Line Restriction Decoupling Scheme

1.2.3.4 Evaporator Fouling Fault

Similar to condenser fouling, evaporator or evaporator filter fouling also develops on the air side and the dominant impact is a reduction of air flow rate. Therefore, the

evaporator air flow rate reduction can be chosen as an independent feature for evaporator fouling. Applying the first thermodynamic law to the evaporator,

$$\dot{m}_{ea} (h_{aie}(T_{aie}, f_{aie}) - h_{aoe}(T_{aoe}, f_{aoe})) = \dot{m}_{ref} (h_{suc}(P_{suc}, T_{suc}) - h_{ll}(P_{ll}, T_{ll})) \quad (1-21)$$

$$\dot{m}_{ea} = \frac{\dot{m}_{ref} (h_{suc}(P_{suc}, T_{suc}) - h_{ll}(P_{ll}, T_{ll}))}{(h_{aie}(T_{aie}, f_{aie}) - h_{aoe}(T_{aoe}, f_{aoe}))} \quad (1-22)$$

where, \dot{m}_{ea} is evaporator air mass flow rate, h_{aoe} is the evaporator outlet air enthalpy, f_{aoe} is the relative humidity of evaporator outlet air, T_{aoe} is evaporator outlet air temperature, h_{aie} is evaporator air inlet enthalpy, T_{aie} is evaporator inlet air temperature, f_{aie} is the relative humidity of evaporator inlet air, h_{suc} is suction line refrigerant enthalpy, P_{suc} is suction line pressure, and T_{suc} is suction line temperature.

All the parameters on the right side of equation (1-22) are measured or estimated, so equation (1-22) is a virtual sensor or observer for measuring $\dot{m}_{ea, meas}$. Figure 1-12 illustrates the above decoupling scheme.

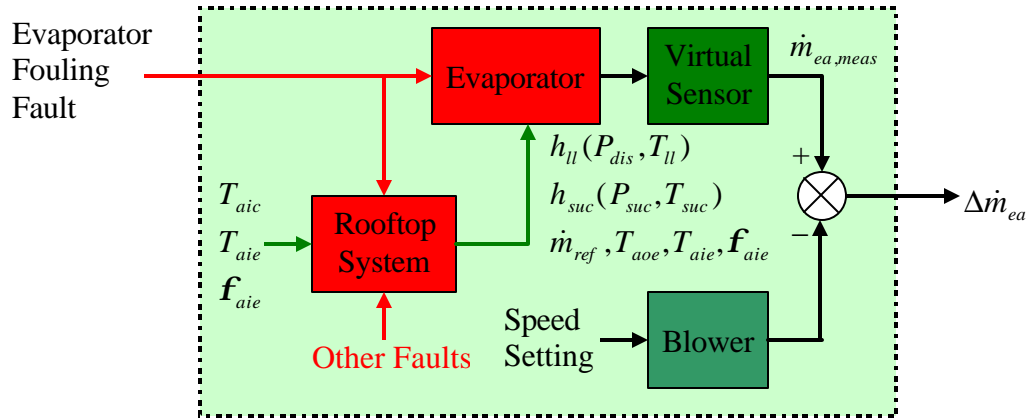


Figure 1-12 Evaporator Fouling Decoupling Scheme

Unlike condenser air mass flow rate, $\dot{m}_{ea, pred}$ normally has more than one speed setting, but it is constant for a given setting. So, the block 'blower' acts as a normal model, whose input is the setting control signal and output is a constant air mass flow rate

$\dot{m}_{ea,pred}$ corresponding to the speed setting. Practically, the actual value of $\dot{m}_{ea,pred}$ would be learned when the FDD scheme is implemented with the assumption of no fouling.

1.2.3.5 Summary of Decoupling Component-Level Faults

After decoupling the 5 component-level faults in the previous sections, the decoupling scheme for component faults can be summarized in Figure 1-13.

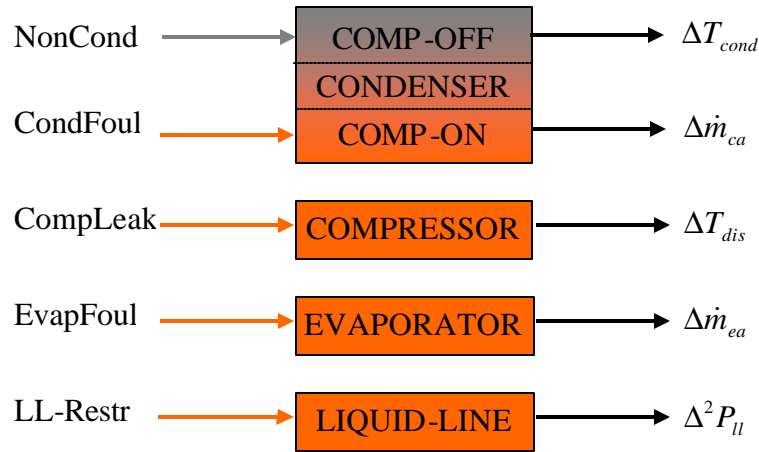


Figure 1-13 Ideal Decoupling Scheme of Component-Level Faults with Refrigerant mass flow measurement

From Figure 1-13, it can be seen that:

1. Immediately after system service has been done and when the system is stopped, ΔT_{cond} is a pseudo-decoupling feature for non-condensable gas;
2. $\Delta \dot{m}_{ca}$ is independent of any faults except for condenser fouling, so it serves as a decoupling feature for condenser fouling;
3. Similar to $\Delta \dot{m}_{ca}$, $\Delta \dot{m}_{ea}$ is the decoupling feature for evaporator fouling;
4. ΔT_{dis} is only dependent on compressor valve leakage fault, so it can be used to break the coupling from compressor valve leakage to any other faults;

5. $\Delta^2 P_{ll}$ deviates drastically from zero only when there is a restriction in the liquid-line and is a decoupling feature for liquid-line restriction.

In decoupling condenser fouling and evaporator fouling faults, a refrigerant mass flow rate measurement \dot{m}_{ref} is necessary. However, a mass flow rate meter is too expensive for this application. So, the decoupling scheme shown in Figure 1-12 is called ideal decoupling. An alternative way to obtain a refrigerant mass flow rate measurement \dot{m}_{ref} is to estimate it indirectly using compressor map data with some readily available measurements. However, using a virtual sensor instead of a real sensor has a penalty. Because the accuracy of real refrigerant mass flow rate measurement has nothing to do with other faults such as a compressor leakage fault, an ideal decoupling among component-level faults can be achieved if a real measurement is used. However, the estimate from a virtual sensor is strongly dependent on the compressor performance. If the compressor has a valve or other fault, the refrigerant mass flow rate could be overestimated. Since condenser and evaporator air mass flow rates are also estimated by virtual sensors, which use refrigerant mass flow rate as an input, overestimated refrigerant mass flow rate would result in underestimated condenser and evaporator air mass flow rate. Therefore, the couplings from compressor leakage to condenser and evaporator fouling are not broken. In other words, use of a virtual sensor would result in unilateral decoupling between a compressor leakage fault and condenser and evaporator fouling faults.

Unlike control applications, in which bilateral decoupling is preferred, unilateral decoupling is sufficient for an FDD application. Later sections will discuss how to do FDD after decoupling. Figure 1-14 modifies the ideal decoupling scheme in Figure 1-13 to an actual decoupling scheme using a virtual sensor for refrigerant flow rate.

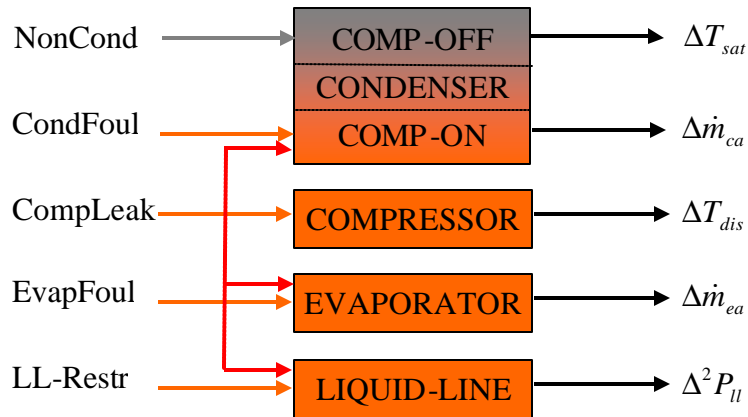


Figure 1-14 Actual Decoupling Scheme of Component-Level Faults without Refrigerant Mass Flow Measurement

1.2.4 Decoupling System-Level Faults

This section interprets relationships among the three system-level faults: refrigerant overcharge, refrigerant undercharge and refrigerant leakage. Although these three faults are system-level faults, from the classification criteria of fault cause, refrigerant overcharge and undercharge faults are service faults while refrigerant leakage is an operational fault. Service faults only happen during service and fault severity would not change, while operational faults normally develop during operation and they would deteriorate. This information contributes to the development of an FDD technique.

From the viewpoint of fault effect, refrigerant undercharge and refrigerant leakage have the same fault effect on the system, low or deficient refrigerant charge, so they can be considered as a single fault when doing fault detection and then can be separated using the fault cause criteria when doing fault diagnosis. Physically, refrigerant deficient and excessive charge faults would not happen simultaneously, so actually there is no coupling among the three system-level faults at all from the sense of fault detection and it is pretty easy to separate them using the fault cause criteria from the sense of fault diagnosis. Figure 1-15 depicts the decoupling scheme for the system-level faults.

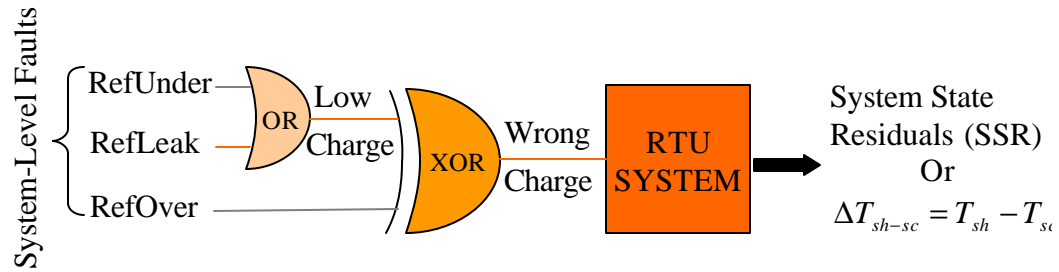


Figure 1-15 The Decoupling Scheme for System Level Faults

So far, couplings among system-level faults and from system-level faults to component-level faults are broken. However, it is necessary to identify a feature that strongly depends on charge.

Since component-level faults can be excluded before handling system-level faults, the system-level faults can be diagnosed independently using the SRB method. However, using the SRB method to do FDD requires system-level normal operation models, which can be expensive to develop. Another lower-cost feature is the difference between suction line superheat and liquid line subcooling, ΔT_{sh-sc} . This is a good feature for the following reasons:

1. Most of the refrigerant charge (more than 80%) accumulates as liquid in the condenser subcooling section and liquid line including the filter/drier. Subcooling is provided by certain heat transfer area in condenser, so the volume of liquid refrigerant is proportional to subcooling.
2. Similarly, superheat is provided by certain heat transfer area in evaporator and the vapor volume is proportional to superheat. So the saturated liquid in the evaporator is inversely proportional to superheat.
3. So the difference between superheat and subcooling should be inversely proportional to refrigerant charge. From the SRB diagnosis rules for both fixed orifice and TXV, it can be seen that the superheat and subcooling residuals change in the same direction for all other faults and in counter directions only for refrigerant charge faults.

The penalty of using this low-cost feature is that it does not include the effects of driving conditions. However, these effects are relatively small. Data collected by Harms (2002) were used to validate this feature. Figure 1-16 shows that the difference between superheat and subcooling is inversely proportional to refrigerant charge. The different symbols represent different operating conditions. There is only very small dependence on different operating conditions for these data because the system uses a TXV, which compensates for variations in operating conditions. For a fixed orifice system, this feature would work as well. Chapter 2 provides a case study for a system having a fixed orifice.

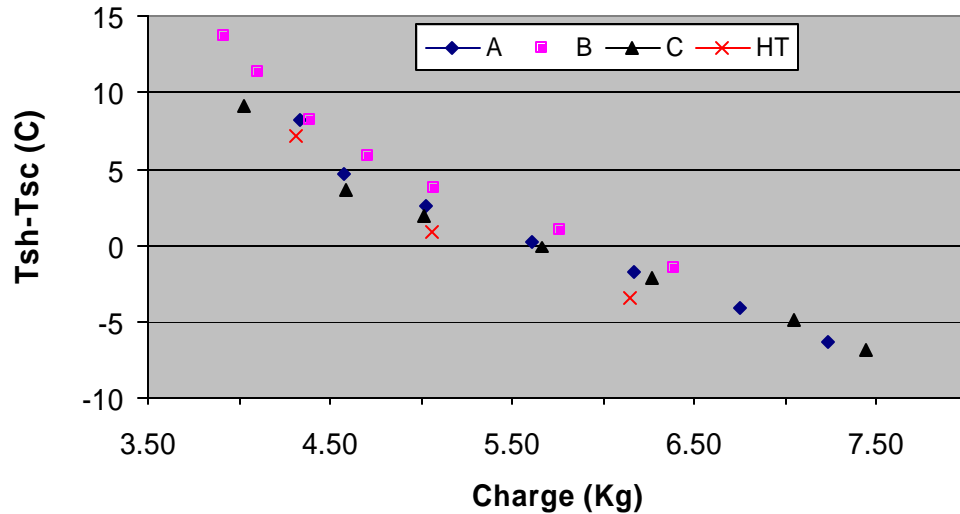


Figure 1-16 ΔT_{sh-sc} with different refrigerant charge levels

Since all the component-level faults can be independently detected and diagnosed, their influence on detecting and diagnosing system-level faults can be eliminated if the component-level faults are considered first. Similar to the unilateral decoupling between non-condensable gas and condenser fouling faults, unilateral decoupling between component-level and system-level faults is also achieved.

1.2.5 Summary of Decoupling Schemes for Rooftop Unit System Faults

So far, couplings among component-level faults, among system-level faults, and from system-level to component-level faults have been broken fully or unilaterally. Figure 1-17 summarizes the decoupling scheme for component and system level faults. Equation (1-23) formulates the decoupling scheme and results of all the rooftop faults. It can be seen that the matrix L of equation (1-23) is sparse and lower triangular. The algorithm described in section 3.1.2.3 can solve this unilateral decoupled problem.

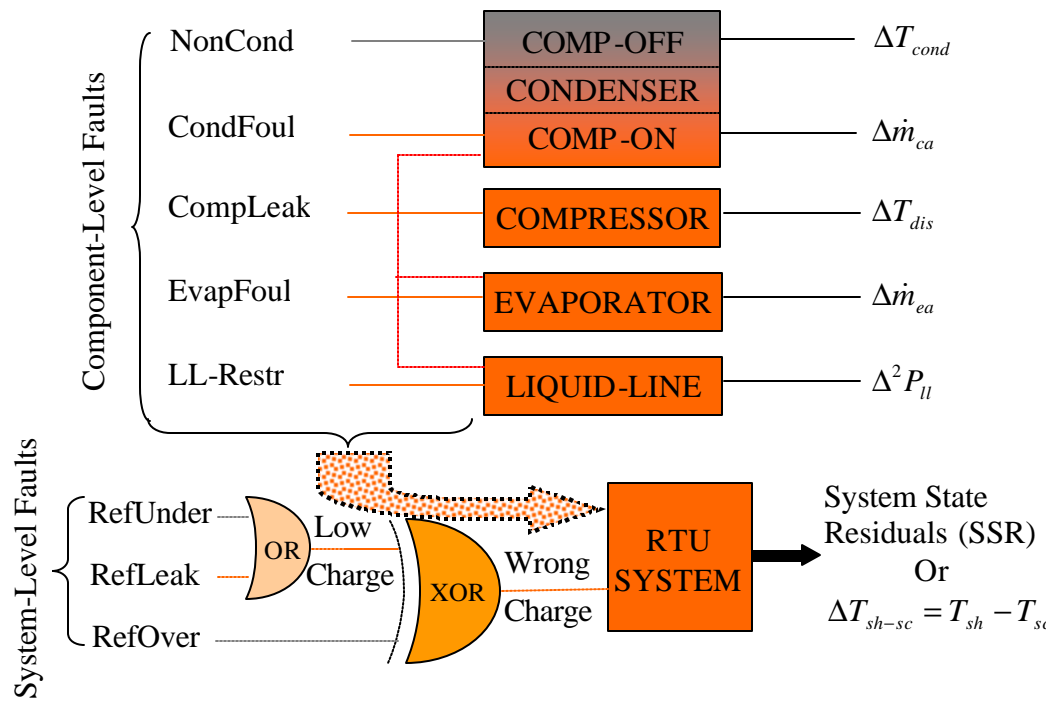


Figure 1-17 The Decoupling Scheme of All Rooftop System Faults

$$\begin{bmatrix} \Delta T_{sat} \\ \Delta T_{dis} \\ \Delta^2 P_{ll} \\ \Delta \dot{m}_{ca} \\ \Delta \dot{m}_{ea} \\ SSR / T_{sh-sc} \end{bmatrix} = Z = LX = \begin{bmatrix} l_{11} & & & & & \\ & l_{22} & & & & \\ & l_{32} & l_{33} & & & \\ & l_{42} & & l_{44} & & \\ & l_{52} & & & l_{55} & \\ l_{61} & l_{62} & l_{63} & l_{64} & l_{65} & l_{66} \end{bmatrix} \begin{bmatrix} NonCond \\ CompLeak \\ LLRestr \\ CondFoul \\ EvapFoul \\ RefCharge \end{bmatrix} \quad (1-23).$$

2 CASE STUDIES

In order to validate the decoupling-based approach, three cases studies are provided in this chapter. Section 2.1 presents an initial case study to validate the decoupling scheme for a 3-ton fixed orifice rooftop unit. Section 2.2 presents an FDD demonstration of multiple-simultaneous faults for a 5-ton TXV rooftop unit installed at the Purdue field site. Section 2.3 provides results for California field sites.

2.1 Case Study of Decoupling Rooftop Unit Faults

Data gathered by Breuker (1997) under controlled conditions in a laboratory were used to evaluate the decoupling scheme for a system with a short-tube expansion device. As described in Deliverables 2.1.3 & 2.1.4, five types of individual faults were artificially introduced at different fault levels and the unit was tested at different load levels with the unit cycling on and off. Although these five kinds of faults are individual instead of multiple-simultaneous faults, they can be used to test whether the proposed decoupling features for each fault are independent of fault and load levels and all other faults.

2.1.1 Compressor Valve Leakage

Figure 2-1 illustrates the discharge line temperature residuals for different fault types with different fault and load levels obtained using predicted compressor power consumption and predicted refrigerant mass flow rate. It can be seen that only the compressor valve leakage fault has a significant influence on the discharge line temperature residual. The small fluctuations with other faults are caused by measurement

noise, system disturbances and modeling error. So, the coupling between compressor valve leakage and other faults is broken successfully using the discharge line temperature residual.

However, there is still some room for improvement. For example, the discharge line temperature residual is impacted a little by large liquid-line restrictions. This may be caused by high suction line superheat at severe liquid-line restrictions, which results in a lower value of the compressor volumetric efficiency. However, this can be improved by improving the compressor model performance and finding some practical means to tune it, which will also eliminate the impact of other faults on the discharge line temperature estimation.

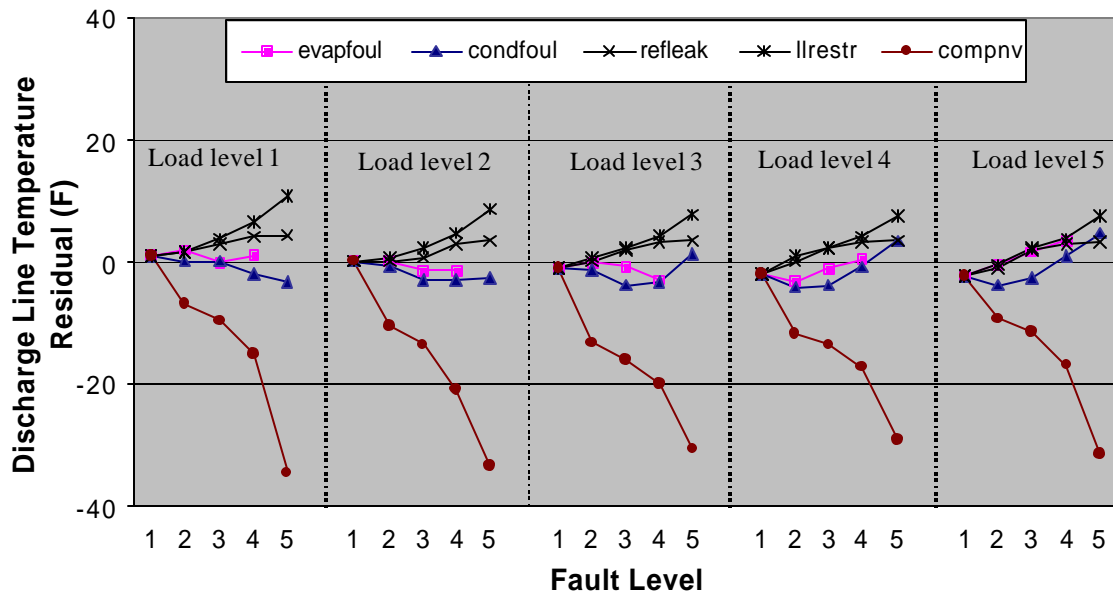


Figure 2-1 Decoupling compressor valve leakage fault using estimated compressor power measurement and estimated refrigerant mass flow rate

2.1.2 Condenser Fouling Decoupling

Figure 2-2 gives the condenser air mass flow rate estimated using a virtual sensor under different fault types with different fault and load levels. In order to show the potential of the decoupling scheme, this virtual sensor uses the actual refrigerant mass flow rate measurement. From 2-2, it can be seen that the condenser air mass flow rate is only influenced by the condenser fouling fault. The reduction of condenser air mass flow rate is proportional to the condenser fault level and independent of load levels and other faults. So full decoupling between condenser fouling fault and other faults is achieved.

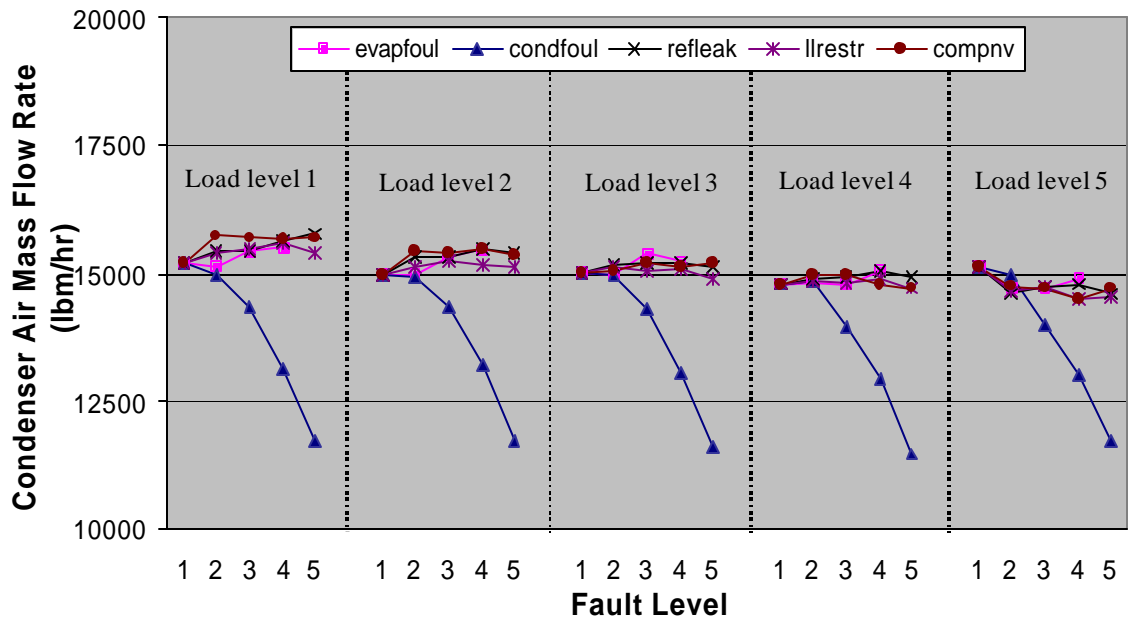


Figure 2-2 Decoupling condenser fouling fault using measured refrigerant mass flow rate

A refrigerant mass flow rate meter is too expensive for this application, so it is estimated using compressor map data. Figure 2-3 shows the condenser mass flow rate estimated using a refrigerant mass flow rate estimate under different fault types with different fault and load levels. It can be seen that the condenser mass flow rate estimate is influenced simultaneously by condenser fouling and compressor valve leakage with inverse directions. The dependence on compressor valve leakage is caused by errors in refrigerant mass flow rate prediction, since the compressor map was built using normal

compressor data. When there is a compressor valve leakage fault, the compressor model over-estimates the refrigerant mass flow rate and this results in an over-estimate of condenser air mass flow rate. So, the coupling from compressor valve leakage to condenser fouling is not broken if the refrigerant mass flow rate is estimated using the compressor map. However, this would not impact the FDD application, because the coupling from condenser fouling to compressor valve leakage has been broken already. In other words, unilateral or partial decoupling can be achieved even if refrigerant mass flow rate is estimated using a compressor map.

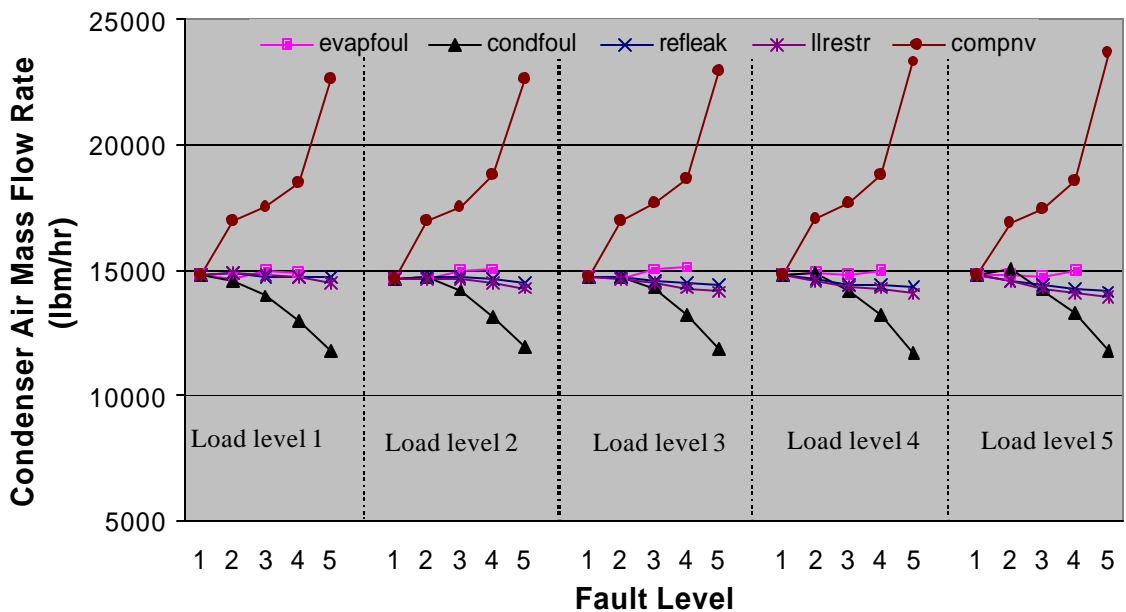


Figure 2-3 Decoupling condenser fouling fault using estimated refrigerant mass flow rate

2.1.3 Evaporator Fouling Decoupling

To quantify the fault levels simulated in this experiment, evaporator air mass flow rate was indirectly calculated from the fan curve using the measurement of the change in differential pressure across the evaporator fan. Figure 2-4 shows the evaporator air mass flow rate measurements. From this figure, it can be seen that in addition to an outlier

point the actual evaporator air mass flow rate has a small variation for different fault types and different fault levels, and the fluctuation band shifts up with the increasing load levels. The outlier point may be caused by experimental error. The small shifting fluctuation with increasing load level may be caused by the variation in the air density at different load levels, and different fault type and fault level also have some influence on the air density. However, this small fluctuation would not change the decoupling feature.

Figure 2-4 Decoupling evaporator fouling fault using measured evaporator air mass flow rate

Evaporator air mass flow rate is not typically measured. Figure 2-5 illustrates the evaporator air mass flow rate estimated using a virtual sensor under different fault types with different fault and load levels. This virtual sensor used the measured refrigerant mass flow rate. From this figure, it can be seen that the existing shifting fluctuation is amplified a little, which may be caused by the systematic error in the measurement of evaporator air inlet and outlet conditions. However, this still does not change the decoupling feature and the change of evaporator air mass flow rate estimate is still dominated by evaporator fouling and also it can be alleviated by improving the measurement scheme.

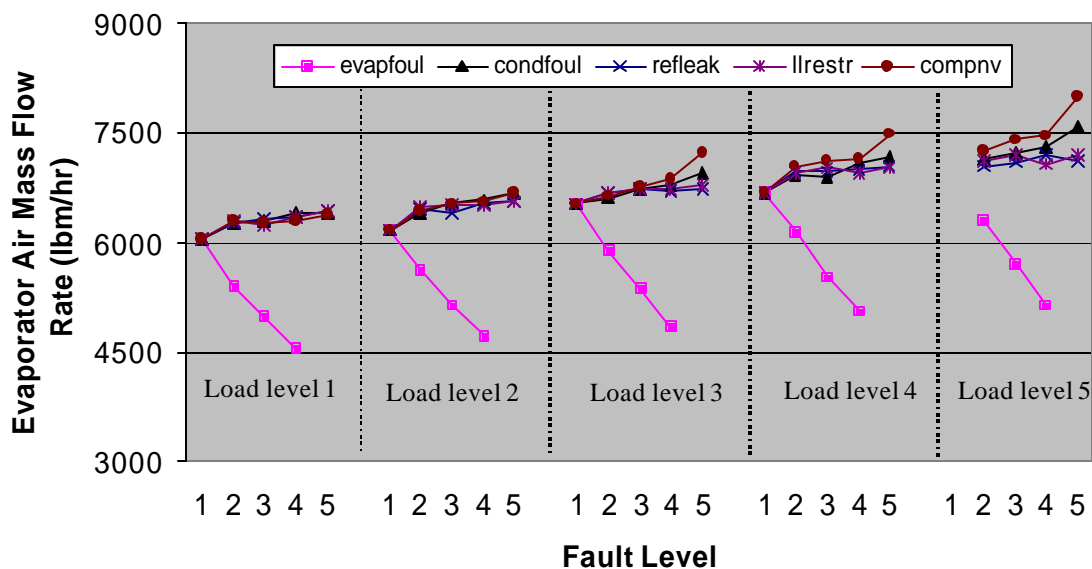


Figure 2-5 Decoupling evaporator fouling fault using measured refrigerant mass flow rate

Figure 2-6 illustrates the evaporator air mass flow rate estimated using estimated refrigerant mass flow rate. As expected, the coupling from compressor valve leakage to evaporator fouling is not broken if refrigerant mass flow rate is estimated by compressor map. For the same reason as condenser fouling, unilateral decoupling is sufficient for FDD application.

Figure 2-6 Decoupling evaporator fouling fault using estimated refrigerant mass flow rate

2.1.4 Liquid-Line Restriction Decoupling

Figure 2-7 illustrates the measured liquid-line pressure drop under different fault types with different fault and load levels. It is obvious that the liquid line pressure drop is only influenced by the liquid-line restriction fault. The decoupling between liquid-line restriction faults and all other faults is broken successfully.

However, it is not practical to measure the inlet and outlet pressures for FDD. The outlet pressure P_{up} should be estimated using a virtual sensor. Figure 2-8 shows the decoupling results using estimated P_{up} and measured P_3 . It can be seen that the accuracy of the P_{up} estimate is within $\pm 5 psi$. In addition, the measurement of P_3 is not available, so Appendix 1 proposed two estimation techniques. Due to limited data, only the second technique, assuming constant pressure drop across the condenser, was tested. Figure 2-9 shows the predict pressure drop between P_{dis} and P_{up} . It seems that a constant pressure drop of $25 psi$ in the condenser can be assumed to estimate P_3 .

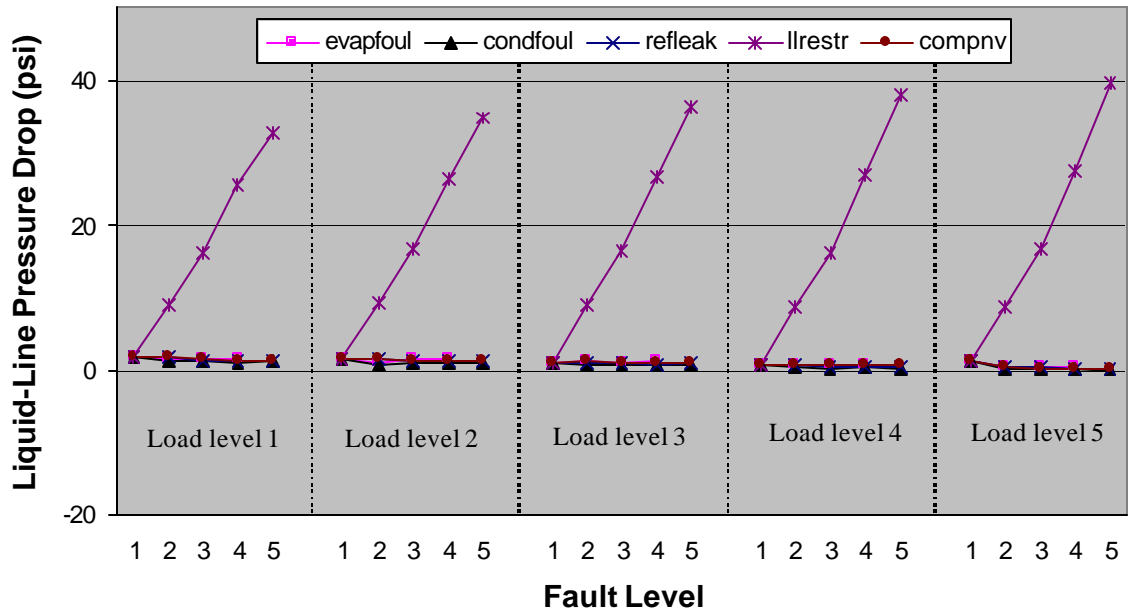


Figure 2-7 Decoupling liquid-line restriction using measured pressure drop

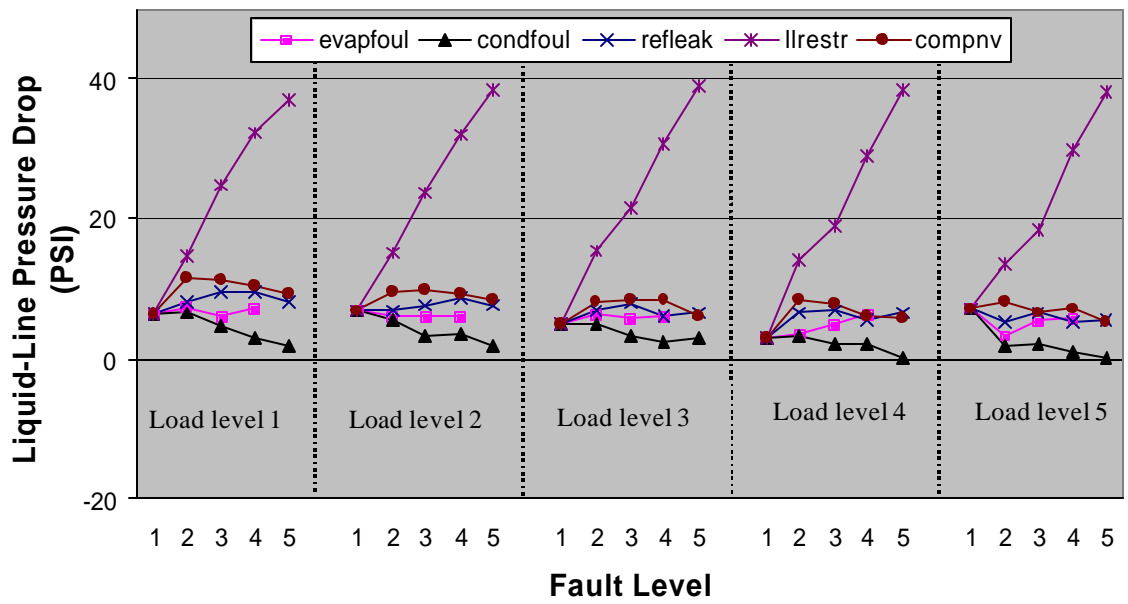


Figure 2-8 Decoupling liquid-line restriction using estimated pressure P_{up} and measured P_3

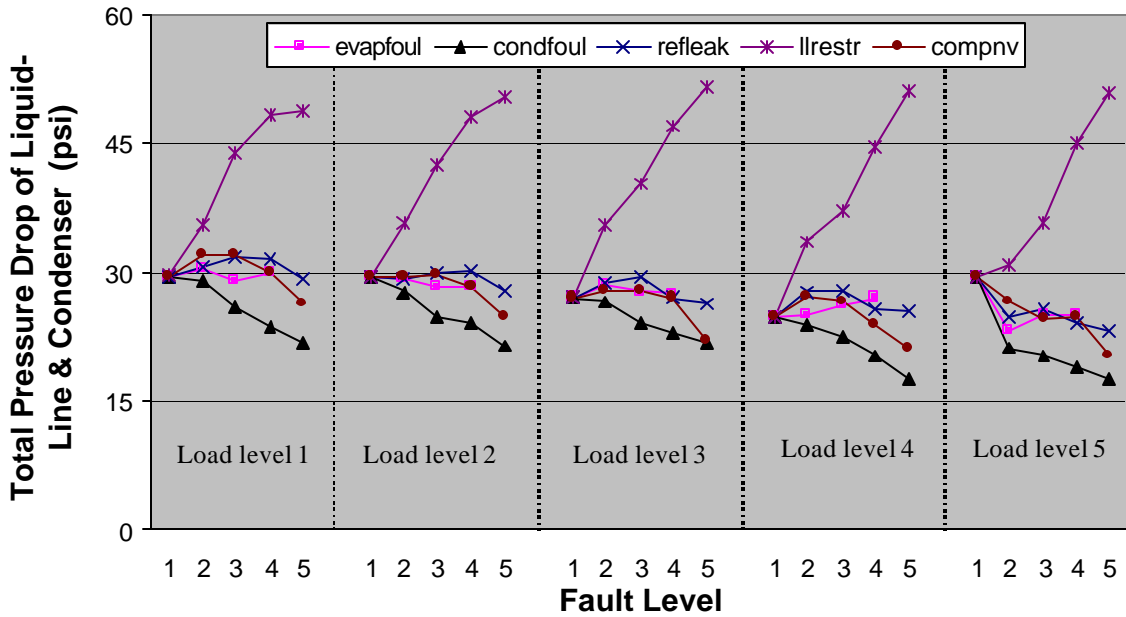


Figure 2-9 Decoupling liquid-line restriction using estimated pressure drop

2.1.5 Refrigerant Leakage Decoupling

Figure 2-10 shows the decoupling feature of ΔT_{sh-sc} for the different fault and load levels. It can be seen that all the faults have impacts on this feature. However, since the refrigerant fault does not have an impact on the other decoupling features (from Figure 2-1 to Figure 2-9) and the value of this feature is proportional to refrigerant leakage fault levels, the unilateral decoupling is achieved successfully.

It should be pointed out that this feature monotonically decreases slightly with load level. This is expected, because no model is used for this feature and a fixed orifice can not compensate for load level variations very well. Although these impacts are a little larger than those of a TXV system, they are still reasonably small. Anyway, it is still advisable to improve this feature furthermore by modifying it using load level.

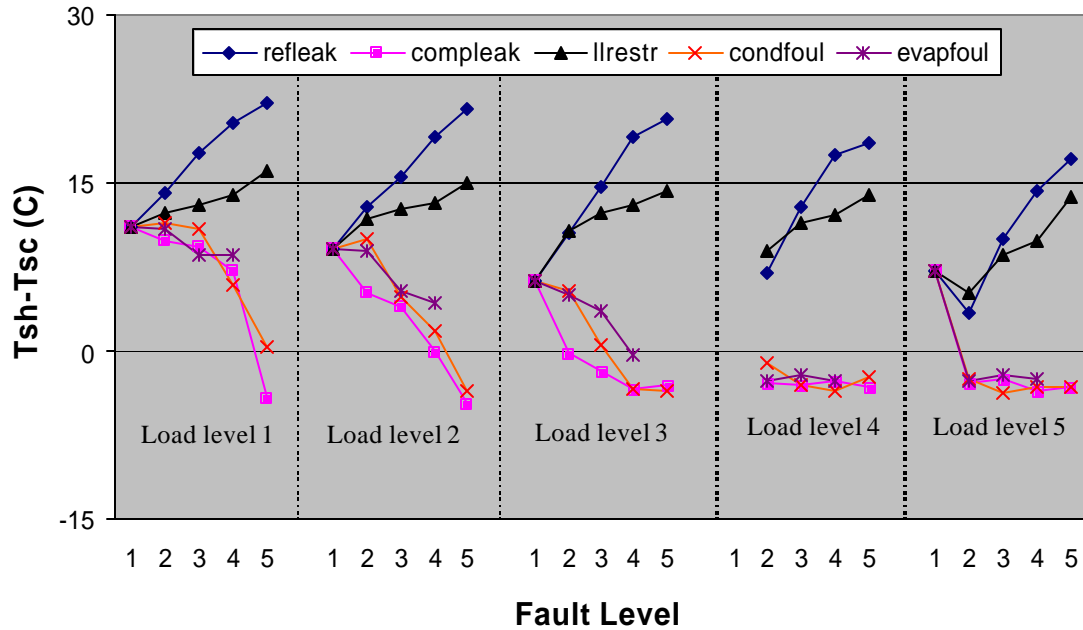


Figure 2-10 Decoupling refrigerant leakage faults using ΔT_{sh-sc}

2.2 Purdue Field Emulation Site's Demonstration

To demonstrate the decoupling-based fault detection and diagnosis approach, multiple-simultaneous faults were artificially introduced to the Purdue field emulation site, which has been described in a previous deliverable.

The decoupling-based fault detection and diagnosis approach described in Chapter 1 was applied to the demonstration. To make the demonstration intuitive, a movie was made to show the whole process. There are four windows shown in the movie: Fault Detection and Diagnosis Window, System Performance and Safety Degradation Window, Fault Simulation Window, and Fault Detection and Diagnosis Window (see Figure 2-11). The following sections describe all the windows in detail and present some sample results.

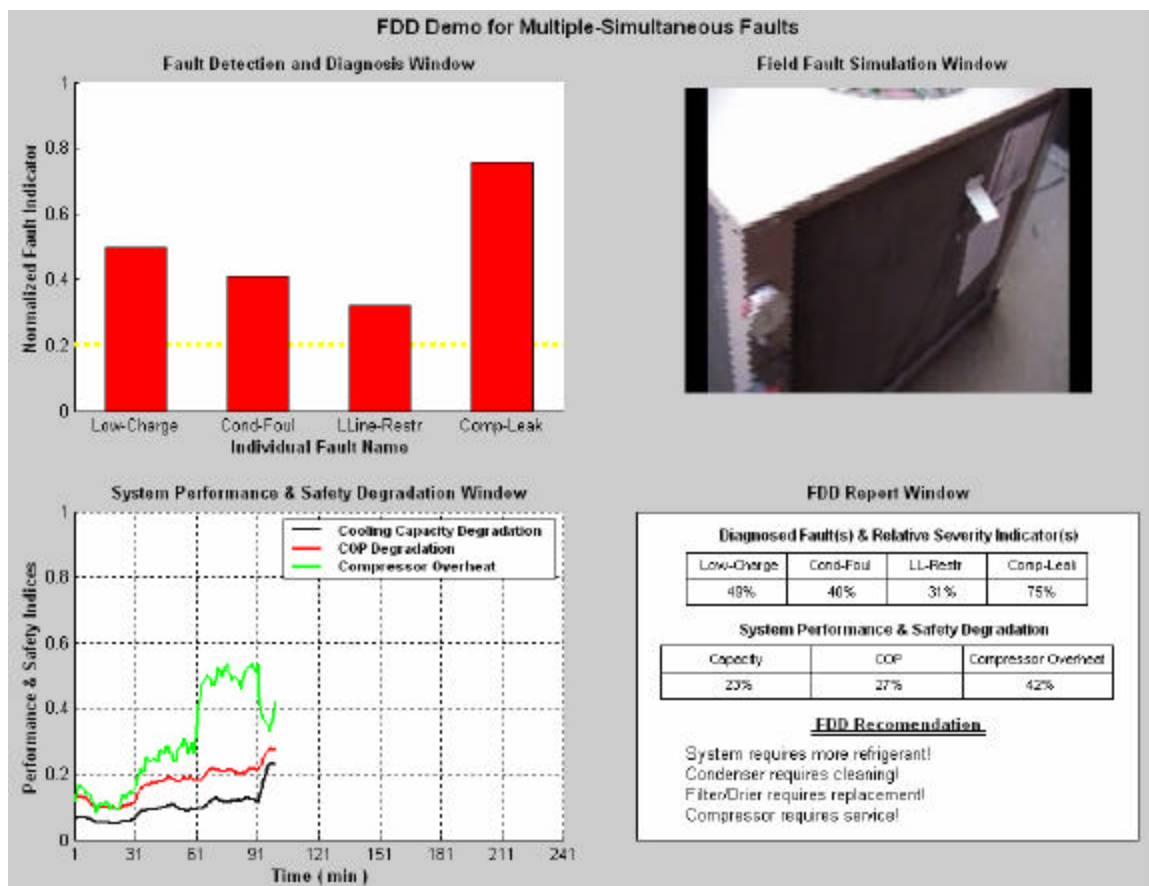


Figure 2-11 Illustration of Demo Movie

2.2.1 Field Fault Simulation Window

For easy access, four faults were artificially introduced: refrigerant low charge, condenser fouling, liquid line restriction and compressor leakage. Since it is not accurate to discharge refrigerant using the recovery system, the refrigerant low charge fault was simulated by charging less refrigerant to the system before running rather than discharging some refrigerant during operation. The fault simulation procedures were divided into the following two stages: added four faults one by one and removed faults one by one. Figure 2-12 illustrates the timeline of the fault simulation.

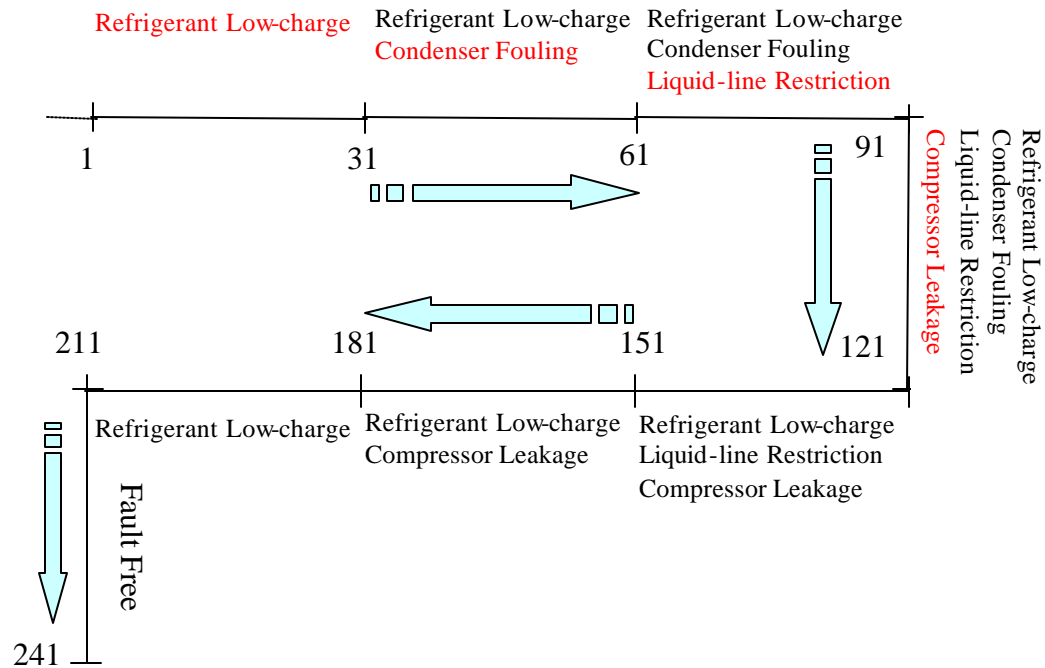


Figure 2-12 Timeline of the fault simulation in minutes.

The following steps describe the addition of faults,

1. Evacuated the system, and then charged the system up to eighty per cent of nominal refrigerant charge. The system ran for half an hour to reach steady state and then data were logged.
2. After logging half an hour of low charge data, the condenser fouling fault was added, by covering thirty per cent of condenser area using paper. At this time, there were two simultaneous faults in the system: refrigerant low charge and condenser fouling.
3. Half an hour later, a liquid line restriction fault was introduced by closing the restriction valve until a twenty psi pressure drop was caused. Three faults existed in the system simultaneously: refrigerant low charge, condenser fouling and liquid line restriction.
4. Half an hour later, a compressor leakage fault was introduced by opening the compressor bypass valve to let fifteen per cent of refrigerant mass flow rate

bypass the compressor. At this time, four faults existed simultaneously in the system: refrigerant low charge, condenser fouling, liquid line restriction, and compressor leakage.

The following steps describe the removal of faults,

5. After the system ran for half an hour under four faults, the paper covering the condenser was removed. There existed three simultaneous faults in the system: refrigerant low charge, liquid line restriction, and compressor leakage, which is a different combination than step three.
6. Half an hour later, the liquid line restriction fault was removed by fully opening the liquid line restriction valve. At this time, refrigerant low charge and compressor leakage existed in the system, which is a different combination than step two.
7. Half an hour later, the compressor bypass valve was closed to remove compressor leakage fault. There was only refrigerant low charge fault in the system.
8. Finally, half an hour later, the system was charged up to a nominal refrigerant level. The system was supposed to run normally.

2.2.2 Fault Detection and Diagnosis Window

This window plots the normalized fault indicator for four individual faults using color bars: refrigerant low charge (Low-Charge), condenser fouling (Cond-Foul), liquid line restriction (LL-Restr), and compressor leakage (Comp-Leak).

The normalized fault indicator is the ratio of the current feature value to the predefined value, which is defined at an individual fault level causing 20% cooling capacity degradation.

$$\text{Normalized_Fault_Indicator} = \frac{\text{current_feature_value}}{\text{predefined_feature_value}}$$

Although the predefined fault level is arbitrary, the author believes that a fault causing 20% cooling capacity degradation is worthwhile to service. The normalized fault indicator indicates the relative severity of the individual faults. However, the refrigerant low charge is a system-level fault and its impact on overall system performance is not only determined by its own charge level but also other faults, so the indicator oscillates a lot. Fortunately, data collected so far shows that this oscillation does not change the decision of the fault detection and diagnosis method.

The normalized fault indicators are plotted using color bars. When an indicator is larger than the threshold, 0.2, it is plotted in red, otherwise in green. According to experience, an indicated fault level with a performance degradation less than $0.2 \times 20\% = 4\%$ is not reliable.

2.2.3 System Performance & Safety Degradation Window

Capacity and COP are usually used as criteria to indicate system performance. The compressor is the most expensive part of the system and too much overheating would result in safety problems such as bad lubrication and motor short-circuit. So degradations of these three indices are plotted in this window. The capacity and COP degradations are defined by,

$$\frac{\text{normal_value} - \text{current_value}}{\text{normal_value}}$$

The normal value is predicted using an overall system performance model which is built based on system manufacturer rating data. The model inputs are condenser inlet air dry-bulb temperature and evaporator wet-bulb temperature.

The compressor overheat degradation is defined by,

$$\frac{\text{current_}T_{dis} - \text{normal_}T_{dis}}{\max_ \Delta T_{dis}}$$

The maximum ΔT_{dis} is found to be around 40 F by Chen's data (2000), which should be confirmed by more investigation. There is difficulty to predict normal values

for T_{dis} because there is no overall system state model available. For this demonstration, it is assumed that the system driving condition is not changed much and the measured value at the fault free condition is used as the normal value. Further research should be done later to find an inexpensive safety indicator for a compressor.

2.2.4 FDD Report Window

To help customers make a decision whether to service the diagnosed fault or not, the FDD Report Window generates a tabular report for the FDD results including diagnosed faults and relative severity indicators and system performance and safety degradation indices, and provides an FDD recommendation. In this demo, the FDD recommendation is based on performance and safety degradation. If the performance degradation is over twenty per cent or the compressor is overheated up to ninety per cent, service is recommended. More investigation is needed for fault recommendation.

2.2.5 Output of the FDD Demonstration

This section provides sample outputs of the FDD demonstration after each fault was added and removed (watch the movie for details).

Figure 2-13 captures a movie frame when the system was running at low refrigerant charge (step 1 of section 2.2.1). The “Fault Detection and Diagnosis window (FDDW)” indicates that there existed a refrigerant low charge fault whose fault severity was around 0.45. The “System Performance & Safety Degradation Window (SPSDW)” plots the overall degradations, all of which were less than 20%. The “FDD Report Window (FDDRW)” summarizes the indicates and generates the FDD report table and recommended that “although there is (are) fault(s) with minor impacts on overall system performance, it may be not worthwhile to service so far”.

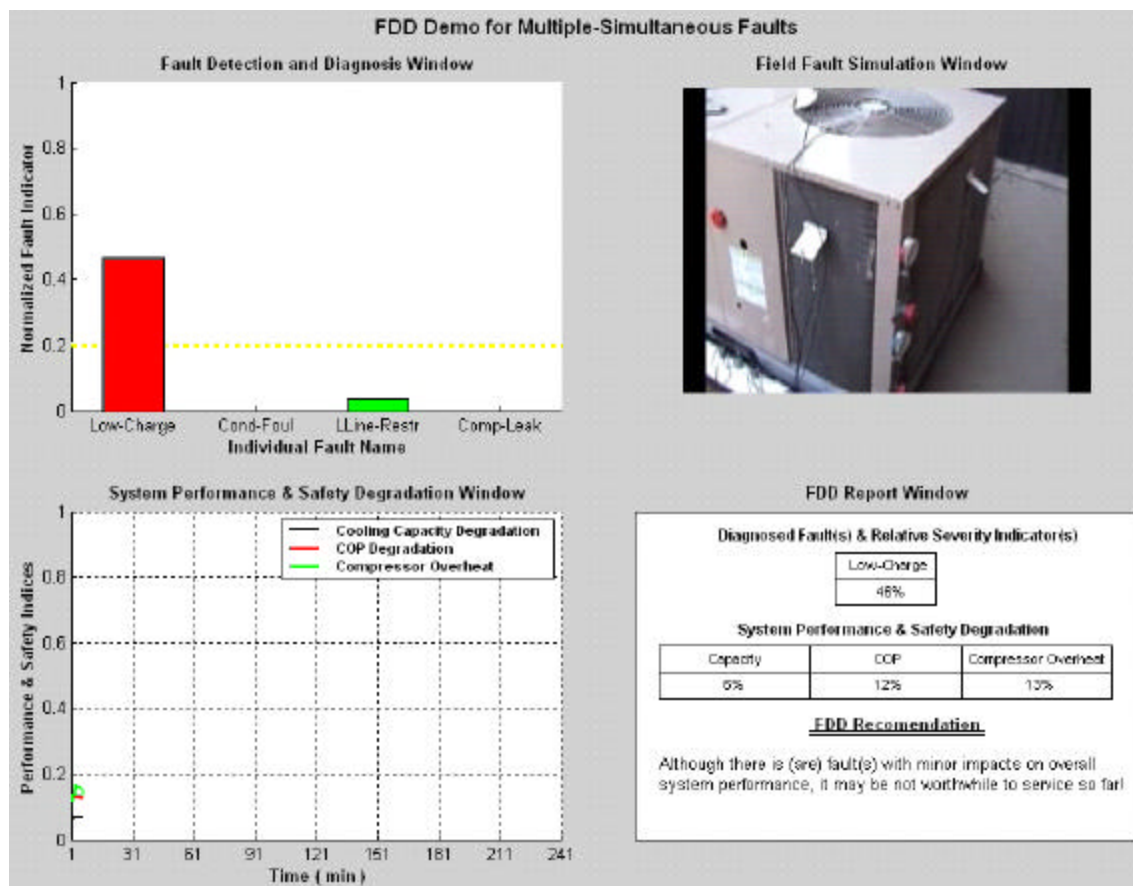


Figure 2-13 Outputs of the FDD demonstration after introduction of low refrigerant charge fault

Figure 214 shows one frame after 30% of the condenser area was covered by paper (step 2 of section 2.2.1). The “Field Fault Simulation Window (FFSW)” shows that some part of the condenser area was covered by paper. FDDW indicates that there existed two faults: refrigerant low charge with the fault severity around 0.45 and condenser fouling with the fault severity around 0.4. Since the overall performance degradations were less than 20% at this moment (see SPSPDW and FDDRW), service was not recommended (see FDDRW).

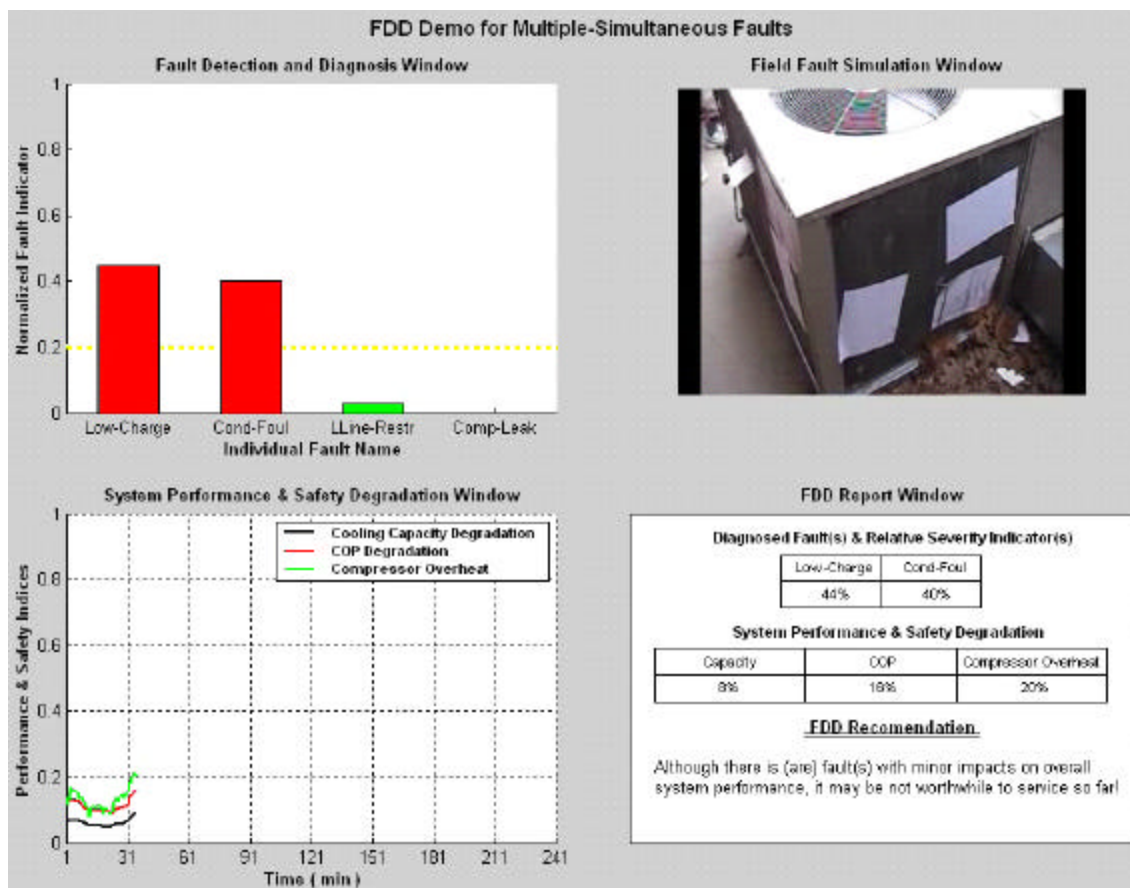


Figure 2-14 Outputs of the FDD demonstration after introduction of condenser fouling fault

Figure 2-15 shows one frame after the liquid line restriction fault was introduced by closing the restriction valve until a twenty psi pressure drop was caused (step 3 of section 2.2.1). The final position of the restriction valve can be seen from the FFSW (see Figure 2-18 for the fully opening position). FDDW indicates that there existed three simultaneous faults: refrigerant low charge with the fault severity over 1.0, condenser fouling with the fault severity around 0.5 and liquid line restriction fault with the severity around 0.35. Since refrigerant charge fault is a system-level fault whose indicator was impacted by other faults, the refrigerant low charge indicator value increased after the liquid line restriction fault was introduced. Since the COP was degraded 21% at this moment (see SPSDW and FDDR), FDDR recommended that: the system requires more refrigerant, the condenser requires cleaning and the filter/drier requires replacement.

Although every individual fault was not severe enough to cause more than a 20% performance degradation, the combination of three simultaneous faults aggravated overall system performance degradations.

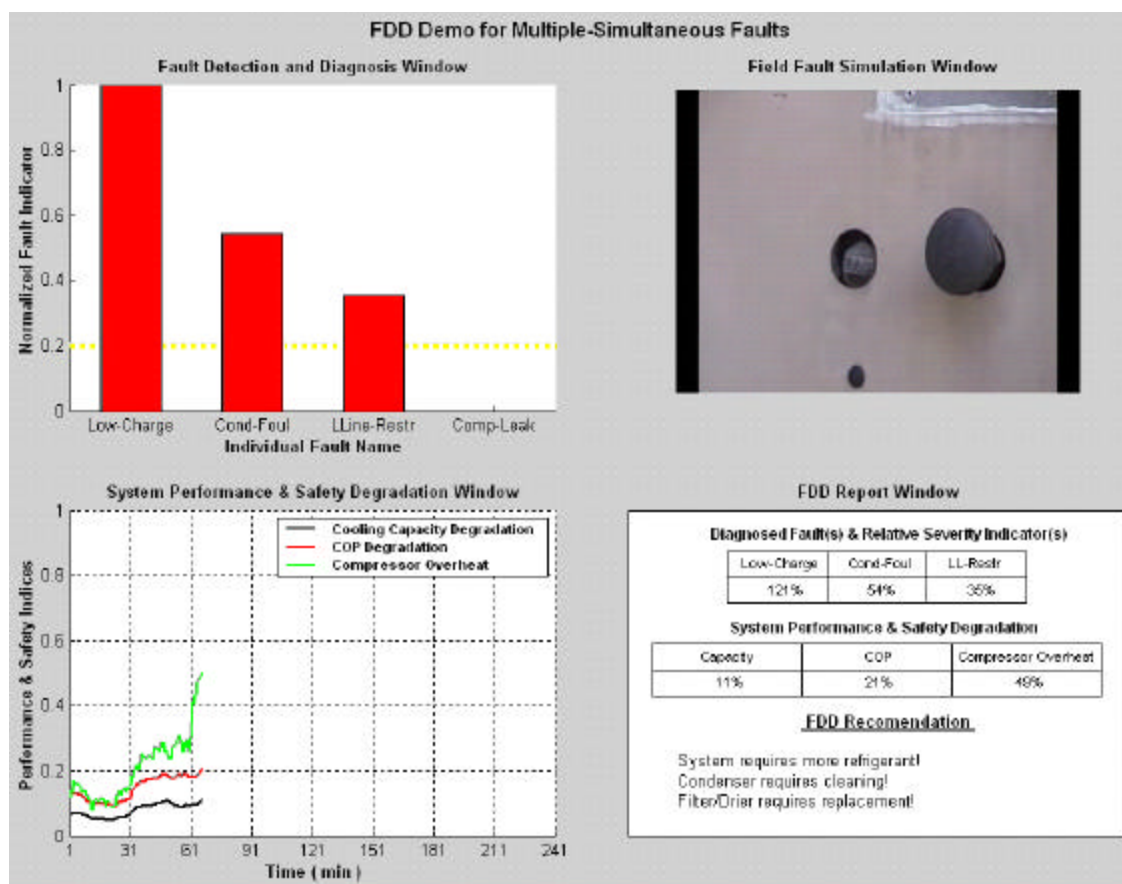


Figure 2-15 Outputs of the FDD demonstration after introduction of liquid line restriction fault

Figure 2-16 shows one frame after the compressor leakage fault was introduced by opening the discharge bypass valve until about 15% of refrigerant mass flow rate was reduced (step 4 of section 2.2.1). FDDW indicates that there existed four simultaneous faults: refrigerant low charge with the fault severity over 0.70, condenser fouling with the fault severity around 0.5, liquid line restriction fault with the fault severity around 0.35 and compressor leakage fault with the fault severity around 0.5. Since the COP was degraded 24% at this moment (see SPSPDW and FDDR), FDDR recommended that:

the system requires more refrigerant, the condenser requires cleaning, the filter/drier requires replacement and the compressor requires service.

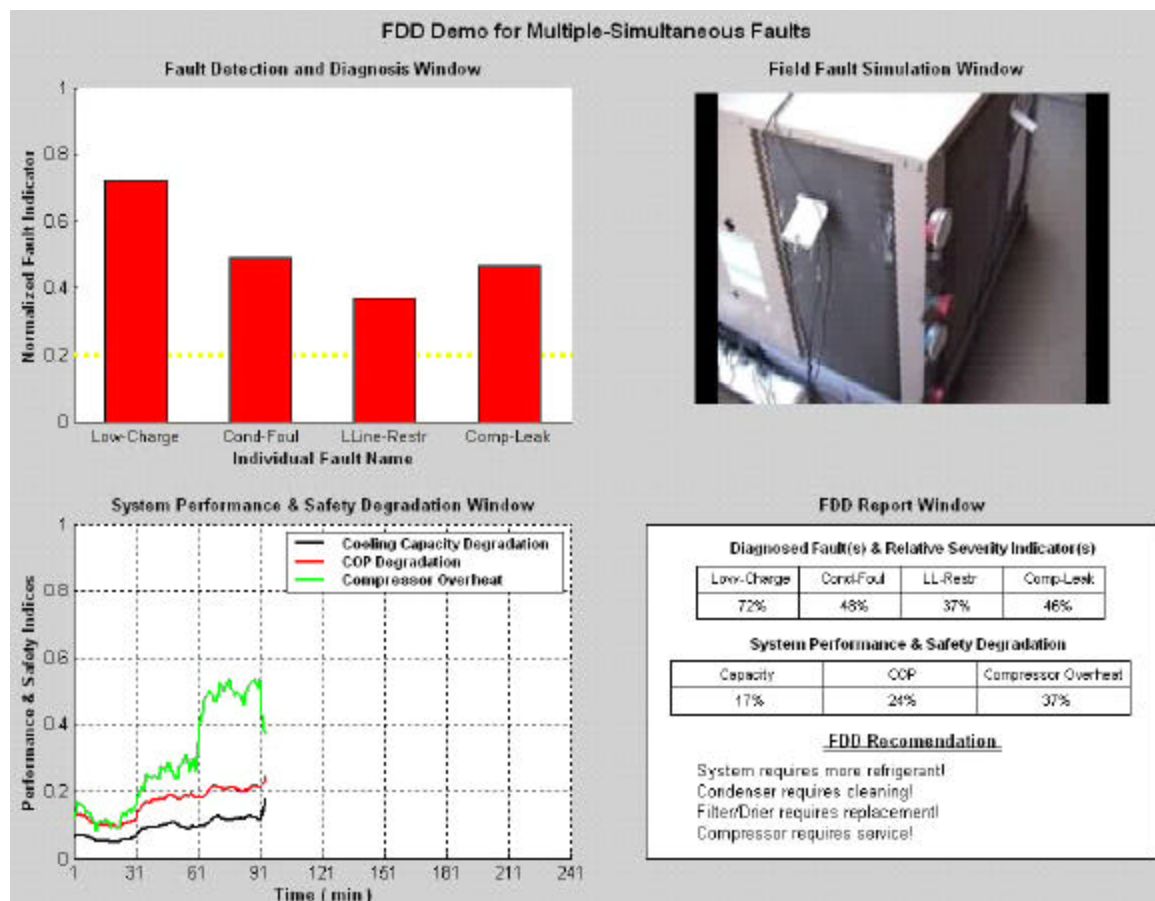


Figure 2-16 Outputs of the FDD demonstration after introduction of compressor leakage fault

Figure 2-17 shows one frame after the condenser fouling fault was removed (step 5 of section 2.2.1). It can be seen from FFSW that the paper covering the condenser was removed. FDDW indicates that there existed three simultaneous faults: refrigerant low charge with the fault severity over 0.60, liquid line restriction fault with the fault severity around 0.3 and compressor leakage fault with the fault severity around 0.8. Since both cooling capacity and COP were degraded 21% at this moment (see SPSPDW and

FDDRW), FDDRW recommended that: the system requires more refrigerant, the filter/drier requires replacement and the compressor requires service.

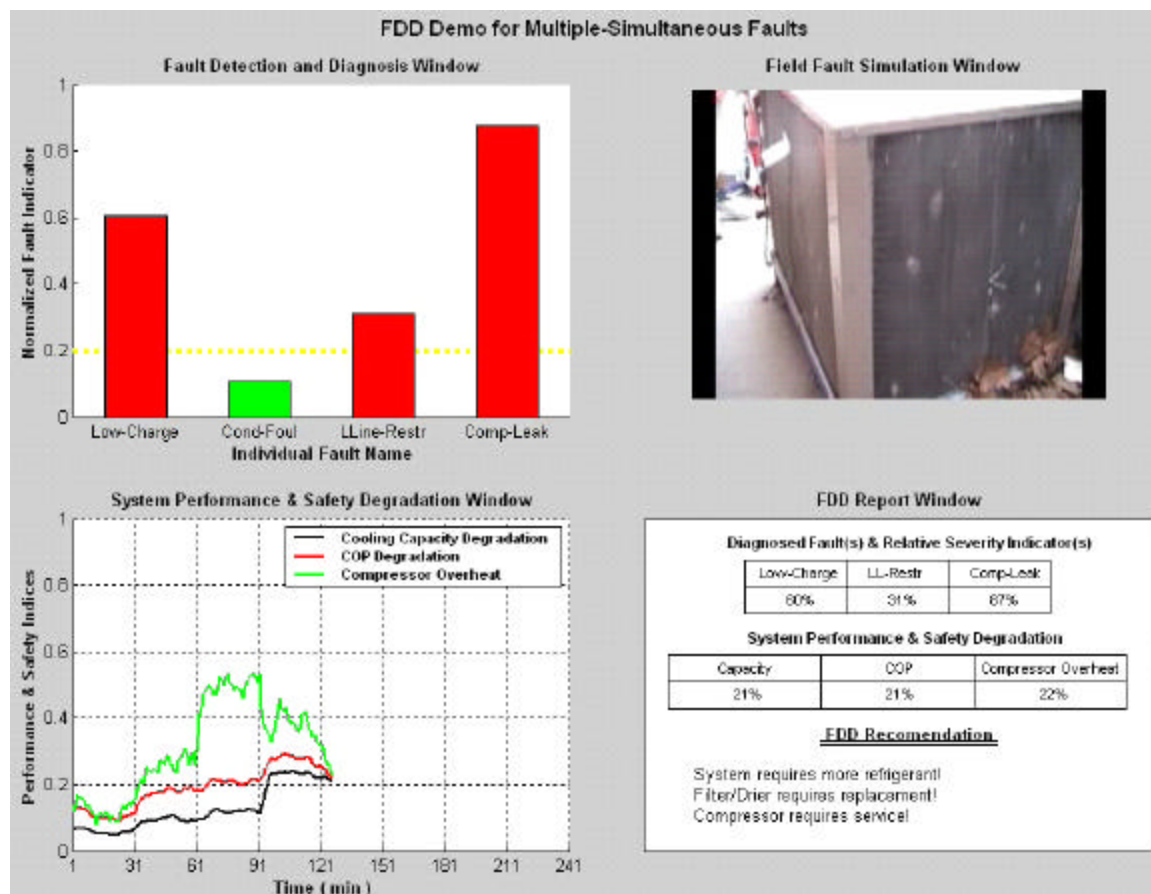


Figure 2-17 Outputs of the FDD demonstration after removal of condenser fouling fault

Figure 2-18 shows one frame after the liquid line restriction fault was removed by opening the liquid line restriction valve (step 6 of section 2.2.1). The final restriction valve position can be seen from FFSW (refer to Figure 2-15 for the fully closing position). FDDW indicates that there existed two simultaneous faults: refrigerant low charge with the fault severity over 0.35 and compressor leakage fault with the fault severity around 0.8. Since COP was degraded 20% at this moment (see SPSDW and FDDRW), FDDRW

recommended that: the system requires more refrigerant and the compressor requires service.

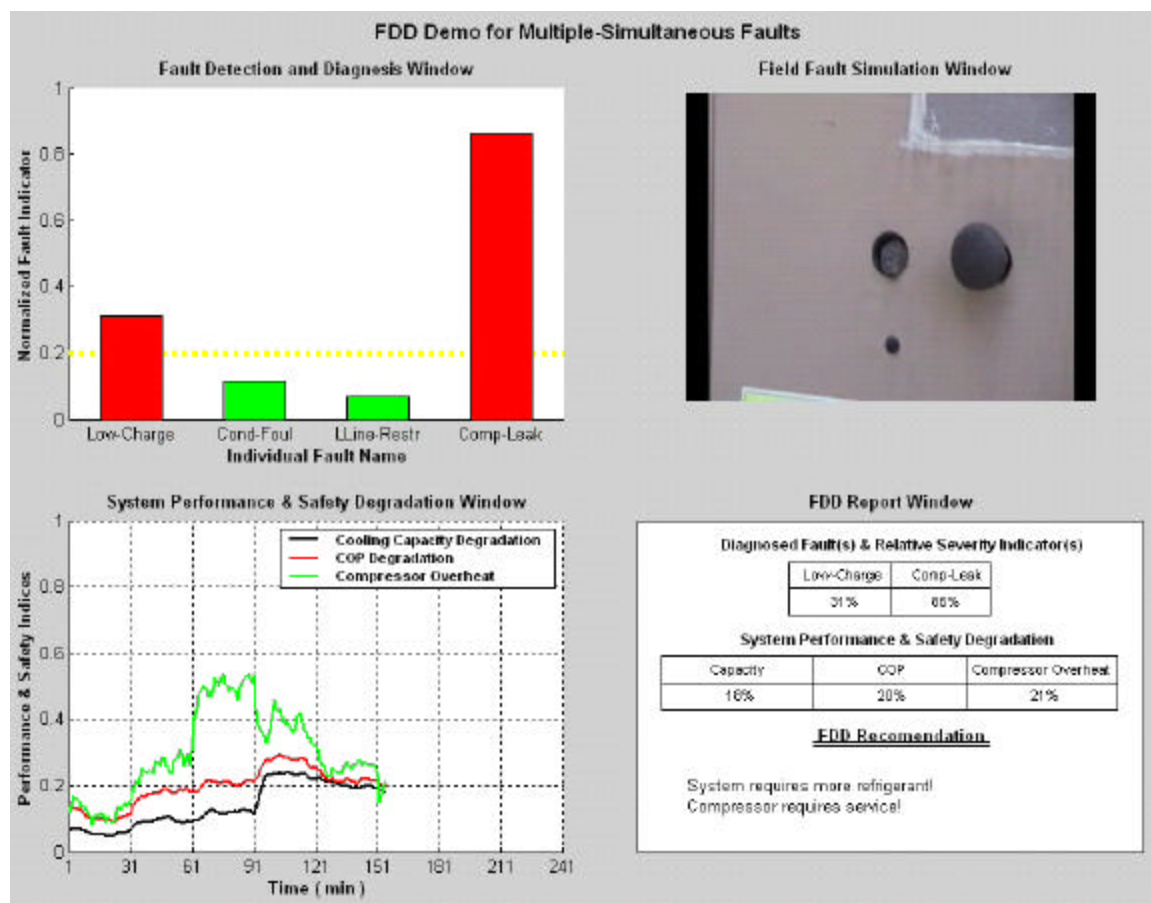


Figure 2-18 Outputs of the FDD demonstration after removal of liquid line restriction fault

Figure 2-19 shows one frame after the compressor leakage fault was removed by closing the discharge line bypass valve (step 7 of section 2.2.1), which was restored to step 1 of section 2.2.1. FDDW indicates that there existed one fault, refrigerant low charge with the fault severity over 0.45. Since the overall performance degradation was less than 20% at this moment (see SPSPDW and FDDRW), no service is recommended.

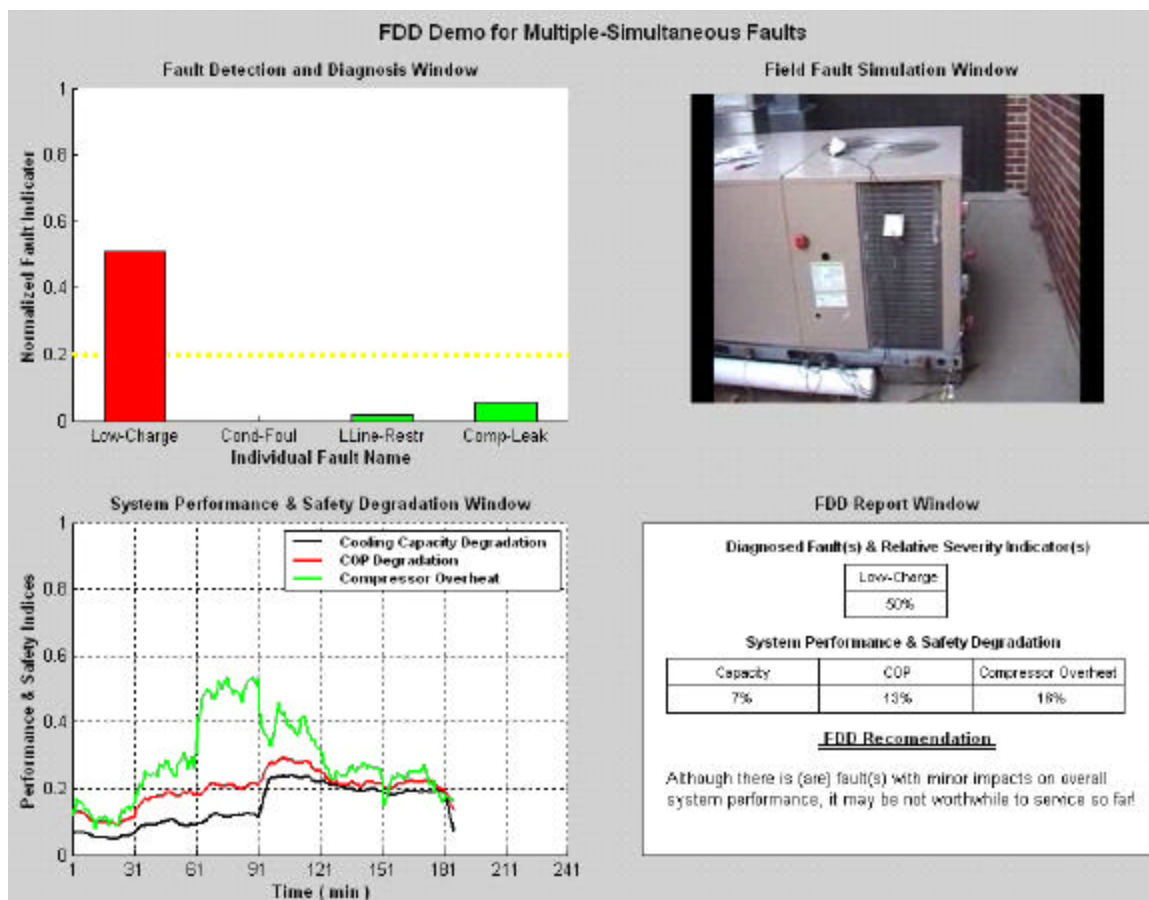


Figure 2-19 Outputs of the FDD demonstration after removal of compressor leakage fault

Figure 2-20 shows one frame after the system was charged up to the nominal level. FDDW indicates that there existed no fault. FDDRW reported that the system was running normally.

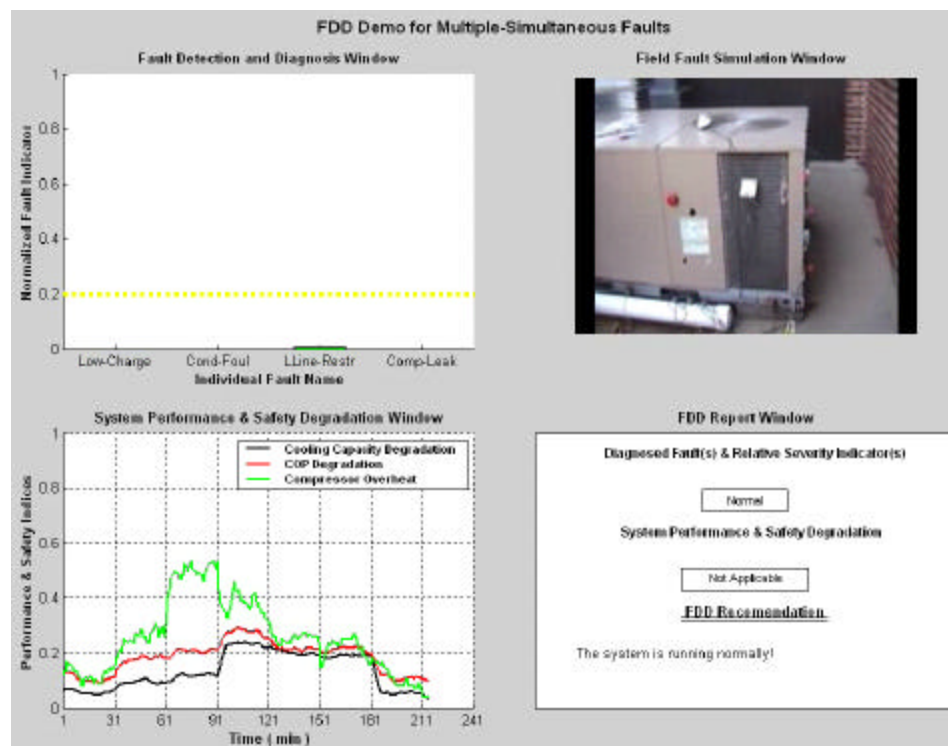


Figure 2-20 Outputs of the FDD demonstration after removal of low refrigerant low charge fault

2.3 Results for California Field Sites

Section 2.1 validated the decoupling scheme using laboratory data and section 2.2 demonstrated the whole approach by artificially introducing faults at the Purdue field emulation site. This section applies the FDD approach to California field sites. Section 2.3.1 presents detailed results for one example site, Milpitas McDonalds restaurant, and section 2.3.2 summarizes the FDD results for other sites.

2.3.1 Milpitas McDonalds Field Site

This site is located in Oakland, California. A 6-ton York rooftop unit (D1CG072N09923C) is installed for this McDonalds restaurant. A Copeland scroll compressor (ZR72KC-TF3) and a TXV are used in this RTU. Data collected from April to October in 2002 were used to do FDD. After filtering the transient data by a steady-state detector and removing the bad data corrupted by the acquisition equipment, 1119 data points (one data point every five minutes) were retained.

Since the RTU has been installed for several years, faults have been fully developed. Unlike the Purdue field emulation site, results of this site are presented in the statistical sense. That is, histogram bar plots are used to present the results.

Figure 2-21 plots the normalized fault indicator for a liquid-line restriction fault. It can be seen that all the steady-state data points are located at the right of the red dotted line, FDD threshold (0.2) and the mean value is around 0.8. That is, all steady-state points indicate that the liquid-line is restricted. Most likely the filter or drier is clogged by debris. If this fault happened individually, it would result in about a 16% cooling capacity degradation.

Figure 2-22 plots the normalized fault indicator for refrigerant charge faults. Similar to Figure 2-21, all the steady-state data points are located at the right of the FDD threshold and the mean value is about 1.6, which means that the system charge is very low. If this fault happened individually, it would result in about 32% cooling capacity degradation. However, since refrigerant charge faults are system level faults, their indicator is impacted by other faults.

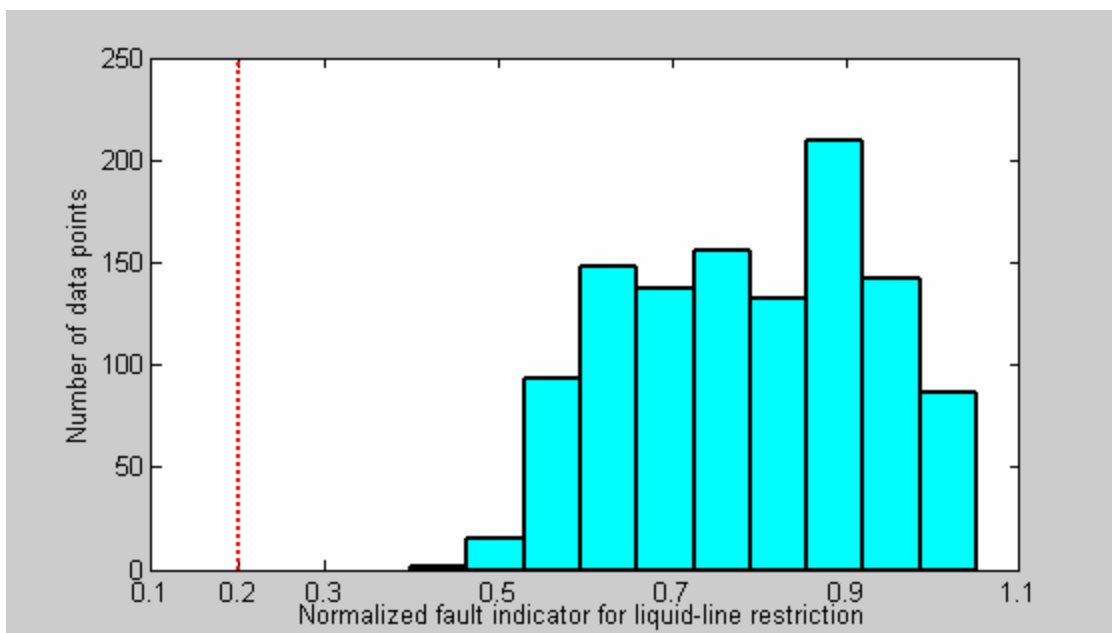


Figure 2-21 Histogram bar plot of the normalized fault indicator for liquid line restriction

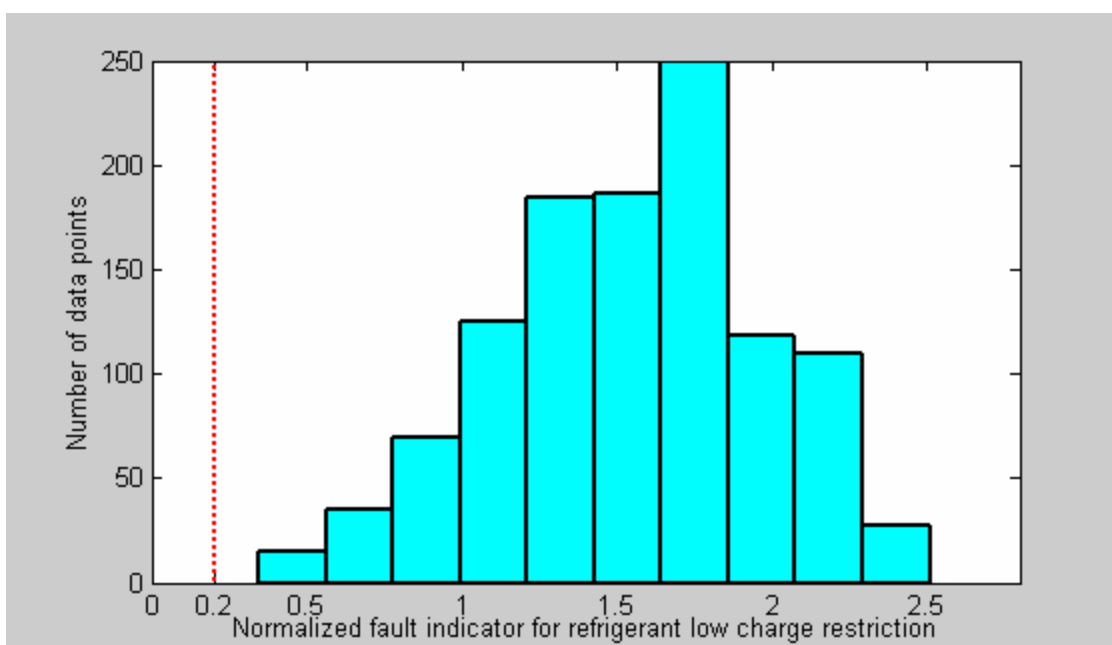


Figure 2-22 Histogram bar plot of the normalized fault indicator for refrigerant low charge

Figure 2-23 plots the normalized fault indicator for a condenser fouling fault. It can be seen that most of the steady-state data points (>95%) are at the right of the FDD threshold and the mean value is about 0.5, which indicates that the condenser is a little dirty. If this fault happened individually, it would result in about 10% cooling capacity degradation.

Figure 2-24 plots the normalized fault indicator for a compressor valve leakage fault. It can be seen that all the steady-state data points are at the left of FDD threshold and the mean value is about -0.7, which indicates that the compressor works properly and the compressor has about 15% heat loss. However, according to heat transfer analysis and our experience with laboratory data, compressors installed in York and Trane RTUs have very small heat loss, less than 5% of the power input and even gain some heat at some operating conditions. The explanation for this discrepancy is probably that the discharge line temperature is not measured accurately using the RTD temperature sensor. Appendix 2 discusses the RTD measuring issue and presents a correction approach. However, Figure 2-24 shows that the discharge line temperature is not corrected accurately as well, which is because the sensor is not installed properly.

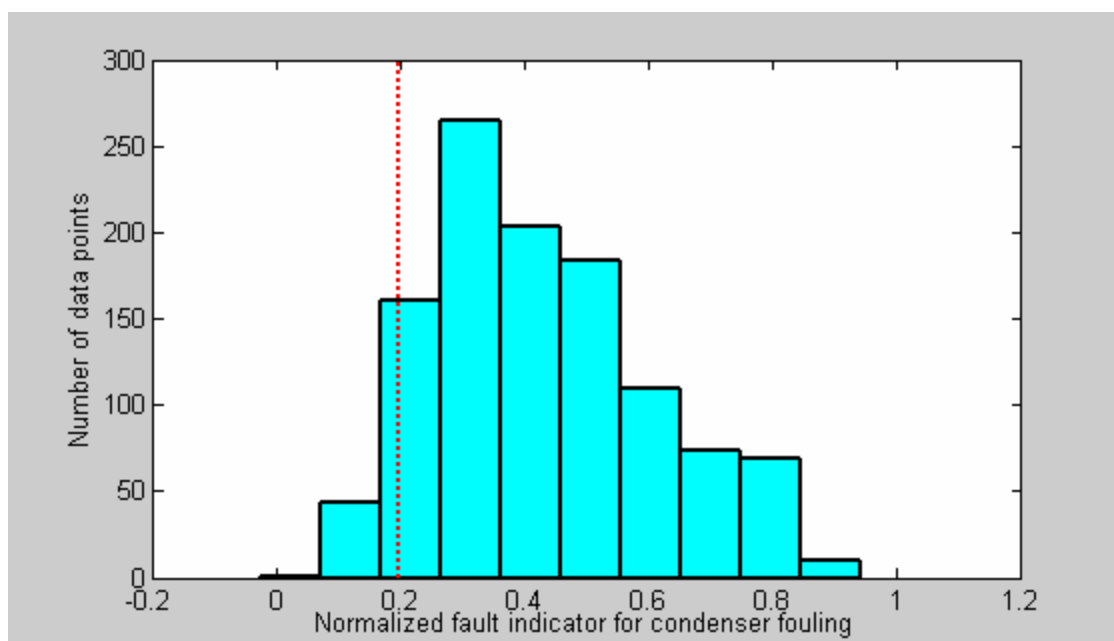


Figure 2-23 Histogram bar plot of the normalized fault indicator for condenser fouling

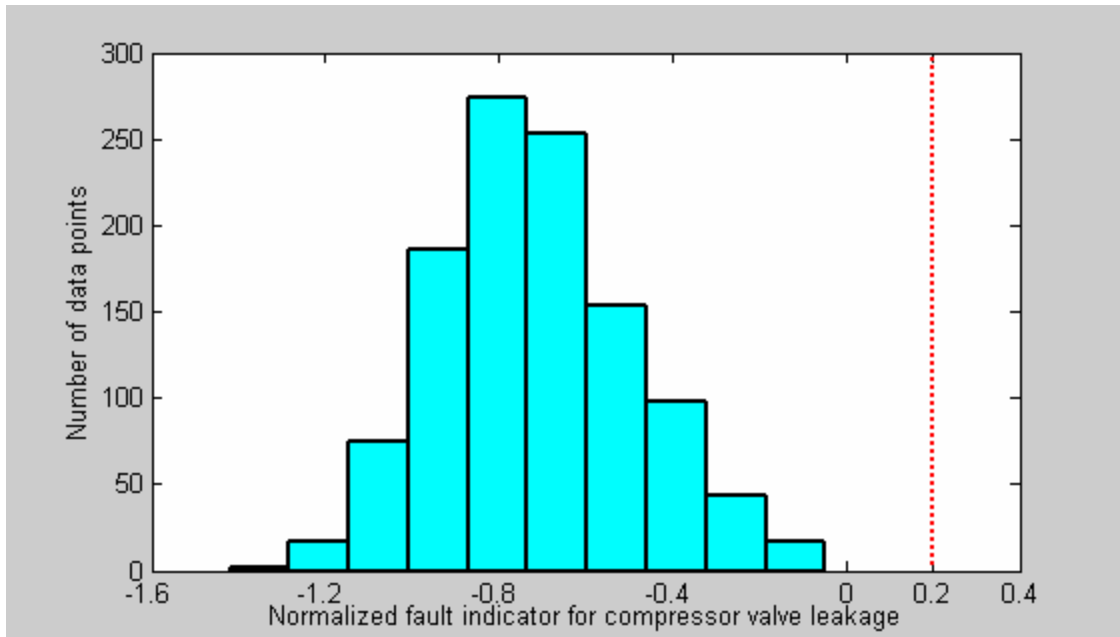


Figure 2-24 Histogram bar plot of the normalized fault indicator for compressor valve leakage

In summary, the system has three faults, low refrigerant charge, liquid line restriction and condenser fouling. To assess the impact of the diagnosed faults on the overall system performance, Figure 2-25 plots the cooling capacity degradation. It can be seen that the system cooling capacity was degraded 23~45% and the average is about 32%, which is coincident with the value indicated by refrigerant charge fault indicator. The cooling capacity degradation can be confirmed by investigating the return air temperature and system running time. It can be seen from Figure 2-26 that the average return air temperature is around 78 F and the highest is 88 F, which does not satisfy the comfort criteria. From Figure 2-27, it can be seen that the system kept running continuously for a long time (average is 2.5 hours and maximum is up to 9 hours) in order to remove the heat load. So, from the comfort criteria, service should be done to correct the diagnosed faults in order to maintain comfort.

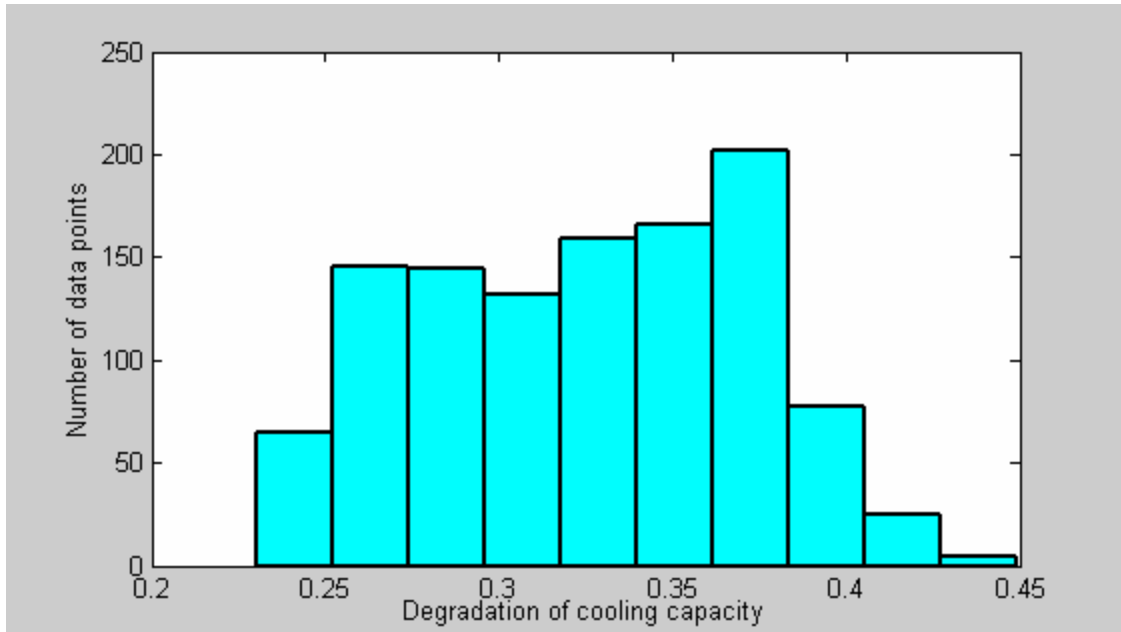


Figure 2-25 Histogram bar plot of the normalized fault indicator for cooling capacity degradation

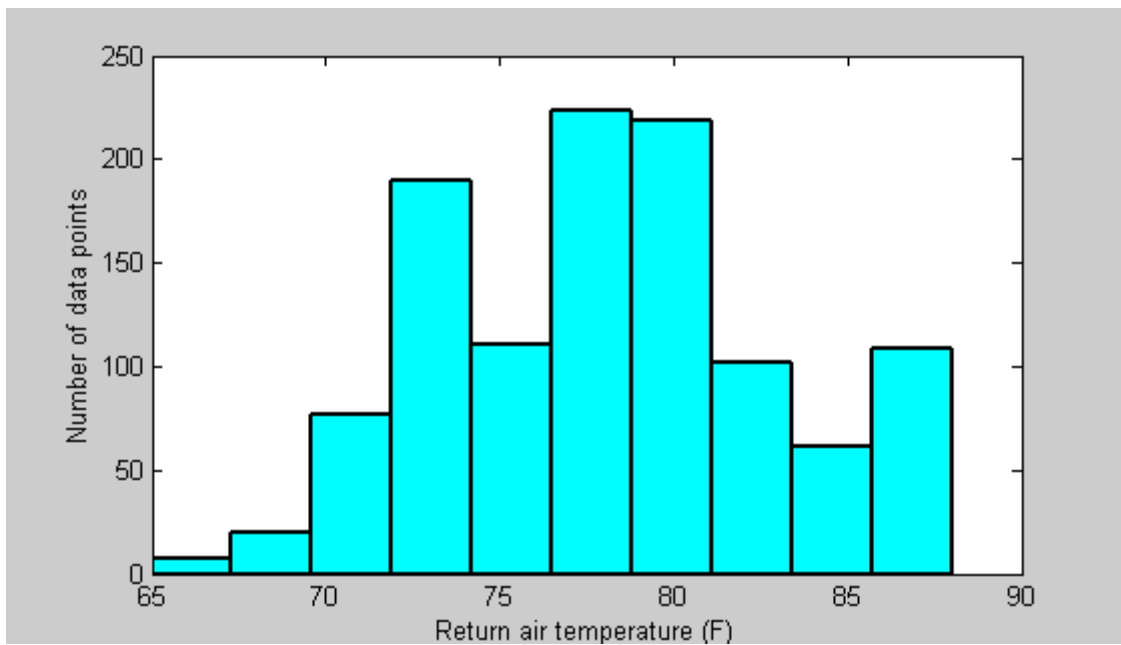


Figure 2-26 Histogram bar plot of the return air temperature

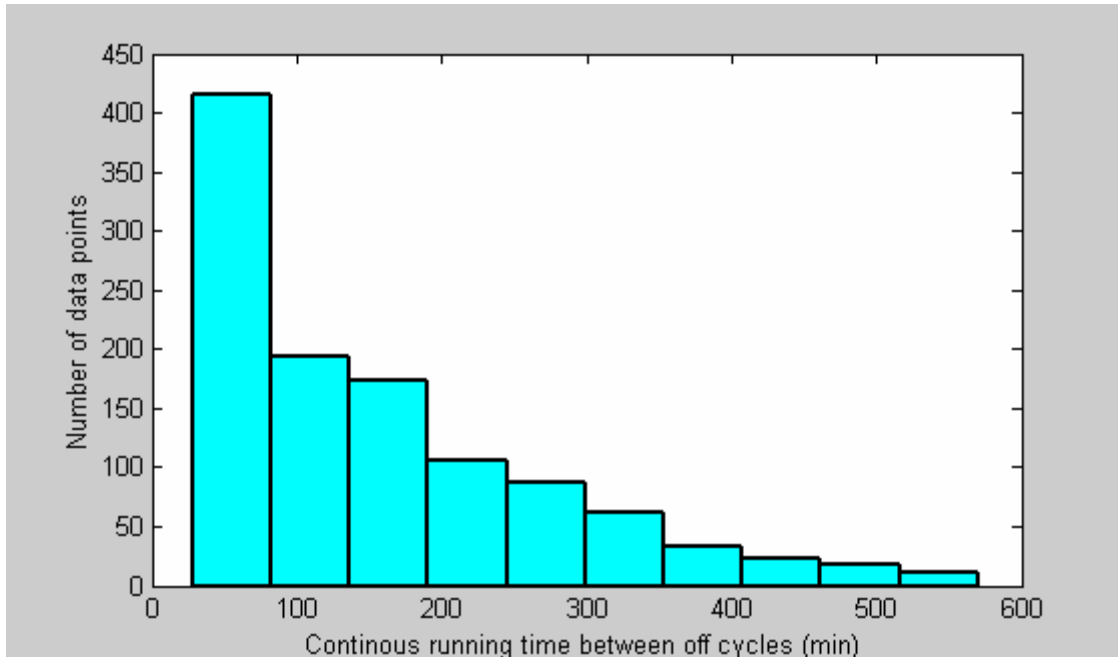


Figure 2-27 Histogram bar plot of the continuous running time between off-cycles of the RTU

In addition to the comfort criteria, Figure 2-28 plots an economic criterion, EER degradation. It can be seen that the system EER degraded about 10~40%, which depends on the operating conditions. Compared with the cooling capacity degradation, the EER degradation was a little smaller. This is because the power consumption was reduced a little but less than the degradation of cooling capacity when the refrigerant mass flow rate was reduced due to faults. Figure 2-29 plots the system power consumption reduction. The average power consumption reduction is about 15%, which is smaller than the average cooling capacity degradation of 32%. In sum, the average EER degradation is 21%, which is a pretty large economic loss. Since costs to recover the system charge, replace the filter or drier, and clean the condenser are not expensive, service to correct the faults is justified.

In summary, from both comfort and economic criteria, it is justified to correct the diagnosed faults as soon as possible.

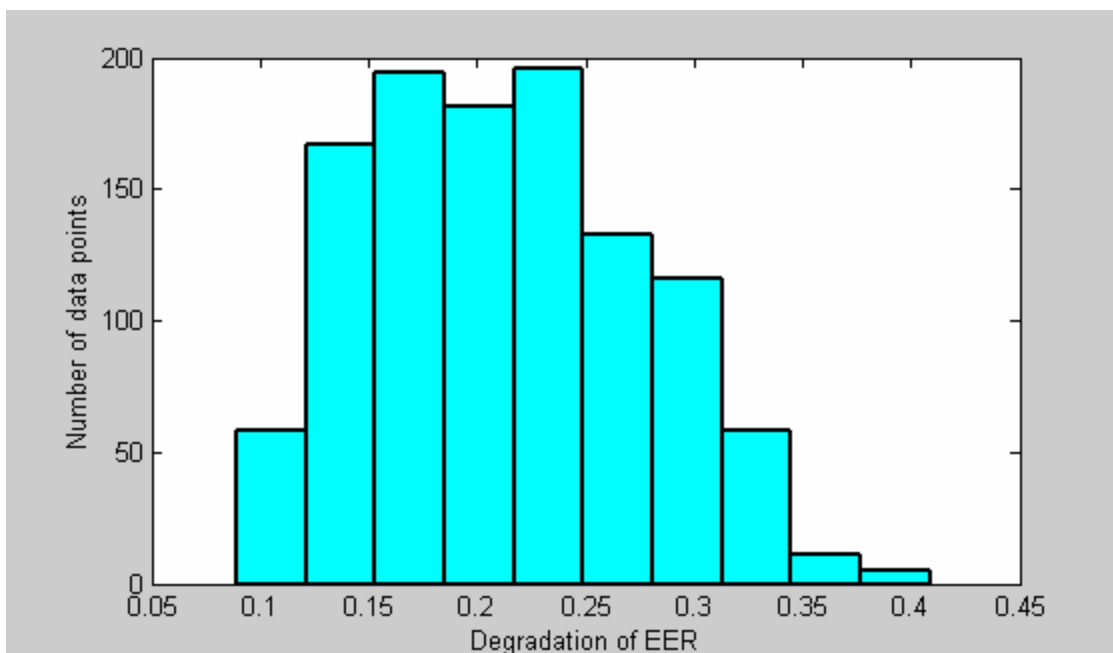


Figure 2-28 Histogram bar plot of the normalized fault indicator for EER degradation

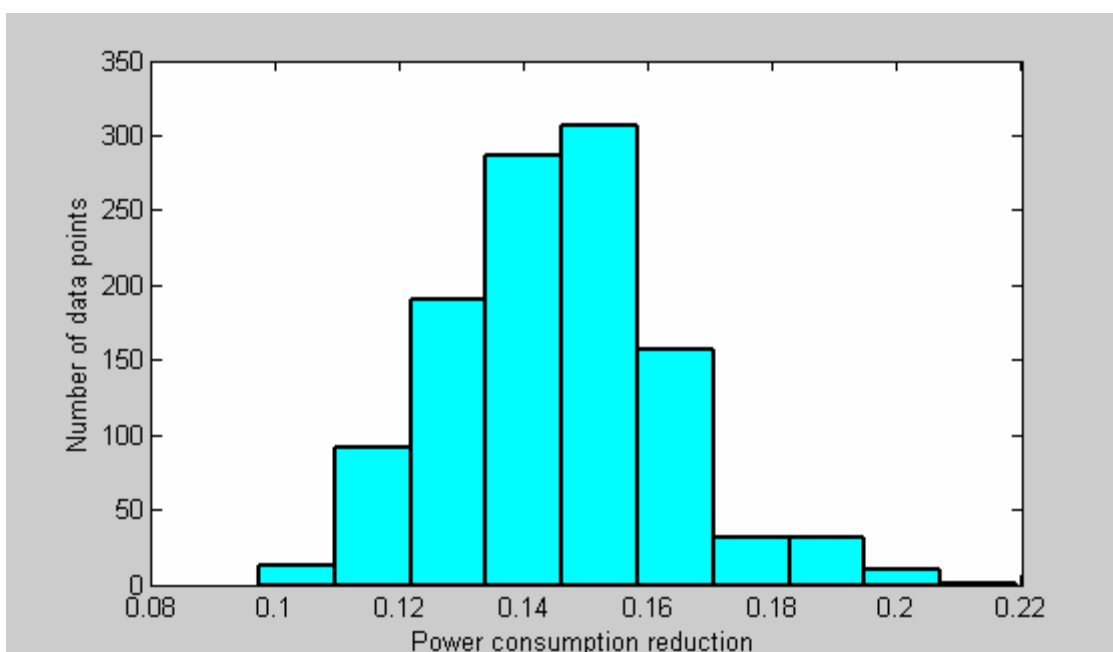


Figure 2-29 System power consumption reduction

2.3.2 Summarized Results for Other Sites

Since some necessary information about compressor and TXV and system configuration is not available so far, the decoupling-based FDD approach was partially applied to the other sites. Comprehensive FDD results and economic assessment will be provided after all the necessary information is obtained. Similar to Milpitas site, data collected from April to October in 2002 were used to do analysis for the following sites.

There are two modular school sites at Woodland and Oakland. At each site there are two 3.5-ton Bard wall-mounted heat-pump RTUs (WH421-A). Table 2-1 summarizes the FDD results for these two sites.

Table 2-1 FDD results of Modular School sites

Faults	Woodland		Oakland	
	RTU1	RTU2	RTU1	RTU2
Refrigerant Charge	Normal	Normal	Normal	Over Charge
Liquid-line Restriction	Restriction	Restriction	Restriction	Normal
Evaporator Fouling	Normal	Normal	Normal	Fouling
Recommended Service	Not yet	Replace filter/drier	Not yet	Discharge some refrigerant and clean the evaporator

Similar to the Milpitas McDonalds site, the Bradshaw McDonalds site uses a 6-ton York RTU. Both Castro Valley and Watt Avenue McDonalds sites have two York two-stage RTUs, but only one RTU in each site was configured for FDD investigation (one is 10 tons and the other is 11 tons). Table 2-2 summarizes the FDD results for these three McDonalds sites.

There are five Trane heat-pump RTUs (one is 6.25 tons and other four are 7.25 tons) installed at the Walgreens Rialto site. Table 2-3 summarizes the FDD results for this site.

Table 2-2 FDD results of McDonalds Restaurant Sites

Faults	Bradshaw	Castro Valley		Watt Avenue	
		Stage 1	Stage 2	Stage 1	Stage 2
Refrigerant Charge	Low Charge	Normal	Normal	Low Charge	Normal
Liquid-line Restriction	Restriction	Normal	Normal	Normal	Normal
Recommended Service	Add some refrigerant	NA	NA	Add some refrigerant	NA

Table 2-3 FDD results of Walgreen Retail Store Sites at Rialto

	RTU1	RTU2	RTU3	RTU4	RTU5
Refrigerant Charge	Extremely Low Charge	A little Low Charge	Normal	Normal	Over Charge
Liquid-line Restriction	Normal	Small Restriction	Normal	Normal	Normal
Recommended Service	Add some refrigerant immediately	Not yet	NA	NA	Discharge a little refrigerant

In summary, initial investigation shows that faults happen very frequently at the field sites. For example, six of the sixteen investigated RTUs have liquid line restriction faults, seven of them have refrigerant charge faults, and four of them have more than two simultaneous faults. Seven of the sixteen investigated RTUs justify service immediately.

3 CONCLUSIONS AND RECOMMENDATIONS

This report first formulated the general model-based FDD methodology in a mathematical way and cast the SRB FDD method within this framework. Inspired by this mathematical formulation, a decoupling-based FDD approach was proposed to handle multiple-simultaneous faults.

Laboratory data collected by Breuker (1998) for a 3-ton fixed orifice RTU validated the proposed decoupling strategy. And then multiple-simultaneous faults were artificially introduced into the Purdue field emulation site to demonstrate the decoupling-based FDD approach. This demonstration showed that the proposed FDD approach can correctly detect and diagnosis multiple-simultaneous faults and it also demonstrates the type of information that could be supplied to a user. Finally, the FDD method was applied to California field sites. Only partial results were obtained for the California field sites because not all of the information on the equipment was obtained so far. However, the results showed that many faults at the field sites can be detected and diagnosed even if the information is not complete. According to the analysis of field data, another conclusion can be drawn that faults occurred frequently and multiple-simultaneous faults were common at the field sites.

More data for multiple-simultaneous faults under wider ranges of operating conditions are needed to test the robustness and quantify the performance of the proposed FDD approach. The instrumentation of the California field sites should to be checked, improved or even modified to obtain more reliable data.

REFERENCE

- Aaron, D. A., and P. A. Domanski. 1990. Experimentation, analysis, and correlation of refrigerant-22 flow through short-tube restrictor. *ASHRAE Transactions* 96(1): 729-742.
- Alistair I. Mees, M. F. Jackson, and Leon O. Chua, 1992. Device Modeling by Radial Basis Functions. *IEEE Transactions on Circuits and Systems-Fundamental Theory and Applications*. 39 (1): 19-27.
- ASHRAE. 1993. *ASHRAE Handbook - 1993 Fundamentals*, Atlanta: American Society of Heating, Refrigerating, and Air Conditioning Engineers, Inc., Atlanta, GA 30329.
- Benjamin, M.W., and J.G. Miller, 1941. The flow of saturated water throttling orifice. *Transactions of the ASME* 63 (5): 419-426
- Braun, J.E. and Li, Haorong. 2001a. Description of Laboratory Setup. Progress report submitted to Architectural Energy Corporation.
- Braun, J.E. and Li, Haorong. 2001b. Description of FDD modeling approach for normal performance expectation. Progress report submitted to Architectural Energy Corporation.
- Braun, J.E. and Li, Haorong. 2002. Description and Evaluation of an Improved FDD Method for Rooftop Air Conditioners. Progress report submitted to Architectural Energy Corporation.
- Breuker, M.S., 1997. Evaluation of a Statistical, Rule-based Detection and Diagnosis Method for Vapor Compression Air Conditioners, Master's Thesis, School of Mechanical Engineering, Purdue University.

- Breuker, M.S. and Braun, J. E., 1997. Evaluation of a Statistical, Rule-based Detection and Diagnosis Method for Vapor Compression Air Conditioners, HL 98-9, Report # 1796-7a, School of Mechanical Engineering, Purdue University.
- Breuker, M.S. and Braun, J.E., 1998. Common Faults and Their Impacts for Rooftop Air Conditioners, HVAC&R Research, Vol. 4, No. 3, pp.303-318.
- Breuker, M.S. and Braun, J.E., 1998. Evaluating the performance of a Fault Detection and Diagnostic System for Vapor Compression Equipment, International Journal of Heating, Ventilating, and Air Conditioning and Refrigerating Research, Vol. 4, No. 4, pp.401-423.
- Cacoullos, 1966. "Estimation of a multivariate density," Ann. Inst. Statist. Math, (Tokyo), Vol. 18, no. 2, pp.179-189.
- Carling, P., 2002. Comparison of Three Fault Detection Methods Based on Field Data of an Air-Handling Unit, ASHRAE Transactions 2002, V. 108, Pt.1.
- Chen, B., 2000. Evaluating the potential of on-line fault detection and diagnosis for rooftop air conditioners, Master's Thesis, School of Mechanical Engineering, Purdue University.
- Chen, Bin and Braun, J.E, 2000. Simple fault detection and diagnostics methods for packaged air conditioners, Proceedings of the 8th international refrigeration conference, Purdue University.
- Chen, Bin and Braun, J.E, 2001. Simple rule-based methods for fault detection and diagnostics applied to packaged air conditioners, ASHRAE Trans., vol. 107, part 1, paper No. AT-01-14-2, 847-837.
- Comstock, M.C., J.E. Braun, and B. Chen, 1999, Literature Review for Application of Fault Detection and Diagnostic Methods to Vapor Compression Cooling Equipment, Purdue University, Ray W. Herrick Laboratories, Report # HL99-19.
- Davis, Coby. 1993. Comparison of steady state detection algorithms. ME 397 Report. Available from Professor Jim Braun, Herrick Labs, Purdue University, West Lafayette, In.

Dexter, Arthur; Pakanen, Jouko (ed.). Demonstrating Automated Fault Detection and Diagnosis Methods in Real Buildings. Espoo. VTT Building Technology, 2001. VTT Symposium 217. 381 p. + app. 13 p.

Dexter, A.L. and Ngo, D., 2001. Fault Diagnosis in Air-Conditioning Systems: A Multi-Step Fuzzy Model-Based Approach, International Journal of Heating, Ventilating, and Air Conditioning and Refrigerating Research, Vol. 7, No. 1, pp.83-102.

Donald F. Specht, 1991. A General Regression Neural Network. IEEE Transactions on Neural Networks. 2 (6): 368-376.

Dyn, N. and Levin, D., 1983. "Iterative solutions of systems originating from integral equations and surface interpolation." SIAM J. Numerical Analysis, vol. 20, pp. 377-390.

Fukunaga, K. 1990. Introduction to Statistical Pattern Recognition, Academic Press, Purdue University, W. Lafayette, IN, USA

Ghiaus, C. 1999. Fault diagnosis of air conditioning systems based on qualitative bond graph, Energy and Buildings 30 (1999) 221-132.

Glass, A.SI, Gruber, P., Roos, and M., Todtli, J., 1993. Qualitative Model-based fault detection in air-handling units, IEEE control systems Magazine, 13(4): 11-22.

Gordon, J. M., and K. C. Ng. 1994. Thermodynamic modeling of reciprocating chillers. Journal of Applied Physics. 76(6):2769-2774.

Grimmelius, H. T., J. Klein Woud, and G. Been. 1993. On-line failure diagnosis for compression refrigeration plants. International Journal of Refrigeration 18(1):31-41.

Isermann, R. 1984. Process Fault Detection Based on Modeling and Estimation - A Survey, Automatica, 20(4): 387-404.

Kim, Y. and O'Neal, D. L., 1994. Two-phase flow of R-22 through short-tube orifices. ASHRAE Transactions 100(1): 323-334.

- Lee, W., House, J.M. and Shin, D.R., 1997. Fault diagnosis and Temperature Sensor Recovery for an Air-handling unit, ASHRAE Transaction, 103(1): 621-633.
- Lee, W.Y. & House, J.M., etc., 1996. Fault diagnosis of an Air-Handling Unit Using Artificial Neural Networks, AHRAE Transactions V.102, Pt.1, pp.340-349,1996
- Li, H. and Braun, J.E. 2003, "An Improved Method for Fault Detection and Diagnosis Applied to Packaged Air Conditioners". Accepted by the American Society of Heating, Refrigerating, and Air Conditioning Engineers (ASHRAE)
- Li, H. and Braun, J.E., "On-Line Models for Use in Automated Fault Detection and Diagnosis for HVAC&R Equipment," Proceedings of the 2002 ACEEE Conference on Energy Efficiency in Buildings, Monterey, CA, 2002.
- Li, X., H. Hvaezi-Nejad, & J.C. Visier, 1996. Development of a fault diagnosis method for heating systems using neural networks. ASHRAE Transactions 102 (1): 607-614.
- Norford, L.K., Wright, J.A., etc., 2002. Demonstration of Fault Detection and Diagnosis Methods for Air-Handling Units, International Journal of Heating, Ventilating, and Air Conditioning and Refrigerating Research, Vol. 8, No. 1, pp.41-71.
- Parzen, 1962. On the estimation of a probability density function and the mode, Ann. Math. Stat., 33, pp. 1063-1076.
- Rossi, T.M., 1993. Detection, Diagnosis, and Evaluation of Faults in Vapor Compression Cycle Equipment, Ph.D. Thesis, School of Mechanical Engineering, Purdue University.
- Rossi, T.M. and Braun, J.E., "Minimizing Operating Costs of Vapor Compression Equipment with Optimal Service Scheduling," International Journal of Heating, Ventilating, Air-Conditioning and Refrigerating Research, Vol. 2, No. 1, pp. 23 - 47, 1996.
- Rossi, T.M. and Braun, J.E., 1997. A Statistical, Rule-Based Fault Detection and Diagnostic Method for Vapor Compression Air Conditioners, International

Journal of Heating, Ventilating, and Air Conditioning and Refrigerating Research, Vol. 3, No. 1, pp.19-37.

Shaw, S.R., Norford, L.K., Luo, D., etc., 2002. Detection and Diagnosis of HVAC Faults Via Electrical Load Monitoring, International Journal of Heating, Ventilating, and Air Conditioning and Refrigerating Research, Vol. 8, No. 1, pp.13-40.

Stylianou, M. & D. Nikanpour. 1996. Performance monitoring, fault detection, and diagnosis of reciprocating chillers. ASHRAE Transactions 114 (4): 613-627.

Yoshida, H. & Kumar, S. 1999. ARX and AFMM model-based on-line real-time data base diagnosis of suddent fault in AHU of VAV system, Energy Conversion & Management 40 (1999) 1191-1206.

Yoshida, H. & Kumar, S. 2001. Development of ARX model based off-line FDD technique for energy efficient buildings, Energy Conversion & Management 22 (2001) 33-39.

Yoshida, H. & Kumar, S. 2001. Online fault detection and diagnosis in VAV air handling unit by RARX modeling, Energy Conversion & Management 33 (2001) 391-401.

APPENDIX 1 PHYSICAL MODELS OF EXPANSION DEVICE

An expansion device is a relatively simple component, whose role is to reduce the pressure and regulate the refrigerant flow to the low side evaporator in accordance with load demands. As mentioned in Section 1, a model of the expansion device can be used to estimate its upstream pressure. There are two kinds of expansion devices used in vapor compression system: fixed-area and adjustable throat-area expansion valve.

A1.1 Fixed-Area Expansion Device Models

The fixed-area expansion devices are typically used on certain small air conditioners and refrigeration systems where operating conditions permit moderately constant evaporator loading and constant condenser pressures. According to their length-to-diameter ratios, L/D , fixed-area expansion devices fall into one of three categories: an orifice with $L/D < 3$, a short-tube with $L/D = 3 \sim 35$, and a capillary tube with $L/D > 20$ (ASHRAE 1998). Among them, capillary tubes are used in home refrigerators and room air-conditioners of small capacity, while short-tubes are widely used in packaged residential and small commercial air-conditioners and heat-pumps of relatively large capacity.

A1.1.1 Orifice Models

Although orifices are seldom used as refrigerant expansion devices nowadays, their operation principles are the basis for the operation of adjustable throat-area control

devices. An equation for liquid mass flow rate across an orifice could be derived from Bernoulli's equation (ASHRAE 1997) as,

$$\dot{m} = C_d A \sqrt{2 \rho (P_{up} - P_{down}) / (1 - b^4)} \quad (A1-1)$$

where, C_d is discharge coefficient, $A = \frac{\pi D^2}{4}$ is the throat area, ρ is density, P_{up} is the upstream pressure, P_{down} is the downstream pressure, and b is the ratio of the orifice diameter, D , to the upstream tube diameter. Since b varies from 0.1 to 0.2, raising b to the fourth power results in a very small number. Therefore, the term of $(1 - b^4)$ could be dropped from the equation.

$$\dot{m} = C_d A \sqrt{2 \rho (P_{up} - P_{down})} \quad (A1-2)$$

Benjamin and Miller (1941) conducted experiments of sharp-edged orifices of $L/D = 0.28 \sim 1$ with saturated water at various upstream pressures and found that

1. Orifices having $L/D < 1$ did not choke the flow at normal operating conditions and therefore could not be used as refrigerant expansion devices.
2. The discharge coefficient found for a two-phase water mixture was approximately the same as that for cold liquid water.

Some other researchers (Roming et al., 1966; Davies and Daniels, 1973) refined the above equation to deal with two-phase situations more accurately by adding an expansion factor, y , which is unity if no vaporization occurs.

$$\dot{m} = C_d y A \sqrt{2 \rho (P_{up} - P_{down})} \quad (A1-3)$$

In summary, the mass flow rate equation of orifices can be generalized as,

$$\dot{m} = C A \sqrt{2 \rho (P_{up} - P_{down})} \quad (A1-4)$$

It should be pointed out that some researchers (Chisholm, 1967; Krakow and Lin 1988) observed that the mass flow rate of a refrigerant through an orifice in a heat pump was primarily dependent on the upstream conditions, which indicates that the flow was choked. This warrants further investigation.

A1.1.2 Short-Tube Models

Many researchers (Bailey, 1951; Zaloudek, 1963; Mei, 1982; Aaron & Domanski, 1990, and Kim & O'Neal, 1994) conducted experimental or theoretical research on short-tubes. Among them, Aaron & Domanski (1990) and Kim & O'Neal (1994) obtained good consistent results and proposed some good correlations. There is no doubt that the flow through a short-tube in air-conditioner applications is choked. Following is the model format for short tubes.

$$\dot{m}_{ref} = C_c A_s \sqrt{2 g_{ca} \mathbf{r} (P_{up} - P_f)} \quad (A1-4)$$

where A_s is the flow area, g_{ca} is the dimensional gravity constant, C_c is a constant that corrects for inlet effect. \mathbf{r} and P_{up} are the upstream refrigerant density and pressure, respectively. For a sharp-edged entrance, $C_c = 1$, otherwise, C_c depends on the inlet chamfer geometry as,

$$C_c = 1.0 + 0.02655(L/D)^{0.70775} (DEPTH/D)^{0.22684}$$

$DEPTH$ is the inlet chamfer depth (45° chamfer angle) and P_f is the flashing pressure, which is approximated by a semi-empirical equation as,

$$P_f = P_{sat} (1.005 + 5.7367(P_{up}/P_c)^{-0.485} (L/D)^{-0.179} SUBC^{0.9948} + 0.268(P_{up}/P_c)^{2.716}) \\ - 0.226 \exp(-0.021(D/D_{ref})(L/D)^2) - 0.092 EVAP$$

where P_{sat} is the liquid saturated pressure corresponding to T_{up} , L/D is the ratio of length to diameter, D/D_{ref} is the non-dimensional diameter with $D_{ref} = 1.35mm$, $SUBC = (T_{sat} - T_{up})/T_c$ with T in absolute temperatures, $EVAP = (P_c - P_4)/P_c$ with P in absolute pressures, T_c and P_c are critical temperature and pressure, respectively, P_4 is the saturated pressure corresponding to T_4 which can be measured, and T_{sat} is the saturated temperature corresponding to P_{up} . Using this model, P_{up} can be estimated if \dot{m}_{ref} can be estimated using a compressor map.

It was reported in the literature that the above model works very well for upstream conditions with positive subcooling and reasonably well down to 10% quality. Our FDD

application falls into the “very well” range, because if the upstream has no subcooling ΔT_{ll} would be used to do FDD for a liquid-line restriction.

A1.1.2 Capillary-Tube Models

Since capillary tubes are used very widely in household refrigerators and room air conditioners, exhaustive research has been conducted for capillary tubes. Similar to a short-tube, the flow through a capillary tube is choked. Since capillary tubes are seldom used in small commercial air-conditioners and many good correlations can be found in the literature, models for them are not repeated here.

A1.2 Adjustable Throat-Area Expansion Valve Models

The drawback associated with fixed-area devices is their limited ability to efficiently regulate refrigerant flow in response to changes in system operating conditions, since they are sized based on one set of conditions. Adjustable throat-area expansion valves provide a better solution to regulating refrigerant flow into a direct expansion type evaporator using certain feedback control strategy. The thermostatic expansion valve (TXV) and the electric expansion valve (EXV) fall into the adjustable throat-area expansion valve. The TXV uses a single variable proportional feedback control scheme to maintain a nearly constant superheat at the evaporator outlet. The fundamental principle of a EXV is the same as a TXV except that it is designed with sophisticated system control strategies including PID and multivariable control.

Although TXVs and EXVs are used widely, modeling literature for them is very limited. When building a simulation model for a system, some researchers ignored them and assumed constant superheat. Some researchers (Harms, 2002) correlated TXV performance using experimental data. Among the limited literature, none discusses fundamentally whether the flow is choked or not. In the limited literature, the following format for a TXV model has been adopted,

$$\dot{m} = CA\sqrt{r(P_{up} - P_{down})} \quad (A1-5)$$

The above equation is the same as that for an orifice except that A is a variable. Therefore, it seems that mass flow rate is a strong function of pressure drop $\Delta P = P_{up} - P_{down}$ and variable restriction area A but a very weak function of upstream refrigerant subcooling T_{sub} . The implicit assumption is that the flow is not choked. Before using this model format, it is advisable to validate this assumption.

A2.2.1 Model Format Validation Using Manufacturers' Rating Data

Whether the flow is choked or not can be checked indirectly by analyzing manufacturers' rating data. Equation (A1-5) can be rearranged as,

$$CA = \frac{\dot{m}_{ref}}{\sqrt{r(P_{up} - P_{down})}} \quad (A1-6)$$

According to ANSI/ASHRAE standard 17 (1998) and ARI standard 750 (2001), maximum throat-area A is nearly fixed by fixing the opening superheat when generating the manufacturers' rating data for a TXV. For a EXV, the maximum throat-area A is exactly fixed at the rating value. So CA for a EXV should be constant and that for a TXV should be relatively constant if the flow is not choked.

Figure A1-1 shows that CA of an ALCO EXV is pretty constant (mean: 6.7881, standard variation: 0.0101, standard variation/mean: 0.15%) over the whole set of rating conditions (evaporator temperature: -40F~40F and Pressure Drop: 50psi~250psi).

For a Sporlan TXV, Figure A1-2 shows that CA has an abrupt change from an air conditioning application (evaporator temperature: -5C ~ 5C) to a refrigeration application (evaporator temperature: -15C). In spite of the abrupt change, its overall variation is still small (mean: 1.1018, standard variation: 0.0323, standard variation/mean: 2.93%). Furthermore, the variation is very small within each application range. For air conditioning applications, the mean is 1.1238, standard variation is 0.0021, and standard variation/mean is 0.19%. For refrigeration applications, the mean is 1.0578, standard variation is 0.0013, and standard variation/mean is 0.12%. Therefore, the TXV model format is accurate and the flow is not choked.

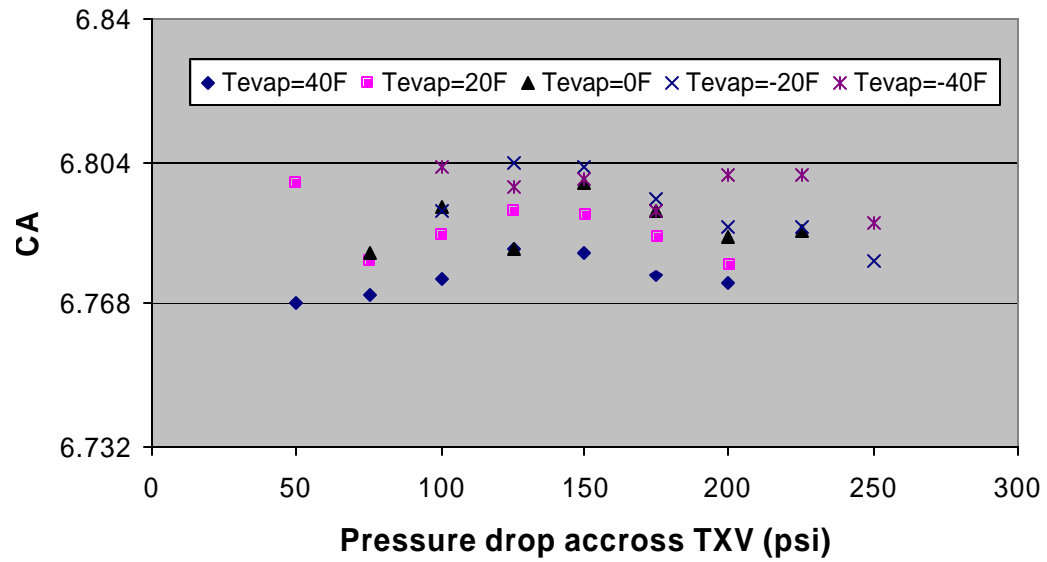


Figure A1-1 The CA value of an ALCO EXV of manufacturer rating conditions

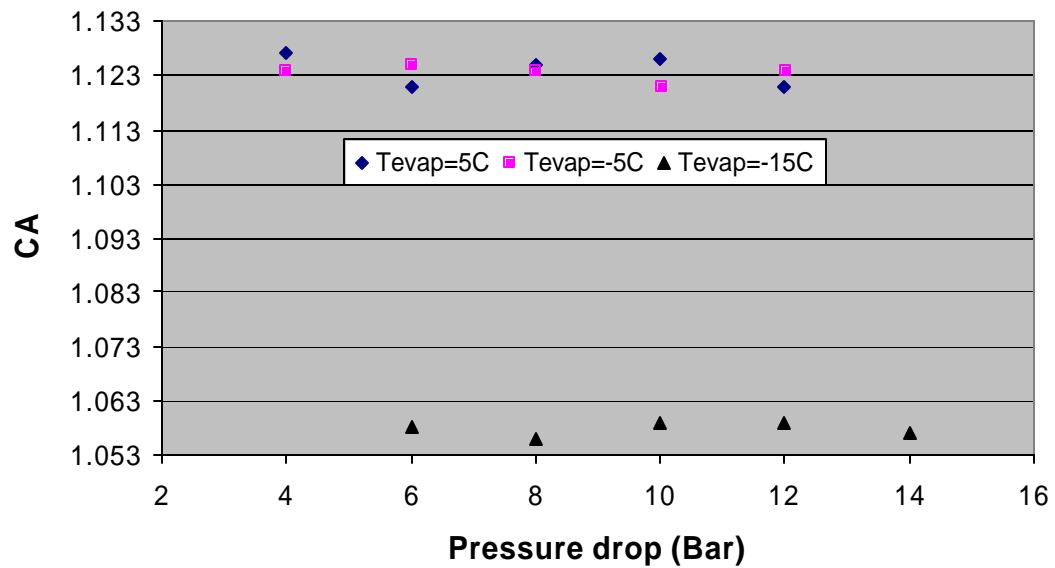


Figure A1-2 The CA value of a SPORLAN TXV of manufacturer rating conditions

The abrupt change of CA for the TXV can be explained by the P-T curve of the thermostatic charge fluid. Figure A1-3 shows that the P-T curve becomes flatter at lower temperature. As a result, a given opening superheat results in less pressure difference across the valve diaphragm at lower evaporating temperatures causing a reduction in valve opening A . For example, the pressure difference caused by 5 C of opening superheat at an evaporating temperature of 5 C is 0.969 bars, which is far larger than 0.584 bars at an evaporating temperature of -15 C. Fortunately, this would not cause a big problem because of the following reasons:

1. The P-T curve is pretty linear if it is divided into three sections: AB, BC and CD. For a given application, the TXV will work in one of the three sections. The TXV used in packaged air conditioning falls into section CD.
2. It can be eliminated or overcome using cross charge. The above analysis is based on liquid charge. As to cross charge, the power fluid is chosen so that the superheat required to open the valve is nearly constant over the entire operating range.

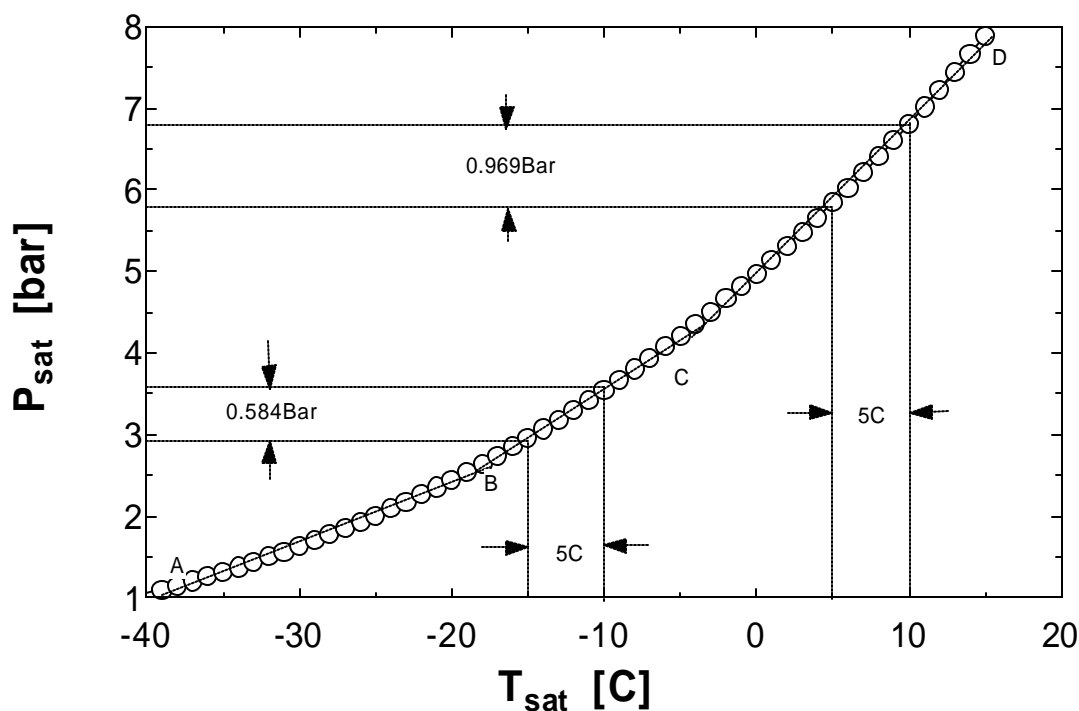


Figure A1-3 P-T saturation curve for R22

In summary, from manufacturers' standard rating data, the flow across a TXV or EXV is not choked and the generally used model format is valid. To specify the TXV or EXV model, the key point is to find the expression for variable throat-area, A , and then specify the constant C using manufacturers' rating data.

Generally speaking, the throat-area, A , is a function of valve position, which is determined by the control strategy used by the valve. Because TXVs and EXVs use different control strategies, the first step is to derive the A in terms of valve position and then develop expressions for valve position.

A1.2.2 Derivation of Throat-Area A Expression

As shown in Figure A1-4, there are three kinds of valves used in TXVs and EXVs and each different type has a different expression for A . Among them, type I and II are used widely and their expression is the same.

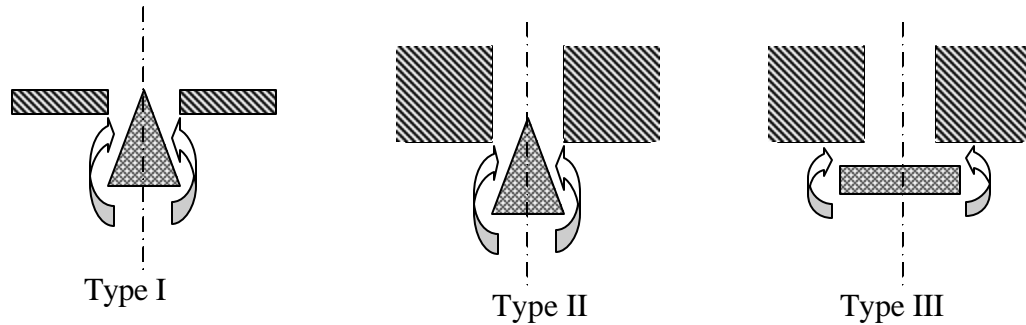


Figure A1-4 Three types of valve geometry

Figure A1-5 shows the geometric model of valve type I and II. At a certain valve position, h ,

$$A = \frac{\pi}{4}(D^2 - d^2),$$

where, $d = 2 \tan \theta (H - h)$ and $\tan \theta = \frac{D}{2H}$, so,

$$d = 2 \frac{D}{2H} (H - h) = D(1 - \frac{h}{H}),$$

These equations can be combined to give,

$$A = \frac{P}{4} (D^2 - D^2 (1 - \frac{2h}{H} + (\frac{h}{H})^2)) = \frac{P}{2} D^2 (\frac{h}{H} - \frac{1}{2} (\frac{h}{H})^2) = \frac{P}{4} \frac{h}{H} D^2 (2 - \frac{h}{H})$$

It is obvious that throat-area, A , is a second order function of valve position, h , which is plotted as Figure A1-6.

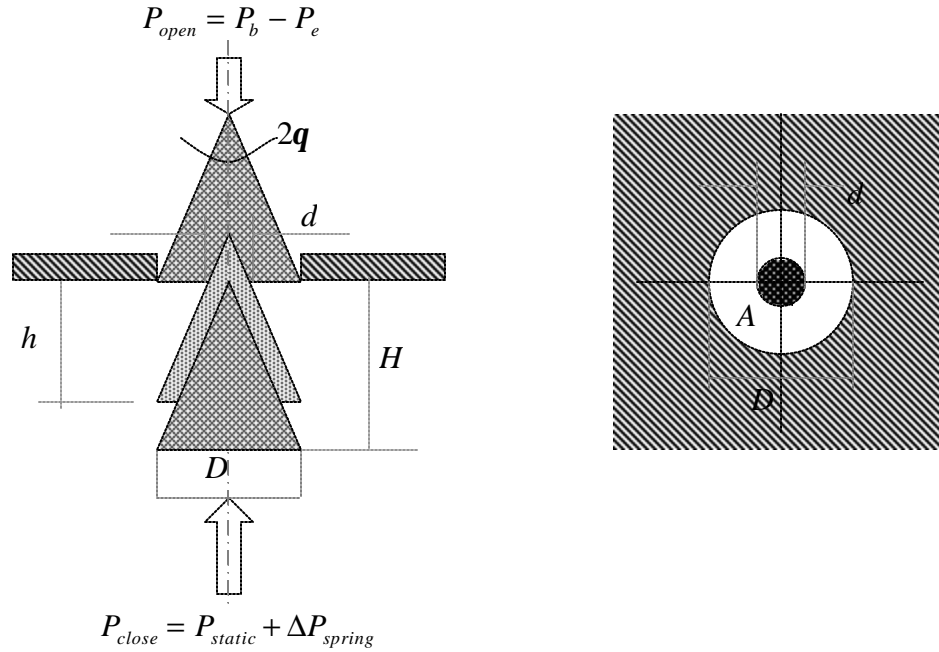


Figure A1-5 Geometric model of type I and II valve

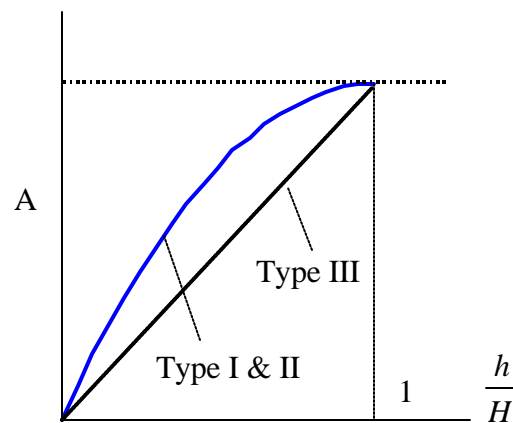


Figure A1-6 Throat-area curves of different valve types

Figure A1-7 shows the geometric model of valve type III. It is very easy to obtain the expression as,

$$A = pDh ,$$

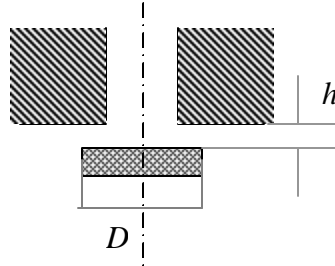


Figure A1-7 Geometric model of valve type III

It is obvious that throat-area, A , is a linear function of valve position, h .

A1.2.3 Valve Position Expression

The valve position for a EXV can be calculated easily by the control signal. As to a TXV, it is the function of superheat. Assume that the pressure difference is a linear function of superheat,

$$P_{open} = k_1 T_{sh,operating} , \quad P_{close} = k_2 (x_{static} + h) .$$

Since the forces exerted on the valve are balanced,

$$k_1 T_{sh,operating} = k_2 (x_{static} + h) ,$$

Rearranging the above equation gives an expression for valve position,

$$\begin{aligned} h &= \frac{k_1}{k_2} T_{sh,operating} - x_{static} = k T_{sh,operating} - x_{static} \\ &= k T_{sh,operating} - k T_{sh,static} = k (T_{sh,operating} - T_{sh,static}) . \\ &= k T_{sh,opening} \end{aligned}$$

As shown in Figure A1-8, it is obvious that the valve position is a linear function of opening superheat.

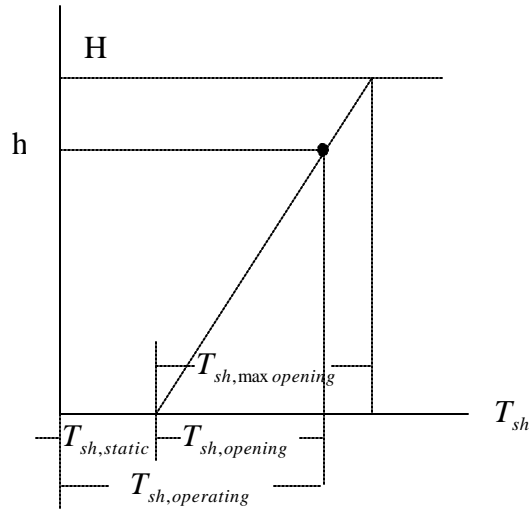


Figure A1-8 Valve position curve

A1.2.4 Overall Mass Flow Rate Model of TXV

The overall mass flow rate model for a TXV can be obtained by substituting the expression of throat-area and valve position expression into the general model equation.

As to type I and II,

$$\begin{aligned}
 A &= \frac{pD^2}{4} \frac{h}{H} \left(2 - \frac{h}{H}\right) = \frac{pD^2}{4} \frac{kT_{sh,opening}}{H} \left(2 - \frac{kT_{sh,opening}}{H}\right) \\
 &= \frac{pD^2}{4} \frac{kT_{sh,max\ opening}}{kT_{sh,max\ opening}} \left(2 - \frac{kT_{sh,opening}}{kT_{sh,max\ opening}}\right) = \frac{pD^2}{4} \frac{T_{sh,opening}}{T_{sh,max\ opening}} \left(2 - \frac{T_{sh,opening}}{T_{sh,max\ opening}}\right) \\
 \dot{m} &= C_d A \sqrt{r(P_{up} - P_{down})} = C_d \frac{pD^2}{4} \frac{T_{sh,opening}}{T_{sh,max\ opening}} \left(2 - \frac{T_{sh,opening}}{T_{sh,max\ opening}}\right) \sqrt{r(P_{up} - P_{down})} \\
 &= C \left(2 \frac{T_{sh,opening}}{T_{sh,max\ opening}} - \left(\frac{T_{sh,opening}}{T_{sh,max\ opening}}\right)^2\right) \sqrt{r(P_{up} - P_{down})}
 \end{aligned}$$

As to type III,

$$\begin{aligned}
 A &= pDkT_{sh,opening} \\
 \dot{m} &= C_d A \sqrt{r(P_{up} - P_{down})} = C_d pDkT_{sh,opening} \sqrt{r(P_{up} - P_{down})} \\
 &= CT_{sh,opening} \sqrt{r(P_{up} - P_{down})}
 \end{aligned}$$

Figure A1-9 shows the refrigerant mass flow rate curves at a fixed pressure drop. It can be seen that:

1. The mass flow rate of type I & II valves is higher than that of a type III valve with the same operation range at the same opening superheat except that the valves are fully open or close. That is, for the valves with the same operation range, type I & II valves require smaller superheat to get the same capacity than type III valve.
2. The mass flow of type III keeps increasing linearly with the opening superheat until the maximum opening superheat arrives, while that of type I & II keeps increasing nonlinearly and the increasing rate decreases smoothly down to zero when the valve is fully open. That is, for type I & II valves to have the same reserve capacity as a type III valve more superheat is required, so type I & II valves would be expected to have smaller reserve capacity (around 10%) than that of type III (up to 40%) in order to avoid abnormally high superheat at high capacity operation. However, a possible advantage is that type I & II valves may help reduce the problem of the TXV alternately overfeeding and underfeeding the evaporator, which is usually termed hunting or cycling.

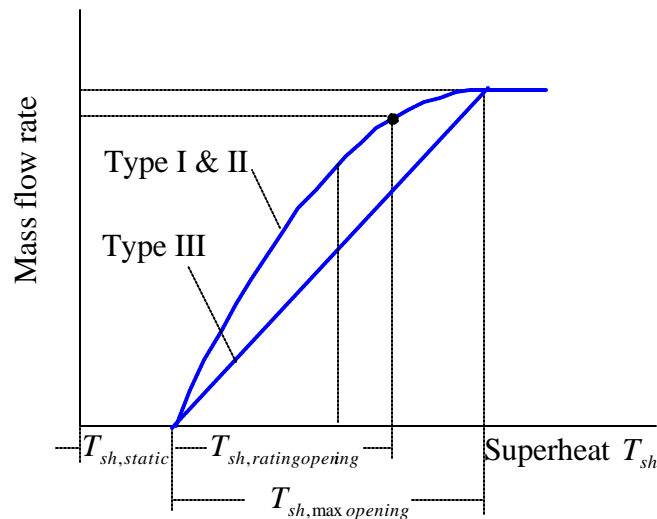


Figure A1-9 Mass flow rate curves at a fixed pressure drop

A1.2.5 Parameter Estimation Method

Having determined the model format, it is important to identify the parameters. From the above analysis, it can be seen that the mass flow rate for type I and II TXVs is a nonlinear function of superheat while that of type III is a linear function of superheat. However, in most of the existing literature, it is assumed that the mass flow rate of all kinds of TXVs is a linear function of superheat. So, in order to simplify the parameter estimation, the global linear assumption can be adopted (no approximation for type III TXV). There are two proposed ways to estimate model parameters using manufacturers' rating or experimental data. One is to use the linear assumption and the other is directly estimate parameters.

A1.3.2.5.1 Global Linear Assumption Method

Under the global linear assumption, the general TXV model is

$$\dot{m} = C(T_{sh,operating} - T_{sh,static})\sqrt{r(P_{up} - P_{down})}$$

Rearranging the above equation,

$$C(T_{sh,operating} - T_{sh,static}) = \frac{\dot{m}}{\sqrt{r(P_{up} - P_{down})}}$$

The parameters of the TXV model can be determined by the following procedure,

1. According to manufacturers' rating data,

$$C(T_{sh,rating} - T_{sh,static}) = CT_{sh,rating,opening} = constant$$

where $T_{sh,rating,opening}$ is fixed by the TXV manufacturer and should be readily available. Although the TXV manufacturer presets the $T_{sh,static}$ as well, the manufacturer of the air conditioning system would adjust it slightly in order to match the rated capacity.

2. IF $T_{sh,rating,opening}$ is available from the manufacturer, go to step 3. If not, roughly guess an initial value according to ARI and ASHRAE standards and manufacturing tradition (Table A1-1).

Table A1-1 TXV rating settings

Source	$T_{sh,rating,opening}$ (C)	$T_{sh,rating}$ (C)	$T_{sh,static}$ (C)	Reserve Capacity
ARI Standard	≤ 4		> 1	
ASHRAE Standard Example	3		3	
ASHRAE Handbook	2 ~ 4			0.1 ~ 0.4
ALCO (recommend)	2.2 ~ 3.3		3.3 ~ 5.6	
SPORLAN(recommend)		4.4 ~ 6.7		
Recommended Initial Guess	3 or 4		3, 4 or 5	0.1

- Determine $C = \frac{constant}{T_{sh,rating,opening}}$.
- Determine $T_{sh,static}$. If the number of rotations adjusted by the system manufacturer is recorded, it could be very easy to calculate the actual static superheat. If not, it could be guessed initially by the manufacturer settings and refined by experimental data.
- Determine $T_{sh,max,opening}$ using the manufacturers' tradition of reserving capacity to set the upper boundary of $(T_{sh,rating} - T_{sh,static})$.

$$\frac{T_{sh,rating,opening}}{T_{sh,max,opening}} \approx 1 - reserve_capacity$$

A1.2.5.2 Nonlinear Parameter Estimation Without Specification Data

The nonlinear model format is

$$\dot{m} = C(2\frac{T_{sh,opening}}{T_{sh,max,opening}} - (\frac{T_{sh,opening}}{T_{sh,max,opening}})^2)\sqrt{r(P_{up} - P_{down})}$$

Rearranging the above equation,

$$C(2\frac{T_{sh,opening}}{T_{sh,max,opening}} - (\frac{T_{sh,opening}}{T_{sh,max,opening}})^2) = \frac{\dot{m}}{\sqrt{r(P_{up} - P_{down})}}$$

The parameters of the TXV model can be determined by the following procedure,

- According to manufacturers' rating data,

$$C(2\frac{T_{sh,rating,opening}}{T_{sh,max,opening}} - (\frac{T_{sh,rating,opening}}{T_{sh,max,opening}})^2) = constant$$
- According to manufacturers' tradition of reserving capacity,

$$\left(2 \frac{T_{sh,rating,opening}}{T_{sh,max\ opening}} - \left(\frac{T_{sh,rating,opening}}{T_{sh,max\ opening}}\right)^2\right) \approx 1 - reserve_capacity$$

$$\Rightarrow C = \frac{constant}{1 - reserve_capacity},$$

and solving the equation,

$$\frac{T_{sh,rating,opening}}{T_{sh,max\ opening}} = 1 - \sqrt{reserve_capacity}$$

3. Determine $T_{sh,static}$ and $T_{sh,rating,opening}$ as described in the last section,
4. Determine $T_{sh,max,opening}$ and set the upper boundary for $(T_{sh,rating} - T_{sh,static})$.

A1.2.5.3 Validation Using Harms' Data

The 5-ton RTU Data collected by Harms (2002) were used to validate the TXV Model (Number: CBB-I-VE-5-VGA). This TXV is a Sporlan model and normally is used specially for heat pumps because it has a check valve inside.

Global Linear Assumption:

According to the manufacturers' rating data,

$$C(T_{sh,rating} - T_{sh,static}) = constant = 1.125$$

From experimental data set A from Harms (2002) with a nominal charge, it can be guessed that

$$T_{sh,rating} = 8^{\circ}C$$

Assuming $T_{sh,rating,opening} = 4^{\circ}C$, so

$$T_{sh,static} = T_{sh,rating} - T_{sh,rating,opening} = 8 - 4 = 4^{\circ}C$$

So,

$$C = \frac{1.125}{4} = 0.2813$$

Assuming the reserve capacity is 10%, since most of valves belong to type I & II,

$$T_{sh,max,opening} \approx \frac{T_{sh,rating,opening}}{1 - reserve_capacity} = \frac{4}{0.9} \approx 4.5$$

So,

$$\begin{aligned} \dot{m} &= C(T_{sh,operating} - T_{sh,static})\sqrt{r(P_{up} - P_{down})} \\ &= 0.2813(T_{sh,operating} - 4)\sqrt{r(P_{up} - P_{down})} \end{aligned}$$

where, the upper boundary of $(T_{sh,rating} - T_{sh,static})$ is set at $4.5^\circ C$.

Nonlinear Parameter Estimation:

Similarly, according to the manufacturers' rating data,

$$C(2\frac{T_{sh,rating,opening}}{T_{sh,max,opening}} - (\frac{T_{sh,rating,opening}}{T_{sh,max,opening}})^2) = constant = 1.125$$

Assuming reserve capacity of 10%,

$$C = \frac{constant}{1 - reserve_capacity} = \frac{1.125}{0.9} = 1.2656$$

and,

$$\frac{T_{sh,rating,opening}}{T_{sh,max,opening}} = 1 - \sqrt{reserve_capacity} = 1 - \sqrt{0.1} = 0.68$$

Similarly, assume $T_{sh,rating,opening} = 4^\circ C$,

$$T_{sh,max,opening} = \frac{4}{0.68} \approx 6^\circ C$$

So,

$$\begin{aligned} \dot{m} &= C(2\frac{T_{sh,opening}}{T_{sh,max,opening}} - (\frac{T_{sh,opening}}{T_{sh,max,opening}})^2)\sqrt{r(P_{up} - P_{down})} \\ &= 1.2656(2\frac{T_{sh,opening}}{6} - (\frac{T_{sh,opening}}{6})^2)\sqrt{r(P_{up} - P_{down})} \end{aligned}$$

where, the upper boundary of $(T_{sh,rating} - T_{sh,static}) = T_{sh,opening}$ is set at $6^\circ C$.

Harms' Result

Harms plotted all four sets of data (see Figure A1-10) and fit the following model by minimizing the least squares error.

$$\dot{m}_{ref} = c_1 (T_{super} - c_2) \left[r_f (P_5 - P_6) \right]^{0.5}$$

Harms determined $c_1 = 0.51 * \sqrt{10}$, $c_2 = 1$. So,

$$\dot{m} = 0.51 * \sqrt{10} (T_{sh,operating} - 1) \sqrt{r(P_{up} - P_{down})}$$

where the upper boundary of $(T_{sh,operating} - 1)$ was set at $8^\circ C$.

Figure A1-10 and Table A1-2 show the results of the global linear assumption and nonlinear parameter estimation approaches. To test how well the experimental data are fitted to a linear model, the model correlated by Harms was tested using the same data used for training. It is obvious that the nonlinear parameter estimation obtained better results than the global linear assumption which is comparable to the interpolation performance of Harms' model. In addition, from the testing of Harms' model, it can be seen that linearization will inherently result in larger errors under many circumstances.

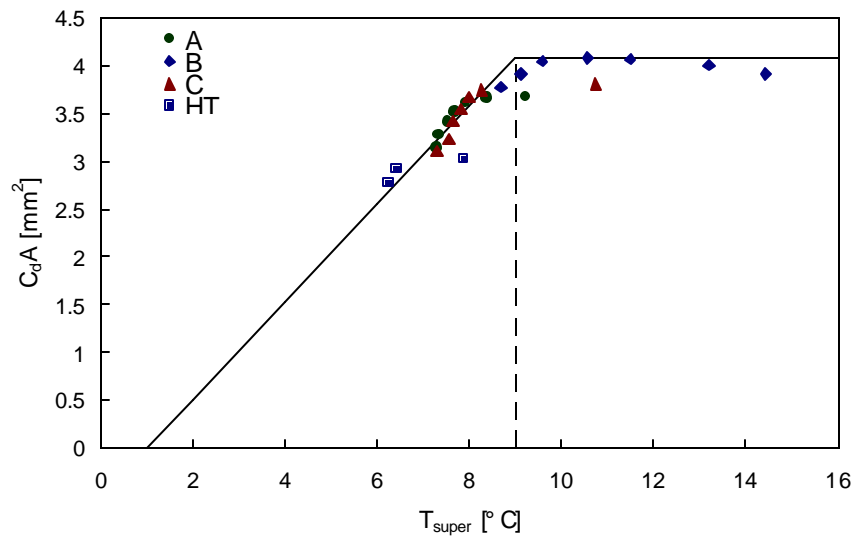


Figure A1-10 The $C_d A$ value of the 5-ton Trane RTU TXV as a function of superheat

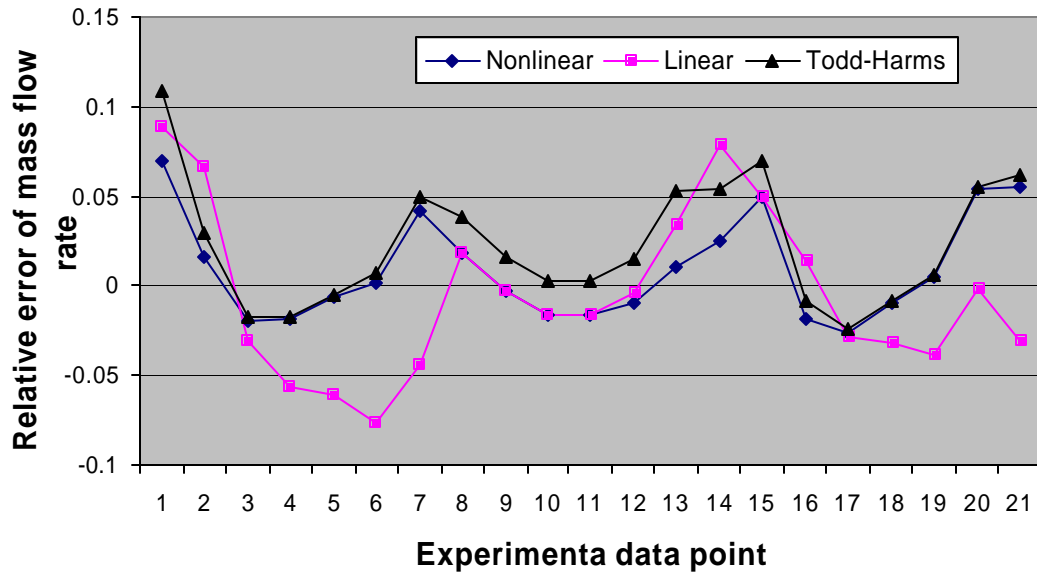


Figure A1-11 Comparison of TXV modeling error

Table A1-2 Comparison of TXV modeling error

	Nonlinear Estimation	Global Linear Estimation	Harms Results
Mean	0.0096	0.0043	0.0235
Std.	0.0291	0.0460	0.0352
Spread	0.0967	0.1647	0.1329

Although Harms' gray-box method may be good for interpolation, it can not be expected to extrapolate well. Mathematically, his method is equivalent to making a local linear assumption (see Figure A1-12). If the experimental data range is limited, parameters C_1 and C_2 will be unreasonable. For example, in his method parameter C_2 of the 5-ton RTU, which is supposed to be the static superheat setting, is equal to 1°C , while the upper boundary of opening superheat is set at 8°C . According to ARI and ASHRAE standards, static superheat should be far larger than 1°C , and 8°C of upper boundary for opening superheat (indicating a 50% of reserve capacity) is too large. For a 7.5 ton RTU considered by Harms, parameter C_2 was correlated to be a negative value, -4.4°C , which is impossible physically.

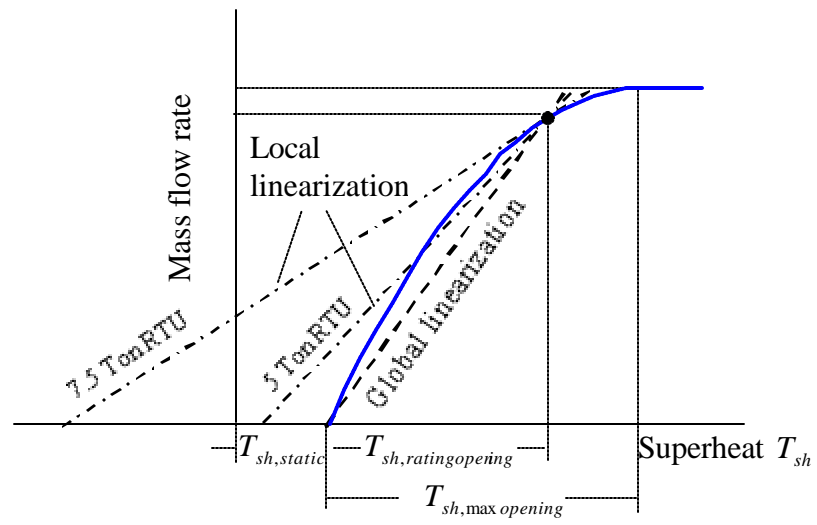


Figure A1-12 Illustration of the three parameter estimation methods

APPENDIX 2 RTD TEMPERATURE SENSOR MEASURING ISSUE

The experiment data collected by Breuker (1997), Chen (2000) and Harms (2002) were measured using thermocouples, so the compressor energy analysis is balanced very well. However, the field data energy analysis shows that there are over 50% heat losses from the compressor, which is impossible from the heat transfer point of view. It was found that the misleading result is caused by inaccurate discharge-line temperature readings measured using RTDs. Figure A2-1 illustrates the RTD measuring scheme.

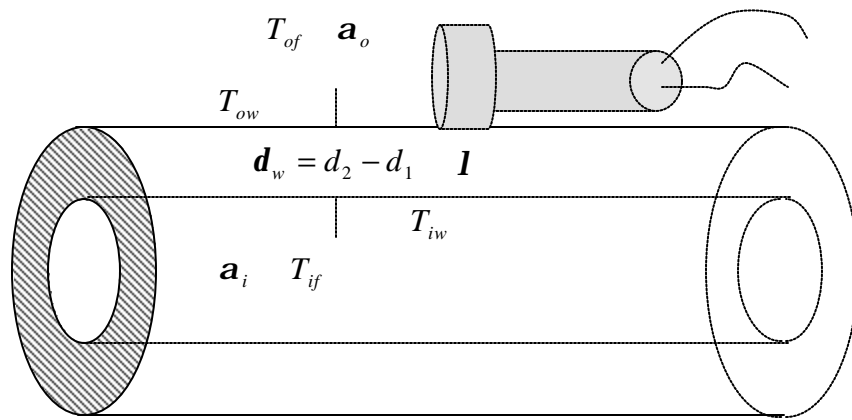


Figure A2-1 RTD measuring scheme

It is described in the literature that: “If the sensor is not insulated, the sensor’s reading would be a weighted average of the tube wall and ambient air temperature”. In addition, the temperature of the sensor is not geometrically distributed uniformly even if the sensor is insulated properly, which is difficult to evaluate. Ideally, assume the

temperature on the RTD is uniform and identical with the tube wall temperature, which is equivalent to thermocouple (see Figure A2-2).

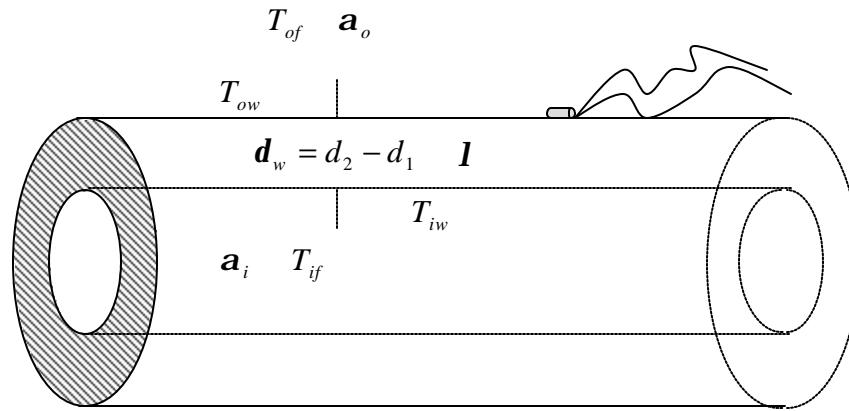


Figure A2-2 Thermocouple measuring scheme

Figure A2-3 sketches the equivalent thermal circuit of the thermocouple measuring scheme and thermal resistance values are listed in Table A2-1. It can be seen that the thermal resistance between refrigerant inside the tube and the thermocouple only accounts for 1.6% of the total thermal resistance, which means that the measuring error would be 1.6 F if there was a 100 F temperature difference between the refrigerant inside the tube and ambient air temperature. So it can be concluded that the thermocouple can measure the refrigerant temperature at reasonably good accuracy.

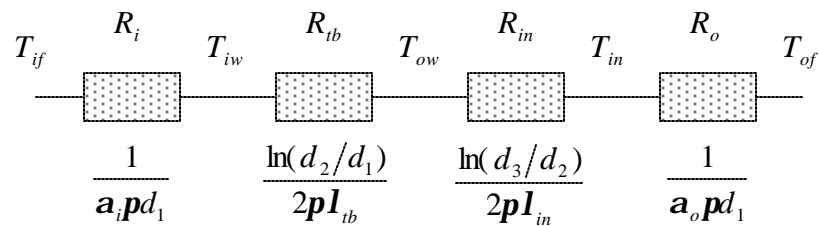


Figure A2-3 Equivalent thermal circuit

Table A2-1 Thermal resistance distribution of thermocouple measuring scheme

Thermal Resistance	R_i	R_{ib}	R_{in}	R_o
Value	0.0278	0.0000765	1.052	0.682
Portion	1.6%	0.004%	59.7%	38.7%
Portion	1.6%		98.4%	

However, there are two additional factors which would impact the measuring accuracy of an RTD. One is the thermal contact resistance between the tube wall and the RTD, and the other is the temperature distribution of RTD. The former is straightforward and impacted only by sensor installation method. If thermal grease is applied and the tube's surface is polished, it would be reduced significantly. However, the latter is difficult to evaluate and is impacted by insulation and the installation method, but its impact on measurement accuracy can be equivalent to that of thermal resistance. So an equivalent thermal contact resistance, $R_{contact}$, which takes both thermal contact resistance and the resistant effect caused by none-uniform temperature distribution. Since it is difficult to evaluate $R_{contact}$ explicitly, experiments are needed in order to determine all the values in Table A2-2.

Table A2-2 Thermal resistance distribution of RTD measuring scheme

Thermal Resistance	R_i	R_{ib}	$R_{contact}$	R_{in}	R_o
Value	0.0278	0.0000765	?	1.052	0.682
Portion	?			?	

Experiments conducted at FDSI using cold water instead of refrigerant showed that the measurement error is around 5% of the total temperature difference between water inside the tube and ambient air if the RTD was insulated and thermal grease was applied. Since liquid water has a larger heat transfer coefficient than refrigerant vapor at the same mass flow rate, the inside thermal resistance value should be modified in order to estimate the equivalent thermal contact resistance, $R_{contact}$. Table A2-3 lists all the value for the cold water application. Using the thermal contact resistance value calculated

in cold water application, it is easy to determine all the values in Table A3-4 for the refrigerant vapor application.

Table A2-3 Thermal resistance distribution of RTD for measuring cold water

Thermal Resistance	R_i	R_{ib}	$R_{contact}$	R_{in}	R_o
Value	0.0278/5=0.00556	0.0000765	0.4087	1.052	6.82
Portion	5%			95%	

Table A2-4 Thermal resistance distribution of RTD for measuring refrigerant vapor

Thermal Resistance	R_i	R_{ib}	$R_{contact}$	R_{in}	R_o
Value	0.0278	0.0000765	0.4087	1.052	0.682
Portion	20%			80%	

From Table A2-4, it can be seen that the subtotal thermal resistance between the refrigerant inside the tube and the RTD is up to 20% of the total, which means that there would be up to 20 F measurement error even under good contact and insulation if there was a 100 F temperature difference between the refrigerant and ambient air.

Besides the thermal resistance, the temperature difference between the refrigerant inside the tube and ambient air is the other important factor (see Equation (A2-1)).

$$\text{Error} = \mathbf{a}(T_{ref} - T_{amb}) \quad (\text{A2-1})$$

\mathbf{a} is the thermal resistance portion (say 20%).

Since the maximum temperature difference occurs between the discharge line refrigerant and ambient air, over 100 F. So either thermocouple or modification is needed (see Equation (A2-2)).

$$T_{ref,mod} = \frac{T_{ref} - \mathbf{a}T_{amb}}{1 - \mathbf{a}} \quad (\text{A2-2})$$

So the key is to determine the thermal resistance portion \mathbf{a} . According to our experience, if the RTD sensor was insulated very well and tube wall was polished before thermal grease was applied, it can be reduced to 5%. However, if the sensor is not properly installed, its value can be very large.

AUTOMATED FAULT DETECTION AND DIAGNOSTICS OF
ROOFTOP AIR CONDITIONERS FOR CALIFORNIA

Deliverables 2.1.6a & 2.1.6b

Final report and economic assessment
submitted to:
Architectural Energy Corporation

For the Building Energy Efficiency Program
Sponsored by:
California Energy Commission

Submitted By:
Purdue University

Principal Investigator: James Braun, Ph.D., P.E.
Research Assistant: Haorong Li

August 2003

Mechanical Engineering
1077 Ray W. Herrick Laboratories
West Lafayette, IN 47907-1077
(765) 496-6008
(765) 494-0787 (fax)

**RAY W. HERRICK
LABORATORIES
PURDUE ENGINEERING**



ACKNOWLEDGEMENTS

The research that resulted in this document was part of the “Energy Efficient and Affordable Small Commercial and Residential Buildings Research Program”, which was a Public Interest Energy Research Program (PIER) sponsored by the California Energy Commission (CEC). We are extremely grateful for the funding from the CEC through PIER. Several organizations and people were involved in the project described in this final report and deserve our many thanks. Chris Scruton of the CEC was very enthusiastic throughout this project and provided valuable insight and encouragement. Vern Smith and Erin Coats of Architectural Energy Corporation (AEC) provided excellent overall project management for the numerous projects within this large program. Todd Rossi and Doug Dietrich of Field Diagnostic Services, Inc. (FDSI) and Lanny Ross of Newport Design Consultants (NDS) were essential in setting up and maintaining the field sites. Martin Nankin of FDSI provided monitoring equipment at cost for this project. Bob Sundberg of Honeywell, Inc. arranged the donation of Honeywell equipment and was an enthusiastic supporter of the research. Adrienne Thomle and Bill Bray at Honeywell, Inc. made sure that equipment was delivered to the field sites and provided replacement equipment and troubleshooting when necessary. We also had excellent support from the organizations that own and/or operate buildings at the field sites. Individual contributors include Jim Landberg for the Woodland schools, Tadashi Nakadegawa for the Oakland schools, Tony Spata and Mike Godlove for McDonalds, and Mike Sheldon, Paul Hamann, Gordon Pellegrinetti, and Tim Schmid for Walgreens.

TABLE OF CONTENTS

ACKNOWLEDGEMENTS.....	1
TABLE OF CONTENTS.....	2
LIST OF FIGURES	5
LIST OF TABLES.....	7
NOMENCLATURE	8
EXECUTIVE SUMMARY	11
1 INTRODUCTION	20
1.1 Background on FDD.....	20
1.2 Literature Review	22
1.2.1 Overview.....	22
1.2.2 Latest Progress.....	24
1.2.2.1 Packaged Air Conditioning Systems	24
1.2.2.2 Other HVAC&R Systems	27
1.2.3 Summary of Literature Review.....	30
1.3 Research Objectives and Approach	31
1.3.1 Motivation and Objectives.....	31
1.3.2 Methodology	33
2 DATA SOURCES USED FOR EVALUATION AND DEMONSTRATION	35
2.1 Overview.....	35
2.2 Previous Data Sources	35
2.2.1 Mark Breuker's Data	35
2.2.1.1 Normal Operation Data.....	36
2.2.1.2 Faulty Operation Data.....	36
2.2.2 Chen's Data.....	37

2.2.3 Todd Harms' Data	37
2.3 Field Test Facilities.....	38
3 IMPROVED SRB FDD METHOD.....	40
3.1 Limitations of the Original SRB FDD Method	41
3.2 Improved SRB Approach.....	42
3.2.1. Steady-State Detector	43
3.2.2 Steady-State Models	43
3.2.3 Normalized Distance Fault detection Classifier	44
3.2.4 Fault Diagnosis	45
3.2.4.1 Fault Diagnosis Rules	45
3.2.4.2 Simple Distance Fault Diagnosis Classifier.....	46
3.3 Results.....	48
4 A DECOUPLING-BASED FDD TECHNIQUE.....	49
4.1 Approach.....	49
4.2 Results.....	54
4.2.1 Case Study of Decoupling Rooftop Unit Faults	54
4.2.1.1 Compressor Valve Leakage	54
4.2.1.2 Condenser Fouling Decoupling	55
4.2.1.3 Evaporator Fouling Decoupling.....	57
4.2.1.4 Liquid-Line Restriction Decoupling	60
4.2.1.5 Refrigerant Leakage Decoupling	62
4.2.2 Purdue Field Emulation Site's Demonstration	63
4.2.2.1 Field Fault Simulation Window (FFSW).....	64
4.2.2.2 Fault Detection and Diagnosis Window (FDDW).....	66
4.2.2.3 System Performance & Safety Degradation Window (SPSDW)	66
4.2.2.4 FDD Report Window (FDDRW).....	67
4.2.2.5 Output of the FDD Demonstration	68
4.2.3 Results for California Field Sites.....	76
4.2.3.1 Milpitas McDonalds Field Site	76
4.2.3.2 Summarized Results for Other Sites	83

5 ECONOMIC ASSESSMENTS	85
5.1 Preventive Maintenance Inspection Savings (PMIS)	86
5.2 Operating Cost Savings (OCS)	87
5.2.1 Utility Cost Savings (UCS).....	88
5.2.2 Equipment Life Savings (ELS).....	92
5.3 Fault Detection and Diagnosis Savings (FDDS)	93
5.3.1 Unnecessary Service (USS)	93
5.3.2 Fault Diagnosis Savings (FDS).....	94
5.4 Smart Service Schedule Savings (SSSS)	95
5.5 Total Equipment Life Savings (TELS)	95
6 SUMMARY AND RECOMMENDATIONS FOR FUTURE WORK.....	100
REFERENCES	103

LIST OF FIGURES

Figure E-1. FDD demonstration output	13
Figure E-2 Histogram of the normalized fault indicator for low refrigerant charge	14
Figure E-3 Histogram of the cooling capacity degradation	14
Figure E-4 Histogram of the EER degradation	15
Figure 1-1 Paper statistics in HVAC FDD with time	23
Figure 1-2 Paper statistics in HVAC FDD with system	23
Figure 1-3 Supervision approach of HVAC&R equipment	25
Figure 3-1 Interactions of Rooftop Unit System	40
Figure 3-2 Structure of the SRB FDD method	42
Figure 3-3 Fault detection classifier scheme for a 2-dimensional case	45
Figure 3-4 Fault detection and diagnosis boundaries	46
Figure 3-5 Distance method for fault diagnosis	47
Figure 4-1 Taxonomy of Rooftop Faults	51
Figure 4-2 Decoupling Scheme of Rooftop System Faults	52
Figure 4-3 Decoupling compressor valve leakage fault using estimated compressor power measurement and estimated refrigerant mass flow rate	55
Figure 4-4 Decoupling condenser fouling fault using measured refrigerant mass flow rate	56
Figure 4-5 Decoupling condenser fouling fault using estimated refrigerant mass flow rate	57
Figure 4-6 Decoupling evaporator fouling fault using measured evaporator air mass flow rate	58
Figure 4-7 Decoupling evaporator fouling using measured refrigerant mass flow rate ...	59
Figure 4-8 Decoupling evaporator fouling using estimated refrigerant mass flow rate ...	59
Figure 4-9 Decoupling liquid-line restriction using measured pressure drop	60
Figure 4-10 Decoupling liquid-line restriction using estimated pressure P_{up} and measured P_3	61
Figure 4-11 Decoupling liquid-line restriction using estimated pressure drop	61
Figure 4-12 Decoupling refrigerant leakage faults using ΔT_{sh-sc}	62
Figure 4-13 Illustration of Demo Movie	63
Figure 4-14 Timeline of the fault simulation in minutes.	64
Figure 4-15 Outputs of the FDD demonstration after introduction of low refrigerant charge fault	68
Figure 4-16 Outputs of the FDD demonstration after introduction of condenser fouling fault	69

Figure 4-17 Outputs of the FDD demonstration after introduction of liquid line restriction fault	70
Figure 4-18 Outputs of the FDD demonstration after introduction of compressor leakage fault	71
Figure 4-19 Outputs of the FDD demonstration after removal of condenser fouling fault	72
Figure 4-20 Outputs of the FDD demonstration after removal of liquid line restriction fault	73
Figure 4-21 Outputs of the FDD demonstration after removal of compressor leakage fault	74
Figure 4-22 Outputs of the FDD demonstration after removal of low refrigerant low charge fault.....	75
Figure 4-23 Histogram bar plot of the normalized fault indicator for liquid line restriction	77
Figure 4-24 Histogram bar plot of the normalized fault indicator for refrigerant low charge.....	77
Figure 4-25 Histogram bar plot of the normalized fault indicator for condenser fouling	78
Figure 4-26 Histogram bar plot of the normalized fault indicator for compressor valve leakage	79
Figure 4-27 Histogram bar plot of the normalized fault indicator for cooling capacity degradation.....	80
Figure 4-28 Histogram bar plot of the return air temperature	80
Figure 4-29 Histogram bar plot of the continuous running time between off-cycles of the RTU.....	81
Figure 4-30 Histogram bar plot of the normalized fault indicator for EER degradation..	82
Figure 4-31 System power consumption reduction	82
Figure 5-1 Interrelationship among different factors affecting RTU performance	88

LIST OF TABLES

Table E-1 FDD results for modular school site	15
Table E-2 FDD results of McDonalds Restaurant Sites	16
Table E-3 FDD results of Walgreen Retail Store Sites at Rialto	16
Table E-4 FDD results of Walgreen Retail Store Sites at Anaheim	16
Table E-5 Conservative Lifetime Total Savings per RTU for Automated FDD	19
Table 2-1 Repeatability analysis during steady-state model testing	36
Table 2-2 Fault levels introduced to different faults	37
Table 2-3 Environmental conditions	38
Table 2-4 Field site information	39
Table 3-1 Fault diagnosis rules	46
Table 3-2 Performance comparison of previous and improved FDD method	48
Table 4-1 FDD results of Modular School sites	83
Table 4-2 FDD results of McDonalds Restaurant Sites	84
Table 4-3 FDD results of Walgreen Retail Store Sites at Rialto	84
Table 4-4 FDD results of Walgreen Retail Store Sites at Anaheim	84
Table 5-1 Planned Preventive Maintenance Costs	87
Table 5-2 Estimates of Utility Costs Savings for a 6-ton RTU A/C	91
Table 5-3 Equipment life savings	93
Table 5-4 Potential for Refrigerant Charge Fault Savings	94
Table 5-5 Potential Savings for Multiple-Service	95
Table 5-6 Equipment Lifetime Operational Savings	98
Table 5-7 Conservative Lifetime Total Savings per RTU (6-ton)	99

NOMENCLATURE

ANN	= Artificial neural network
AHU	= Air handling unit
α	= False alarm threshold
α	= EER degradation factor
β	= Fault diagnosis threshold
β	= Cooling capacity degradation factor
BP	= Back-propagation
c	= Distance from fault point to axes
C_e	= Cost of electricity
$\chi^2(n)$	= Chi-square distribution
d_i^2	= Normalized distance square
d_{\max}	= Maximum normalized distance
ΔT_{ca}	= Condenser air temperature difference
ΔT_{ea}	= Evaporator air temperature difference
ΔT_{sh-sc}	= Difference between suction line superheat and liquid line subcooling
E	= Energy consumption
EER	= Equipment efficiency ratio
EER_{Normal}	= Equipment efficiency ratio at normal operation
ELS	= Equipment life savings
η_v	= Compressor volumetric efficiency
$E_{savings}$	= Energy savings
FDD	= Fault detection and diagnosis
FDDRW	= FDD report window
FDDS	= Fault detection and diagnosis savings
FDDW	= Fault detection and diagnosis window
FDS	= Fault diagnosis savings
FFSW	= Field fault simulation window
F_i	= Fault points
f_i	= Frequency
GRNN	= General regression neural network
HVAC	= Heating, Ventilating, and Air-Conditioning

IA	= Independence Assumption
λ_i	= Eigenvalue of Σ
Λ	= Eigenvalue matrix
M	= Mean vector of residuals
ma	= Mixed air
M_{normal}	= Mean vector for normal operation
$M_{current}$	= Mean vector for current operation
MCS	= Monte-Carlo Simulation
\dot{m}_r	= Refrigerant mass flow rate
μ	= Mean
μ_{normal}	= Mean value for normal operation
M_X	= Mean vector for sample X
M_Y	= Mean vector for sample Y
N	= Number of generated sample points
N_X	= Normal distribution for sample X
OCS	= Operation costs savings
Ω_X	= Area for probability evaluation
P_{dis}	= Discharge pressure
Φ	= Eigenvector matrix
P_i	= Data points
P_Ω	= Probability within area Ω_X
ϕ_{ra}	= Relative humidity of return air
P_{dis}	= Discharge pressure
PMIS	= Preventive maintenance service savings
P_{suc}	= Suction pressure
\dot{Q}_{cap}	= Cooling capacity
$\overline{\dot{Q}_{cap}}$	= Average cooling capacity
$\overline{\dot{Q}_{cap,Normal}}$	= Average cooling capacity at normal operation
Q_{Load}	= Building cooling load
ra	= Return air
$ratio_{dist}$	= Distance ratio
RBF	= Radial basis function
RMS	= Root mean square
SPSDW	= System performance & safety degradation window
SRB	= Statistical rule-based
SSR	= System state residual
SSSS	= Smart service schedule savings
RTU	= Rooftop unit

σ	= Standard deviation
σ_{normal}	= σ for normal operation
Σ	= Covariance matrix
$\Sigma_{assumption}$	= Σ with independence assumption
$\Sigma_{current}$	= Σ for current operation
Σ_{normal}	= Σ for normal operation
Σ_{true}	= True covariance matrix
Σ_X	= Covariance matrix for X
T	= Runtime
T_{amb}	= Ambient temperature
T_{cond}	= Condensing temperature
T_{dis}	= Discharge line temperature
TELS	= Total equipment life savings
T_{evap}	= Evaporating temperature
T_{ll}	= Liquid line temperature
T_{ma}	= Mixed air temperature
T_{oa}	= Outdoor air temperature
T_{ra}	= Return air temperature
T_{sc}	= Sub-cooling
T_{sh}	= Superheat
T_{wb}	= Wet bulb temperature
UCS	= Utility cost savings
USS	= Unnecessary service savings
VAV	= Variable air volume
v_1	= Specific volume of compressor inlet refrigerant
X_i	= Sample point in original space
Y_i	= Sample point in transformed space
\dot{W}	= Power consumption
$\overline{\dot{W}}$	= Average power consumption
W_{ma}	= Mixed air humidity ratio
W_{oa}	= Outdoor air humidity ratio
W_{ra}	= Return air humidity ratio

EXECUTIVE SUMMARY

Packaged air conditioning equipment is used extensively throughout small commercial and institutional buildings. However, compared to larger systems, they tend to be not well maintained. Widespread application of automated fault detection and diagnosis (FDD) to packaged equipment will significantly reduce energy use and peak electrical demand, down time and maintenance costs. However, techniques for online FDD reported in the literature are expensive to apply because of requirements for model training and large computation, have only been tested in the laboratory, and can not handle multiple-simultaneous faults. Furthermore, no one has performed economic assessments of FDD. Economic assessment is a complicated problem that requires field evaluations. The primary goals of the research described in this report were to 1) develop a practical automated FDD technique having low cost, robust performance, and the capability to handle multiple-simultaneous faults and 2) to perform an initial economic assessment of FDD applied to vapor compression equipment in California.

The process of developing and evaluating the performance of FDD methods involved the use of both laboratory and field data. Laboratory data from previous studies were used to provide rigorous performance evaluations. In addition, a number of field sites were established in small commercial buildings in California to allow consideration of practical issues. An additional field site was set up at Purdue to allow artificial implementation of faults in order to provide more controlled evaluation of the FDD techniques under realistic operating conditions.

Two different FDD approaches were developed in this research. First of all, the statistical rule-based (SRB) FDD method presented by Rossi and Braun (1997) was modified to improve sensitivity and robustness and reduce computational requirements. The following components of the FDD method were improved: 1) models for predicting

normal state variables, 2) steady-state detector, 3) fault detection classifier, and 4) fault diagnosis classifier. The resulting method is simpler to implement and was shown to have significantly better sensitivity for detecting and diagnosing faults than the original method. However, it was not possible to modify the method to handle multiple-simultaneous faults. Furthermore, the application of this method to the field sites proved to be difficult because of the requirement for training models using field data. The method is better suited to implementation in original equipment than for retrofit to field applications.

A second FDD method was developed to handle multiple-simultaneous faults and to eliminate the need for model training using field data. The ability to handle multiple faults was addressed by identifying features that decouple the impacts of individual faults. The need for on-line models was eliminated by employing manufacturers' rating data such as compressor and TXV maps. These data are readily available at no cost and are generic and reasonably accurate. The performance of the decoupling-based FDD method was initially tested using laboratory data. A prototype software implementation was developed and a demonstration was created for illustration purposes using the Purdue field site with faults artificially introduced. Finally, the FDD methodology was applied to California field sites to understand the condition of the equipment and highlight the potential for FDD.

Figure E-1 shows output from the FDD demonstration at a point where four faults had been introduced. The bar chart in the upper-left quadrant shows individual fault indicators relative to a threshold for detection and diagnosis. Each of the fault indicators have been normalized so that full scale (i.e., 1.0) corresponds to an individual fault causing a 20% degradation in cooling capacity. The graph in the lower-left quadrant shows impacts of the faults on performance and safety factors as a function of time during the demonstration. The factors include cooling capacity, COP, and overheating of the compressor. The capacity and COP are reductions relative to values for equipment operating normally. The compressor overheating is the difference between the current and normal compressor discharge temperature normalized by a value considered to be harmful to the compressor life. The table in the lower right quadrant summarizes the

current values of the fault indicators and performance and safety factors. Also shown are current recommendations provided by the FDD method. The demonstration has been very useful in testing the FDD method for single and multiple faults and for illustrating the potential for application of FDD.

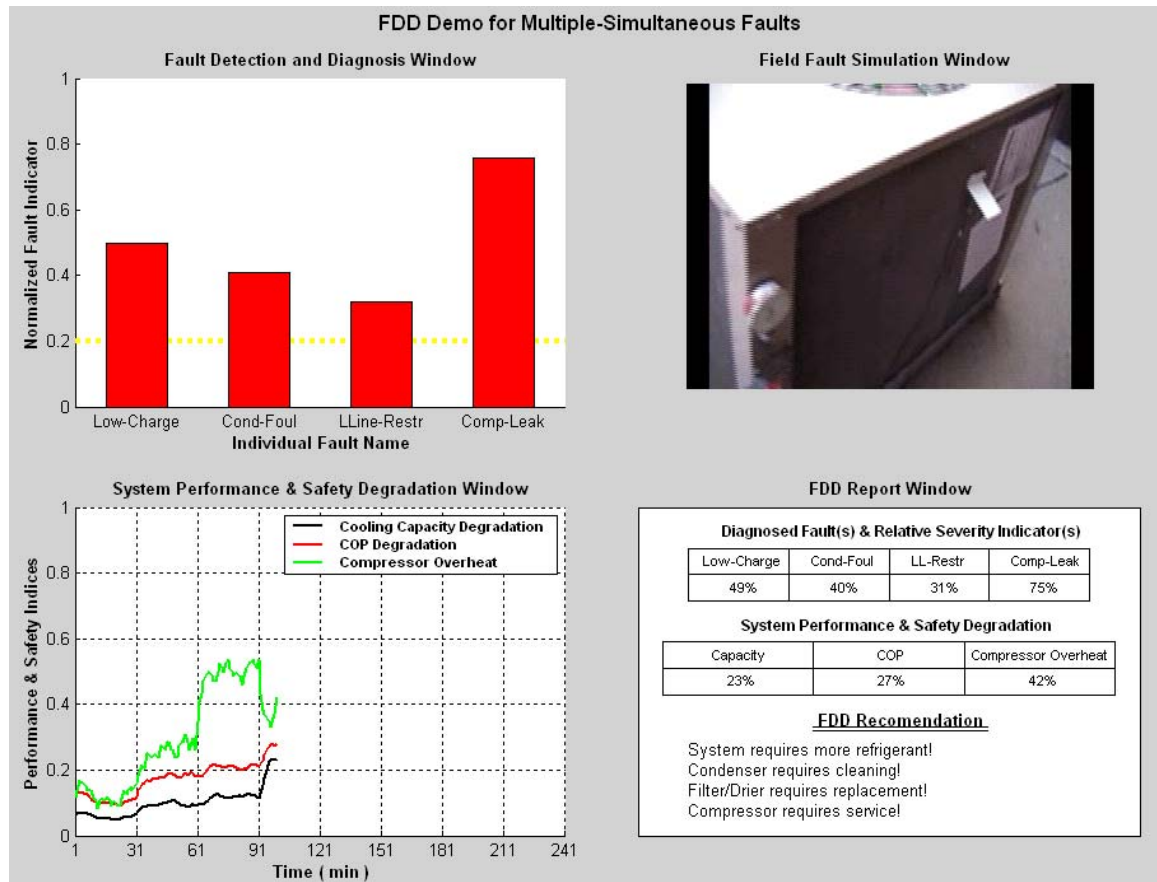


Figure E-1. FDD demonstration output

The decoupling-based method was then applied to field data. Figure E-2 shows example results for a rooftop unit at the Milpitas McDonalds field site determined over an entire cooling season. This plot is a histogram of the normalized fault indicator for a low refrigerant charge. All the steady-state data points are located at the right of the FDD threshold and the mean value is about 1.6, which means that the system charge is very low. In addition to low refrigerant charge, the FDD method identified a clogged filter-drier and a fouled condenser coil for this site.

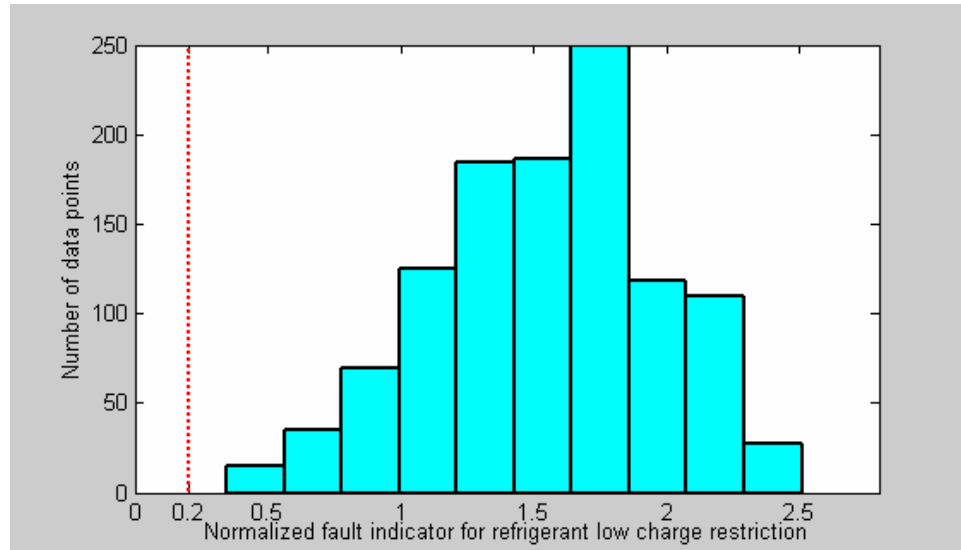


Figure E-2 Histogram of the normalized fault indicator for low refrigerant charge

Figures E-3 and E-4 show the degradation in cooling capacity and EER for the Milpitas site. The system cooling capacity was degraded between 23 and 45%, with an average degradation of 32%. The cooling capacity degradation was confirmed by analyzing zone temperature and system runtime data. The rooftop unit at this site was not maintaining comfort conditions at all times. The system EER degraded between about 10 and 40%, with an average of 21%.

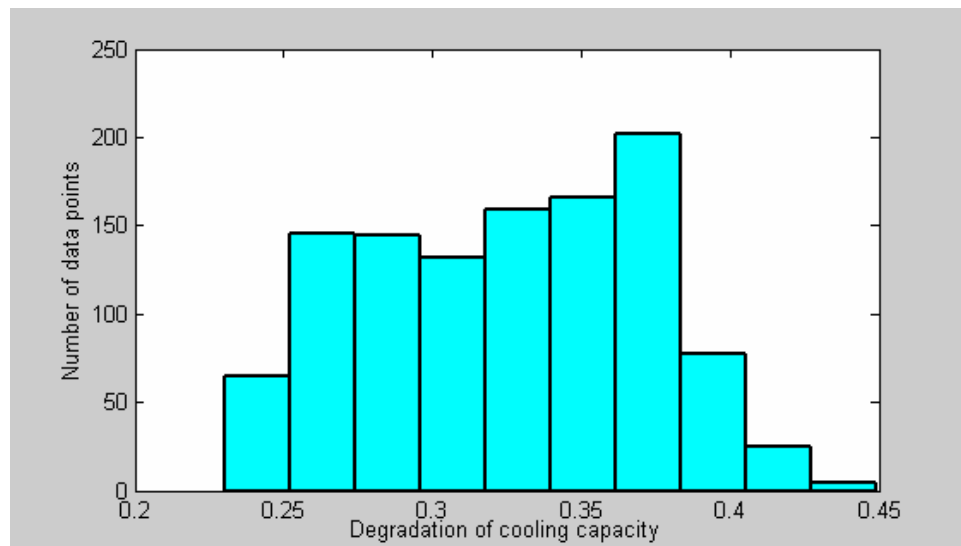


Figure E-3 Histogram of the cooling capacity degradation

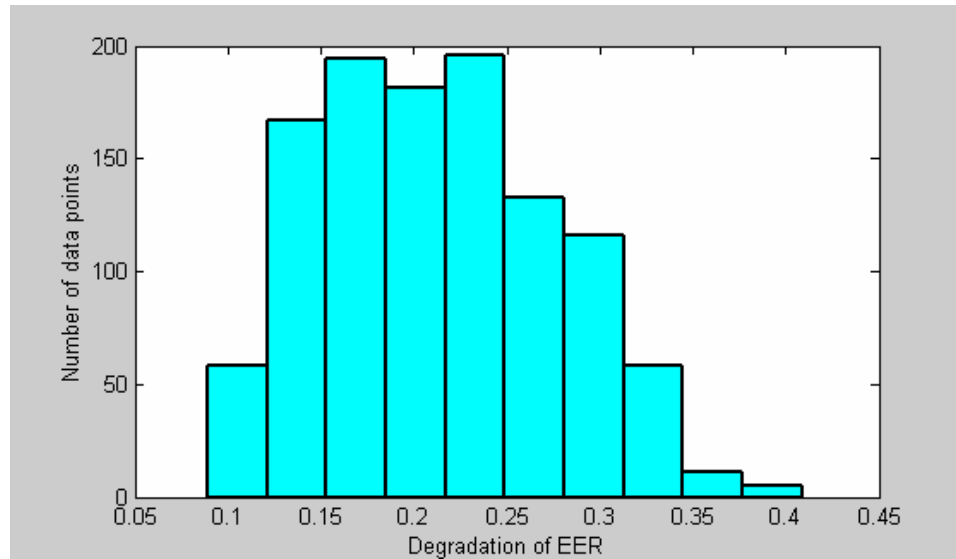


Figure E-4 Histogram of the EER degradation

Tables E-1, E-2, E-3, and E-4 summarize FDD results for the other field sites. Eleven of the twenty-one investigated RTUs have liquid-line restriction faults, ten of them have refrigerant charge faults, and eight of them have more than two simultaneous faults. Service would be justified for nine of the twenty-one investigated RTUs.

Table E-1 FDD results for modular school site

Faults	Woodland		Oakland	
	RTU1	RTU2	RTU1	RTU2
Refrigerant Charge	Normal	Normal	Normal	Over Charge
Liquid-line Restriction	Restriction	Severe Restriction	Restriction	Normal
Evaporator Fouling	Normal	Normal	Normal	Fouling
Recommended Service	Not yet	Arrange Service	Not yet	Arrange Service

Table E-2 FDD results of McDonalds Restaurant Sites

Faults	Bradshaw	Castro Valley		Watt Avenue	
		Stage 1	Stage 2	Stage 1	Stage 2
Refrigerant Charge	Low Charge	Normal	Normal	Low Charge	Normal
Liquid-line Restriction	Restriction	Normal	Normal	Normal	Normal
Recommended Service	Arrange Service	NA	NA	Not yet	NA

Table E-3 FDD results of Walgreen Retail Store Sites at Rialto

	RTU1	RTU2	RTU3	RTU4	RTU5
Refrigerant Charge	Extremely Low Charge	Low Charge	Normal	Normal	Over Charge
Liquid-line Restriction	Normal	Small Restriction	Normal	Normal	Normal
Recommended Service	Require Service	Arrange Service	NA	NA	Not yet

Table E-4 FDD results of Walgreen Retail Store Sites at Anaheim

	RTU1	RTU2	RTU3	RTU4	RTU5
Refrigerant Charge	Low Charge	Low Charge	Normal	Low Charge	Normal
Liquid-line Restriction	Small Restriction	Severe Restriction	Small Restriction	Small Restriction	Small Restriction
Recommended Service	Arrange Service	Require Service	Not yet	Arrange Service	Not yet

Some initial estimates of the economics of FDD were made based upon the field results. Opportunities for cost savings with automated FDD that were included in this analysis are:

1. Savings associated with eliminating planned preventive maintenance services. Instead, the FDD system would schedule service when it is most economical.

2. Operational cost savings, which include two parts: utility cost and equipment life savings. The utility cost savings should include both energy and peak demand savings associated with equipment operating more efficiently due to better maintenance. Equipment life savings are due to two effects resulting from better maintenance: less adverse operating conditions for the compressor and decreased runtime due to cooling capacity that is closer to rated performance.
3. Fault detection and diagnosis savings, which includes two parts: unnecessary service and fault diagnosis savings. Unnecessary service includes regular service, such as coil cleaning, that is not justified and unnecessary repairs that are based upon incorrect fault diagnoses. Fault diagnosis savings are due to reduced technician time associated with diagnosing a problem.
4. Smart service schedule savings. The primary savings are associated with reducing the total service calls by only performing service when it is economically justified and by scheduling multiple service tasks during each service visit.

In order to quantify the net savings, the following conservative assumptions were made:

1. A 10-year equipment life under normal operating conditions with no replacement of major components, such as the compressor and fan motors during the life of the equipment. Actual equipment life might be longer, but with major service required including compressor and fan motor replacements. These major service requirements are not considered in this analysis.
2. No effect of adverse operating conditions on equipment life. This is a conservative assumption, since improved maintenance due to FDD will reduce adverse operating conditions for the compressor (i.e., liquid slugging and overheating). The only equipment life impact considered was reduced runtime due to improved cooling capacity.

3. Elimination of preventative maintenance for a savings of \$2000 per RTU over the life of the unit.
4. On average, the performance of the system was degraded for 40% of its lifetime with an *EER* and cooling capacity degradation of 21% and 30%, respectively. This assumption is based upon limited field results and should be confirmed through additional analysis.
5. No demand savings. This is a very conservative assumption and should be considered in more detail in future studies.
6. One coil cleaning service can be saved per year through automated FDD.
7. A 60% probability that a refrigerant charge fault will occur once during the equipment lifetime.
8. A 60% probability that a filter/drier restriction fault will occur once during the equipment lifetime.
9. A 6-ton RTU having an initial cost of \$4500.
10. A cost for the FDD system of \$300.

Table E-5 gives estimates of total lifetime net savings (total savings minus FDD system cost) for an individual RTU operating in different buildings and locations. The estimated savings over the life of the unit range from \$4000 to \$10,000 per RTU. The annual net savings range from \$400 to \$1,000 and the estimated payback period is less than one year. Greater savings are possible in hotter climates due to larger cooling requirements. The savings would be greater for heat pumps because they operate throughout the whole year.

Table E-5 Conservative Lifetime Total Savings per RTU for Automated FDD

Location	Building Type	Net Savings (\$)
North California	Modular School	4,328
	Restaurant	4,800
	Retail Store	5,804
South California	Modular School	5,496
	Restaurant	6,772
	Retail Store	9,756

Research on further improvements and evaluations of the FDD methodology will continue as follows:

1. Obtain more detailed information on the rooftop units for all the California field sites and apply the proposed FDD technique more completely to these sites.
2. Further improve the performance of the unified FDD technique by improving the modeling approach that is based on manufacturers' data and find an efficient and practical way to tune these models using low-cost sensors. Improve other virtual sensors' performance and consider trying to remove pressure and humidity sensors.
3. Improve the overall performance model for assessing performance degradations of packaged air conditioning equipment under faulty operation using limited sensor and manufacturers' rating data.
4. Expand the service cost database and build a more detailed economic assessment model to more accurately evaluate the potential savings associated with the FDD technique and to provide guidelines for the fault evaluation and decision step.
5. Conduct more field tests under multiple-simultaneous faults and, if necessary, conduct more laboratory tests to test the proposed decoupling-based FDD technique.
6. Consider additional control related diagnoses, such as economizer and controller diagnoses.

1 INTRODUCTION

1.1 Background on FDD

FDD is an acronym for fault detection and diagnosis. Fault detection involves identifying whether the supervised system deviates from normal operation and fault diagnosis is diagnosing or isolating the detected fault(s) from other possible faults. Some literature uses the acronym FDI to refer to fault detection and isolation.

FDD has been successfully applied to critical systems such as space exploration and nuclear power plants, in which early identification of small malfunctions would prevent loss of life and damage of equipment. In these applications, FDD sensitivity is a vital feature. However, false alarm rate is also an important index because of economic concerns. A high false alarm rate could result in unnecessary economic loss due to stoppage of equipment operation. In order to increase FDD sensitivity and decrease false alarm rate, FDD techniques generally use multiple hardware such as sensors and computation sources for the same purpose. The high cost of hardware redundancy has limited the application of FDD to non-critical systems such as HVAC&R systems. However, with the growing realization of the benefits brought by FDD and the decreasing cost of hardware especially for computation, more and more applications of FDD have been attempted for non-critical equipment such as HVAC&R systems.

HVAC systems often do not function as well as expected due to faults introduced during initial installation or developed in routine operation. Rooftop and other packaged air conditioners are used extensively throughout small commercial and institutional buildings, but compared to larger systems, they tend to be not well maintained. As a result, widespread application of automated FDD will significantly reduce energy use and peak electrical demand, down time and maintenance costs. Unlike critical systems, FDD for HVAC systems, especially for small packaged air conditioners, is subject to economic

constraints. Economic constraints bring special difficulties and issues, which do not need to be considered in critical systems.

First, since a packaged air conditioner is relatively inexpensive, the cost to realize FDD for HVAC systems in terms of software and hardware should be low. Therefore some relatively expensive measurements such as flow rate cannot be used, and use of pressure and humidity sensors is limited. This is a particular problem in fault diagnosis since some faults may have similar symptoms and more sensors can help in distinguishing them. On the one hand, features as sensitive as possible should be extracted from limited available measurements, and on the other hand, the diagnosis method should be as sensitive as possible to isolate several faults with similar symptoms and insensitive features. Computation should be small enough to be implementable within a microprocessor.

Second, since HVAC equipment are used in diverse weather and climates, the behavior of the HVAC plant will vary drastically. In addition, since single-point sensor placement is generally used, many measurements often are biased and noisy. So the FDD system should be able to handle biased measurements and be robust to different operating modes and against noise and disturbances.

Third, unlike critical systems in which faults have zero tolerance, a fault evaluation and decision step should be added to assess the impact of a fault on overall system performance and make a decision whether the benefit of servicing the fault justifies its expense.

Fourth, unlike a critical FDD system which is engineered for a specific large system, FDD for HVAC systems needs to be adaptive and generic (system-independent) to the same type of system, or at least to similar models from the same product family. This would reduce the per-unit costs, which need to be low, compared to the HVAC equipment price.

Finally, multiple-simultaneous faults are pretty common for air conditioners, so the FDD technique should be capable of handling them. This feature has been neglected for previous developments and evaluations of FDD techniques.

In order to reduce hardware costs, FDD for HVAC systems should use analytical redundancy, which means the information from system measurements should be preprocessed extensively before it is used to detect and diagnose faults. Furthermore, the characteristics of being adaptive and generic and capable of handling multiple-simultaneous faults should be emphasized when developing FDD for HVAC systems.

The rest of this chapter presents a literature review about FDD for HVAC systems with emphasis on rooftop and other vapor compression air conditioners, provides the motivation for the proposed research, summarizes the specific research objectives, and discusses the general approach to evaluating the proposed FDD methods. Chapter 2 describes data sources used to validate and demonstrate the proposed approaches. Chapters 3 and 4 describe the FDD methodology. Chapter 5 describes the economic assessment. Chapter 6 summarizes the major completed work and provides some recommendations for future work

1.2 Literature Review

1.2.1 Overview

In the late 1980's, some researchers investigated common faults and methods for fault detection and diagnosis in simple vapor compression cycles, such as a household refrigerator. With the growing realization of the benefits brought by FDD, many more papers about HVAC FDD have appeared in the last ten years. Figures 1-1 and 1-2 show the paper statistics for HVAC FDD over the past 13 years.

From these two figures, it can be seen that the number of papers significantly increased since 1996 and most of the papers focused on variable air volume (VAV) air handling units (AHU). Since Comstock, Chen, and Braun (1999) did a very detailed and comprehensive literature review in 1999, the next section of this report will briefly refer to some significant contributions before 1999 and concentrate on up-to-date progress after that.

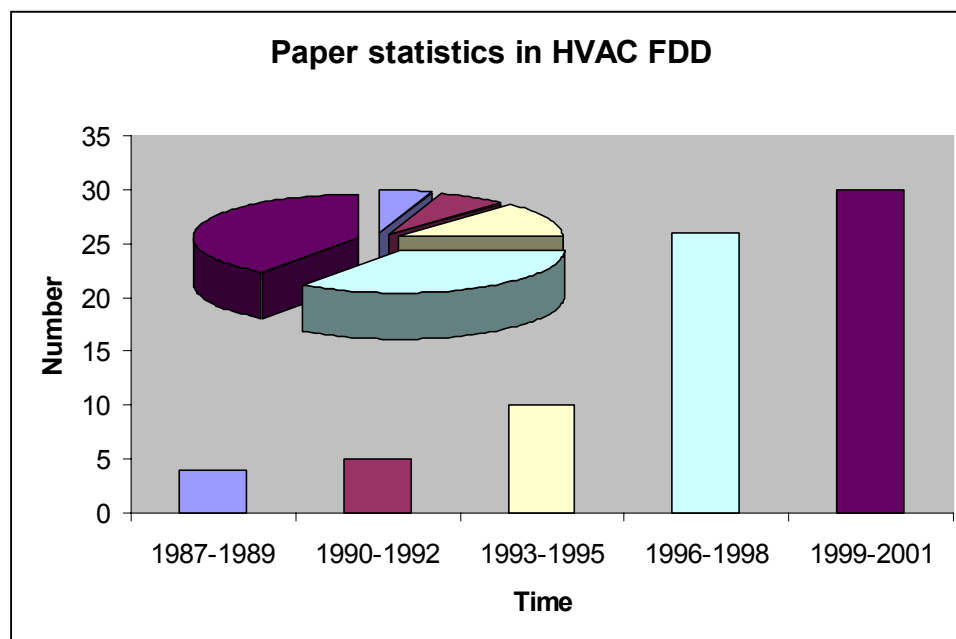


Figure 1-1 Paper statistics in HVAC FDD with time

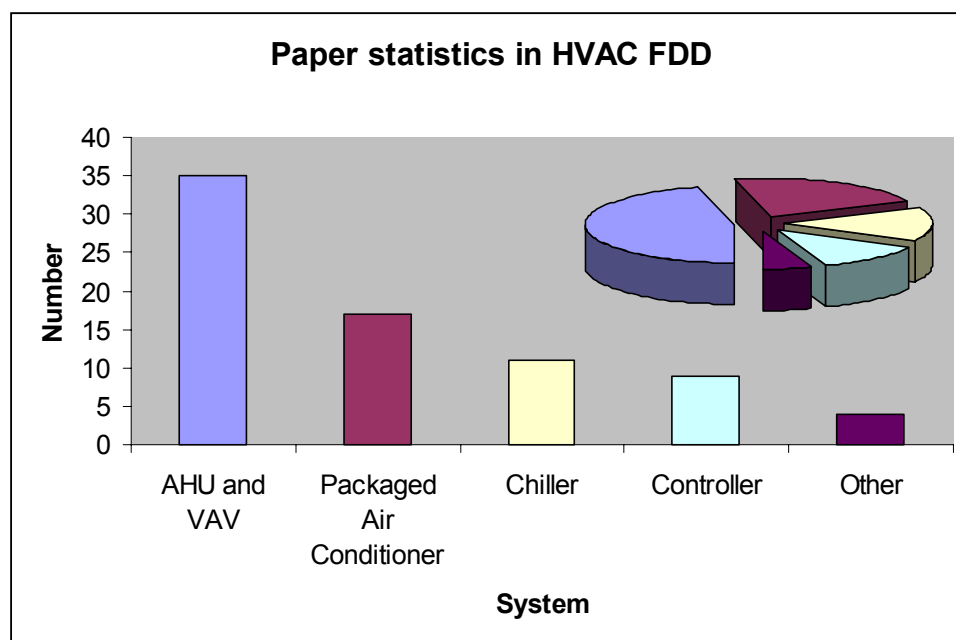


Figure 1-2 Paper statistics in HVAC FDD with system

1.2.2 Latest Progress

Since 1999, about 30 papers have been published on FDD for HVAC systems. According to the IEA ANNEX 34 final report edited by Dexter and Pakanen (2001),

- Twenty-three prototype FDD performance monitoring tools and three validation tools have been developed.
- Thirty demonstrations have been taken place in twenty buildings.
- Twenty-six FDD tools have been tested in real buildings.
- Four performance monitoring schemes have been jointly evaluated on three documented data sets from real buildings.
- A test shell has been developed to simplify the comparative testing of FDD tools.

1.2.2.1 Packaged Air Conditioning Systems

Rossi and Braun (1996 and 1997) modified the general FDD supervision methodology first described by Isermann (1984) for non-critical HVAC system as shown in Figure 1-3 and developed a statistical rule-based (SRB) FDD technique for vapor compression air conditioners. This technique uses only nine temperatures and one relative humidity. Among the ten measurements, ambient air temperature T_{amb} , return air temperature T_{ra} , and return air relative humidity Φ_{ra} (or wet-bulb temperature T_{wb}) are considered to be driving conditions. The other seven measurements (evaporating temperature T_{evap} , condensing temperature T_{cond} , suction line superheat T_{sh} , liquid line subcooling T_{sc} , compressor discharge temperature T_{dis} , air temperature rise across the condenser ΔT_{ca} , and air temperature drop across the evaporator ΔT_{ea}) are used to specify the system operating state. A steady-state model is used to describe the relationship between the driving conditions and the expected output states in a normally operating condition. By comparing the measurements of the output states with those predicted by the steady-state model, residuals are generated. These residuals are statistically evaluated to perform fault detection and compared with a set of rules based

on directional changes to identify the most likely cause of the faulty behavior (diagnosis). In addition, four fault impact evaluation criteria, ECONOMIC CRITERIA, COMFORT CRITERIA, SAFETY CRITERIA, and ENVIRONMENTAL CRITERIA, were developed. Based on estimated impacts, the FDD technique further made a decision on how to respond to the fault: tolerate, repair ASAP, adapt control, or stop to repair. This research laid a blueprint for later research, whose strengths and weaknesses were discussed in Deliverables 2.1.3, 2.1.4 and 2.1.5 and Li & Braun (2003).

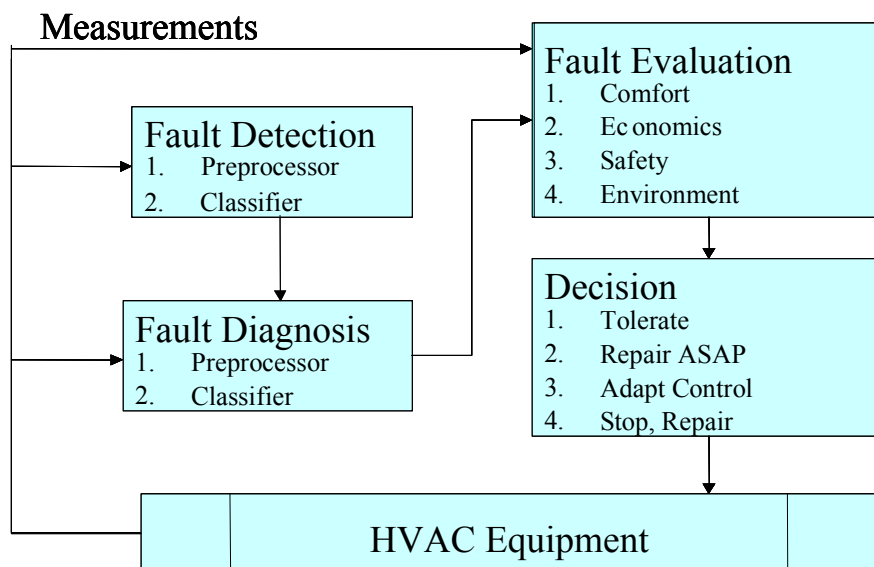


Figure 1-3 Supervision approach of HVAC&R equipment.

Following this research, Breuker and Braun (1997a, 1998a, 1998b) first identified important faults and their impacts on rooftop air conditioners through interactions with industry personnel, and then did a detailed evaluation of the performance of the FDD technique presented by Rossi and Braun (1997). It was found that by the frequency of occurrence, approximately 40% of the failure incidents of "no air conditioning" were electrical or controls related and the other 60% were mechanical. By the service occurrences, refrigerant leakage (12%) dominated among the mechanical faults while the occurrences of faults relating to condenser (7%), air handling (7%), evaporator (6%), and compressor (3%) are similar. By the service costs, the faults related to compressor failure dominated with 24% of total service costs. Controls related faults were the second-rated

class of high cost fault, accounting for 10% of total service costs. Further analysis showed that, although most failures in hermetic compressors are diagnosed as a failure in the motor, those failures usually result from mechanical problems such as overload or liquid refrigerant in the compressor. Based on their survey and analysis, Breuker and Braun concluded that five fault types should be considered for systems with fixed expansion devices: (1) refrigerant leakage; (2) condenser fouling; (3) evaporator filter fouling; (4) liquid line restriction; and (5) compressor valve leakage.

To evaluate the FDD technique presented by Rossi and Braun, the above five faults were introduced within a 3-ton fixed orifice air conditioner in well-controlled environmental chambers under various fault levels and cooling load levels. Results showed that refrigerant leakage, condenser fouling, and liquid line restriction faults could be detected and diagnosed before an 8% reduction in COP occurred; compressor valve leakage was detected and diagnosed before a 12% reduction occurred; and the least sensitivity was evaporator fouling at 20%. These results are compared with the improved FDD technique later in the current report.

To keep track of the up-to-date research, Comstock, Chen, and Braun (1999) performed an exhaustive literature review of FDD in HVAC. This review provided a solid background and guide for later research.

The fault characteristics on a system with a TXV are different from those with a fixed orifice for which Rossi and Braun originally developed the statistical rule-based technique. Chen (2000a) modified and evaluated the original FDD technique for a 5-ton rooftop unit with a TXV as the expansion device. To simplify the FDD method, two innovative and easy-to-implement methods were proposed (Chen & Braun, 2000b & 2001). The first method, termed the “Sensitivity Ratio Method”, used measurements and model predictions of temperatures for normal system operation to compute ratios that are sensitive to individual faults. The second method, termed the “Simple Rule-Based Method”, dispensed with any on-line model but used performance indices computed from raw measurements that are relatively independent of operating state but are sensitive to faults. Both methods were tested using experimental data for different fault types and

fault levels at different operation conditions. Also, a 7.5-ton unit from the same product family as the 5-ton unit was used for a robustness test.

Ghiaus (1999) presented a bond graph method for a packaged air conditioning system. The bond graph is a graph in which nodes represent conservation of energy equations, and terminal nodes represent either system elements (such as resistance, capacitance, inertia) or sources. A bond is a power connection between two parts of the system: A and B. The power is the product of power variables: effort and flow. Effort represents force, torque, pressure, voltage, or absolute temperature, while flow represents velocity, rotational frequency, volume flow rate, current, or entropy flow rate. For the air conditioning system, a thermal bond graph used temperature as effort and entropy flow rate as flow. Two faults: reducing the heat removed by the evaporator (by slowing the evaporator fan) and reducing the heat rejected by the condenser (by slowing the condenser fan) were considered. The advantage of the method is that it could diagnose a fault without any a priori knowledge of the possible faults and implementation of the fault inference algorithm is fast and simple due to its recursive nature. However, there are several drawbacks for this method. Firstly, the method does not consider impact of variation in driving conditions on the bond graph, so it cannot tell driving condition effects from faulty effects. Secondly, only two simple faults were considered. If there is a refrigerant fault such as leakage or flow restriction, the technique described in the paper could not make the correct diagnosis, due to the assumption of constant refrigerant flow rate.

1.2.2.2 Other HVAC&R Systems

There is a large body of literature on other HVAC systems, especially variable air volume (VAV) air handling units (AHU) and chillers. Since this project is focused on rooftop and other packaged air conditioners, only recent and representative research is discussed here.

Shaw and Norford (2002) presented two techniques for using electrical power data for detecting and diagnosing a number of faults in AHUs. One technique relies on gray-box correlations of electrical power with such exogenous variables as airflow or

motor speed. This technique was developed to detect and diagnose a limited number of air handler faults and was shown to work well with data taken from a test building. The other method relies on physical models of the electromechanical dynamics that occur immediately after a motor is turned on. This technique has been demonstrated with sub-metered data for a pump and for a fan. Tests showed that several faults could be successfully detected from motor startup data alone. While the method relies solely on generally stable and accurate voltage and current sensors, thereby avoiding problems with flow and temperature sensors used in other fault detection methods, it requires electrical data taken directly at the motor, down-stream of variable-speed drives, where current sensors would not normally be installed for control or load-monitoring purposes. Later Norford and Wright (2002) presented some results from controlled field tests and concluded that: the first-principles-based method misdiagnosed several faults and required a larger number of sensors than the electrical power correlation models, while the latter method demonstrated greater success in diagnosis (limited number of faults addressed in the tests may have contributed to this success) but required power meters that were not typically installed.

Yoshida and Kumar (1999) presented a model-based methodology for online fault detection for VAV HVAC systems. Two models, Auto Regressive Exogenous (ARX) and Adaptive Forgetting through Multiple Models (AFMM), were trained and validated on data obtained from a real building. Based on the results, it was concluded that the variation of parameters rather than the difference between the predicted and actual output is more prominent and reflective of a sudden fault in the system. The AFMM could detect any change in the system but required a long window length and therefore may not detect faults of low magnitude. The ARX model, on the other hand, could be used with very short window length and was more robust. Yoshida and Kumar (2001a) further put forth an off-line analysis based on ARX method. It was concluded that off-line analysis of data by this model was likely to detect most of the faults. To evaluate the robustness of this technique, Yoshida and Kunmar (2001b) developed a recursive autoregressive exogenous algorithm (RARX) to build the frequency response dynamic model for VAV AHUs. It

was concluded that the method was quite robust against sensor error and could detect and diagnose several types of faults.

Carling (2002) presented a comparison of three fault detection methods for AHUs. The three methods were: a qualitative method that compares controller outputs and model-based predictions, a rule-based method that examines measured temperatures and controller outputs, and a model-based method that analyzes residuals based on steady-state models. The author concluded that the first method was easy to set up and generated few false alarms. However, it detected only a few faults of those introduced. The second method is straightforward and detected more faults while requiring some analysis during setup. The third method also detected more faults but it also generated more false alarms and demanded considerably more time for setup. The third method may have generated more false alarms because of poor steady-state detector performance and a bad detection and diagnosis threshold. In this paper, an exponentially weighted variance steady-state detector was used. Our investigation, which will be discussed in a later part of the report shows that the variance method, either the exponentially weighted method or fixed moving window method, is not robust enough and should be used together with a slope method for steady-state detection.

Dexter and Ngo (2001) proposed a multi-step fuzzy model-based approach to improve their earlier diagnosis results for AHUs. A computer simulation study demonstrated that a more precise diagnosis can be obtained and experimental results also showed that the proposed scheme does not generate false alarms. This method was based on the use of two kinds of reference models, the fault-free reference model and one of the reference models describing faulty behavior, to perform multiple-diagnosis. Although this new technique overcame some weaknesses of the fuzzy method, the difficulty to summarize or generate fuzzy rules when the number of fault types and levels and load levels increased could not be eliminated.

In addition to fuzzy methods, several investigators (Lee & Park, 1996, Li & Vaezi 1997) attempted to use artificial neural network (ANN) directly to do FDD for AHUs. The common feature of ANN FDD is to use an ANN to map the symptoms to the fault indicators. The network must first be trained to recognize the symptoms of the possible

faults, which requires tremendous data for different load levels, fault levels and types. For complicated problems with many fault types and levels and operating conditions, it is difficult, if not possible, to gather so much data. So recently there seems to be no research on ANN for HVAC FDD. It should be clarified that although it is difficult to directly use ANN to do FDD, it is very useful to use ANN to build fault-free reference models for model-based FDD.

Finally, in the literature of HVAC FDD, some researchers (Salsbury & Diamond 2001, Liu & Dexter 2001) attempted to deal with FDD in control loop problems or use the information from the controller to do FDD.

1.2.3 Summary of Literature Review

So far, online FDD for HVAC is primarily at the laboratory or field demonstration stage and commercialization of FDD is a big challenge, since many practical and economic issues should be addressed. In particular, none of the previous methods can handle multiple simultaneous faults, which limits their applicability. The SRB FDD method was one of the first comprehensive techniques applied to packaged air conditioners and was the most extensively validated through experimental testing. Significant contributions of this work included:

1. The method was validated by experimental tests and shown to have reasonably good performance in handling individual faults.
2. The method only requires nine low-cost temperature measurements and one humidity measurement, which is vital for practical use and commercialization.
3. This work was the first to introduce fault evaluation to HVAC&R equipment FDD and four fault evaluation criteria were introduced.
4. A detailed simulation model was developed and used to test FDD methods.
5. The method involved the successful conversion of an infinite-classification problem into multiple single-classification problems.
6. The work laid a blueprint for later research.

However, several improvements are possible, including:

1. Removing the assumption that the covariance matrix $\Sigma_{current}$ for current operation is the same as the normal covariance matrix Σ_{normal} . When the system deviates from normal operation, it is possible for $\Sigma_{current}$ to vary significantly from Σ_{normal} .
2. Eliminating the independence assumption originally used to simplify the probability computation, which results in some loss of FDD sensitivity.
3. Extending the methods to handle multiple-simultaneous faults. Neglecting the different fault levels, 3 kinds of faults may have 31 ($\binom{5}{1} + \binom{5}{2} + \binom{5}{3} + \binom{5}{4} + \binom{5}{5} = 2^5 - 1$) combinations while 7 would have 127 combinations, so it is difficult, if it is not impossible, to find so many rules for each combination.
4. Extending the methods to achieve system-independence. TXV systems have different rules from fixed orifice systems and are not handled using the original SRB method.

1.3 Research Objectives and Approach

1.3.1 Motivation and Objectives

Based on the background literature review, the motivation for the proposed research can be summarized as:

1. Packaged air conditioning equipment is an excellent application for FDD. This type of equipment is used extensively throughout small commercial and institutional buildings. However, compared to larger systems, they tend to be not well maintained. For instance, one study showed that more than 60% of residential systems in California were not properly charged (Levins, Rice, and Baxter, 1996). Widespread application of automated FDD to packaged equipment will significantly reduce energy use and peak electrical demand, down time and maintenance costs.

2. Existing techniques for online FDD mainly have three drawbacks. First, they are expensive to apply practically because of requirements for model training and large computational demand. Second, they have only been tested in the laboratory and have not considered factors that occur in the field. Third, they can not handle multiple-simultaneous faults.
3. No one has performed economic assessments of FDD. It is a complicated problem that requires field evaluations.

So, a general objective of this research was to develop a practical automated FDD technique, whose cost is low enough to be affordable for packaged air conditioners and heat pumps, and whose performance is robust and capable of handling multiple-simultaneous faults. Another objective was to perform an initial economic assessment of FDD applied to vapor compression equipment in California.

The biggest technical difficulties associated with development of a practical FDD method are associated with the economic constraints. To realize the general objective, some sub-objectives should be achieved.

1. Only inexpensive hardware can be used, which means that redundant analyses should be conducted using limited computation and memory resources. This is a particular problem in fault diagnosis since some faults may have similar symptoms and more sensors can help in distinguishing them. On the one hand, features as sensitive as possible should be extracted from limited inexpensive measurements, and on the other hand, the diagnosis method should be as sensitive as possible to isolate several faults with similar symptoms and insensitive features. Computation should be small enough to be implementable within a microprocessor.
2. Packaged air conditioners are used in diverse weather and climates, so their behavior will vary drastically. Unmeasured ambient weather conditions, such as solar radiation, rain, and strong wind on the condenser can impact performance. Since the mixing chamber is small, outdoor air and return air are not mixed well and varying damper positions even exaggerate this impact. In addition, since single-

point sensor placement is generally used, many measurements often are biased and noisy. The FDD should be able to handle these practical difficulties.

3. Multiple-simultaneous faults are common for packaged air conditioners, so the FDD technique should be capable of handling them.

1.3.2 Methodology

There are two aspects to the general approach proposed for achieving the objectives: 1) actively create favorable conditions for application of the FDD techniques and 2) provide improved FDD methodologies to handle multiple-simultaneous faults and reduced model training requirements.

Because of economic constraints, some practical difficulties are impossible to overcome passively. For example, it is not possible for a single-point sensor to measure the mixing box temperature accurately under varying damper position. To reduce measurement uncertainty and bias and dimensionality, favorable conditions for FDD can be created proactively as follows:

1. Schedule application of the FDD methods at special times (e.g. night time) instead of around the clock to eliminate the unfavorable impact of weather conditions, such as solar radiation, and occupant intervention.
2. Override routine controls to fix the speed of the condenser fan and evaporator blower and damper position. Constant condenser fan and evaporator blower speed is equivalent to constant air mass flow rate under normal operation condition. Fixed damper position eliminates the mixing problem with single-point sensor.

From a methodology point of view,

1. Existing FDD methods were examined to identify their advantages and drawbacks. The statistical rule-based (SRB) FDD method proposed by Rossi & Braun only uses low cost sensor and has good performance under laboratory test, so it provided a start for further improvement.
2. The FDD problem was analyzed from a control and mathematical point of view. From the control point of view, decoupling is an efficient way to handle

interactions among multiple factors. From the perspective of mathematics, transformation could result in decoupling.

3. The underlying physics for HVAC&R equipment were utilized wherever possible. By analyzing the different faults deeply, the commonness and characteristics of faults and decoupling features could be found. Deep understanding of the physics of the system also contributed to development of models (virtual sensors) that can be used to estimate some measurements that would require expensive measurements.
4. Manufacturers' rating data such as compressor maps, TXV maps and system capacity rating data were used extensively, because they are not only readily available at no cost, but also are generic and reasonably accurate.
5. The focus was on development of generic FDD methods for packaged air conditioners. Unlike a critical FDD system which is engineered for a specific large system, FDD for packaged equipment needs to be adaptive and generic (system-independent) for the same type of system, or at least for similar models from the same product family. The application of generic FDD methods would reduce the per-unit costs.

Both laboratory and field data were used to validate the proposed techniques as follows:

1. Field setups were used to investigate the impact of practical factors on FDD application.
2. Laboratory setups will be used to test overall performance of FDD methods in a controlled environment with individual and multiple-simultaneous faults artificially imposed at known levels.

Field data were also used to evaluate the impact of faults on system performance and to perform initial economic assessments for FDD.

2 DATA SOURCES USED FOR EVALUATION AND DEMONSTRATION

2.1 Overview

There is a lot of test data available from earlier research projects performed at Herrick laboratories for the purpose of validating FDD techniques and models for packaged air conditioning equipment. Data taken by Breuker (1997b), Chen (2000), and Harms (2002) were used to validate the FDD techniques presented in this report.

The earlier laboratory data sets do not include some factors that would be experienced in the field. Examples include ambient weather conditions that appear in the field but are typically not measured and were not considered during laboratory testing, such as solar radiation, rain, and wind. These factors can influence the performance of the unit through an impact on the condenser heat transfer characteristics. Also the damper position changes the air flow rate, while the laboratory experimental data was collected with a constant air flow rate. Since the mixing chamber is small, outdoor air and return air are not mixed well and different damper positions also have some impact on mixing. If not properly considered, changes in damper position could lead to classification errors. The impacts of these factors are unknown and deserve further research in a field situation.

2.2 Previous Data Sources

2.2.1 Mark Breuker's Data

Two types of laboratory data were collected by Breuker (1997b) under controlled conditions for a 3-ton Carrier rooftop air conditioner with a short-tube as the expansion device. One is normal operation data, which were used to build a normal operation model, and the other is faulty operation data, which were collected under various simulated faults and used to evaluate FDD performance.

2.2.1.1 Normal Operation Data

The normal operation data set was obtained at a number of controlled normal operating conditions. There are two sets of normal operation data. A large set of data was gathered at combinations of indoor dry bulb temperatures (T_{ra}) of 70, 73, 76, 79, and 82 F, indoor wet bulb temperatures (T_{wb}) of 33, 38, 61, 64, and 67 F, and ambient temperatures (T_{amb}) of 60, 70, 80, 90, and 100 F. A smaller set of data was gathered at indoor dry bulb temperatures of 71.3, 74.3, 77.3, and 80.3 F, indoor wet bulb temperatures of 36.3, 39.3, 62.3, and 63.3 F, and ambient temperatures of 63, 73, 83, and 93 F. The conditions were selected because they completely cover the normal comfort region defined by ASHRAE (1993).

To ensure that there were no faults developing in the test unit during the test period and to quantify experimental noise which is present in the operation of the test unit, a test condition at $T_{amb} = 83$ F, $T_{ra} = 76$ F, $T_{wb} = 61$ F was retested every few days. The results of this repeatability test for all of the measurements used by the FDD technique are shown in Table 2-1. Because of the smaller heat capacity associated with vapor (as compared with liquid), the noisiest measurements are the suction superheat and hot gas temperatures.

Table 2-1 Repeatability analysis during steady-state model testing

Data (deg. F)	T_{evap}	T_{sh}	T_{dis}	T_{cond}	T_{sc}	ΔT_{ca}	ΔT_{ea}
Mean	43.76	8.42	193.11	108.69	7.03	11.72	19.14
Std. Dev.	0.39	1.73	1.23	0.40	0.23	0.09	0.17
Spread	1.21	4.80	4.04	1.28	0.60	0.26	0.64

2.2.1.2 Faulty Operation Data

In addition, five types of artificial faults were introduced at different fault levels and the unit was tested at different load levels in order to evaluate the performance of the FDD technique.

The five types of faults are refrigerant leakage, compressor valve leakage, condenser fouling, evaporator fouling and liquid line restriction. Each fault was introduced at four or five different levels (see Table 2-2) and tested at five different load levels (20%, 40%, 60%, 80% and 100%). In all, there are 120 sets of fault data available to test the proposed FDD method. For each of the different load levels, the unit was on for different amounts of time. The total cycle time was held constant at 43 minutes and the on time was varied for the different load levels. For example at 20% load, the unit ran for 9 minutes and was off for 36 minutes. Two consecutive transient start-up responses were generated and data were recorded at 3-second intervals at each of the conditions and fault levels.

Table 2-2 Fault levels introduced to different faults

Fault Level	Refrigerant Leakage	Liquid-line Restriction	Compressor Valve Leakage	Condenser Fouling	Evaporator Fouling
1	0	0	0	0	0
2	3.5%	5.0%	7.0%	14.6%	12%
3	7.0%	10%	14%	29.2%	24%
4	10%	15%	19%	41.4%	35%
5	14%	20%	28%	56.1%	NA

2.2.2 Chen's Data

Similar to Breuker's data, two sets of laboratory data were collected under controlled conditions for two packaged York rooftop air conditioners with TXV as the expansion device: a 5-ton one stage system and a 7.5-ton two-stage system by Chen (2000). In addition to the five faults considered by Breuker (1997b), two more faults, refrigerant overcharge and non-condensable gas, were simulated.

2.2.3 Todd Harms' Data

Although the data collected by Todd Harms were originally used for refrigerant charge inventory research, they are useful to test modeling approaches and refrigerant

charge faults for TXV RTU systems. Three Trane RTUs (a 2.5-ton split system, a 5-ton packaged system and a 7.5-Ton split system) were tested under four operation conditions (see Table 2-3) with various charge levels.

Table 2-3 Environmental conditions.

Test Condition	T _{outdoor} , °C	T _{indoor} , °C	T _{dew point} , °C
A	35.00	26.67	15.77
B	27.78	26.67	15.77
C	27.78	26.67	< 3.06
HT	48.89	26.67	15.77

2.3 Field Test Facilities

All the field-sites in California are small commercial buildings that utilize packaged air conditioning and heating equipment. The criteria used for selecting the field-sites included: 1) building occupancy type and size; 2) HVAC system installed, and 3) climate region. The types of building include smaller retail stores, restaurants and modular schoolrooms. The HVAC systems installed include different rooftop and wall mounted units with different capacities and manufactured by York, Trane and Bard. The climates include two different macroclimate types: coastal and inland. Table 2-4 summarizes information about all sites (refer to Deliverables 2.1.1a & 2.1.1b for details).

The Purdue field setup is meant to mimic field setups in California in order to aid in the identification of installation and operational problems locally. In addition, this setup allows us to test alternative sensors and to artificially introduce faults, both of which would be logistically difficult to perform in California (refer to Deliverables 2.1.1a & 2.1.1b).

Table 2-4 Field site information

Occupation Type	Climate Location	Model	Cap (Tons)	Stage No.	VM No.	RTU/COMP Model No.
Storage room	Inland Purdue	York	5	1	1	D1EE 060 A23 Copeland Model ZR37K3-TF3
Schoolroom	Inland Woodland	Bard HP	3.5	1	1	WH421-A CopelandRecip. CR42K6-PFV
	2					
	Coastal Oakland				1	
	2					
McDonalds	Inland Sacramento	York	10	2	WattAve	D3CG120N20023MKD Bristol Inertia H23A36QDBLA
	Coastal Oakland		6	1	Bradshaw	D1CG072N07923ECC CopelandScroll ZR72KC-TF3
					Milpitas	D1CG072N09923C CopelandScroll ZR72KC-TF3
			12	2	Castro	D4CG130N16323MDB Bristol Inertia H26A72QDBLA
Walgreens	Inland Rialto	Trane HP	6.25	1	3	WCD073C30BBC
			7.5		1	WFD090C30BBC
					5	
					2	
					4	
	Coastal Anaheim		5	1	1	WSCO60A3R0A01H0A
			6.25		2	WCD073C30CBC
					3	
			7.5		4	WCD090C30CBC
					5	

3 IMPROVED SRB FDD METHOD

As depicted in Figure 3-1, a rooftop unit (RTU) can be represented as a black-box, which is driven by faults, disturbances and overall system driving conditions, including condenser inlet air temperature T_{aic} , evaporator inlet air temperature T_{aie} , and relative humidity ϕ_{aie} , and outputs overall system state variables, including evaporator temperature T_{evap} , suction line superheat T_{sh} , discharge line temperature T_{hg} , condensing temperature T_{cond} , liquid line subcooling T_{sc} , evaporator air temperature difference ΔT_{ea} , condenser air temperature difference ΔT_{ca} , and liquid line pressure drop ΔP_{ll} . The objective of the FDD technique is to infer some of the inputs from the outputs. There are two ways to fulfill this.

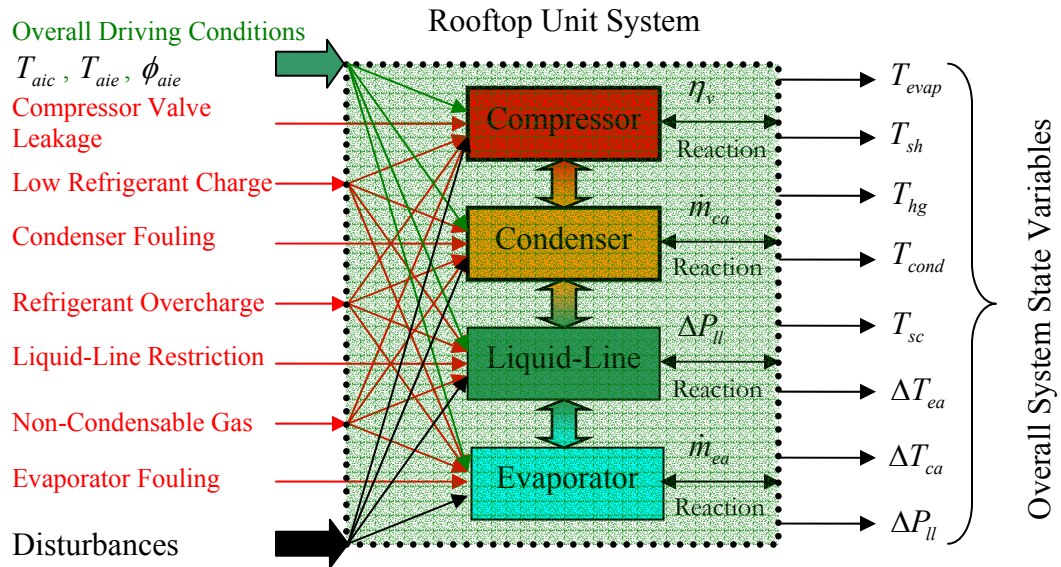


Figure 3-1 Interactions of Rooftop Unit System

The SRB FDD method determines which factors contribute to the current operation state directly from overall state variables. This method uses normal state models to predict the normal operation states according to the overall driving conditions and generates residuals to decouple the interactions between driving conditions and faults, and further uses statistical analysis to further decouple the actions from disturbances. This chapter summarizes an improved SRB FDD method (refer to Deliverables 2.1.3 & 2.1.4 or Li & Braun (2003) for details). However, this method leaves the couplings among the different faults untouched, so it cannot handle multiple-simultaneous faults. A method for handling multiple-simultaneous faults is described in the next chapter.

3.1 Limitations of the Original SRB FDD Method

Although the SRB FDD method proposed by Rossi and Braun (1997) has reasonably good performance, there are two disadvantageous assumptions which impact FDD performance. One is that the covariance matrix of the probability distributions for all faulty operation is constant and the same as that of normal operation. This assumption is important for this method, because it is difficult to obtain the covariance matrix for different faulty conditions. When implementing fault diagnosis, a further assumption, a diagonal co-variance matrix, is made. The diagonal assumption greatly simplifies the calculation of the probabilities associated with the occurrence of each of the faults, changing the problem from the integration of a 7-dimensional probability density function into a problem of seven 1-dimensional integrals. The first assumption is difficult to validate and the second one, a diagonal co-variance matrix, leads to some loss in FDD sensitivity. Deliverables 2.1.3 & 2.1.4 and Li & Braun (2003) evaluated the second assumption using Monte-Carlo Simulation. Section 3.2 summarizes the improved SRB FDD method and section 3.3 provides some comparisons with the original method.

3.2 Improved SRB Approach

Figure 3-2 depicts the overall structure of the SRB FDD method presented by Rossi and Braun (1997). Data (including system driving conditions and state variables) gathered from HVAC equipment are fed into the preprocessor, which includes a steady-state model and a preprocessor for the steady-state detector. The steady-state detector determines whether the system is considered to be at steady state, a necessary condition for the fault detection and diagnosis steps, and provides a binary output to a switch (SW), which ignores the output of the detection and diagnostic classifiers unless the system is in steady-state. The steady-state model uses the measured driving conditions (ambient dry-bulb temperature, mixed air temperature and wet-bulb) to predict state variables under normal operation (evaporation temperature, suction superheat, condensing temperature, condenser subcooling, compressor hot gas temperature, condenser and evaporator air temperature differences). The residuals between current measured and predicted normal operating states are used by fault detection and diagnostic classifiers.

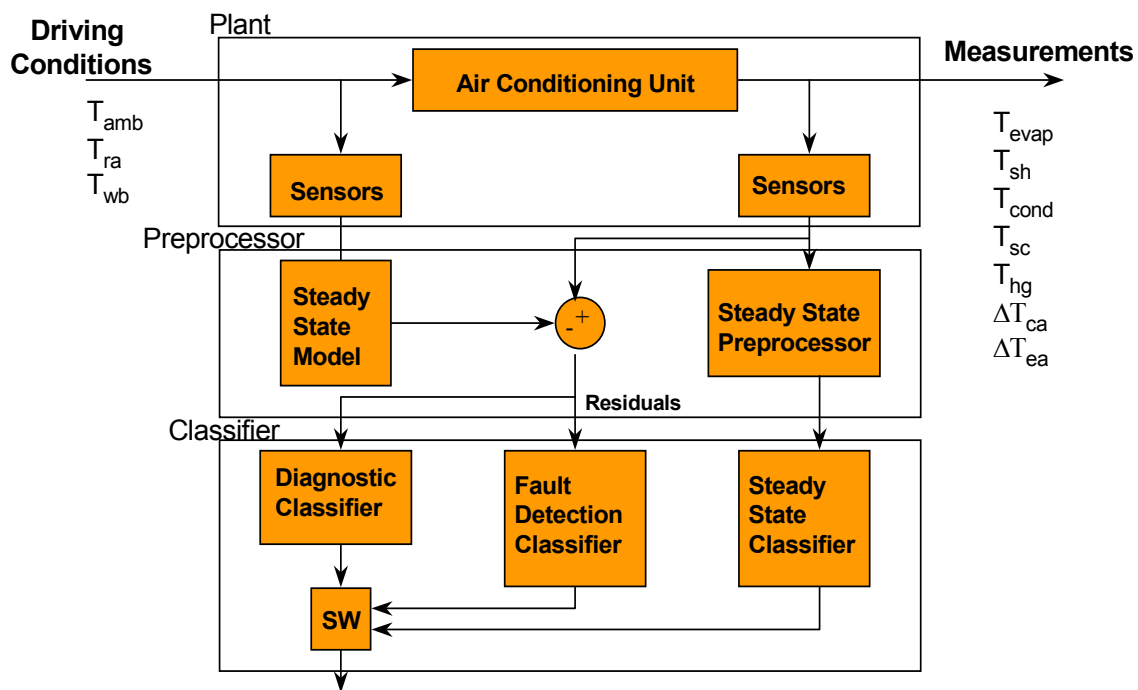


Figure 3-2 Structure of the SRB FDD method

The following sections describe specific improvements that have been made with respect to the steady-state detector, steady-state models, fault detection classifier, and diagnostic classifier.

3.2.1. Steady-State Detector

Two kinds of detection methods, a slope method and two variance methods, have been proposed to decide whether the system has approached steady-state (see Breuker (1997a)). If the variance threshold is set low enough, variance methods can filter out data with both deterministic and random variations. Although the slope method can filter out data with deterministic variations, it has difficulty distinguishing data with pure large oscillating magnitude from those with pure small oscillating magnitude. The combination of the slope and variance methods was proposed to improve the overall performance. This combined steady-state detection method can filter both deterministic and random variations at reasonable threshold and therefore is more robust (see Deliverables 2.1.3 & 2.1.4 and Li & Braun (2003)).

3.2.2 Steady-State Models

Breuker and Braun (1998b) used low-order polynomial (i.e, 1st and 2nd-order) models to predict steady-state operating states for normal operation. The advantage of low-order models is that relatively little data is required for training and the models work reasonably well to extrapolate beyond the range of training data. However, higher-order models can provide a better representation when sufficient training data are available. Li and Braun (2002) proposed a hybrid model that combines a low-order polynomial with a general regression neural network (GRNN). A GRNN is a memory-based network that incorporates a one-pass learning algorithm with a highly parallel structure (Donald, 1991). The low-order polynomial model is fit to the training data and the GRNN model is trained using residuals between the polynomial predictions and the data. Li and Braun (2002) demonstrated that in comparison to the low-order polynomial models, the hybrid

model has better performance in predicting states that are within the range of training data, with no penalty for extrapolating beyond the range.

3.2.3 Normalized Distance Fault detection Classifier

Deliverables 2.1.3, 2.1.4 & 2.1.5 and Li & Braun (2003) present details of a normalized distance fault detection classifier that can be used for both individual and multiple-simultaneous faults. The classifier evaluates the following inequality.

$$(Y - M_{normal})^T \Sigma_{normal}^{-1} (Y - M_{normal}) \underset{\omega_2: Faulty}{\overset{\omega_1: Normal}{\leq}} (\chi^2)^{-1}\{(1-\alpha), m\} \quad (3-1)$$

where $(Y - M_{normal})^T \Sigma_{normal}^{-1} (Y - M_{normal})$ is the normalized distance, $(\chi^2)^{-1}\{(1-\alpha), m\}$ is the threshold of normalized distance for normal operation, $(\chi^2)^{-1}\{, \}$ is the inverse of the chi-square cumulative distribution function, α is the false alarm rate, and m is the degree of freedom or dimension which is equal to the number of chosen state variables. Due to modeling error M_{normal} is not exactly zero, so equation (3-1) takes modeling error into account to statistically evaluate whether Y is zero or not.

The above fault detection scheme can be illustrated using Figure 3-3. The residual distribution of normal operation can be characterized in terms of the covariance matrix Σ_{normal} and mean vector M_{normal} and depicted in the residual space plane as in Figure 3-3. In the residual space plane, any operating states (points) outside the normal operating region are classified as faulty while those inside the normal operation region are classified as normal. The normal operating ellipse is the fault detection boundary.

Practically, normal operation information, such as the mean and covariance matrix, is more accessible and more reliable, compared to faulty operation data. In addition, this scheme is intuitive in that the opposite of normal operation is abnormal operation. If the current operation point is not inside the normal operation region at a certain confidence according to reliable prior information, it should be classified as faulty operation. Another advantage is that the fault detection decision is based on individual

points rather than on a distribution, so it is more computational efficient for online application.

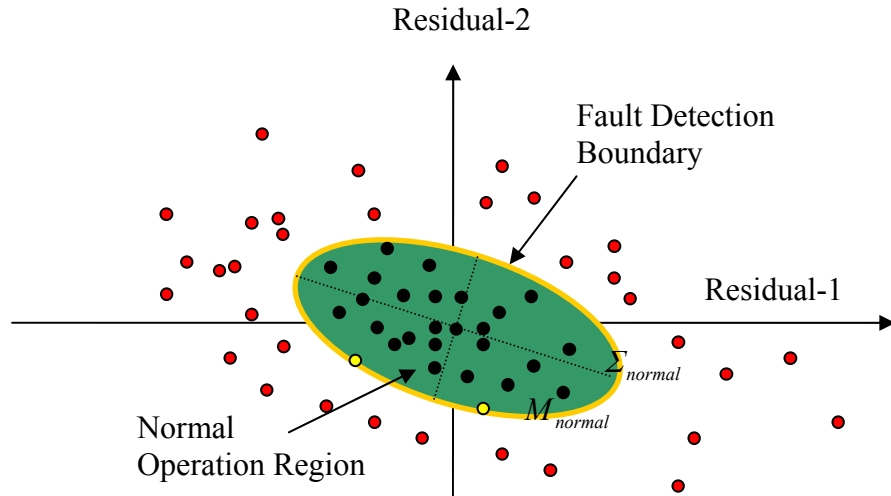


Figure 3-3 Fault detection classifier scheme for a 2-dimensional case

3.2.4 Fault Diagnosis

The SRB FDD method relies on a set of diagnosis rules to do fault diagnosis. Based on the fault diagnosis rules, fault diagnosis classifier separates the detected faults from the possible fault candidates.

3.2.4.1 Fault Diagnosis Rules

Fault diagnosis rules (see Table 3-1) can be expressed as positive and negative changes in residuals, so that each fault type corresponds to a unique quadrant of a multi-dimensional residual space. To decide which fault is the most probable is equivalent to identifying which quadrant the current measurement belongs to. Combined with the normal operating ellipse, coordinate axes form the fault diagnosis boundary (see Figure 3-4).

Table 3-1 Fault diagnosis rules

Fault type	T_{evap}	T_{sh}	T_{cond}	T_{sc}	T_{hg}	ΔT_{ca}	ΔT_{ea}
Refrigerant leakage	-	+	-	-	+	-	-
Comp. Valve Leak	+	-	-	-	-	-	-
Liquid Restriction	-	+	-	+	+	-	-
Condenser Fouling	+	-	+	-	+	+	-
Evaporator Fouling	-	-	-	-	-	-	+

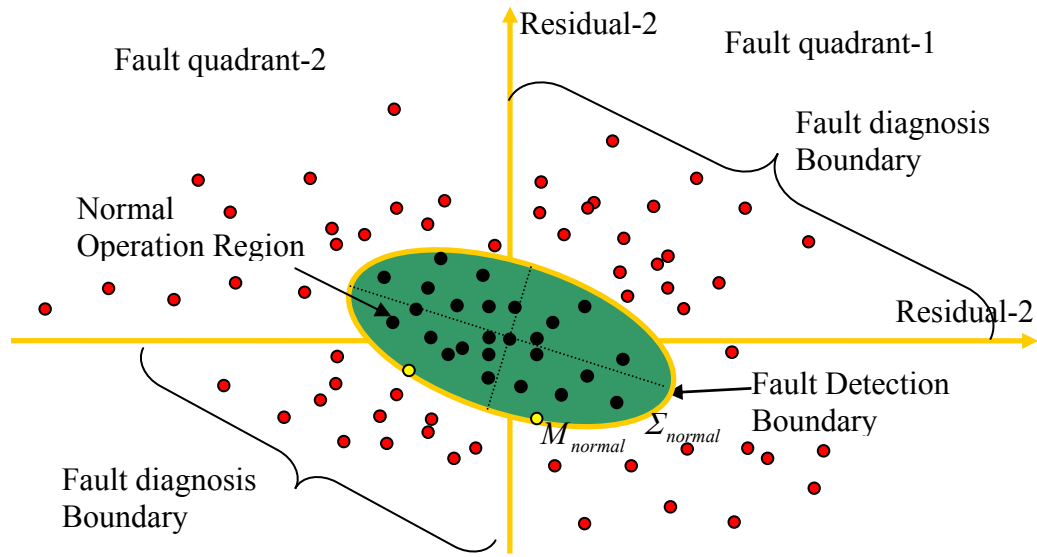


Figure 3-4 Fault detection and diagnosis boundaries

3.2.4.2 Simple Distance Fault Diagnosis Classifier

To eliminate the independence assumption and improve fault diagnosis performance, a simple distance fault diagnosis classifier, which does not require integration of the probability distributions, was developed and validated.

This method is briefly illustrated in Figure 3-5 using a two-dimensional case. Based on the predefined fault points (i.e., F_1 and F_2) corresponding to the fault quadrants (I and II), the distance ratio of the smallest distance to the second smallest distance (as to

current operation point P_1 , $ratio_{dist} = \frac{\|P_1 F_2\|}{\|P_1 F_1\|}$) is calculated, and when the distance ratio is less than a preset threshold β , then a fault corresponding to the minimum distance will be indicated. In Figure 3-5, the fault point with the minimal distance for P_1 is F_2 while for P_7 is F_1 , and if the distance ratio is lower than a preset threshold, fault II would be indicated for P_1 while fault I for P_7 .

The performance of the method is good in that the distance ratio monotonously decreases with increasing fault level (P_1 has the same fault level as P_2 and P_4 but a higher fault level than P_5 and lower fault level than P_3 and P_6), and is relatively insensitive to the choice of parameters c (P_6 can be classified correctly in Figure 3-5) and different operating conditions over a wide range (refer to Deliverables 2.1.3, 2.1.4 & 2.1.5 and Li & Braun (2003) for details).

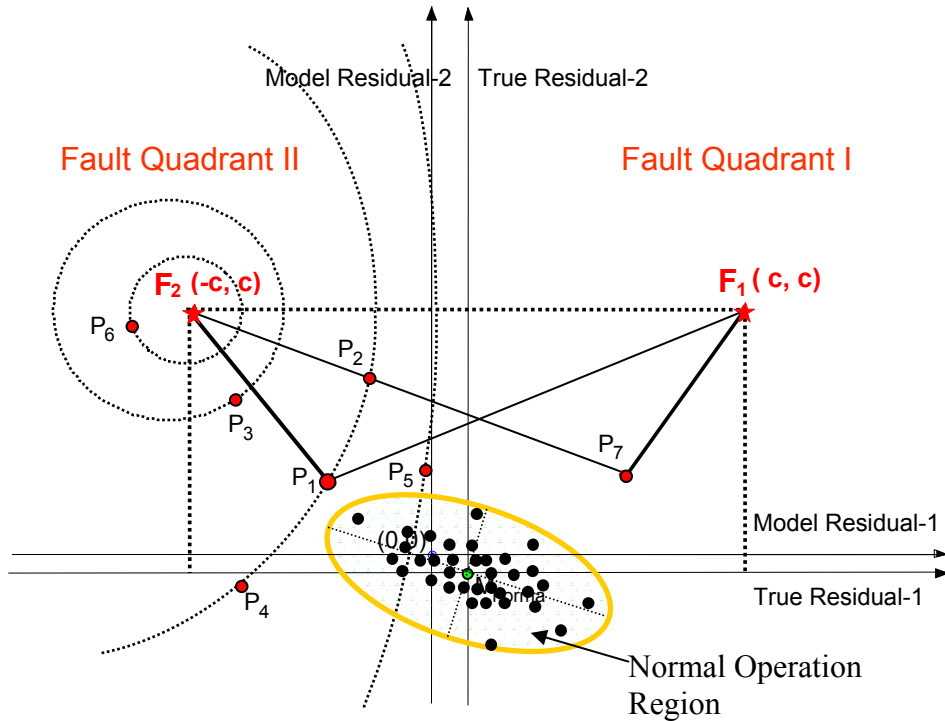


Figure 3-5 Distance method for fault diagnosis

3.3 Results

Table 3-2 gives comparative results for the two methods in terms of FDD sensitivity. Compared with the results obtained by Breuker and Braun (1998b), the improved SRB FDD method has superior performance. Breuker and Braun (1998b) presented results in terms of a “1st Detected” and “All Detected” level. The “1st Detected” level is the level at which the fault was first successfully detected and diagnosed throughout the data set. The “All Detected” level is the level at which the fault was detected and diagnosed during all steady-state operating conditions. As an example, the “1st Detected” refrigerant leakage fault level is 3.5% for the improved method and 7.8% for the original SRB method, whereas the “All Detected” refrigerant leakage fault levels are 7% and 9.5%, respectively. Similar results occur for the other faults. The results of Breuker and Braun do show some “1st Detected levels” that are below the lowest level of fault that was introduced. This is because their results were calculated by interpolating the impact of the fault level. This was not done for the current study. For a direct comparison without interpolation, the original SRB results should be rounded up to the next discrete fault level (shown in parenthesis for each fault type). For example, the “1st Detected” refrigerant leakage fault level for the original SRB, 7.8%, would be rounded up to the next discrete fault level, 10%. With this fairer comparison, the improvements in performance with the new method are more dramatic.

Table 3-2 Performance comparison of previous and improved FDD method

FDD results	Refrigerant leakage (3.5,7,10,14)%		Liquid-line restriction (5,10,15,20)%		Compressor valve leakage (7,14,19,28)%		Condenser fouling (14.6,29.2,41.4,56.1)%		Evaporator fouling (12,24,35)%	
	1 st	All	1 st	All	1 st	All	1 st	All	1 st	All
Original SRB	7.8	9.5	6.2	8.1	6.5	14.2	11.6	15.1	11.1	30.9
Improved SRB	3.5	7	5	5	7	7	14.6	14.6	12	12

4 A DECOUPLING-BASED FDD TECHNIQUE

Although the improved SRB FDD method has good performance for individual faults, it requires measurements over a wide range of conditions for training reference models. The development of these models can be time consuming and costly. Furthermore, SRB FDD methods can only handle individual faults. This section summarizes a new method, termed the decoupling-based FDD method, which reduces engineering and installed costs for FDD and handles multiple-simultaneous faults. This methods are evaluated using both laboratory and field data. Additional details of the method and evaluation are given in Deliverable 2.1.5.

4.1 Approach

To handle multiple-simultaneous faults, the interactions among different faults should be decoupled (refer to Figure 3-1). That is, if one independent feature, which is impacted only by one fault, can be found for each individual fault, then multiple-simultaneous faults are decoupled. For a linear system or some special nonlinear systems, a transformation can be found to diagonalize a transfer function matrix to decouple the system if a detailed system physical model is available. However, to obtain such a detailed physical model taking faults into account for a rooftop unit system is extremely difficult. Another way to decouple the system is to unfold the black-box representing the rooftop unit system to view it from a microscopic point of view and find some independent features with physical meaning for component-level faults, and isolate service faults from operation faults immediately after service is done and when the system stops. There is an important and practical restriction for the independence features. They should be able to be expressed as functions of low-cost measurements such as temperature and pressure.

In order to extend the easily-implemented SRB fault diagnosis idea to handle multiple-simultaneous faults, Deliverable 2.1.5 proposed a decoupling-based method, which decouples the interactions between the transformed FDD features Z and faults X (see Equation (4-1)). That is, it makes each entry of the feature vector Z only correspond to unique fault entries of the fault vector X and vice versa.

$$Z = \begin{bmatrix} \lambda_1 & & & \\ & \lambda_2 & & \\ & & \ddots & \\ & & & \lambda_n \end{bmatrix} X \quad (4-1)$$

Based on the decoupled features, the SRB FDD technique can be applied to handle multiple-simultaneous faults. That is, the $n - dimensional$ FDD problem has been decoupled to be $n - 1 - dimensional$ SRB FDD problems. In addition, the decoupling-based diagnosis method simplifies fault detection from a high-D problem to $n - 1$ -D ones. Equation (3-1) boils down to the following $n - 1$ -D equations,

$$\frac{(z_i - \mu_{i,normal})^2}{\sigma_{i,normal}^2} \begin{matrix} \omega_1: normal \\ \leq \\ \omega_2: faulty \end{matrix} (\chi^2)^{-1}\{(1-\alpha), 1\} \quad (4-2A)$$

or

$$\frac{|z_i - \mu_{i,normal}|}{\sigma_{i,normal}} \begin{matrix} \omega_1: normal \\ \leq \\ \omega_2: faulty \end{matrix} N^{-1}\{(1-\alpha), 0, 1\} \quad (4-2B)$$

where, $(\chi^2)^{-1}\{\cdot\}$ is the inverse chi-square cumulative distribution function, $N^{-1}\{\cdot\}$ is the inverse normal cumulative distribution function, α is the false alarm rate, and $i = 1, 2, \dots, n$.

Fault diagnosis automatically is achieved without any extra computation immediately after fault detection is finished, so the fault diagnosis classifier is not required.

This approach overcomes the drawback of the SRB diagnosis method and handles multiple-simultaneous faults diagnosis and becomes more generic and system-independent and does not require complicated rules, which depend on the system.

The above approach is based on decoupled features. Mathematically, there exists an infinite number of decoupled features, but for HVAC systems only those with intuitive physical meaning and those that are readily available (low-cost) are practical. Deliverable 2.1.5 develops a methodology or guidelines to find these kinds of features. This methodology or guideline first classifies the RTU faults from two criteria. From microscopic and macroscopic points of view, the seven faults can be divided into two classes: component-level and system-level faults, which are shown in Figure 4-1. If classified from the view of fault cause, they can be divided into: operational and service faults.

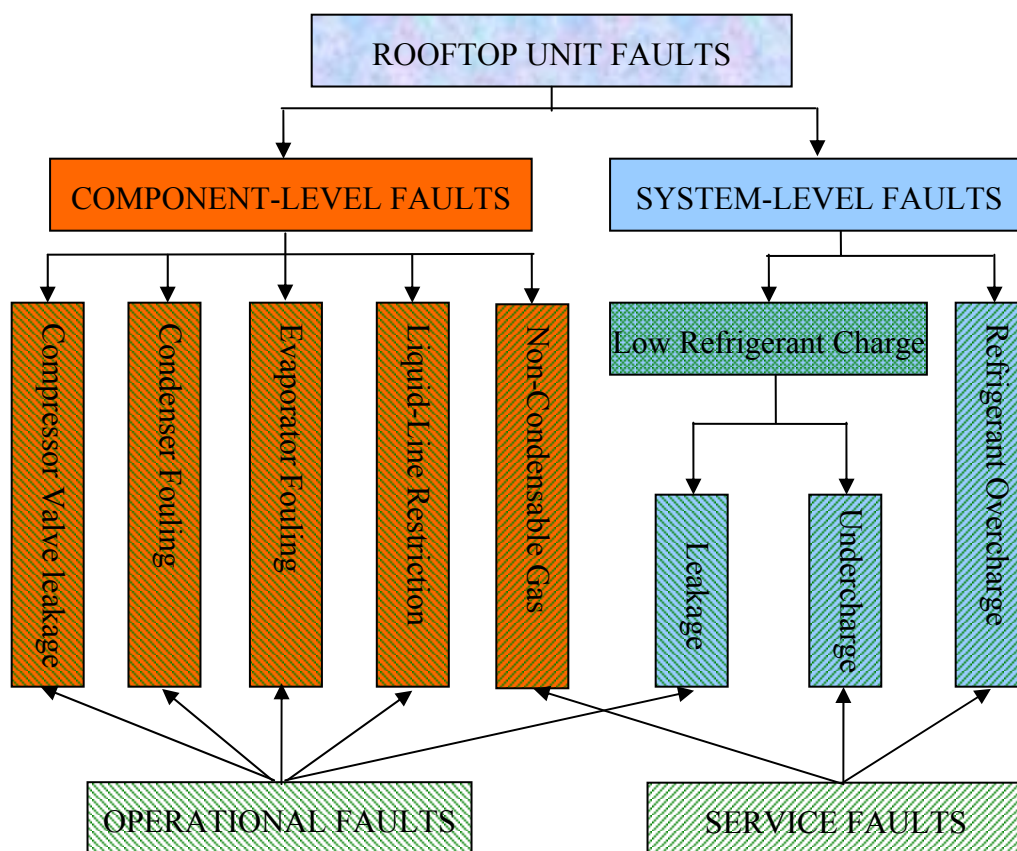


Figure 4-1 Taxonomy of Rooftop Faults

The characteristic of component-level faults is that their source impact can be confined to a component and this source impact is independent of other faults locally. So, the independence features for individual component-level faults can be found by investigating their source impacts. The independence features for service faults can be found by investigating their impact when the system stops.

Deliverable 2.1.5 described the details about how to decouple the RTU faults based on the taxonomy. Figure 4-2 summarizes the decoupling scheme for component and system level faults. Equation (4-3) formulates the decoupling scheme and results of all the rooftop faults. It can be seen that the matrix L of equation (4-3) is sparse and lower triangular. The algorithm described in Deliverable 2.1.5 can solve this unilateral decoupled problem.

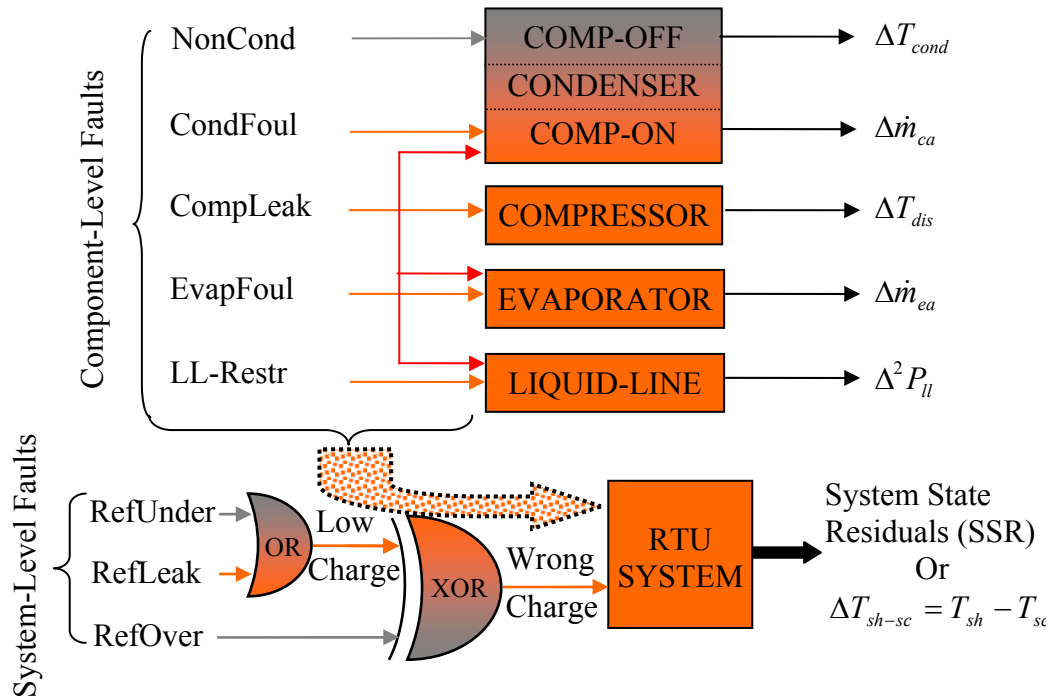


Figure 4-2 Decoupling Scheme of Rooftop System Faults

$$\begin{bmatrix} \Delta T_{cond} \\ \Delta T_{dis} \\ \Delta^2 P_{ll} \\ \Delta \dot{m}_{ca} \\ \Delta \dot{m}_{ea} \\ SSR / T_{sh-sc} \end{bmatrix} = Z = LX = \begin{bmatrix} l_{11} & & & & & \\ & l_{22} & & & & \\ & l_{32} & l_{33} & & & \\ & l_{42} & & l_{44} & & \\ & l_{52} & & & l_{55} & \\ l_{61} & l_{62} & l_{63} & l_{64} & l_{65} & l_{66} \end{bmatrix} \begin{bmatrix} NonCond \\ CompLeak \\ LLRestr \\ CondFoul \\ EvapFoul \\ RefCharge \end{bmatrix} \quad (4-3)$$

where ΔT_{cond} is the temperature difference between the condensing temperature and saturated temperature based on condensing pressure, $\Delta \dot{m}_{ca}$ is condenser air mass flow rate residual, $\Delta \dot{m}_{ea}$ is evaporator air mass flow rate residual, $\Delta^2 P_{ll}$ is the liquid line pressure drop residual, SSR is the system state residual, and ΔT_{sh-sc} is the difference between suction line superheat and liquid line subcooling.

4.2 Results

In order to validate the decoupling-based approach, three cases studies are provided in this section. Section 4.2.1 presents an initial case study to validate the decoupling scheme for a 3-ton fixed orifice rooftop unit. Section 4.2.2 presents an FDD demonstration of multiple-simultaneous faults for a 5-ton TXV rooftop unit installed at the Purdue field site. Section 4.2.3 provides results for California field sites.

4.2.1 Case Study of Decoupling Rooftop Unit Faults

Data gathered by Breuker (1997b) under controlled conditions in a laboratory were used to evaluate the decoupling scheme for a system with a short-tube expansion device. As described in Chapter 2, five types of individual faults were artificially introduced at different fault levels and the unit was tested at different load levels with the unit cycling on and off. Although these five kinds of faults are individual instead of multiple-simultaneous faults, they can be used to test whether the proposed decoupling features for each fault are independent of fault and load levels and all other faults.

4.2.1.1 Compressor Valve Leakage

Figure 4-3 illustrates the discharge line temperature residuals for different fault types with different fault and load levels obtained using predicted compressor power consumption and predicted refrigerant mass flow rate. It can be seen that only the compressor valve leakage fault has a significant influence on the discharge line temperature residual. The small fluctuations with other faults are caused by measurement noise, system disturbances and modeling error. So, the coupling between compressor valve leakage and other faults is broken successfully using the discharge line temperature residual.

However, there is still some room for improvement. For example, the discharge line temperature residual is impacted a little by large liquid-line restrictions. This may be caused by high suction line superheat at severe liquid-line restrictions, which results in a lower value of the compressor volumetric efficiency. However, this can be improved by

improving the compressor model performance and finding some practical means to tune it, which will also eliminate the impact of other faults on the discharge line temperature estimation.

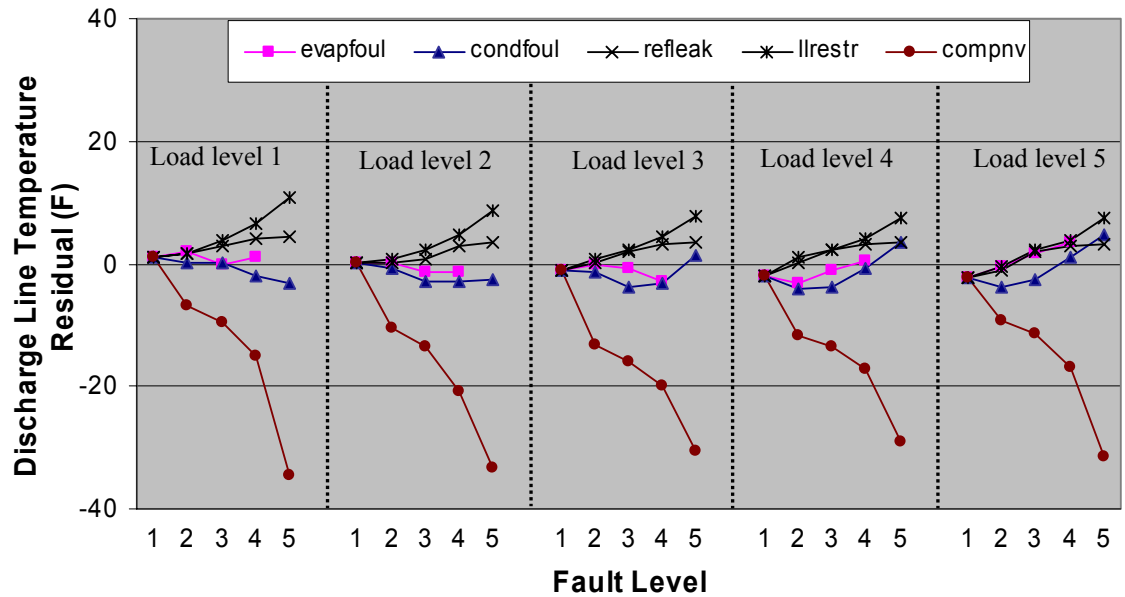


Figure 4-3 Decoupling compressor valve leakage fault using estimated compressor power measurement and estimated refrigerant mass flow rate

4.2.1.2 Condenser Fouling Decoupling

Figure 4-4 gives the condenser air mass flow rate estimated using a virtual sensor under different fault types with different fault and load levels. In order to show the potential of the decoupling scheme, this virtual sensor uses the actual refrigerant mass flow rate measurement. From Figure 4-4, it can be seen that the condenser air mass flow rate is only influenced by the condenser fouling fault. The reduction of condenser air mass flow rate is proportional to the condenser fault level and independent of load levels and other faults. So full decoupling between condenser fouling fault and other faults is achieved.

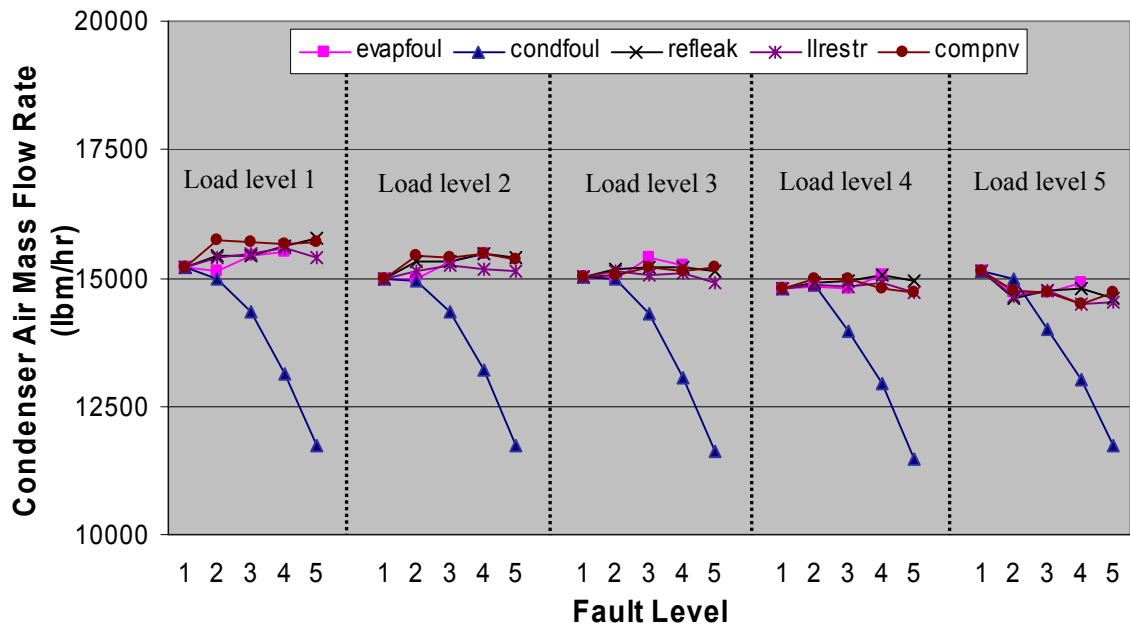


Figure 4-4 Decoupling condenser fouling fault using measured refrigerant mass flow rate

A refrigerant mass flow rate meter is too expensive for this application, so it is estimated using compressor map data. Figure 4-5 shows the condenser mass flow rate estimated using a refrigerant mass flow rate estimate under different fault types with different fault and load levels. It can be seen that the condenser mass flow rate estimate is influenced simultaneously by condenser fouling and compressor valve leakage with inverse directions. The dependence on compressor valve leakage is caused by errors in refrigerant mass flow rate prediction, since the compressor map was built using normal compressor data. When there is a compressor valve leakage fault, the compressor model over-estimates the refrigerant mass flow rate and this results in an over-estimate of condenser air mass flow rate. So, the coupling from compressor valve leakage to condenser fouling is not broken if the refrigerant mass flow rate is estimated using the compressor map. However, this would not impact the FDD application, because the coupling from condenser fouling to compressor valve leakage has been broken already. In other words, unilateral or partial decoupling can be achieved even if refrigerant mass flow rate is estimated using a compressor map.

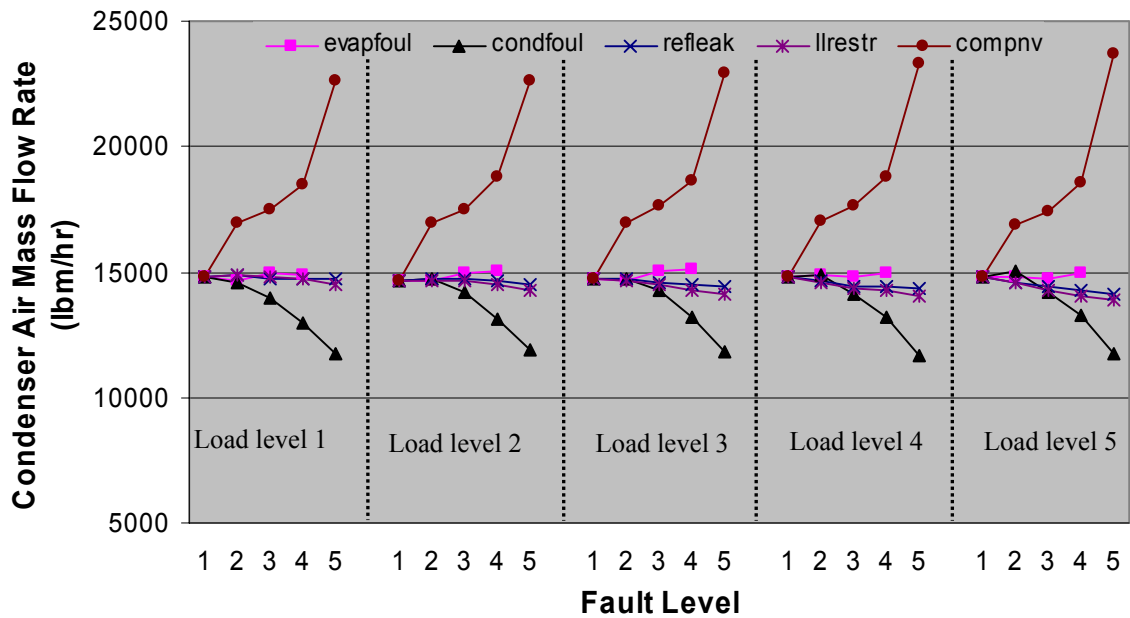


Figure 4-5 Decoupling condenser fouling fault using estimated refrigerant mass flow rate

4.2.1.3 Evaporator Fouling Decoupling

To quantify the fault levels simulated in this experiment, evaporator air mass flow rate was indirectly calculated from the fan curve using the measurement of the change in differential pressure across the evaporator fan. Figure 4-6 shows the evaporator air mass flow rate measurements. From this figure, it can be seen that in addition to an outlier point the actual evaporator air mass flow rate has a small variation for different fault types and different fault levels, and the fluctuation band shifts up with the increasing load levels. The outlier point may be caused by experimental error. The small shifting fluctuation with increasing load level may be caused by the variation in the air density at different load levels, and different fault type and fault level also have some influence on the air density. However, this small fluctuation would not change the decoupling feature.

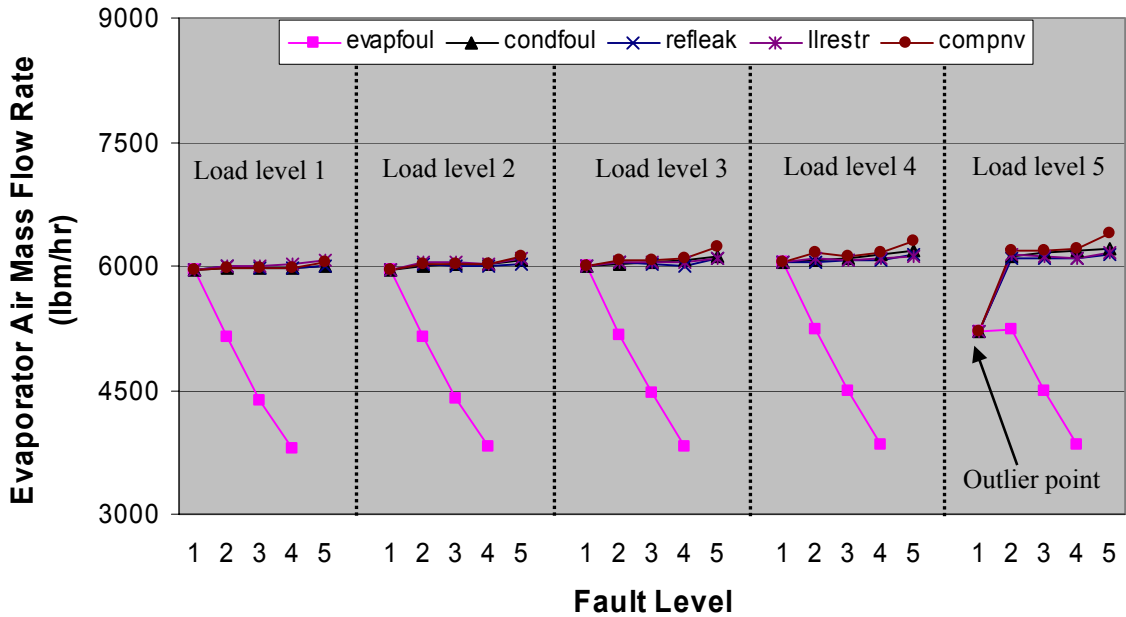


Figure 4-6 Decoupling evaporator fouling fault using measured evaporator air mass flow rate

Evaporator air mass flow rate is not typically measured. Figure 4-7 illustrates the evaporator air mass flow rate estimated using a virtual sensor under different fault types with different fault and load levels. This virtual sensor used the measured refrigerant mass flow rate. From this figure, it can be seen that the existing shifting fluctuation is amplified a little, which may be caused by the systematic error in the measurement of evaporator air inlet and outlet conditions. However, this still does not change the decoupling feature and the change of evaporator air mass flow rate estimate is still dominated by evaporator fouling and also it can be alleviated by improving the measurement scheme.

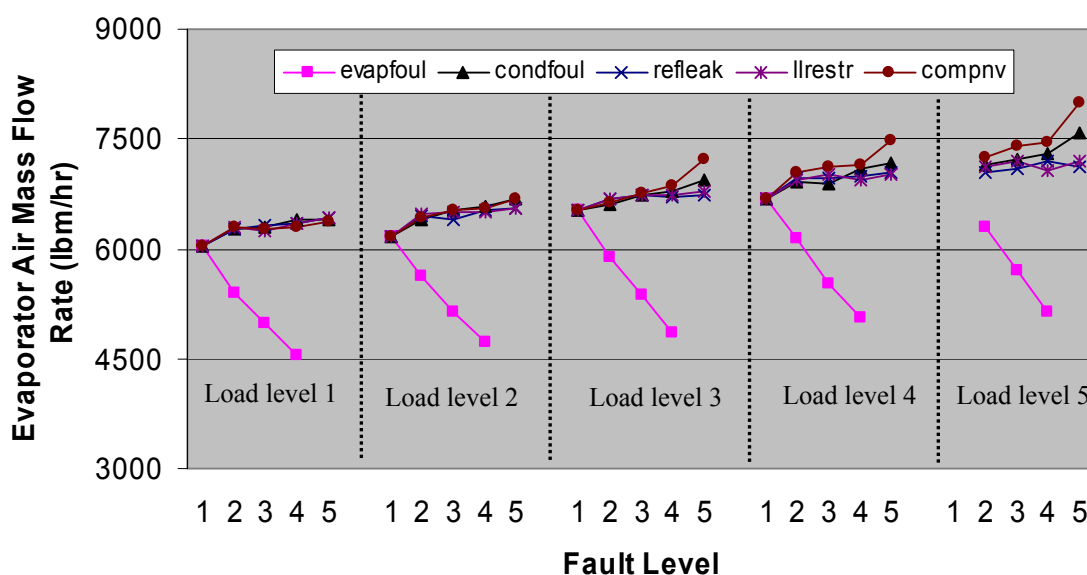


Figure 4-7 Decoupling evaporator fouling using measured refrigerant mass flow rate

Figure 4-8 illustrates the evaporator air mass flow rate estimated using estimated refrigerant mass flow rate. As expected, the coupling from compressor valve leakage to evaporator fouling is not broken if refrigerant mass flow rate is estimated by compressor map. For the same reason as condenser fouling, unilateral decoupling is sufficient for FDD application.

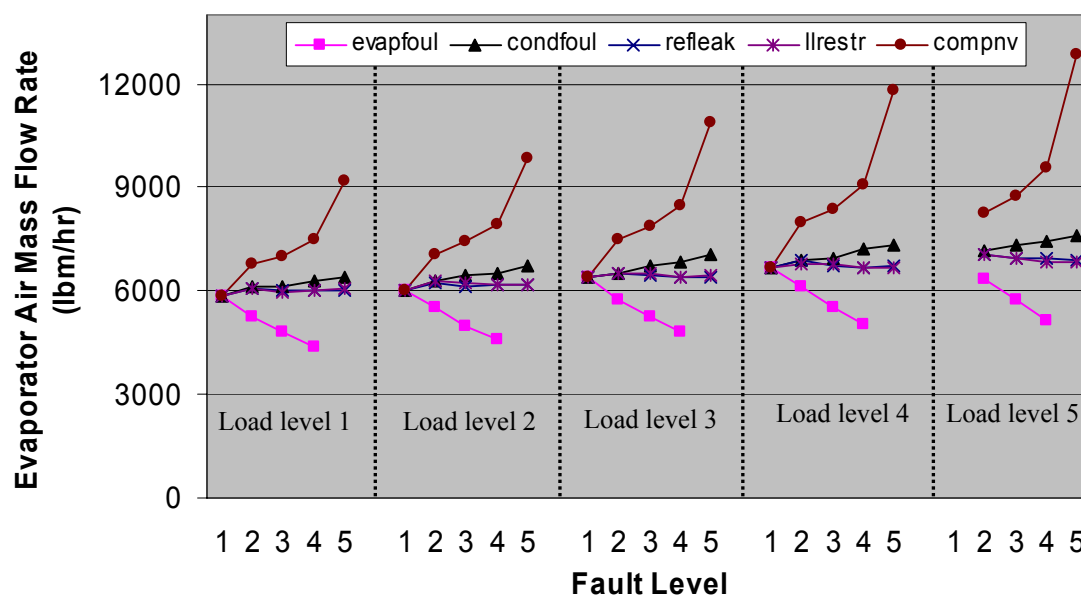


Figure 4-8 Decoupling evaporator fouling using estimated refrigerant mass flow rate

4.2.1.4 Liquid-Line Restriction Decoupling

Figure 4-9 illustrates the measured liquid-line pressure drop under different fault types with different fault and load levels. It is obvious that the liquid line pressure drop is only influenced by the liquid-line restriction fault. The decoupling between liquid-line restriction faults and all other faults is broken successfully.

However, it is not practical to measure the inlet and outlet pressures for FDD. The outlet pressure P_{up} should be estimated using a virtual sensor. Figure 4-10 shows the decoupling results using estimated P_{up} and measured P_3 . It can be seen that the accuracy of the P_{up} estimate is within $\pm 5\text{psi}$. In addition, the measurement of P_3 is not available, so Deliverable 2.1.5 proposed two estimation techniques. Due to limited data, only the second technique, assuming constant pressure drop across the condenser, was tested. Figure 4-11 shows the predict pressure drop between P_{dis} and P_{up} . It seems that a constant pressure drop of 25psi in the condenser can be assumed to estimate P_3 .

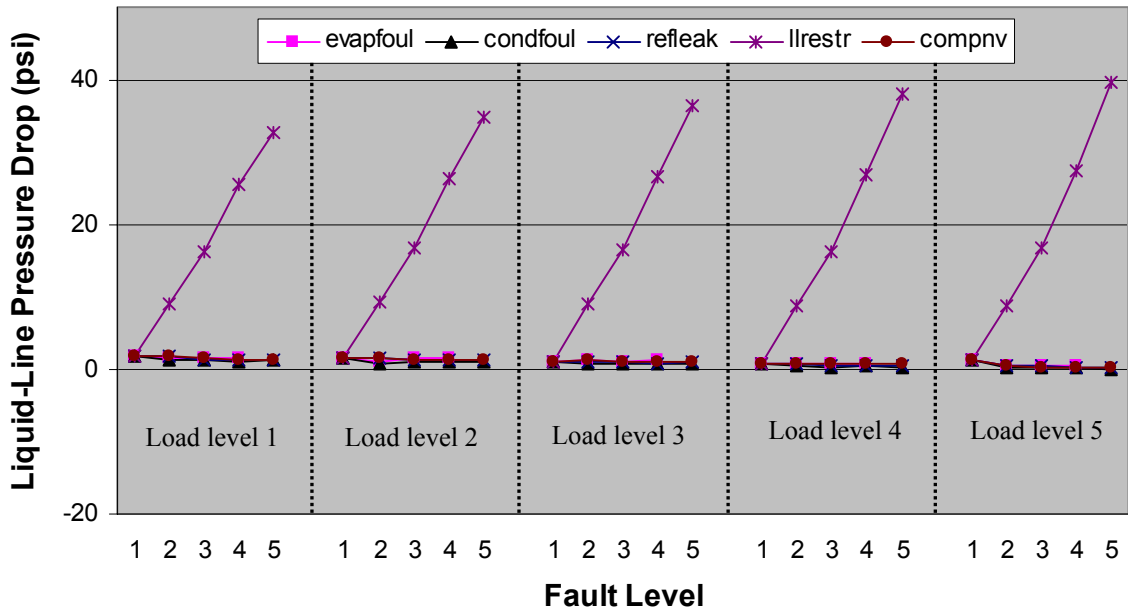


Figure 4-9 Decoupling liquid-line restriction using measured pressure drop

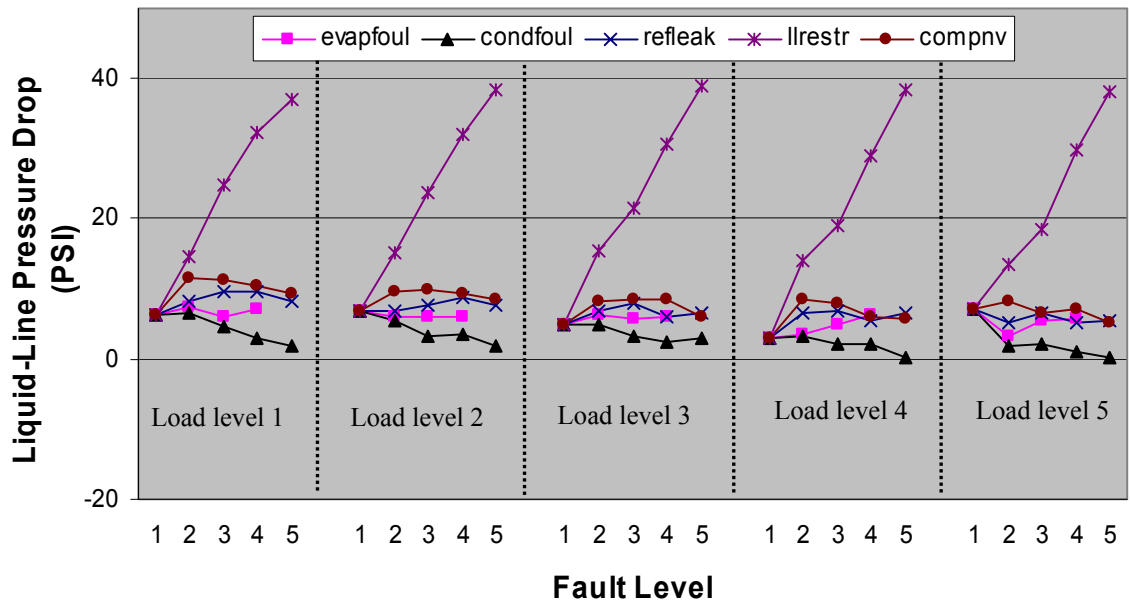


Figure 4-10 Decoupling liquid-line restriction using estimated pressure P_{up} and measured P_3

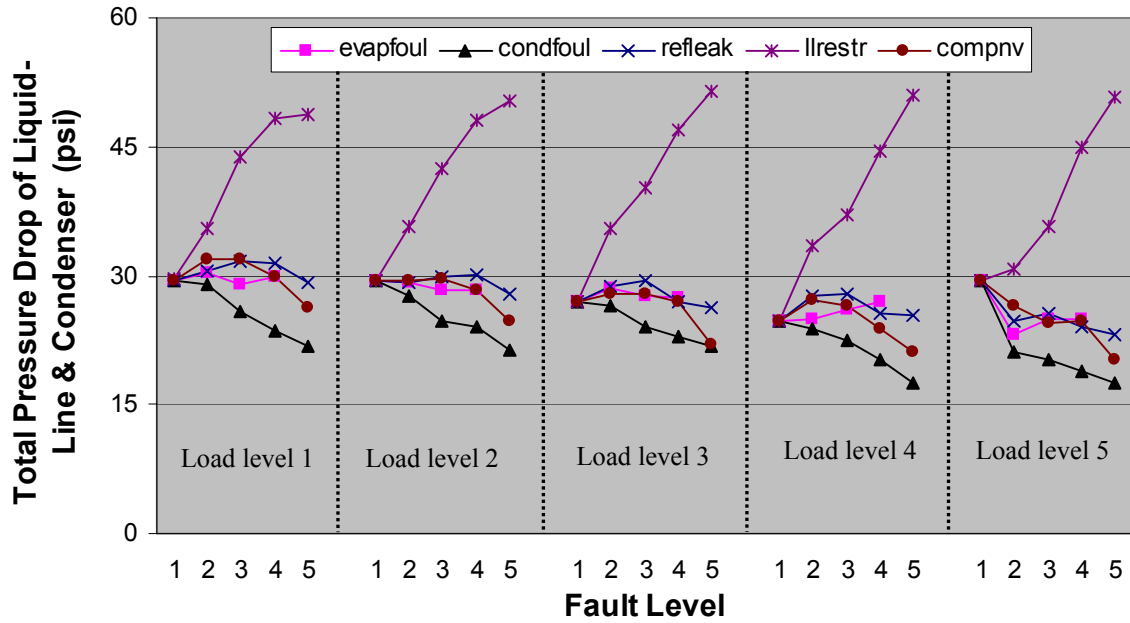


Figure 4-11 Decoupling liquid-line restriction using estimated pressure drop

4.2.1.5 Refrigerant Leakage Decoupling

Figure 4-12 shows the decoupling feature of ΔT_{sh-sc} for the different fault and load levels. It can be seen that all the faults have impacts on this feature. However, since the refrigerant fault does not have an impact on the other decoupling features and the value of this feature is proportional to refrigerant leakage fault levels, the unilateral decoupling is achieved successfully.

It should be pointed out that this feature monotonically decreases slightly with load level. This is expected, because no model is used for this feature and a fixed orifice can not compensate for load level variations very well. Although these impacts are a little larger than those of a TXV system, they are still reasonably small. Anyway, it is still advisable to improve this feature furthermore by modifying it using load level.

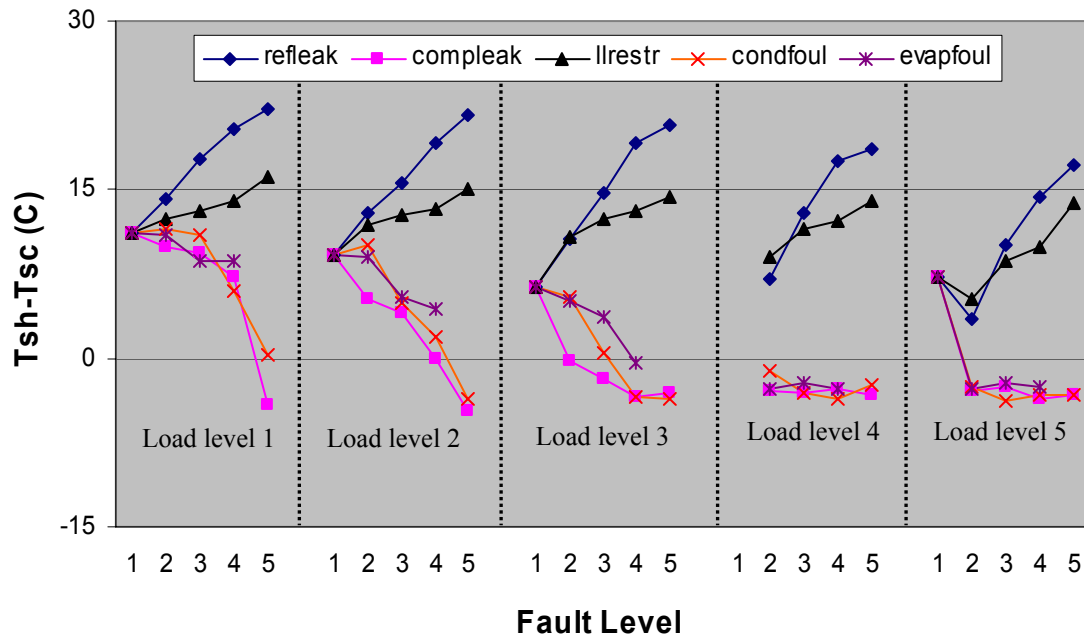


Figure 4-12 Decoupling refrigerant leakage faults using ΔT_{sh-sc}

4.2.2 Purdue Field Emulation Site's Demonstration

To demonstrate the decoupling-based fault detection and diagnosis approach, multiple-simultaneous faults were artificially introduced to the Purdue field emulation site, which has been described in a previous deliverable.

The decoupling-based fault detection and diagnosis approach was applied to the demonstration. To make the demonstration intuitive, a movie was made to show the whole process. There are four windows shown in the movie: Fault Detection and Diagnosis Window, System Performance and Safety Degradation Window, Fault Simulation Window, and Fault Detection and Diagnosis Window (see Figure 4-13). The following sections describe all the windows in detail and present some sample results.

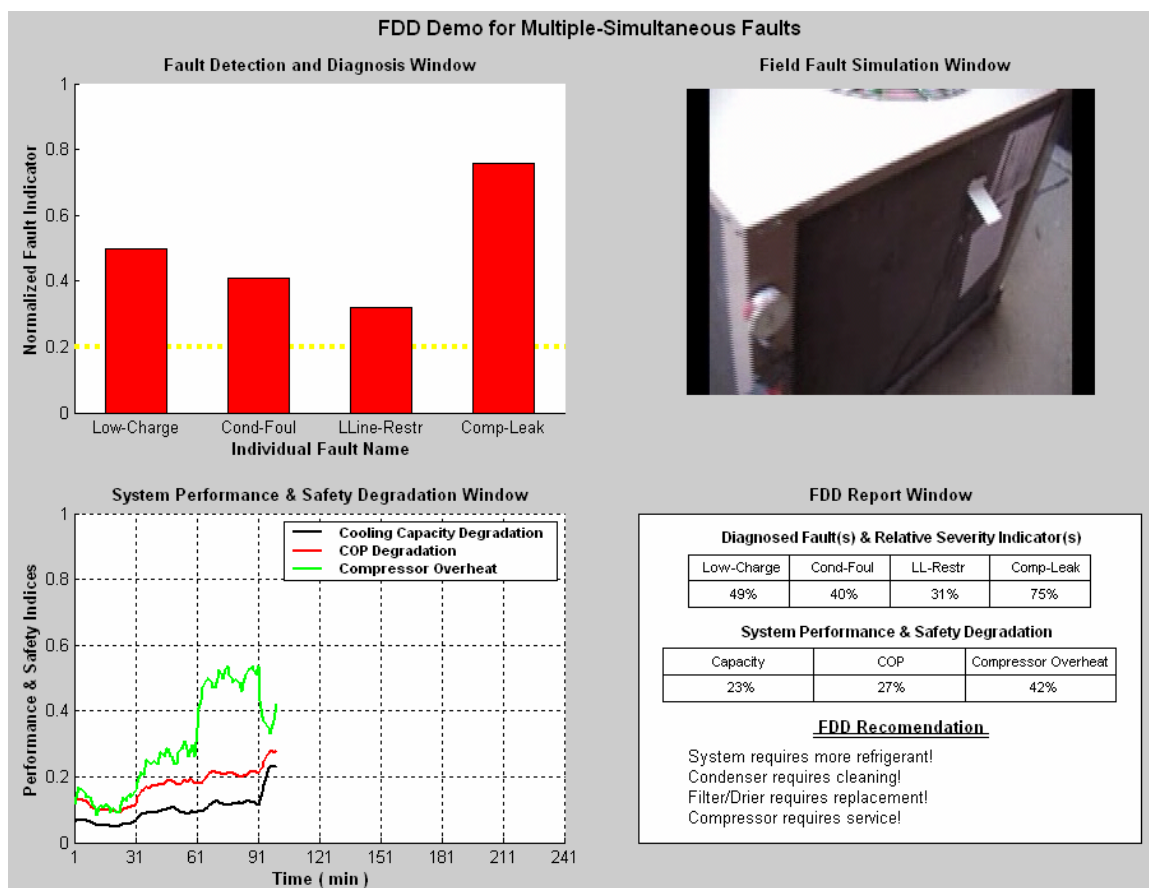


Figure 4-13 Illustration of Demo Movie

4.2.2.1 Field Fault Simulation Window (FFSW)

For easy access, four faults were artificially introduced: refrigerant low charge, condenser fouling, liquid line restriction and compressor leakage. Since it is not accurate to discharge refrigerant using the recovery system, the refrigerant low charge fault was simulated by charging less refrigerant to the system before running rather than discharging some refrigerant during operation. The fault simulation procedures were divided into the following two stages: added four faults one by one and removed faults one by one. Figure 4-14 illustrates the timeline of the fault simulation.

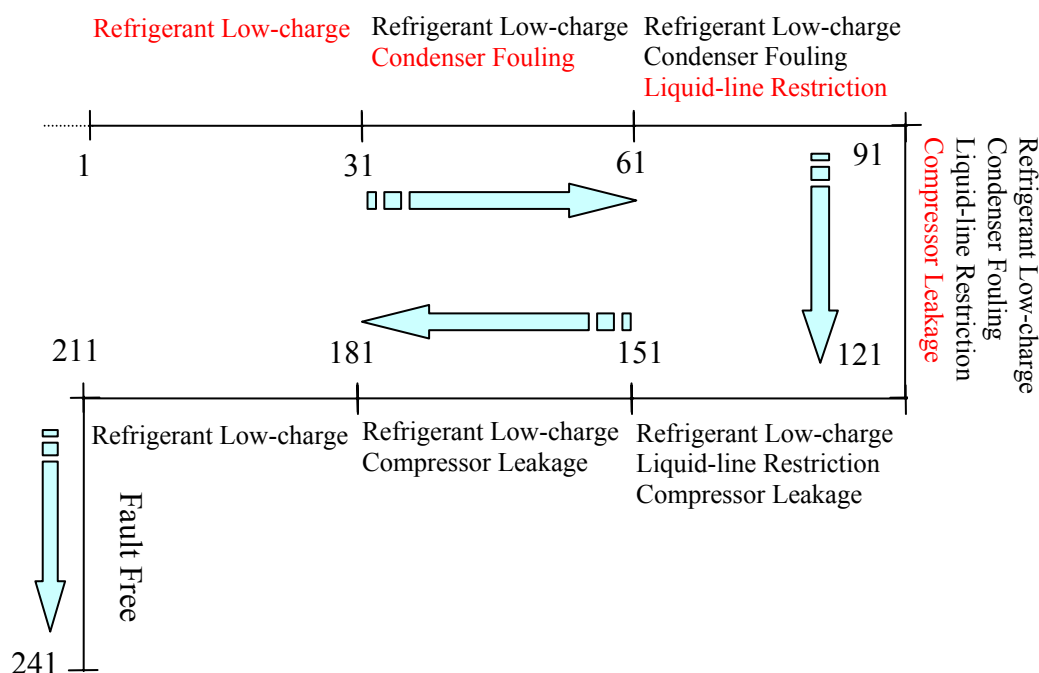


Figure 4-14 Timeline of the fault simulation in minutes.

The following steps describe the addition of faults:

1. Evacuated the system, and then charged the system up to eighty per cent of nominal refrigerant charge. The system ran for half an hour to reach steady state and then data were logged.
2. After logging half an hour of low charge data, the condenser fouling fault was added, by covering thirty per cent of condenser area using paper. At this time, there were two simultaneous faults in the system: refrigerant low charge and condenser fouling.
3. Half an hour later, a liquid line restriction fault was introduced by closing the restriction valve until a twenty psi pressure drop was caused. Three faults existed in the system simultaneously: refrigerant low charge, condenser fouling and liquid line restriction.
4. Half an hour later, a compressor leakage fault was introduced by opening the compressor bypass valve to let fifteen per cent of refrigerant mass flow rate bypass the compressor. At this time, four faults existed simultaneously in the system: refrigerant low charge, condenser fouling, liquid line restriction, and compressor leakage.
5. The following steps describe the removal of faults,
6. After the system ran for half an hour under four faults, the paper covering the condenser was removed. There existed three simultaneous faults in the system: refrigerant low charge, liquid line restriction, and compressor leakage, which is a different combination than step three.
7. Half an hour later, the liquid line restriction fault was removed by fully opening the liquid line restriction valve. At this time, refrigerant low charge and compressor leakage existed in the system, which is a different combination than step two.
8. Half an hour later, the compressor bypass valve was closed to remove compressor leakage fault. There was only refrigerant low charge fault in the system.
9. Finally, half an hour later, the system was charged up to a nominal refrigerant level. The system was supposed to run normally.

4.2.2.2 Fault Detection and Diagnosis Window (FDDW)

This window plots the normalized fault indicator for four individual faults using color bars: refrigerant low charge (Low-Charge), condenser fouling (Cond-Foul), liquid line restriction (LL-Restr), and compressor leakage (Comp-Leak).

The normalized fault indicator is the ratio of the current feature value to the predefined value, which is defined at an individual fault level causing 20% cooling capacity degradation.

$$\text{Normalized_Fault_Indicator} = \frac{\text{current_feature_value}}{\text{predefined_feature_value}}$$

Although the predefined fault level is arbitrary, the author believes that a fault causing 20% cooling capacity degradation is worthwhile to service. The normalized fault indicator indicates the relative severity of the individual faults. However, the refrigerant low charge is a system-level fault and its impact on overall system performance is not only determined by its own charge level but also other faults, so the indicator oscillates a lot. Fortunately, data collected so far shows that this oscillation does not change the decision of the fault detection and diagnosis method.

The normalized fault indicators are plotted using color bars. When an indicator is larger than the threshold, 0.2, it is plotted in red, otherwise in green. According to experience, an indicated fault level with a performance degradation less than $0.2 \times 20\% = 4\%$ is not reliable.

4.2.2.3 System Performance & Safety Degradation Window (SPSDW)

Capacity and COP are usually used as criteria to indicate system performance. The compressor is the most expensive part of the system and too much overheating would result in safety problems such as bad lubrication and motor short-circuit. So degradations of these three indices are plotted in this window. The capacity and COP degradations are defined by,

$$\frac{normal_value - current_value}{normal_value}$$

The normal value is predicted using an overall system performance model which is built based on system manufacturer rating data. The model inputs are condenser inlet air dry-bulb temperature and evaporator wet-bulb temperature.

The compressor overheat degradation is defined by,

$$\frac{current_T_{dis} - normal_T_{dis}}{max_ \Delta T_{dis}}$$

The maximum ΔT_{dis} is found to be around 40 F by Chen's data (2000), which should be confirmed by more investigation. There is difficulty to predict normal values for T_{dis} because there is no overall system state model available. For this demonstration, it is assumed that the system driving condition is not changed much and the measured value at the fault free condition is used as the normal value. Further research should be done later to find an inexpensive safety indicator for a compressor.

4.2.2.4 FDD Report Window (FDDRW)

To help customers make a decision whether to service the diagnosed fault or not, the FDD Report Window generates a tabular report for the FDD results including diagnosed faults and relative severity indicators and system performance and safety degradation indices, and provides an FDD recommendation. In this demo, the FDD recommendation is based on performance and safety degradation. If the performance degradation is over twenty per cent or the compressor is overheated up to ninety per cent, service is recommended. More investigation is needed for fault recommendation.

4.2.2.5 Output of the FDD Demonstration

This section provides sample outputs of the FDD demonstration after each fault was added and removed (watch the movie for details). Figure 4-15 captures a movie frame when the system was running at low refrigerant charge (step 1 of section 4.2.3.1). The FDDW indicates that there existed a refrigerant low charge fault whose fault severity was around 0.45. The SPSDW plots the overall degradations, all of which were less than 20%. The FDDRW summarizes indicators and generates the FDD report table and recommended that “although there is (are) fault(s) with minor impacts on overall system performance, it may be not worthwhile to service so far”.

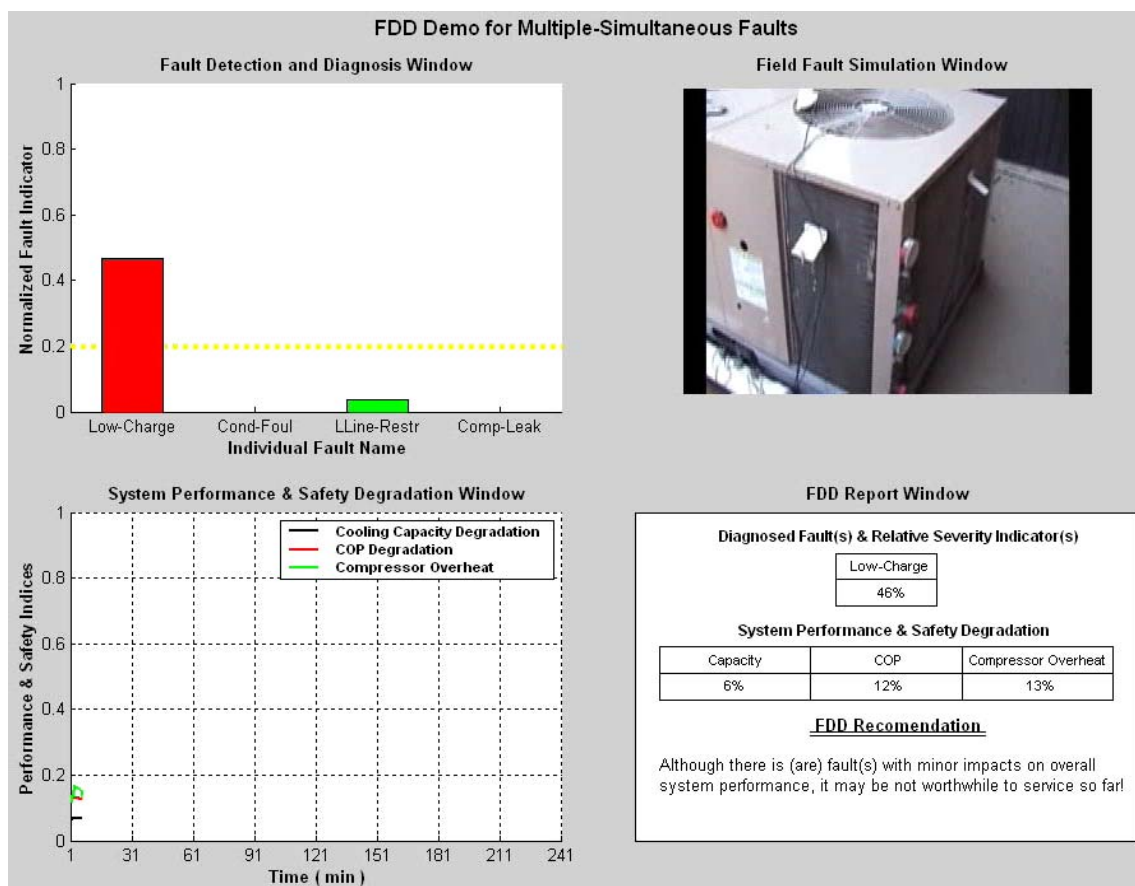


Figure 4-15 Outputs of the FDD demonstration after introduction of low refrigerant charge fault

Figure 4-16 shows one frame after 30% of the condenser area was covered by paper (step 2 of section 4.2.3.1). The FFSW shows that some part of the condenser area was covered by paper. FDDW indicates that there existed two faults: refrigerant low charge with the fault severity around 0.45 and condenser fouling with the fault severity around 0.4. Since the overall performance degradations were less than 20% at this moment (see SPSDW and FDDRW), service was not recommended (see FDDRW).

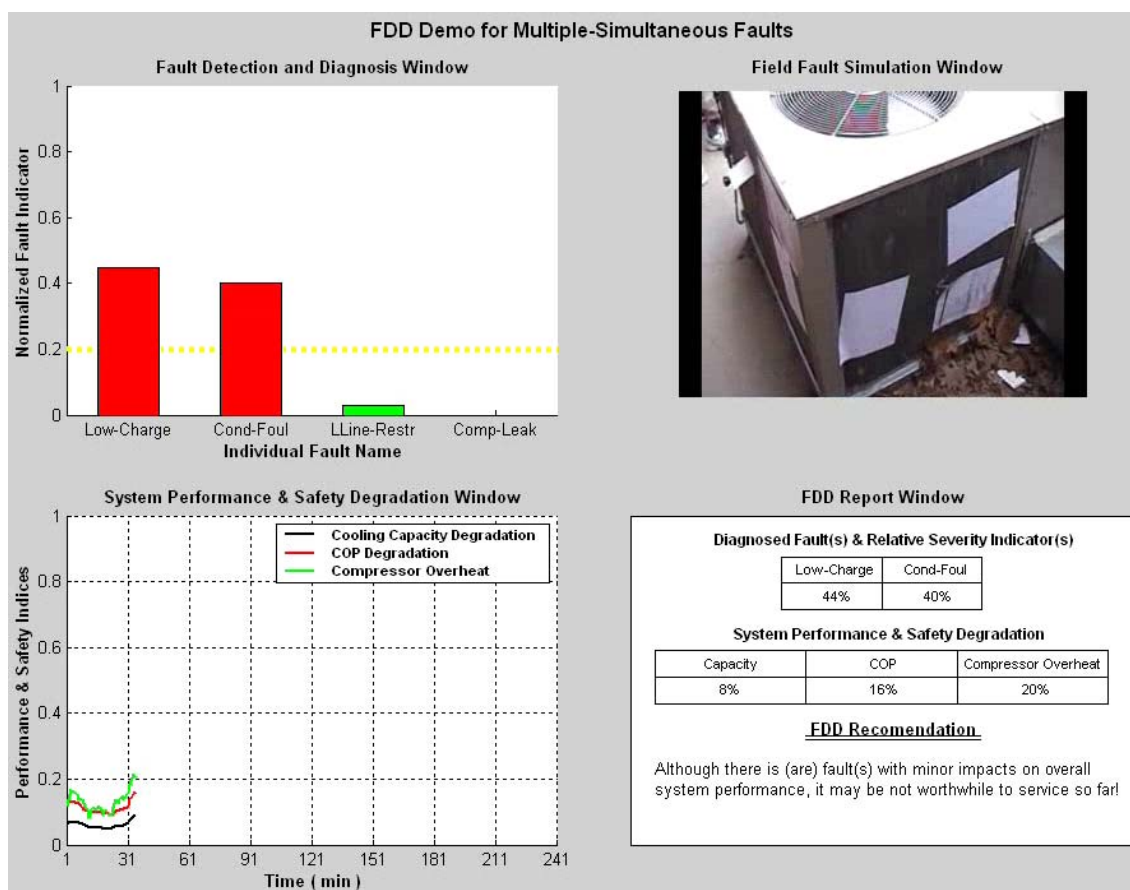


Figure 4-16 Outputs of the FDD demonstration after introduction of condenser fouling fault

Figure 4-17 shows one frame after the liquid line restriction fault was introduced by closing the restriction valve until a twenty psi pressure drop was caused (step 3 of section 4.2.3.1). The final position of the restriction valve can be seen from the FFSW (see Figure 4-20 for the fully opening position). FDDW indicates that there existed three

simultaneous faults: refrigerant low charge with the fault severity over 1.0, condenser fouling with the fault severity around 0.5 and liquid line restriction fault with the severity around 0.35. Since refrigerant charge fault is a system-level fault whose indicator was impacted by other faults, the refrigerant low charge indicator value increased after the liquid line restriction fault was introduced. Since the COP was degraded 21% at this moment (see SPSDW and FDDRW), FDDRW recommended that: the system requires more refrigerant, the condenser requires cleaning and the filter/drier requires replacement. Although every individual fault was not severe enough to cause more than a 20% performance degradation, the combination of three simultaneous faults aggravated overall system performance degradations.

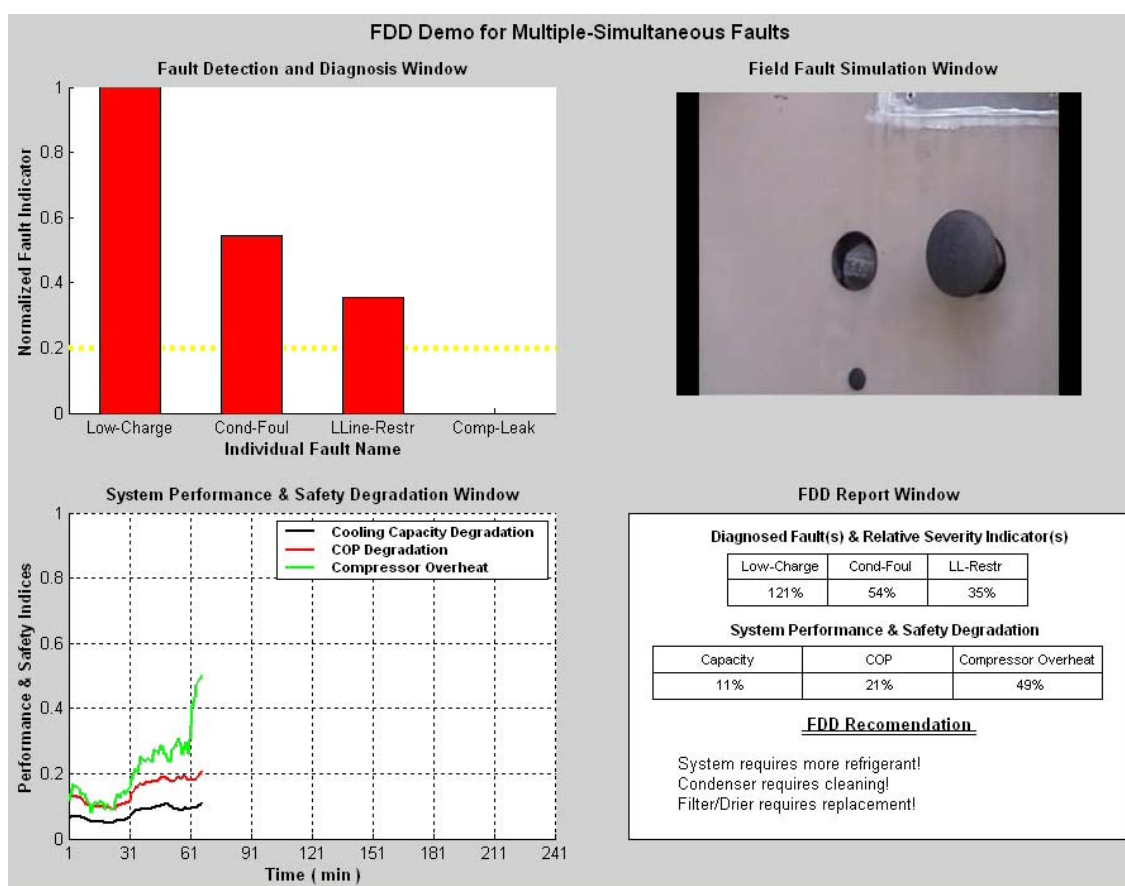


Figure 4-17 Outputs of the FDD demonstration after introduction of liquid line restriction fault

Figure 4-18 shows one frame after the compressor leakage fault was introduced by opening the discharge bypass valve until about 15% of refrigerant mass flow rate was reduced (step 4 of section 4.2.3.1). FDDW indicates that there existed four simultaneous faults: refrigerant low charge with the fault severity over 0.70, condenser fouling with the fault severity around 0.5, liquid line restriction fault with the fault severity around 0.35 and compressor leakage fault with the fault severity around 0.5. Since the COP was degraded 24% at this moment (see SPSDW and FDDRW), FDDRW recommended that: the system requires more refrigerant, the condenser requires cleaning, the filter/drier requires replacement and the compressor requires service.

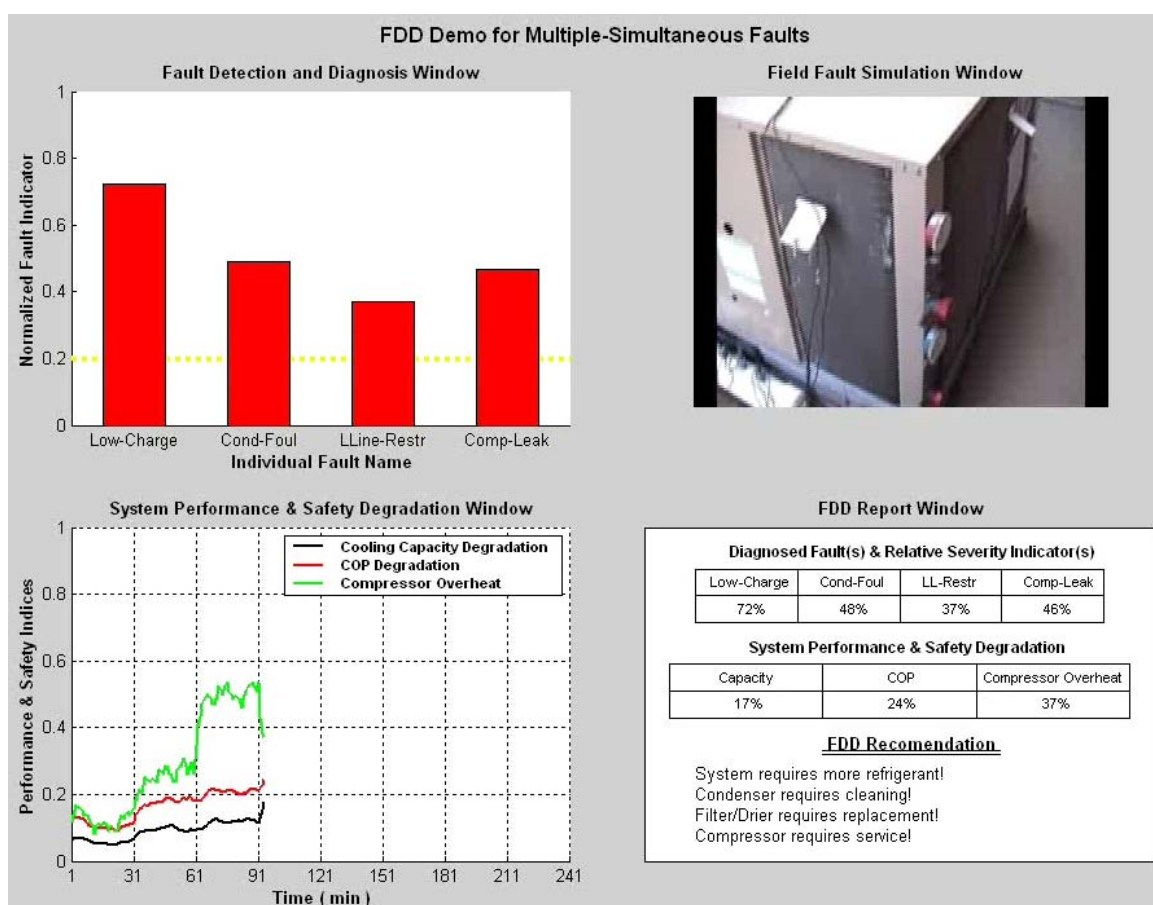


Figure 4-18 Outputs of the FDD demonstration after introduction of compressor leakage fault

Figure 4-19 shows one frame after the condenser fouling fault was removed (step 5 of section 4.2.3.1). It can be seen from FFSW that the paper covering the condenser was removed. FDDW indicates that there existed three simultaneous faults: refrigerant low charge with the fault severity over 0.60, liquid line restriction fault with the fault severity around 0.3 and compressor leakage fault with the fault severity around 0.8. Since both cooling capacity and COP were degraded 21% at this moment (see SPSDW and FDDRW), FDDRW recommended that: the system requires more refrigerant, the filter/drier requires replacement and the compressor requires service.

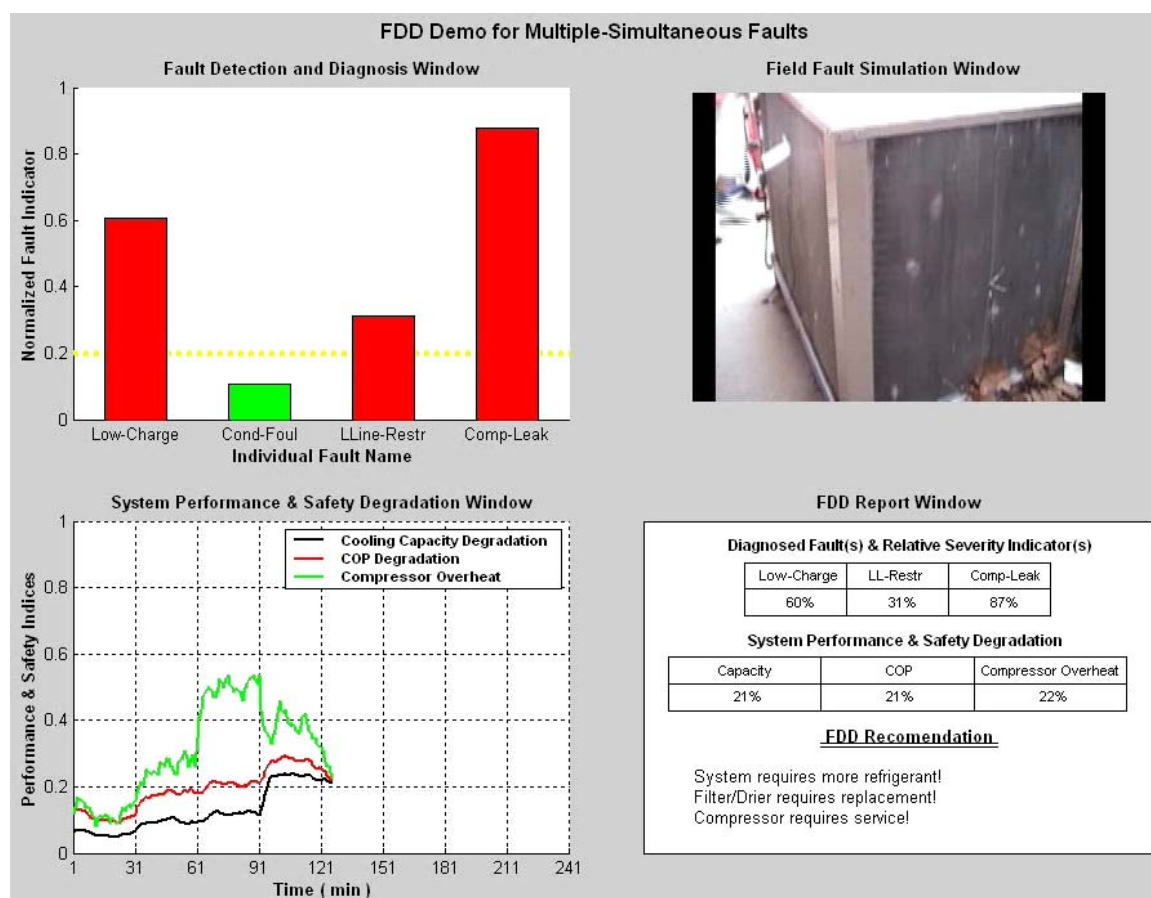


Figure 4-19 Outputs of the FDD demonstration after removal of condenser fouling fault

Figure 4-20 shows one frame after the liquid line restriction fault was removed by opening the liquid line restriction valve (step 6 of section 4.2.3.1). The final restriction

valve position can be seen from FFSW (refer to Figure 4-17 for the fully closing position). FDDW indicates that there existed two simultaneous faults: refrigerant low charge with the fault severity over 0.35 and compressor leakage fault with the fault severity around 0.8. Since COP was degraded 20% at this moment (see SPSDW and FDDRW), FDDRW recommended that the system requires more refrigerant and the compressor requires service.

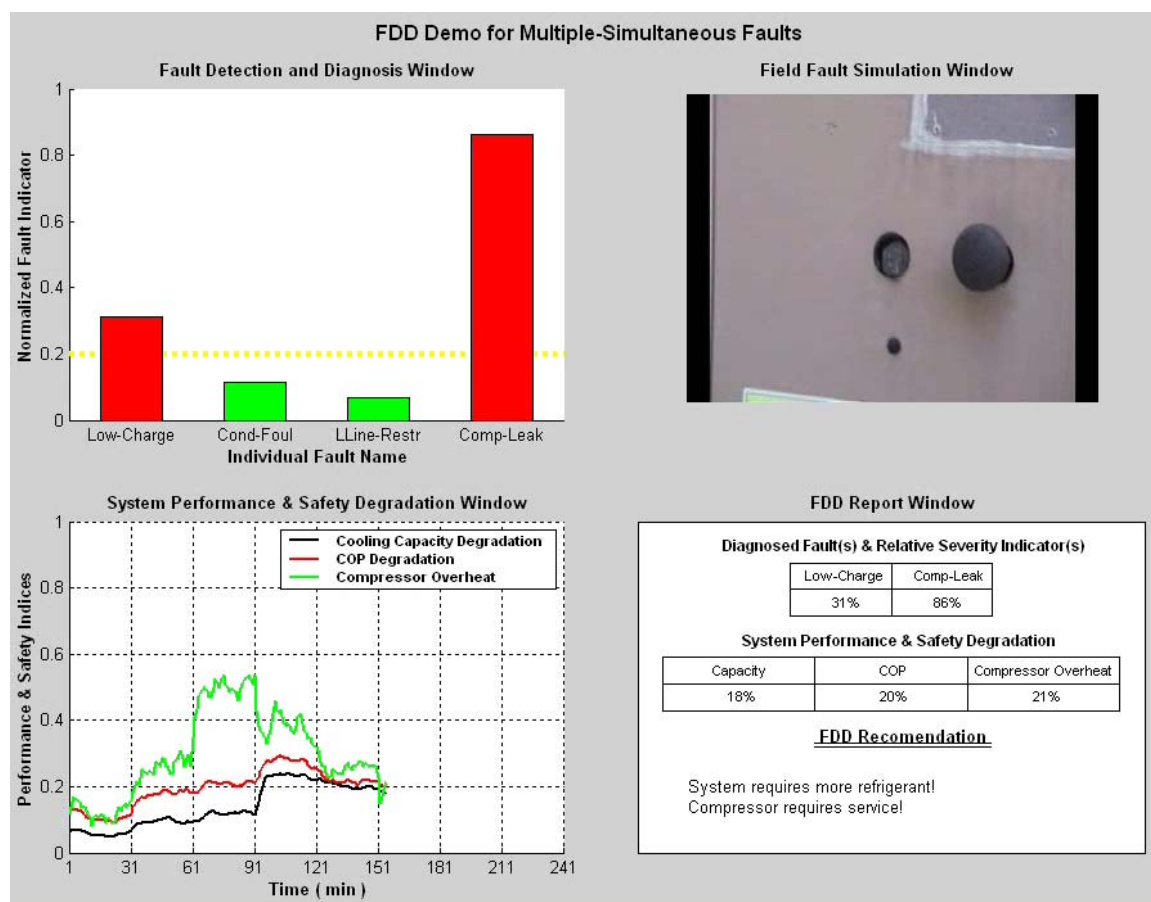


Figure 4-20 Outputs of the FDD demonstration after removal of liquid line restriction fault

Figure 4-21 shows one frame after the compressor leakage fault was removed by closing the discharge line bypass valve (step 7 of section 4.2.3.1), which was restored to step 1 of section 4.2.3.1. FDDW indicates that there existed one fault, refrigerant low

charge with the fault severity over 0.45. Since the overall performance degradation was less than 20% at this moment (see SPSDW and FDDRW), no service is recommended.

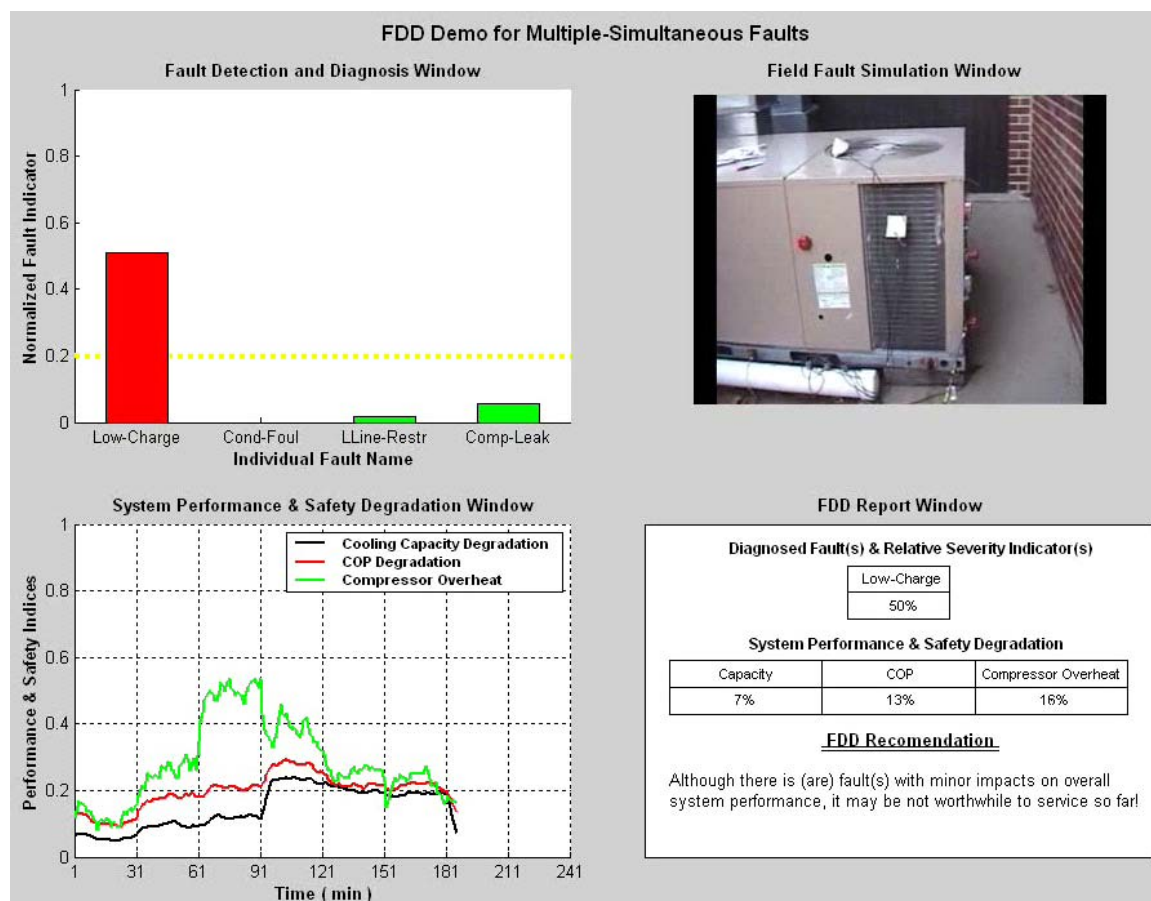


Figure 4-21 Outputs of the FDD demonstration after removal of compressor leakage fault

Figure 4-22 shows one frame after the system was charged up to the nominal level. FDDW indicates that there existed no fault. FDDRW reported that the system was running normally.

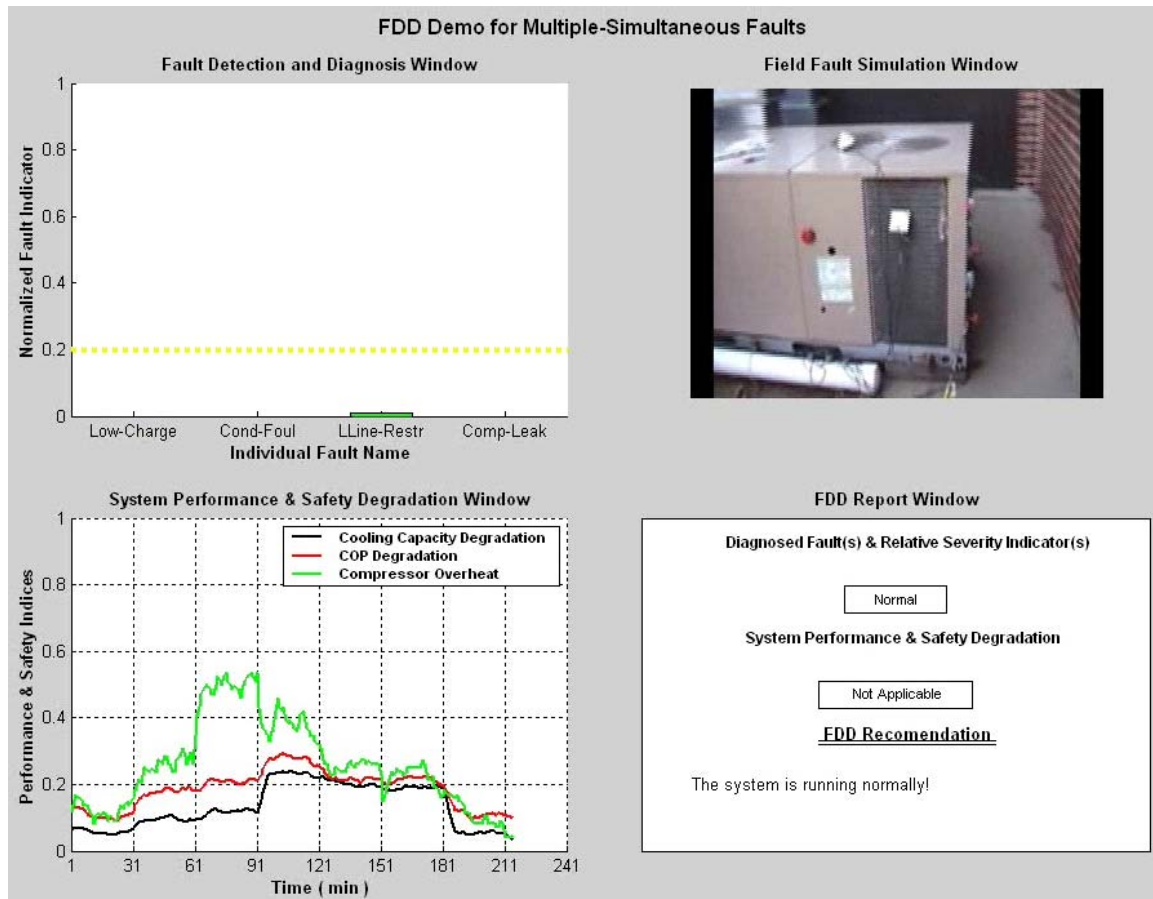


Figure 4-22 Outputs of the FDD demonstration after removal of low refrigerant low charge fault

4.2.3 Results for California Field Sites

Section 4.2.1 validated the decoupling scheme using laboratory data and section 4.2.2 demonstrated the whole approach by artificially introducing faults at the Purdue field emulation site. This section applies the FDD approach to California field sites. Section 4.2.3.1 presents detailed results for one example site, Milpitas McDonalds restaurant, and section 4.2.3.2 summarizes the FDD results for other sites.

4.2.3.1 Milpitas McDonalds Field Site

This site is located in Oakland, California. A 6-ton York rooftop unit is installed for this McDonalds restaurant. A Copeland scroll compressor and a TXV are used in this RTU. Data collected from April to October in 2002 were used to do FDD. After filtering the transient data by a steady-state detector and removing the bad data corrupted by the acquisition equipment, 1119 data points (one data point every five minutes) were retained. Since the RTU has been installed for several years, faults have been fully developed. Unlike the Purdue field emulation site, results of this site are presented in the statistical sense. That is, histogram bar plots are used to present the results.

Figure 4-23 plots the normalized fault indicator for a liquid-line restriction fault. It can be seen that all the steady-state data points are located at the right of the red dotted line, FDD threshold (0.2) and the mean value is around 0.8. That is, all steady-state points indicate that the liquid-line is restricted. Most likely the filter or drier is clogged by debris. If this fault happened individually, it would result in about a 16% cooling capacity degradation.

Figure 4-24 plots the normalized fault indicator for refrigerant charge faults. Similar to Figure 4-23, all the steady-state data points are located at the right of the FDD threshold and the mean value is about 1.6, which means that the system charge is very low. If this fault happened individually, it would result in about 32% cooling capacity degradation. However, since refrigerant charge faults are system level faults, their indicator is impacted by other faults.

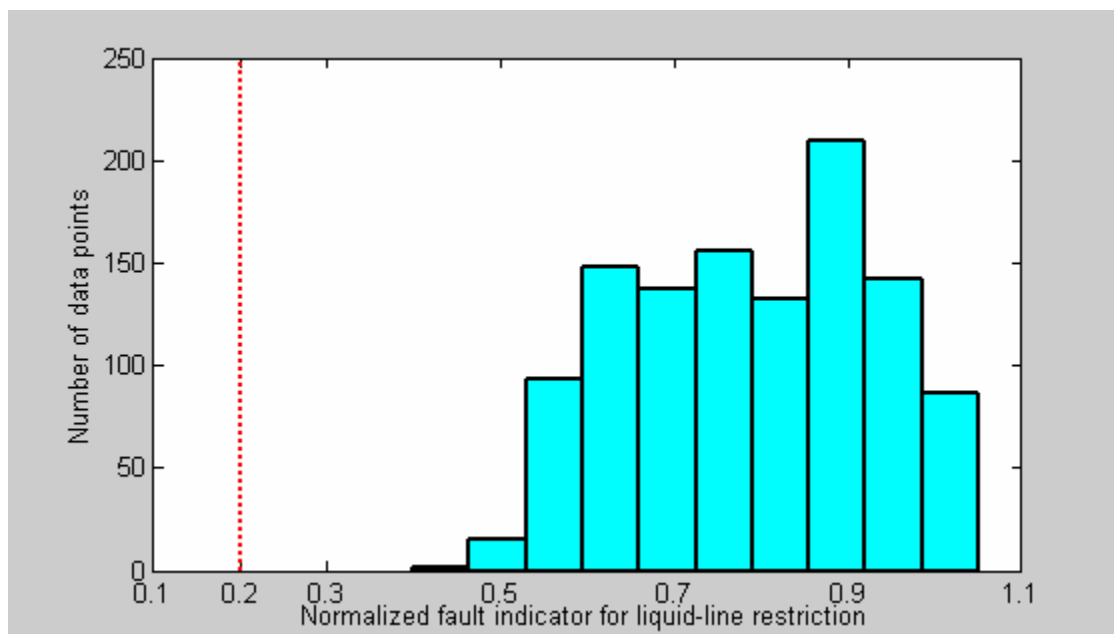


Figure 4-23 Histogram bar plot of the normalized fault indicator for liquid line restriction

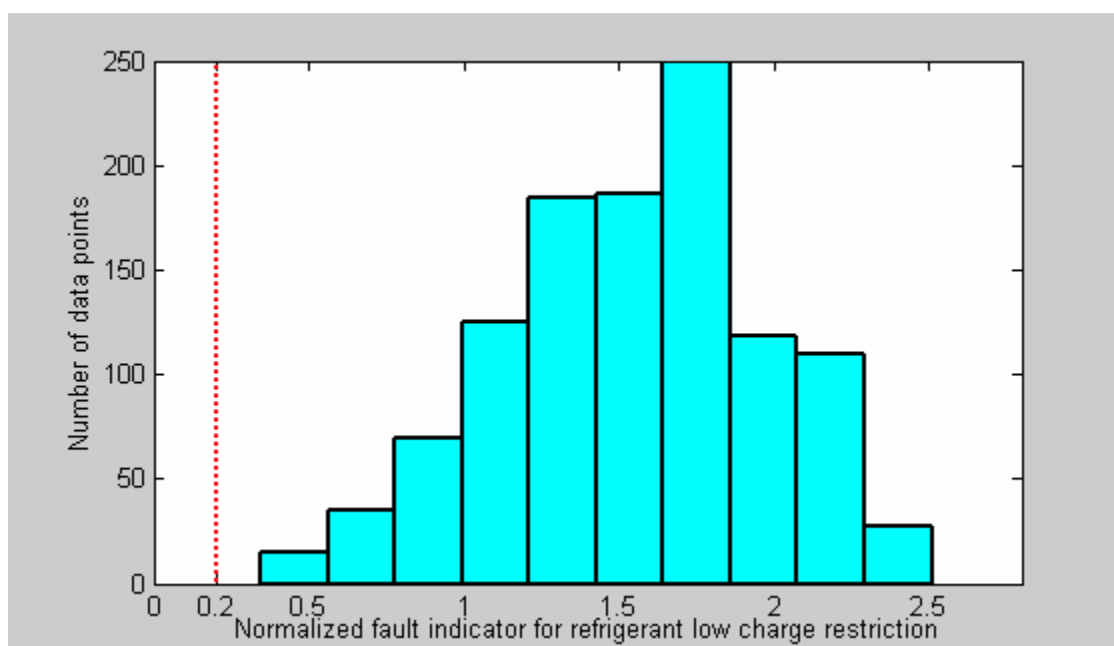


Figure 4-24 Histogram bar plot of the normalized fault indicator for refrigerant low charge

Figure 4-25 plots the normalized fault indicator for a condenser fouling fault. It can be seen that most of the steady-state data points (>95%) are at the right of the FDD threshold and the mean value is about 0.5, which indicates that the condenser is a little dirty. If this fault happened individually, it would result in about 10% cooling capacity degradation.

Figure 4-26 plots the normalized fault indicator for a compressor valve leakage fault. It can be seen that all the steady-state data points are at the left of FDD threshold and the mean value is about -0.7, which indicates that the compressor works properly and the compressor has about 15% heat loss. However, according to heat transfer analysis and our experience with laboratory data, compressors installed in York and Trane RTUs have very small heat, less than 5% of the power input and even gain some heat at some operating conditions. The explanation for this discrepancy is probably that the discharge line temperature is not measured accurately using the RTD temperature sensor. Deliverable 2.1.5 discusses the RTD measuring issue and presents a correction approach. However, Figure 4-26 shows that the discharge line temperature is not corrected accurately as well, which is because the sensor is not installed properly.

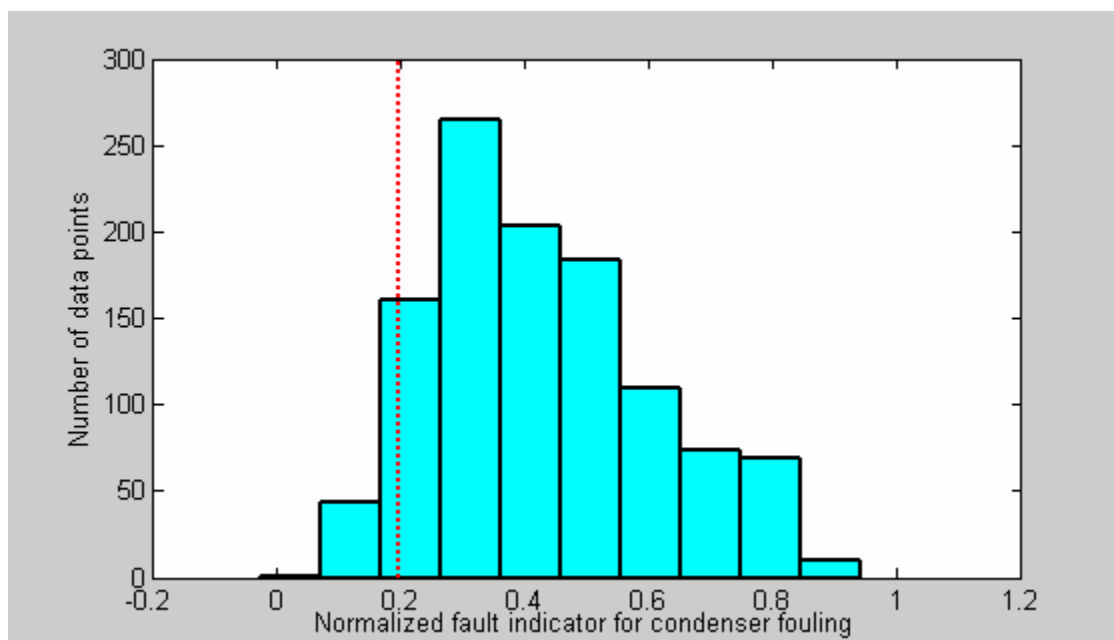


Figure 4-25 Histogram bar plot of the normalized fault indicator for condenser fouling

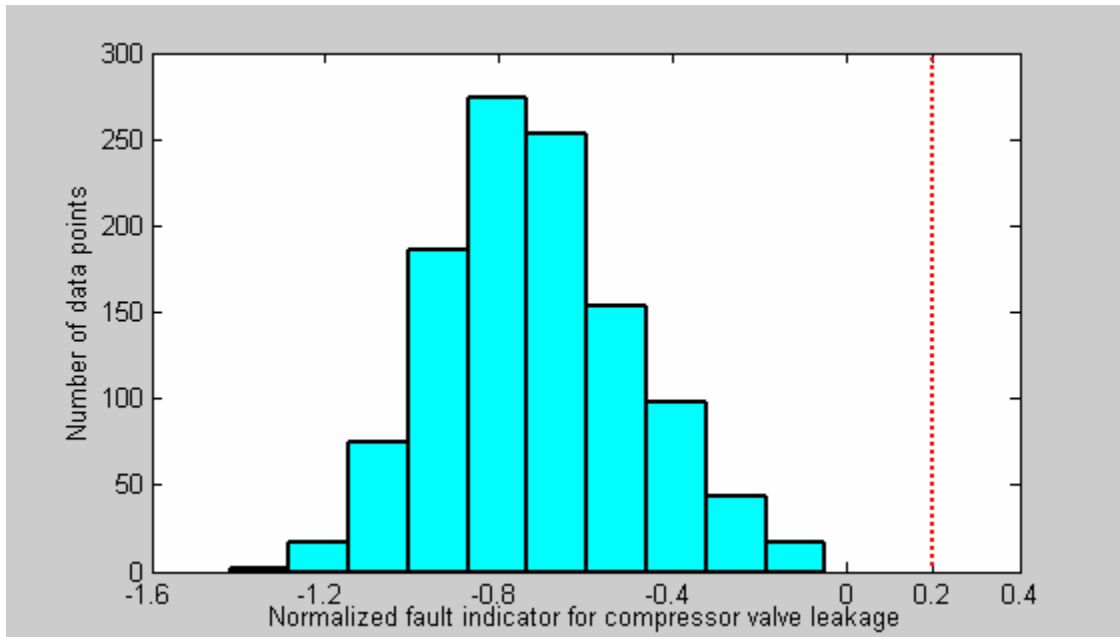


Figure 4-26 Histogram bar plot of the normalized fault indicator for compressor valve leakage

In summary, the system has three faults, low refrigerant charge, liquid line restriction and condenser fouling. To assess the impact of the diagnosed faults on the overall system performance, Figure 4-27 plots the cooling capacity degradation. It can be seen that the system cooling capacity was degraded 23~45% and the average is about 32%, which is coincident with the value indicated by refrigerant charge fault indicator. The cooling capacity degradation can be confirmed by investigating the return air temperature and system running time. It can be seen from Figure 4-28 that the average return air temperature is around 78 F and the highest is 88 F, which does not satisfy the comfort criteria. From Figure 4-29, it can be seen that the system kept running continuously for a long time (average is 2.5 hours and maximum is up to 9 hours) in order to remove the heat load. So, from the comfort criteria, service should be done to correct the diagnosed faults in order to maintain comfort.

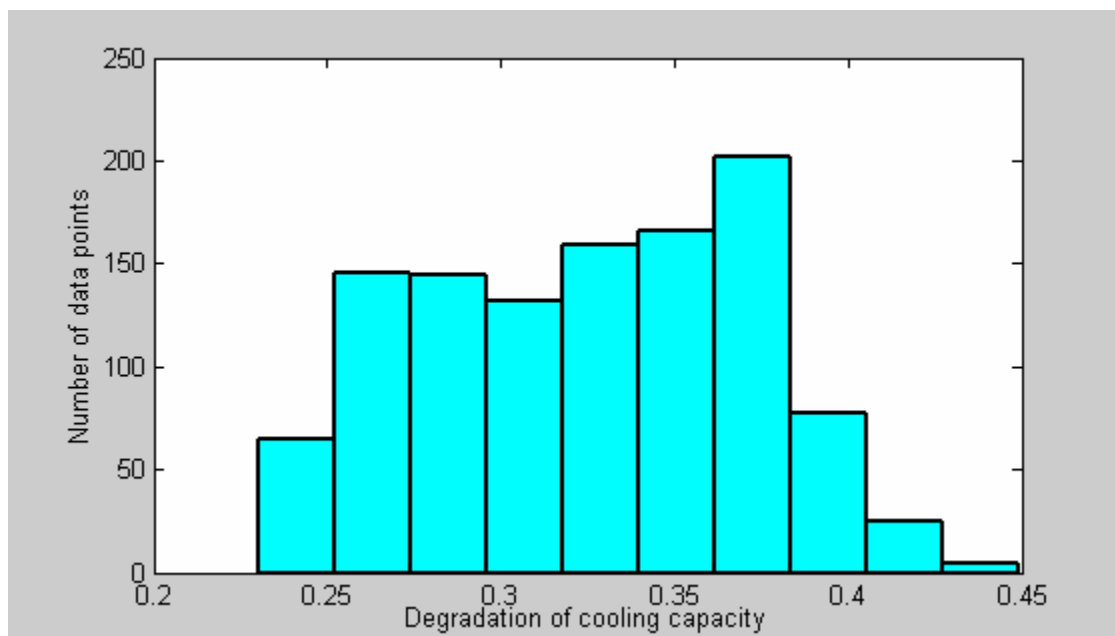


Figure 4-27 Histogram bar plot of the normalized fault indicator for cooling capacity degradation

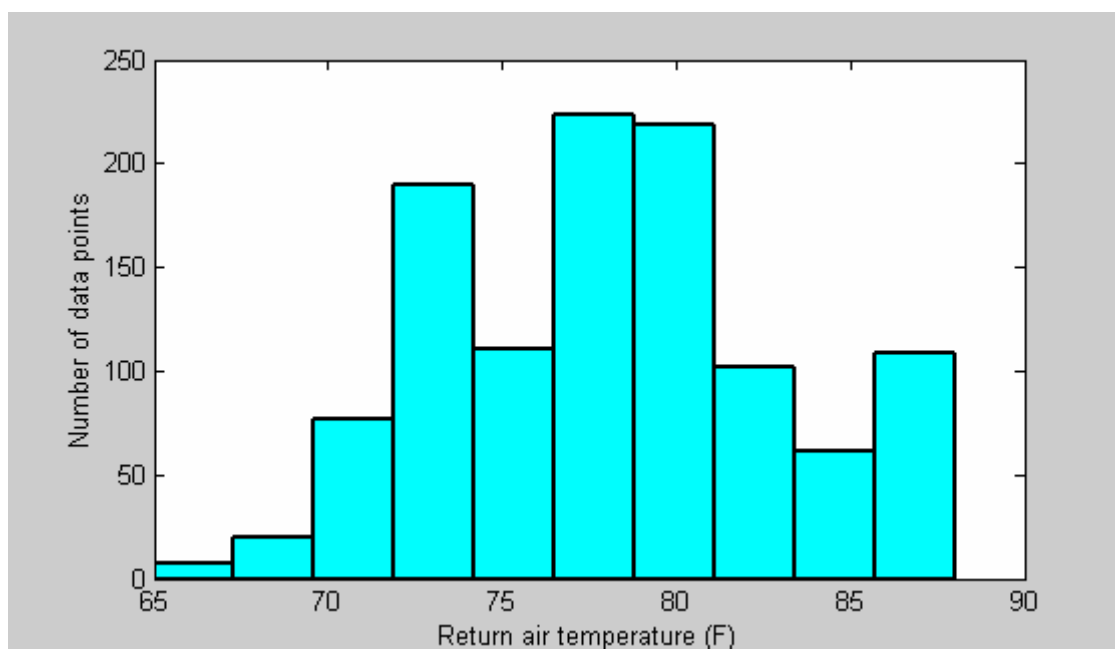


Figure 4-28 Histogram bar plot of the return air temperature

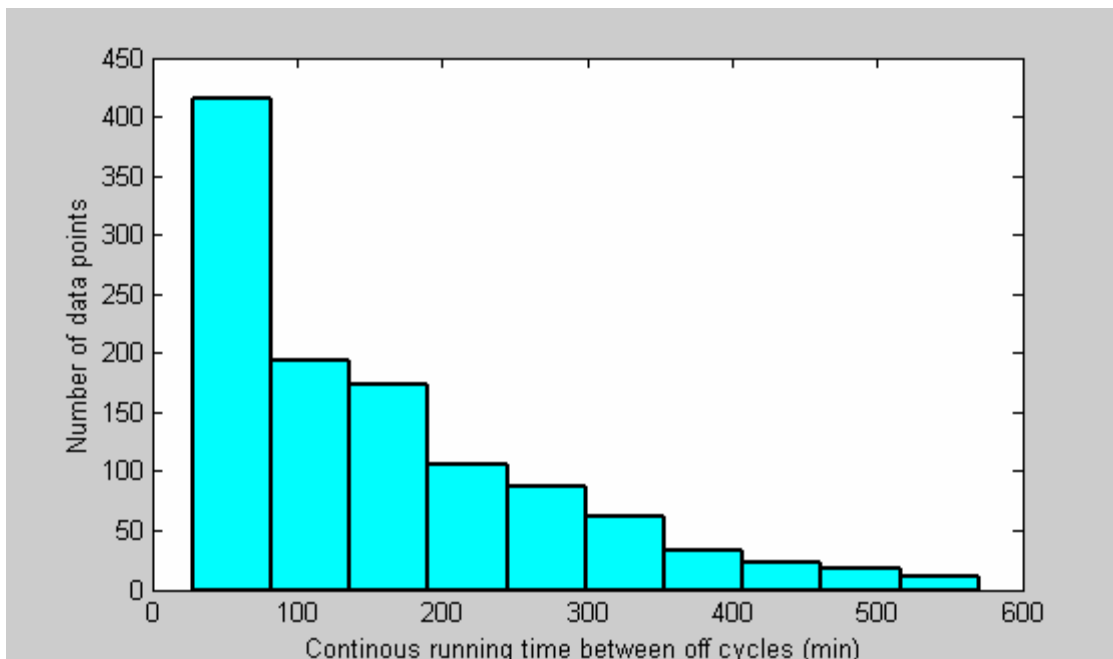


Figure 4-29 Histogram bar plot of the continuous running time between off-cycles of the RTU

In addition to the comfort criteria, Figure 4-30 plots an economic criterion, EER degradation. It can be seen that the system EER degraded about 10~40%, which depends on the operating conditions. Compared with the cooling capacity degradation, the EER degradation was a little smaller. This is because the power consumption was reduced a little but less than the degradation of cooling capacity when the refrigerant mass flow rate was reduced due to faults. Figure 4-31 plots the system power consumption reduction. The average power consumption reduction is about 15%, which is smaller than the average cooling capacity degradation of 32%. In sum, the average EER degradation is 21%, which is a pretty large economic loss. A rough and conservative estimate in Chapter 5 shows that a direct operation savings would be \$252/year for this economical application (in North California), which does not consider the dangerous impact of faults on compressor safety (cost about \$1000 to replace a compressor). Since multiple-service costs to add some refrigerant, replace the filter/drier, and clean the condenser are around \$500, service to correct the faults is justified. In summary, from both comfort and economic criteria, it is justified to correct the diagnosed faults as soon as possible.

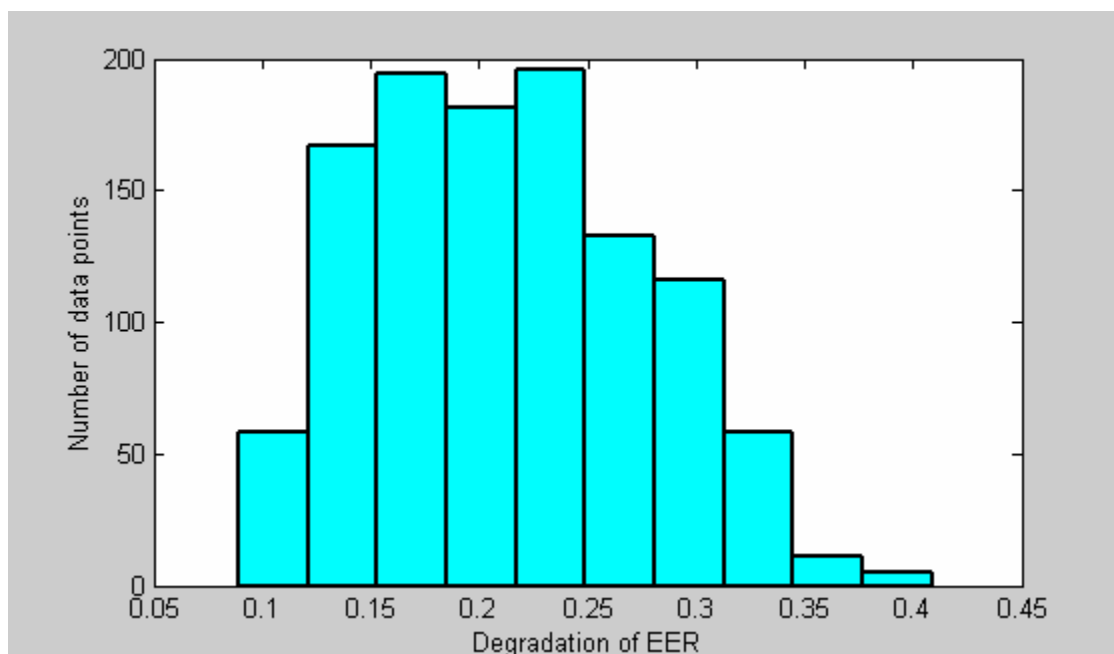


Figure 4-30 Histogram bar plot of the normalized fault indicator for EER degradation

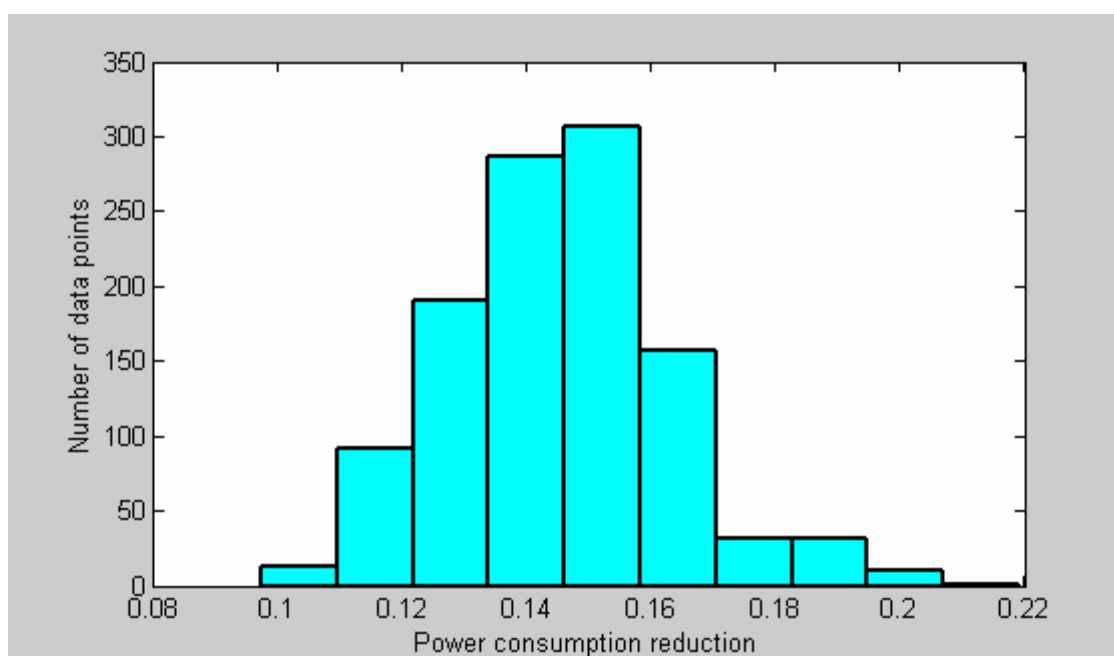


Figure 4-31 System power consumption reduction

4.2.3.2 Summarized Results for Other Sites

Since some necessary information about compressor and TXV and system configuration is not available so far, the decoupling-based FDD approach was partially applied to the other sites. Comprehensive FDD results and economic assessment will be provided after all the necessary information is obtained. Similar to Milpitas site, data collected from April to October in 2002 were used to do analysis for the following sites except for the Walgreens Anaheim site, which is based on data collected in 2003.

There are two modular school sites at Woodland and Oakland. At each site there are two 3.5-ton Bard wall-mounted heat-pump RTUs (WH421-A). Table 4-1 summarizes the FDD results for these two sites.

Table 4-1 FDD results of Modular School sites

Faults	Woodland		Oakland	
	RTU1	RTU2	RTU1	RTU2
Refrigerant Charge	Normal	Normal	Normal	Over Charge
Liquid-line Restriction	Restriction	Severe Restriction	Restriction	Normal
Evaporator Fouling	Normal	Normal	Normal	Fouling
Recommended Service	Not yet	Arrange Service	Not yet	Arrange Service

Similar to the Milpitas McDonalds site, the Bradshaw McDonalds site uses a 6-ton York RTU. Both Castro Valley and Watt Avenue McDonalds sites have two York two-stage RTUs, but only one RTU in each site was configured for FDD investigation (one is 10 tons and the other is 11 tons). Table 4-2 summarizes the FDD results for these three McDonalds sites.

There are five Trane heat-pump RTUs (one is 6.25 tons and other four are 7.25 tons) installed at the Walgreens Rialto and Anaheim sites. Tables 4-3 and 4-4 summarize the FDD results for these sites.

Table 4-2 FDD results of McDonalds Restaurant Sites

Faults	Bradshaw	Castro Valley		Watt Avenue	
		Stage 1	Stage 2	Stage 1	Stage 2
Refrigerant Charge	Low Charge	Normal	Normal	Low Charge	Normal
Liquid-line Restriction	Restriction	Normal	Normal	Normal	Normal
Recommended Service	Arrange Service	NA	NA	Not yet	NA

Table 4-3 FDD results of Walgreen Retail Store Sites at Rialto

	RTU1	RTU2	RTU3	RTU4	RTU5
Refrigerant Charge	Extremely Low Charge	Low Charge	Normal	Normal	Over Charge
Liquid-line Restriction	Normal	Small Restriction	Normal	Normal	Normal
Recommended Service	Require Service	Arrange Service	NA	NA	Not yet

Table 4-4 FDD results of Walgreen Retail Store Sites at Anaheim

	RTU1	RTU2	RTU3	RTU4	RTU5
Refrigerant Charge	Low Charge	Low Charge	Normal	Low Charge	Normal
Liquid-line Restriction	Small Restriction	Severe Restriction	Small Restriction	Small Restriction	Small Restriction
Recommended Service	Arrange Service	Require Service	Not yet	Arrange Service	Not yet

In summary, initial investigation shows that faults happen very frequently at the field sites. For example, eleven of the twenty-one investigated RTUs have liquid line restriction faults, ten of them have refrigerant charge faults, and eight of them have more than two simultaneous faults. Nine of the twenty-one investigated RTUs justify service immediately.

5 ECONOMIC ASSESSMENTS

Since the primary consequences of faults in HVAC systems are economic, FDD systems must be assessed based upon economic considerations. In order to performed economic assessments, the following factors should be considered:

1. RTU systems are relatively inexpensive, around \$750-1000 per ton for installed equipment. A 6-ton RTU only costs about \$5000. As a result, it is difficult to persuade RTU manufacturers or customers to spend an additional \$300 for an automated FDD.
2. Utility costs are not very significant compared to other costs for a business. For the northern California McDonalds sites, the monthly utility costs for a 6-ton RTU are about \$100. For the southern California Walgreens site, the monthly costs are around \$600.
3. Service costs are very high, \$115 for each visit plus \$60/hour (\$50~75/hour) for service. For example, a three-hour service visit costs \$295.

In order to perform economic assessments, the following assumptions were employed:

1. Service is required whenever the RTU cannot maintain comfort due to the presence of one or more faults. This assumption implies that there is a high cost associated with not maintaining comfort.
2. For a given building over a given time period, the cooling load is independent of whether an RTU fault exists.
3. A technician will only detect and diagnose severe and obvious faults. In the absence of preventative maintenance, technicians would typically be called to

perform emergency service when an air conditioner is not working or is unable to maintain comfort. Even if preventive maintenance is performed, the procedures only involve routine checks that can only detect severe and obvious faults. According to the analysis of California site data, some systems degraded significantly due to faults which were not detected during preventive maintenance service.

4. Compared with service costs, most HVAC hardware replacement costs are small (with the exception of a faulty compressor). A liquid line filter/drier costs around \$15, while the labor fee for replacement costs about \$300. An evaporator filter costs around \$2, while the labor fee for replacement costs \$30. R-22 refrigerant costs less than \$2/lb, while leak checking plus recharging costs more than \$400.
5. An automated FDD technique can detect and diagnose common faults, which has been demonstrated through laboratory and field tests.

Based on the above assumptions, the following sections analyze the potential savings associated with FDD.

5.1 Preventive Maintenance Inspection Savings (PMIS)

According to discussions with service technicians, regular preventive maintenance inspections are often applied to RTU systems for commercial use. Table 5-1 lists the costs of planned preventative maintenance inspections done by a technician. These costs only cover inspections and some easy maintenance. Power washing of condenser and evaporator coils is quoted separately. It can be seen that the average annual planned maintenance inspection costs are around \$270.

If an automated FDD system were applied, most (e.g, 75%) of the planned preventative maintenance inspection fees of \$270 would be saved. If the average equipment life for an RTU is 10 years, then the life-long preventive maintenance

inspection savings would be \$2,027 per RTU. This is a significant initial savings for FDD, which is usually not considered.

Table 5-1 Planned Preventive Maintenance Costs

Location	No. of RTU	Total Annual Costs (\$)	Costs per Inspection (\$)	Annual Costs per RTU (\$)
1	4	1,119.00	279.75	279.75
2	5	1,377.00	344.25	275.40
3	6	1,635.00	408.75	272.50
4	7	1,893.00	473.25	270.43
5	8	2,151.00	537.75	268.88
6	9	2,409.00	602.25	267.67
7	10	2,667.00	666.75	266.70
8	11	2,925.00	731.25	265.91
9	12	3,183.00	795.75	265.25

5.2 Operating Cost Savings (OCS)

Many systems are affected by faults that are not detected during preventive maintenance inspections and that lead to significant system performance degradations. For example, Proctor and Downey (see Levins, Rice, and Baxter, 1996) investigated refrigerant charge levels in residential systems in California:

1. One study found that 31% of the units were undercharged and 69% were either properly charged or overcharged.
2. Another study in 1990-1991 found that about 60% of the units were undercharged or overcharged, and 40% were properly charged.
3. A third study found 22% undercharged units, 33% overcharged units, and 45% properly charged units.

According to our initial investigation of California field sites, fifteen of the twenty-one systems (71%) are significantly impacted by faults: eleven (52%) have filter/drier restrictions, ten (48%) have refrigerant charge fault, and eight have (38%) have both low charge and filter/drier restriction faults. As an example, the EER and cooling capacity of the RTU at the Milpitas site degraded 21% and 30%, respectively.

5.2.1 Utility Cost Savings (UCS)

Figure 5-1 illustrates the interrelationship among the system performance indices and other factors. Generally speaking, the total cooling load of a specific building over a specific time period, Q_{Load} , is independent of the RTU cooling capacity, \dot{Q}_{Cap} , and its operating status (fault or normal) as long as comfort conditions are maintained. However, cooling capacity is very dependent on operating status (fault or normal). So, in order to satisfy the cooling load, the RTU run time varies according to whether a fault exists or not. If cooling capacity degrades due to one or more faults, the RTU must operate longer.

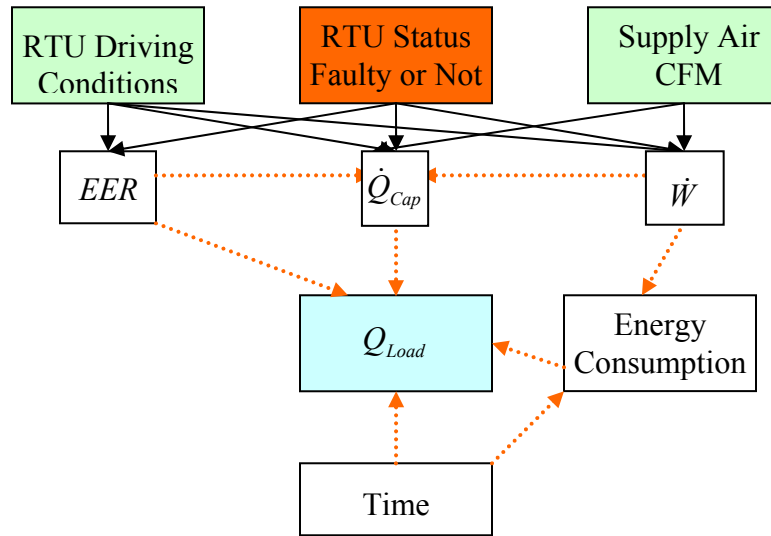


Figure 5-1 Interrelationship among different factors affecting RTU performance

In order to estimate the impact on utility costs, the cooling load is related to the average cooling capacity and total runtime according to equation (5-1).

$$Q_{Load} = \bar{\dot{Q}_{Cap}} \times T \quad (5-1)$$

Power consumption, \dot{W} , is also highly dependent on operating status (fault or normal). The relationship between EER , \dot{W} and \dot{Q}_{Cap} is given by equation (5-2).

$$\dot{Q}_{Cap} = \dot{W} \times EER \quad (5-2)$$

The energy consumption is estimated as the product of the average power consumption (\bar{W}) and the runtime (T) for mechanical cooling/heating according to equation (5-3).

$$E = \bar{W} \times T \quad (5-3)$$

Substituting equations (5-1) and (5-2) into equation (5-3) gives

$$E = \frac{Q_{Load}}{EER} \quad (5-4)$$

If the EER were degraded by a factor of α ($EER_{fault} = (1 - \alpha)EER_{Normal}$), then the energy consumption would increase by a factor of $\frac{\alpha}{1 - \alpha}$. For example, if the EER degraded 21%, the energy consumption would increase 26.6%. In other words, if faults were corrected the energy savings would be 26.6%. In general, the maximum energy savings associated with maintaining the equipment at normal performance levels are

$$E_{Savings} = \frac{\alpha}{1 - \alpha} \times E = \frac{\alpha}{1 - \alpha} \times \frac{Q_{Load}}{EER_{Normal}} \quad (5-5)$$

The cooling load can be related to the cooling capacity and run time according to

$$Q_{Load} = \dot{Q}_{Cap,Normal} (1 - \beta)T \quad (5-6)$$

where β is a degradation factor for cooling capacity due to faults and $\bar{\dot{Q}}_{Cap,Normal}$ is the RTU cooling capacity for normal operation. Substituting equation (5-6) into equation (5-5) gives

$$E_{Savings} = \frac{\alpha}{(1-\alpha)EER_{Normal}} \bar{\dot{Q}}_{Cap,Normal} (1-\beta)T \quad (5-7)$$

Neglecting demand costs, the utility cost savings (UCS) are calculated as

$$UCS = \left(\frac{\alpha}{(1-\alpha)EER_{Normal}} \bar{\dot{Q}}_{Cap,Normal} (1-\beta)T \right) C_e \quad (5-8)$$

where C_e is the cost of electricity (\$/kWh). Neglecting demand savings is a conservative assumption. Significantly greater utility cost savings would be possible if demand costs were considered. Roughly, the weighted average utility rate between on-peak and mid-peak periods in North California is 0.08\$/kWh and that in South California is around \$0.21/kWh.

According to the simple relationship given in equation (5-8), the utility cost savings associated with automated FDD applied to an individual RTU depend on the following factors:

1. the normal ERR (EER_{Normal}) and the degradation in EER due to the faults, α .
The lower the normal EER and the greater the EER degradation, the greater the opportunity for utility cost savings. The savings are particularly sensitive to the EER degradation factor.
2. the normal cooling capacity ($\bar{\dot{Q}}_{Cap,Normal}$) and the degradations in cooling capacity (β). Greater savings are associated with larger cooling capacities and cooling capacity degradations.
3. runtime (T). Utility cost savings increase linearly with increasing runtime.

4. electricity costs (C_e). Utility cost savings increase linearly with increasing energy costs. A similar result would apply to demand costs if they were considered.

Table 5-2 gives estimates of utility cost savings for different buildings and locations in California obtained with equation (5-8). For these calculations, the degradation factors determined for the RTU installed at Milpitas were used. This site uses RTU a 6-ton York air conditioning system with a nominal *EER* equal to 9 and its *EER* and cooling capacity degraded 21% and 30%, respectively due to faults. The runtimes for different sites, which only include the operation time for mechanical cooling, are estimated using data collected in 2002.

Table 5-2 Estimates of Utility Costs Savings for a 6-ton RTU A/C

Location	Electricity Costs (\$/kWh)	Building Type	Monthly Runtime (hour per month)	Months per Year	Annual Runtime (hour per year)	Utility Savings per Year (\$)
North California	0.08	Modular School	120	4	480	57
		Restaurant	150	6	900	107
		Retail Store	300	6	1800	214
South California	0.21	Modular School	180	5	900	281
		Restaurant	225	7	1575	492
		Retail Store	450	7	3150	985

From Table 5-2, it can be seen that:

1. The savings are greater in southern California than in northern California, because the climate is hotter and the electricity costs are higher. The differences might be less if demand charges were included.

2. The savings are greatest for retail store and lowest for the modular school. This is because the retail store has the highest cooling loads and the modular school has the lowest cooling loads.

5.2.2 Equipment Life Savings (ELS)

Faults can have a direct effect on equipment life through adverse operating conditions associated with the compressor, such as high operating temperatures or liquid entering the compressor. If the faults were severe enough to result in compressor failure, it would be very costly (about \$1,000 to replace a 6-ton compressor including labor fees). However, it is difficult to quantitatively evaluate the impact of faults on the compressor life. Faults also affect equipment life indirectly due to an increase in the required runtime to maintain comfort. This effect is much easier to quantify. Rearranging equation (5-6) gives the run time as

$$T = \frac{Q_{Load}}{\dot{Q}_{Cap,Normal} (1 - \beta)} \quad (5-9)$$

If the system cooling capacity were degraded by β , then the run time would increase by $\frac{\beta}{1 - \beta}$. The equipment life is dictated by the run time, e.g., 8 (hours) * 30 (days) * 5 (months) * 10 (years) = 12000 hours. Assuming an RTU cost of 750\$/ton and equipment life of 12,000 runtime hours, a unit cost per hour is \$0.0625/ (ton-hour). Then, the savings related to equipment life would be

$$ELS = 0.0625 \cdot \bar{\dot{Q}}_{Cap,Normal} \frac{\beta}{1 - \beta} T \quad (5-10)$$

Table 5-3 lists estimates of equipment life savings for different building types and locations in California, assuming characteristics of the RTU installed at Milpitas. From Table 5-3, the savings potential associated with equipment life is comparable to the utility cost savings and the trends are the same. This significant savings has not been considered by other investigators. Even greater savings would result if the direct effect of faults on equipment life were considered.

Table 5-3 Equipment life savings

Location	Building Type	Monthly Runtime (hour per month)	Months per Year	Annual Runtime (hour per year)	Equipment Savings per Year (\$)
North California	Modular School	120	4	480	77
	Restaurant	150	6	900	145
	Retail Store	300	6	1800	289
South California	Modular School	180	5	900	145
	Restaurant	225	7	1575	253
	Retail Store	450	7	3150	506

5.3 Fault Detection and Diagnosis Savings (FDDS)

Without automated FDD, there are significant costs associated with a service technician responding to an emergency call, performing a diagnosis, and providing repairs. In addition, unnecessary service is sometimes performed due to inaccurate diagnosis.

5.3.1 Unnecessary Service (USS)

Often, condenser cleaning and evaporator filter replacement occur on a regular basis (e.g, twice a year). However, the rate of fouling depends on the environment and the runtime of the unit. Furthermore, significant fouling is required before an impact on

performance is realized. According to Breuker's (1998a) investigation, cooling capacity and COP only degraded 6.1% and 10%, respectively when 35% of the condenser area was covered. Cleaning a condenser coil and replacing an evaporator filter costs about \$120 per service and is typically done twice a year. If automated FDD were applied, service could be based upon a quantitative assessment of the impact and unnecessary service could be reduced. If, for example, one regular service could be saved per year, the savings would be \$120 per year, which is significant compared to other costs.

5.3.2 Fault Diagnosis Savings (FDS)

Upon receiving an emergency call, a technician needs to go to the site, open the system, and perform a diagnosis. Typically, service costs are calculated based upon a charge for the visit (e.g., \$115) plus an hourly rate (e.g., \$65/hour). For example, to open the system, check for refrigerant leakage and recover the system requires about four hours. A four-hour service would cost about \$375. There are three kinds of refrigerant charge faults: refrigerant leakage, refrigerant low charge and refrigerant overcharge. The former requires manual leakage checking, while the latter two could be diagnosed with an automated FDD system. Furthermore, with the help of the automated FDD technique, refrigerant could be added or removed without the requirement for recovering the entire system charge, which is very time-consuming and costly. Table 5-4 lists the potential savings for refrigerant charge faults associated with the use of automated diagnostics.

Table 5-4 Potential for Refrigerant Charge Fault Savings

Refrigerant Charge Faults	Manual FDD Costs Plus Service (\$)	Automated Costs Plus Service (\$)	Savings (\$)
Leakage	375	150	225
Low Charge	375	75	300
Over Charge	375	75	300

5.4 Smart Service Schedule Savings (SSSS)

Automated FDD has the benefit of allowing service to be scheduled in an optimum manner. The primary savings are associated with reducing the number of emergency and total service calls according to the following schemes:

1. Find a tradeoff between cost savings and service costs. If the savings do not justify the service costs, service is not recommended. Since operating costs are higher for southern California sites than in northern California, more frequent service is expected.
2. Schedule multiple service tasks whenever possible. A significant part of the cost is associated with making the service visit. Furthermore, certain tasks should always be done in together. For example, replacing the filter/drier in combination with repairing a refrigerant leak reduces service costs considerably when compared to two separate service tasks. Table 5-5 lists potential savings associated with multiple service tasks.

Table 5-5 Potential Savings for Multiple-Service

Faults	Individual Service (\$)	Multiple Service (\$)	Savings (\$)
Refrigerant Leakage	375	500	250
Filter/Drier Restriction	375		
Coil Fouling	120	65	55

5.5 Total Equipment Life Savings (TELS)

As discussed in previous sections, potential savings for automated FDD include the following:

1. Planned preventive maintenance service savings, which are about \$2,000 for each RTU.
2. Operational cost savings, which include two parts: utility cost and equipment life savings. The utility cost savings should include both energy and peak demand savings. However, more work is needed to evaluate the peak demand savings effect.
3. Fault detection and diagnosis savings, which include two parts: unnecessary service savings and fault diagnosis savings.
4. Smart service schedule savings.

The last three items are difficult to quantify, because they are related to the rate of occurrence and level of faults. As previously mentioned, around 60% of packaged systems in California are improperly charged. According to our initial investigation of California field sites, fifteen of the twenty-one systems (71%) are impacted by faults, eleven of them (52%) are impacted by filter/drier restrictions, ten of them (48%) are impacted by refrigerant charge faults, and eight of them (38%) are impacted by both low charge and filter/drier restriction faults.

In order to quantify the net savings, the following conservative assumptions were made:

1. 10-year equipment life under normal operating conditions.
2. No replacement of major components, such as the compressor and fan motors during the life of the equipment.
3. On average, the performance of the system is assumed to be degraded for 40% of its lifetime with an *EER* and cooling capacity degradation of 21% and 30%, respectively.
4. One coil cleaning service can be saved per year through automated FDD.
5. A 60% probability that a refrigerant charge fault will occur once during the equipment lifetime.
6. A 60% probability that a filter/drier restriction fault will occur once during the equipment lifetime.

7. A 6-ton RTU having a cost of \$4500.
8. A cost for the FDD system of \$300.

The total equipment lifetime savings were estimated with the following steps:

1. Lifetime preventive maintenance service savings (PMIS),
 $10 \text{ (years)} * 0.75 * 270.28 = \$2,027$
2. Lifetime operational costs savings (OCS), $0.4 * 10 * (\text{UCS} + \text{ELS})$. Table 5-6 list the lifelong operation costs savings for different building types and locations.
3. Lifetime fault detection and diagnosis savings, which are the sum of
 $\text{USS} (10 \text{ (year)} * 120 = 1200) + \text{FDS} (0.6 * (225 + 300 + 300) / 3 = 165) = \1365
4. Lifetime smart service schedule savings (SSSS), $0.6 * 250 + 55 * 10 = \$700$

Table 5-6 Equipment Lifetime Operational Savings

Location	Building Type	Utility Savings per Year (\$)	Equipment Savings per Year (\$)	Lifetime Operation Savings (\$)
North California	Modular School	57	77	536
	Restaurant	107	145	1008
	Retail Store	214	289	2012
South California	Modular School	281	145	1704
	Restaurant	492	253	2980
	Retail Store	985	506	5964

The total lifetime net savings (see Table 5-7) are the total savings minus the cost of the FDD system (\$300). From Table 5-7, conservative estimates of the lifetime net savings range from \$4000 to \$10,000 per RTU, annual net savings range from \$400 to \$1,000, and the payback period would be less than one year. The savings would be greater for heat pumps because they operate through the whole year.

Table 5-7 Conservative Lifetime Total Savings per RTU (6-ton)

Location	Building Type	PMIS (\$)	OCS (\$)	FDDS (\$)	SSSS (\$)	TELS (\$)	Net Savings (\$)
North California	Modular School	2,027	536	1365	700	4,628	4,328
	Restaurant		1008			5,100	4,800
	Retail Store		2012			6,104	5,804
South California	Modular School		1704			5,796	5,496
	Restaurant		2980			7,072	6,772
	Retail Store		5964			10,056	9,756

6 SUMMARY AND RECOMMENDATIONS FOR FUTURE WORK

The following work was completed during this project:

1. A literature review about FDD application in HVAC&R was conducted in order to enhance the understanding of FDD. (Chapter 1 and Deliverables 2.1.3 & 2.1.4)
2. More than twenty field-sites, with unit one at Purdue and 20 units in California, were set up. The Purdue field-setup is meant to mimic field-setups in California in order to aid in the identification of installation and operational problems locally. The field-sites in California have different building occupancies, climate conditions, and packaged air conditioning equipment from different manufacturers (Deliverables 2.1.1a & 2.1.1b).
3. The FDD problem has been formulated in a mathematical way and a decoupling-based unified FDD technique was proposed to handle multiple-simultaneous faults and provide a more generic and system-independent method (Deliverables 2.1.5). The SRB method was re-examined in detail and then two new fault detection and diagnostic classifiers were presented that are simpler to implement and provide improved FDD sensitivity as compared with the original SRB method (Deliverables 2.1.3 & 2.1.4 and ASHRAE paper)
4. Various component models and virtual sensors were proposed to estimate features and overall system performance indices at low cost. For situations where physical or map-based models are not practical, a Polynomial plus GRNN modeling approach was developed that provides both good interpolation and extrapolation performance when training data are readily available (Deliverable 2.1.2 and Li and Braun (2002)).

5. Three case studies were investigated to validate the proposed approaches. (Deliverable 2.1.5). One case study provided initial validation of the decoupling-based FDD approach using laboratory data where single faults were artificially introduced into a 3-ton Trane rooftop unit (RTU) with a fixed-orifice as the expansion device. The second case study demonstrated the whole FDD methodology by artificially introducing multiple-simultaneous faults into the Purdue field emulation site, where a 5-ton York RTU with a TXV as the expansion device is installed. Finally, the decoupling-based FDD approach was applied to California field sites.
6. Finally, an initial economic assessment of the proposed FDD technique was performed. Conservative estimates of the lifetime net savings ranged from \$4,000 to \$10,000 per RTU, with annual net savings ranging from \$400 to \$1,000 and a payback period of less than one year.

Research on further improvements and evaluations of the FDD methodology will continue as follows:

1. Obtain more detailed RTU information for all the California field sites and apply the proposed FDD technique more completely to these field sites.
2. Further improve the performance of the unified FDD technique by improving the modeling approach that is based on manufacturers' data and find an efficient and practical way to tune these models using low-cost sensors. Improve other virtual sensors' performance and consider trying to remove pressure and humidity sensors.
3. Improve the overall performance model for assessing performance degradations of packaged air conditioning equipment under faulty operation using limited sensor and manufacturers' rating data.
4. Expand the service cost database and build a more detailed economic assessment model to more accurately evaluate the potential savings associated with the FDD technique and to provide guidelines for the fault evaluation and decision step.

5. Conduct more field tests under multiple-simultaneous faults and, if necessary, conduct more laboratory tests to test the proposed decoupling-based FDD technique.
6. Consider additional control related diagnoses, such as economizer and controller diagnoses.

REFERENCES

- Aaron, D. A., and P. A. Domanski. 1990. Experimentation, analysis, and correlation of refrigerant-22 flow through short-tube restrictor. *ASHRAE Transactions* 96(1): 729-742.
- Alistair I. Mees, M. F. Jackson, and Leon O. Chua, 1992. Device Modeling by Radial Basis Functions. *IEEE Transactions on Circuits and Systems-Fundamental Theory and Applications*. 39 (1): 19-27.
- ASHRAE. 1993. *ASHRAE Handbook - 1993 Fundamentals*, Atlanta: American Society of Heating, Refrigerating, and Air Conditioning Engineers, Inc., Atlanta, GA 30329.
- Benjamin, M.W., and J.G. Miller, 1941. The flow of saturated water throttling orifice. *Transactions of the ASME* 63 (5): 419-426
- Braun, J.E. and Li, Haorong. 2001a. Description of Laboratory Setup. Progress report submitted to Architectural Energy Corporation.
- Braun, J.E. and Li, Haorong. 2001b. Description of FDD modeling approach for normal performance expectation. Progress report submitted to Architectural Energy Corporation.
- Braun, J.E. and Li, Haorong. 2002. Description and Evaluation of an Improved FDD Method for Rooftop Air Conditioners. Progress report submitted to Architectural Energy Corporation.
- Braun, J.E. and Li, Haorong. 2003. A Decoupling-Based FDD Approach for Multiple-Simultaneous Faults. Progress report submitted to Architectural Energy Corporation.

- Breuker, M.S., 1997a. Evaluation of a Statistical, Rule-based Detection and Diagnosis Method for Vapor Compression Air Conditioners, Master's Thesis, School of Mechanical Engineering, Purdue University.
- Breuker, M.S. and Braun, J. E., 1997b. Evaluation of a Statistical, Rule-based Detection and Diagnosis Method for Vapor Compression Air Conditioners, HL 98-9, Report # 1796-7a, School of Mechanical Engineering, Purdue University.
- Breuker, M.S. and Braun, J.E., 1998a. Common Faults and Their Impacts for Rooftop Air Conditioners, HVAC&R Research, Vol. 4, No. 3, pp.303-318.
- Breuker, M.S. and Braun, J.E., 1998b. Evaluating the performance of a Fault Detection and Diagnostic System for Vapor Compression Equipment, International Journal of Heating, Ventilating, and Air Conditioning and Refrigerating Research, Vol. 4, No. 4, pp.401-423.
- Cacoullos, 1966. "Estimation of a multivariate density," Ann. Inst. Statist. Math, (Tokyo), Vol. 18, no. 2, pp.179-189.
- Carling, P., 2002. Comparison of Three Fault Detection Methods Based on Field Data of an Air-Handling Unit, ASHRAE Transactions 2002, V. 108, Pt.1.
- Chen, Bin, 2000a. Evaluating the potential of on-line fault detection and diagnosis for rooftop air conditioners, Master's Thesis, School of Mechanical Engineering, Purdue University.
- Chen, Bin and Braun, J.E, 2000b. Simple fault detection and diagnostics methods for packaged air conditioners, Proceedings of the 8th international refrigeration conference, Purdue University.
- Chen, Bin and Braun, J.E, 2001. Simple rule-based methods for fault detection and diagnostics applied to packaged air conditioners, ASHRAE Trans., vol. 107, part 1, paper No. AT-01-14-2, 847-837.
- Comstock, M.C., J.E. Braun, and B. Chen, 1999, Literature Review for Application of Fault Detection and Diagnostic Methods to Vapor Compression Cooling Equipment, Purdue University, Ray W. Herrick Laboratories, Report # HL99-19.

- Davis, Coby. 1993. Comparison of steady state detection algorithms. ME 397 Report. Available from Professor Jim Braun, Herrick Labs, Purdue University, West Lafayette, In.
- Dexter, Arthur; Pakanen, Jouko (ed.). Demonstrating Automated Fault Detection and Diagnosis Methods in Real Buildings. Espoo. VTT Building Technology, 2001. VTT Symposium 217. 381 p. + app. 13 p.
- Dexter, A.L. and Ngo, D., 2001. Fault Diagnosis in Air-Conditioning Systems: A Multi-Step Fuzzy Model-Based Approach, International Journal of Heating, Ventilating, and Air Conditioning and Refrigerating Research, Vol. 7, No. 1, pp.83-102.
- Donald F. Specht, 1991. A General Regression Neural Network. IEEE Transactions on Neural Networks. 2 (6): 368-376.
- Dyn, N. and Levin, D., 1983. "Iterative solutions of systems originating from integral equations and surface interpolation." SIAM J. Numerical Analysis, vol. 20, pp. 377-390.
- Fukunaga, K. 1990. Introduction to Statistical Pattern Recognition, Academic Press, Purdue University, W. Lafayette, IN, USA
- Ghiaus, C. 1999. Fault diagnosis of air conditioning systems based on qualitative bond graph, Energy and Buildings 30 (1999) 221-132.
- Glass, A.SI, Gruber, P., Roos, and M., Todtli, J., 1993. Qualitative Model-based fault detection in air-handling units, IEEE control systems Magazine, 13(4): 11-22.
- Gordon, J. M., and K. C. Ng. 1994. Thermodynamic modeling of reciprocating chillers. Journal of Applied Physics. 76(6):2769-2774.
- Grimmelius, H. T., J. Klein Woud, and G. Been. 1993. On-line failure diagnosis for compression refrigeration plants. International Journal of Refrigeration 18(1):31-41.

- Isermann, R. 1984. Process Fault Detection Based on Modeling and Estimation - A Survey, *Automatica*, 20(4): 387-404.
- Kim, Y. and O'Neal, D. L., 1994. Two-phase flow of R-22 through short-tube orifices. *ASHRAE Transactions* 100(1): 323-334.
- Lee, W., House, J.M. and Shin, D.R., 1997. Fault diagnosis and Temperature Sensor Recovery for an Air-handling unit, *ASHRAE Transaction*, 103(1): 621-633.
- Lee, W.Y. & House, J.M., etc., 1996. Fault diagnosis of an Air-Handling Unit Using Artificial Neural Networks, *ASHRAE Transactions* V.102, Pt.1, pp.340-349.
- Levins, W., Rice, C. and Baxter, V., 1996. Modeled and Measured Effects of Compressor Downsizing in an Existing Air Conditioner/ Heat Pump in the Cooling Mode, *ASHRAE Transactions* V. 102, Pt. 2, pp. 22-33.
- Li, H. and Braun, J.E. 2003, "An Improved Method for Fault Detection and Diagnosis Applied to Packaged Air Conditioners". Accepted by the American Society of Heating, Refrigerating, and Air Conditioning Engineers (ASHRAE)
- Li, H. and Braun, J.E., 2002, "On-Line Models for Use in Automated Fault Detection and Diagnosis for HVAC&R Equipment," *Proceedings of the 2002 ACEEE Conference on Energy Efficiency in Buildings*, Monterey, CA, 2002.
- Li, X., H. Hvaezi-Nejad, & J.C. Visier, 1996. Development of a fault diagnosis method for heating systems using neural networks. *ASHRAE Transactions* 102 (1): 607-614.
- Norford, L.K., Wright, J.A., etc., 2002. Demonstration of Fault Detection and Diagnosis Methods for Air-Handling Units, *International Journal of Heating, Ventilating, and Air Conditioning and Refrigerating Research*, Vol. 8, No. 1, pp.41-71.
- Parzen, 1962. On the estimation of a probability density function and the mode, *Ann. Math. Stat.*, 33, pp. 1063-1076.

- Rossi, T.M., 1995. Detection, Diagnosis, and Evaluation of Faults in Vapor Compression Cycle Equipment, Ph.D. Thesis, School of Mechanical Engineering, Purdue University.
- Rossi, T.M. and Braun, J.E. , 1996, "Minimizing Operating Costs of Vapor Compression Equipment with Optimal Service Scheduling," International Journal of Heating, Ventilating, Air-Conditioning and Refrigerating Research, Vol. 2, No. 1, pp. 23 - 47, 1996.
- Rossi, T.M. and Braun, J.E., 1997. A Statistical, Rule-Based Fault Detection and Diagnostic Method for Vapor Compression Air Conditioners, International Journal of Heating, Ventilating, and Air Conditioning and Refrigerating Research, Vol. 3, No. 1, pp.19-37.
- Shaw, S.R., Norford, L.K., Luo, D., etc., 2002. Detection and Diagnosis of HVAC Faults Via Electrical Load Monitoring, International Journal of Heating, Ventilating, and Air Conditioning and Refrigerating Research, Vol. 8, No. 1, pp.13-40.
- Stylianou, M. & D. Nikanpour. 1996. Performance monitoring, fault detection, and diagnosis of reciprocating chillers. ASHRAE Transactions 114 (4): 613-627.
- Yoshida, H. & Kumar, S. 1999. ARX and AFMM model-based on-line real-time data base diagnosis of suddent fault in AHU of VAV system, Energy Conversion & Management 40 (1999) 1191-1206.
- Yoshida, H. & Kumar, S. 2001a. Development of ARX model based off-line FDD technique for energy efficient buildings, Energy Conversion & Management 22 (2001) 33-39.
- Yoshida, H. & Kumar, S. 2001b. Online fault detection and diagnosis in VAV air handling unit by RARX modeling, Energy Conversion & Management 33 (2001) 391-401.